Development and Mechanistic Investigation of HDAC6 Degraders and Small Molecule PCSK9 Modulators

By

Ka Yang

A dissertation submitted in partial fulfillment of the requirements for the degree of

Doctor of Philosophy

(Pharmaceutical Sciences)

at the

UNIVERSITY OF WISCONSIN–MADISON

2019

Date of final oral examination: 06/10/2019

The dissertation is approved by the following members of the Final Oral Committee:

Weiping Tang, Professor, Pharmaceutical Sciences
Lingjun Li, Professor, Pharmaceutical Sciences
Wei Xu, Professor, Oncology
Charles Lauhon, Associate Professor, Pharmaceutical Sciences
Jennifer Golden, Assistant Professor, Pharmaceutical Sciences

Abstract

Small-molecule drugs are bioactive chemicals that can modulate important cellular functions responsible for diseases. In addition to the therapeutic significance, bioactive small molecules are also important probes for dissecting the function of macromolecules in biological systems.

Proteolysis targeting chimeras (PROTACs) are bifunctional molecules designed to knock down functional proteins. By tethering two ligands together, PROTACs are able to recruit E3 ligase to proteins of interest and promote the ubiquitination-mediated degradation via proteasome. Most histone deacetylases (HDACs) are epigenetic regulators that control the acetylation level of histones. As class IIb HDACs, HDAC6 modulates the acetylation of cytoplasmatic proteins such as α-tubulin and HSP90. HDAC6 is involved in multiple disease-relevant pathways. We designed and developed the first degrader for HDAC6 by linking a non-selective HDAC inhibitor to E3 ubiquitin ligase ligand pomalidomide. Our mechanistic investigations indicated that both CRBN E3 ligase and the ubiquitination-proteasome system are critical for the PROTAC-induced degradation of HDAC6. We subsequently developed the second generation of HDAC6 degraders by using selective HDAC6 inhibitor Nexturastat A as the ligand of HDAC6. The new generation of degraders exhibited improved potency and selectivity. The most potent degrader has a 1.6 nM of DC_{50} for HDAC6 and inhibits the proliferation of multiple myeloma (MM) cells at low nM concentrations. We also developed in-cell ELISA for high-throughput screening of degraders and third-generation degraders that could recruit VHL E3 ligase.

Cardiovascular diseases (CVDs) are one of the leading causes of death in United States and worldwide. High levels of low-density-lipoprotein-cholesterol (LDL-c) is clinically known as hypercholesterolemia or hyperlipidemia and significantly increases the risk of CVDs such as atherosclerosis. To lowing cholesterol, statin drugs are the major clinical therapy, but over 20% patients cannot achieve the desired LDL-c level due to the side effects associated with statin. Proprotein Convertase Subtilisin/Kexin Type 9 (PCSK9) is a validated therapeutic target to control LDL-c by regulating the degradation of LDL receptor (LDLR). Combination of statin and anti-PCSK9 mAbs successfully reduced 40-60% LDL-c in statin-resist patients. Comparing with macromolecule drugs, small-molecule drugs have several advantages such as ease of delivery and lower costs. To date, several small-molecule PCSK9 modulators have been reported, such as berberine, LDL-1dlnr, PF-06446846 and Heparin I. However, all of them remain low potency. The selectivity can be an issue under such high concentration for further clinical development. We have identified a class of heterocyclic compounds that can reduce the PCSK9 level selectively in cell-based phenotypic screening. We further improved the potency and other pharmacological properties by structure-relationship-study (SAR). Some of the most potent compounds have picomolar IC_{50}s for the reduction of secreted PCSK9 in media. Meantime, we also investigated the mechanism of action of our PCSK9 modulators by various methods including RNA-seq based transcriptome studies, proteomic studies, and chemical probe-based target identification studies. Our effort uncovered the intricate and novel regulatory pathway of PCSK9 through AhR.

Acknowledgments

Doctoral career is not an easy journey. All my progress and achievement in research are contributed by so many wonderful peoples in my life. Dr. Weiping Tang owns most credit in guiding me the research, scientific ethics and this thesis. I really appreciate his patience, motivation and immense knowledge. Besides my advisor, I would like to thank the rest of my thesis committee: Dr. Lingjun Li, Dr. Wei Xu, Dr. Charles Lauhon and Dr. Jennifer Golden. I benefit a lot from their encouragement and support to my research and career development.

Furthermore, tons of credit go to our medicinal chemists for the synthesis of so many fascinating molecules. I would like to thank Dr. Haibo Xie for synthesis of all PCSK9 modulators and Dr. Hao Wu created so many remarkable PROTAC degraders. I must acknowledge Dr. Gabrielle Noel Winston-McPherson for guide me in biochemical experiments. I would like also thanks lab alumni such as Dr. Haoyuan Wang, Dr. Wangze Song, who I worked with in chemistry when I firstly joined Tang lab. Our collaborators Dr. Alan Attie, Dr. Lingjun Li, Dr. Christina Kendziorski and their lab members have so many intellectual and experimental contributions to the PCSK9 projects.

I must thank my parents who sincerely supported me during my PhD life. I couldn’t make even one step without them as my strongest supporters.

Table of Content

List of Figures

List of Tables

List of Scheme

1. Review of Proteolysis Targeting Chimera (PROTAC)

1.1. Introduction

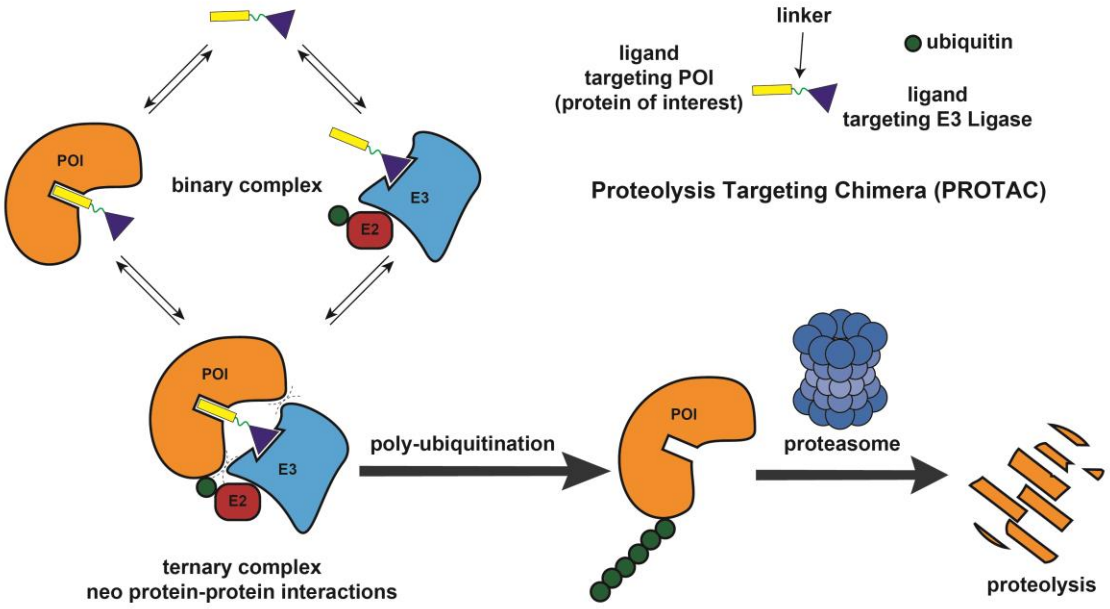

Figure 1.1.1. Mechanism of PROTAC-Mediated Protein Degradation

Genetic knockout or knockdown of certain cellular proteins is an important method for biological research and drug discovery. CRISPR-Cas9 and siRNA are the primary tools for the control of protein expression by changing the genomic content or blocking transcription[1,2]. Both of them have been used extensively for the study of various biological pathways and the validation of drug targets. However, both of them also have a number of limitations such as 1) off-target effects, 2) difficulty in delivery to cells and living organisms, 3) metabolic instability and 4) irreversible editing[3–6].

Ubiquitination-proteasome system (UPS) is one of the major pathways for protein degradation [7]. About 80% of proteins in our proteome are degraded by the UPS. Proteolysis

targeting chimera (PROTAC) is an emerging technique that can induce efficient degradation of targeted protein via UPS[8]. As illustrated in **Figure 1.1**, PROTAC is a rationally designed bifunctional molecule by tethering together a E3 ligase ligand and a ligand for protein of interest (POI). The chemical chimera binds to either POI or E3 ligase to form binary complex first[9]. A subsequent ternary complex formation recruits E3 ligase to the POI and promote its ubiquitination. Poly-ubiquitinated POI is subsequently recognized by escort protein complexes and delivered to proteasome for degradation. Various functional proteins were artificially targeted for ubiquitination-degradation by different E3 ligases using the PROTAC strategy[10]. The E3 ligase and the targeted protein(s) don't have to be biologically relevant. Beside inducing rapid degradation, PROTAC has multiple potential advantages over traditional inhibitor, such as overcoming drug resistance, sustained downstream effects and offering selectivity for isoforms of proteins that are otherwise difficult to differentiate[11]. Those features underscore the significance of targeted protein degradation (TPD) by PROTAC in both therapeutic development and serving as powerful tools for biological research. In this Chapter, I will briefly review the history of PROTAC development, highlight some key features in drug discovery, and discuss applications of PROTACs as chemical probes.

1.2. History of the PROTAC Development

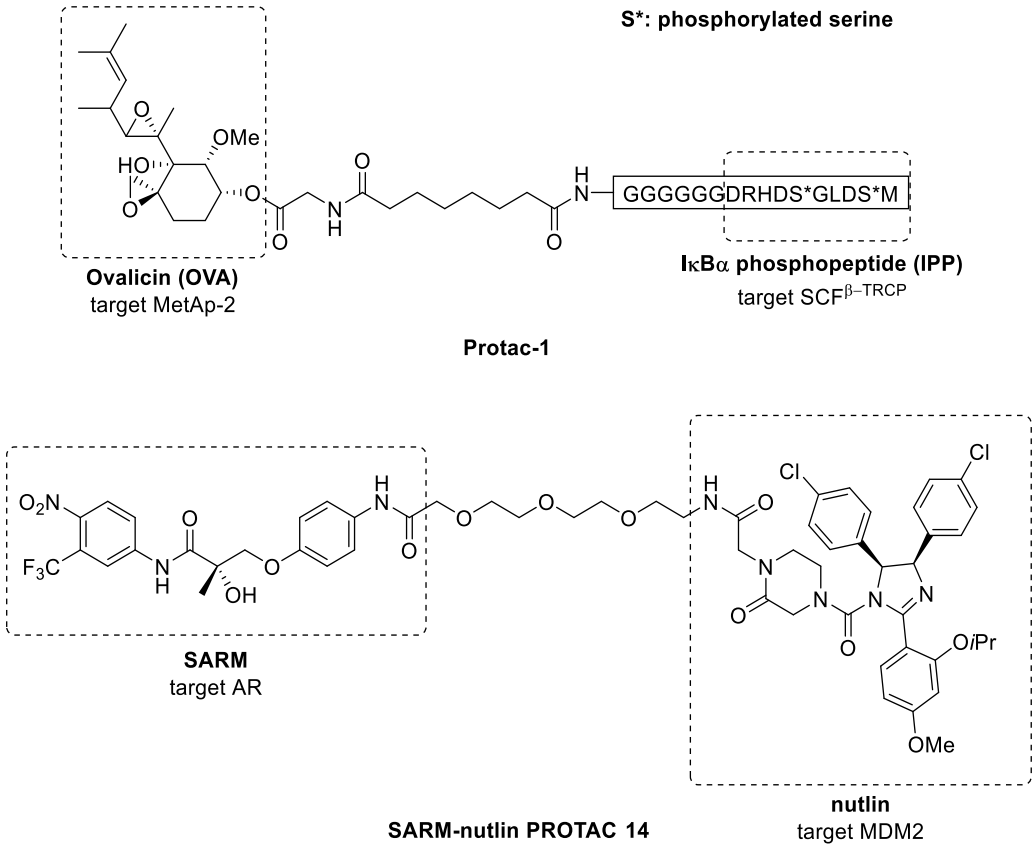

Figure 1.2.1 First peptide-based and all-small-molecule PROTACs

In 2001, Sakamoto's lab at UCLA, Deshaies's lab at Caltech, and Crews's lab at Yale first introduced the peptide based PROTAC molecule[12]. They employed IκBα phosphopeptide (IPP) and ovalicin (OVA) as the ligands of E3 ubiquitin ligase and the POI, respectively, to form the first PROTAC (Protac-1, **Figure 1.2.1**). IPP mimicked the phosphorylated 10 amino acids moiety of IκBα and was able to bind the heterotetrameric Skp1-Cullin-F box complex on β-TRCP/E3RS[13]. SCF$^{β-TRCP}$ is one of SCF E3 complexes responsible for the destruction of various proteins[14]. On the other side, angiogenesis inhibitor OVA can covalently bind to MetAp-2[15], which had not been reported as the ubiquitination target of

any SCFs. Protac-1 successfully recruited MetAp-2 to $SCF^{\beta\text{-}TRCP}$ *in vitro* and resulted in augmenting its degradation via ubiquitination-proteasome pathway. Because cell-permeability is a major issue for peptide-based compounds, the effect of PROTAC-1 on ubiquitination and degradation was only demonstrated in xenopus egg extracts. Nevertheless, PROTAC-1 was the first proof of concept study. It then took about 14 years for the development of cell permeable PROTACs with in-vivo efficacy, and another four years to launch the first human clinical trial for PROTACs, as shown in **Figure 1.2.2**. Between 2015 and 2019, almost all major pharmaceutical companies established internal programs on PROTAC-based targeted protein degradation. Most published PROTAC-based degraders are summarized in **Table 1.1**.

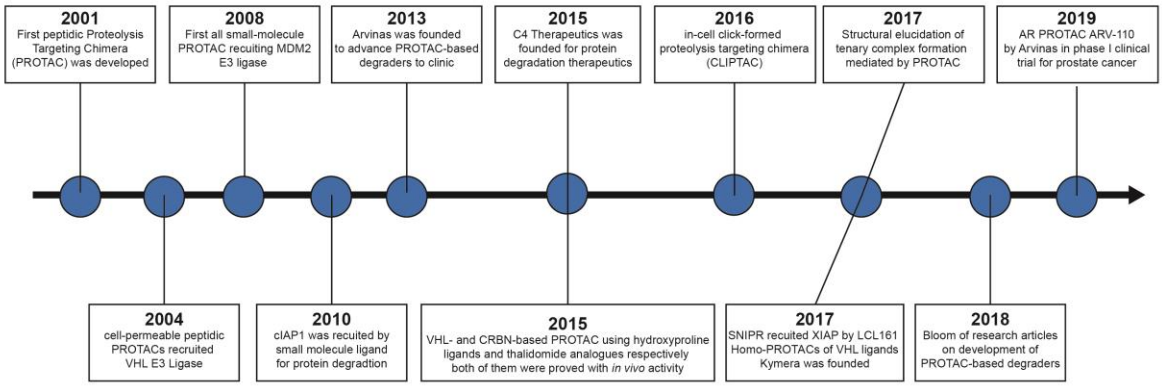

Figure 1.2.2 Chronicle of events in PROTAC development

For early peptidic degraders, limited cell penetration restricted their applications[15,16]. To solve that problem, cell permeable Protac-4 and Protac-5 targeting FK506 binding protein 12 (FKBP12) mutant F36V ($FKBP12^{F36V}$)and androgen receptor (AR) were developed[17]. The E3 binding moiety for these PROTACs was a short peptidic sequence ALAPYIP of

HIF-1α that could recruit von Hippel-Lindau (VHL) tumor suppressor protein E3 ligase[18]. Both degraders successfully "knocked out" targeted proteins via UPS in cultured cells. In 2008, the first non-peptidic PROTAC (PROTAC **14**, **Figure 1.2.1**), or all small-molecule PROTAC, was created by assembling selective androgen receptor modulator (SARM) with nutlin[19], which disrupts the protein-protein interaction (PPI) of MDM2 E3 ligase and p53 by binding to MDM2[20]. However, relatively high concentration of this probe was required to induce intracellular depletion of protein targets. There is no evidence showing that the MDM2 E3 ligase is actually involved in the degradation of androgen receptor. In late 2018, the second PROTAC that recruits MDM2 E3 ligase was reported[21].

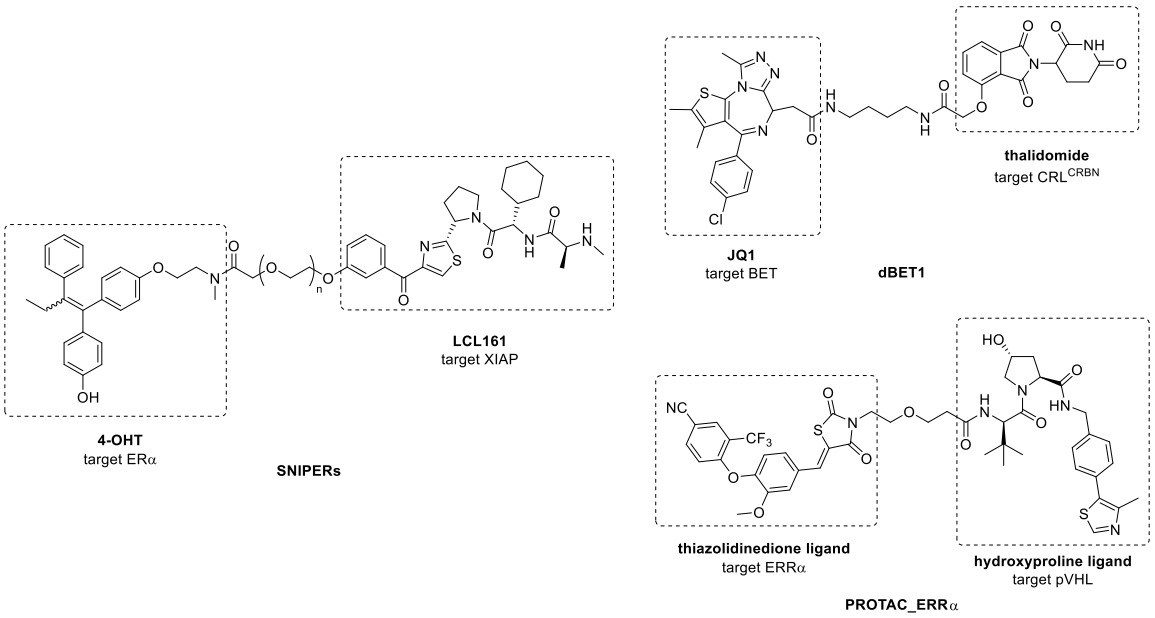

Figure 1.2.3 Featured PROTACs recruiting IAP, VHL and CRBN E3 ligases

The putative number of E3 ligases in human genome is over 600[22]. However, only inhibitor of apoptosis protein (IAP), VHL and cereblon (CRBN) together with their ligands were exploited to PROTAC degraders for various protein targets[23]. In 2010, specific and

nongenetic IAP-dependent protein erasers (SNIPER) was introduced based on the same concept as PROTAC[24]. The first SNIPER used Methyl Bestatin (MeBS) to recruit cellular inhibitor of apoptosis protein 1 (cIAP1) E3 ligase and all-trans retinoic acid (ATRA) to target cellular retinoic acid binding protein 1 and 2 (CRABP-I and CRABP-II). However, the first SNIPER promoted the degradation of both cIAP1 and the targeted proteins in cellular context. The variation of linking method was able to overcome the auto-ubiquitination of cIAP itself. The conversion of ester-type linking to amide-type linking resulted in degradation only targeted protein despite low potency[25,26]. Subsequently, new series of SNIPERs (**Figure 1.2.3**) adopted novel ligand LCL161 to recruit X-linked IAP (XIAP) instead of cIAP1[27]. Degraders using this E3-ligand have better potency for a number of targets such as ERα, BCR-ABL, Brd4 and PDE4 proteins. The versatility of using XIAP as E3 ligase was validated for future PROTAC design.

VHL E3 ligase was first employed in peptidic PROTAC with seven amino acids[17]. Aiming to develop more pharmacologically modifiable VHL ligands, Crews's group *de novo* designed and optimized small-molecule peptidomimetic ligands based on the critical binding moiety, hydroxyproline (Hyp) of HIF-1α, a protein substrate targeted by VHL[28,29]. Once ligands with high binding affinity were identified, they exploited those ligands by constructing various PROTAC molecules (**Figure 1.2.3**)[3,30]. Those VHL-PROTACs selectively targeting estrogen-related receptor alpha (ERRα), receptor-interacting serine/threonine-protein kinase 2 (RIPK2) and Brd4 showed impressive degradation efficacy in cells and even *in vivo*. Since then, VHL ligands have been used extensively used in developing effective degraders that can recruit VHL E3 ligase[31–35].

Thalidomide was once notorious of causing birth defects in infant when used as sedative for pregnant women[36]. After being withdrew from the market, thalidomide and its analogues were found to possess multiple other functions such as anti-inflammation, anti-angiogenesis and immune modulation, including T-cell co-stimulation and NK cell activation[37]. Decades later, they were proved for the treatment of multiple myeloma as immunomodulatory drugs (IMiDs). Cereblon (CRBN) can assemble with DDB1 to form E3 complex and was proposed as the cellular target of IMiDs[38,39]. Thalidomide and its derivatives activated CRBN's E3 ligase activity towards Ikaros family zinc finger proteins 1 and 3 (IKZF1 and IKZF3)[40]. The degradation of IKZFs was responsible for the anti-proliferative effects in multiple myeloma. In 2015, thalidomide and derivatives were first applied in PROTAC technology for targeting disease-relevant proteins Brd4 and FKBP12 (**Figure 1.2.3**)[41,42]. Potent bromodomain protein degrader dBET1 was one of the first PROTAC degraders showed efficacy in animals, including degradation and anti-tumor effect. Thalidomide and its derivatives are much smaller than the peptidomimetic ligands of IAP and VHL, which are less drug-like[40]. Thus, the IMiDs gained popularity quickly for the development of degraders targeting various proteins[5,33,43–45]. However, PROTACs bearing IMiDs preserved IKZF1/3 degradation as off-targets effects of CRBN E3 ligases[44,46–48]. This may be a concern for degraders of this type.

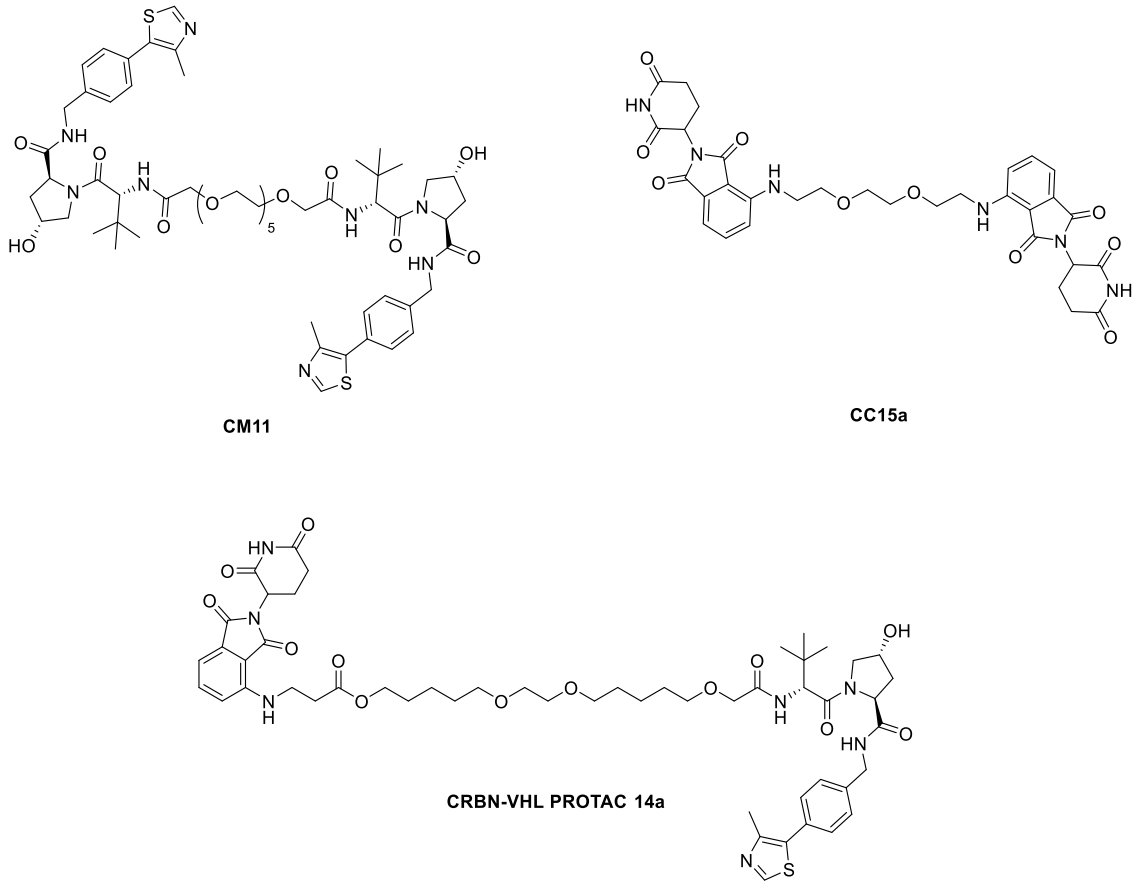

Figure 1.2.4 PROTACs mediated interaction between E3 ligases

PROTACs targeting E3 ligases was also created to study the interaction between same or different E3 ligases (**Figure 1.2.4**). Homo-PROTACs were the homodimers of ligands of VHL (CM11) or CRBN (CC15a) and triggered the self-ubiquitination and proteasomal degradation[49,50]. Heterodimer which tethers pomalidomide and hydroxyproline derivative was named Hetero-PROTAC or CRBN-VHL PROTAC[51,52]. The two different E3 ligases are bridged by this hetero-PROTAC and unexpectedly resulted the favorable degradation of CRBN but not VHL. The preference of CRBN degradation was not fully understood and required further investigation to elucidate the detailed mechanism.

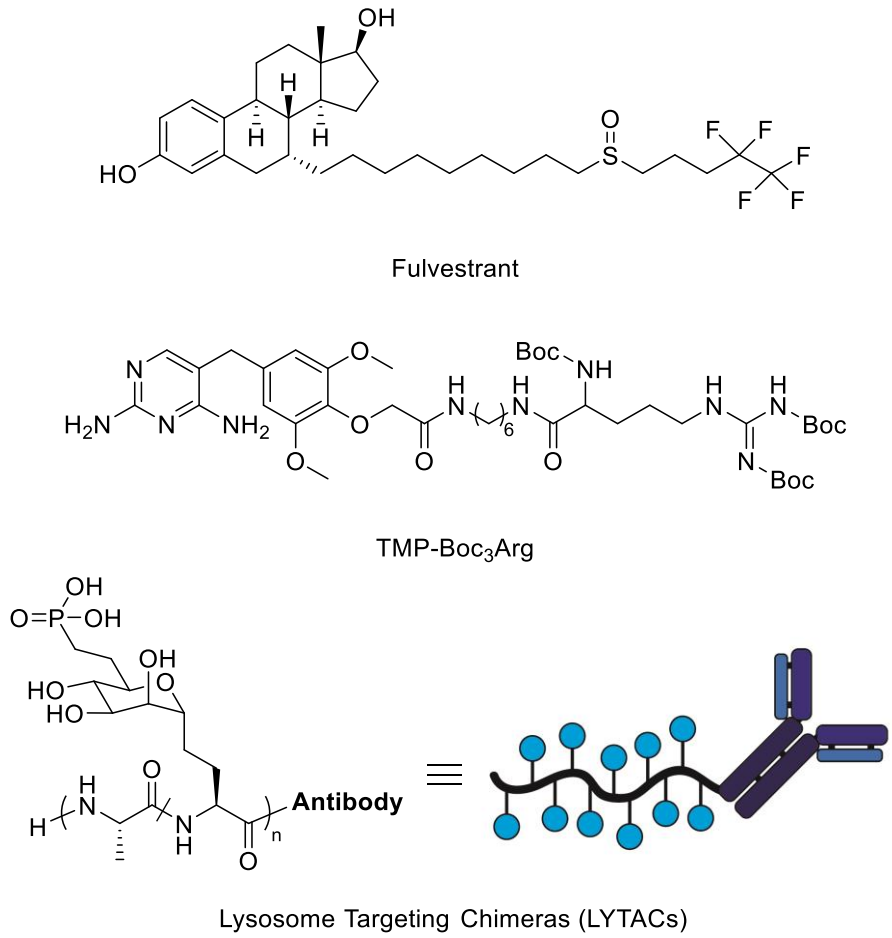

Figure 1.2.5 Other technologies for targeted protein degradation (TPD)

In addition to the above strategies, several other related targeted protein degradation technologies were also developed (**Figure 1.2.5**). For example, selective estrogen/androgen receptor degraders (SERDs and SARDs), such as Fulvestrant and UT-155, can bind to ER and induced subsequent degradation[53,54]. Novel SERDs developed recently with excellent anti-tumor activity were advanced to clinical trials[55,56]. Small molecule tagged with hydrophobic groups like adamantane[57] or Boc_3Arg[58] could also recruit cellular degradation machinery for depletion of targeted proteins. To complement the PROTAC strategy, which only degrade intracellular proteins, Bertozzi and co-workers

designed and synthesized lysosome targeting chimeras (LYTACs) to recruit cation-independent mannose-6-phosphate receptor (CI-M6PR) to degrade secreted and membrane proteins[59]. CI-M6PR is lysosomal targeting receptor (LTR) on cell surface and transports substrate proteins to lysosome[60]. They used mannose-6-phosphonate (M6Pn) glycopolypeptides to recruit CI-M6PR and antibody to bind to targeted proteins. LYTACs were able to deliver membrane or secreted proteins, such as epidermal growth factor receptor (EGFR) and Apolipoprotein-E4, to lysosome for degradation. This strategy expanded the scope of TPD to extracellular proteins.

Up to date, there are many disease-relevant proteins that have been degraded by PROTACs. PROTACs targeting estrogen receptor (ER)[27], AR[61], mouse double minute 2 homolog (MDM2)[62] or bromodomain and extra-terminal motif (BET) proteins[41,43,63] exhibited excellent antitumor activity in *in vivo* tumor models. Those pre-clinical evidences underlined the significance of PROTAC in drug discovery. Arvinas was found by Crews in 2013 aiming to advance the pre-clinical and clinical development of PROTACs. Recently, they launched the first clinical trial for treatment of prostate cancers using their AR PROTAC degrader ARV-110 (NCT03888612). A number of other biotech companies were also launched recently to develop PROTAC-based therapeutics. It will take years of time and enormous amount of resources to develop PROTAC-based therapeutics, similar to the development of any small molecule drugs. Besides the therapeutic applications, PROTACs are also useful chemical probes for target validation[44] and modulation of the functions of intracellular proteins[64]. As discussed before, small molecule PROTACs have

many advantages over CRISPR and siRNA and PROTAC can complement these two powerful technologies in basic biological research.

Table 1.1. Comprehensive Summary of Featured PRTOAC-Based Degraders in Literatures

Name	Year	POI	Ligand of POI	E3 ligase	E3 ligand	Functionality	Animal Study	Ref
Protac-1 (peptidic)	2001	MetAp-2	ovalicin (OVA)	$SCF^{\beta\text{-}TRCP}$	IκBα phosphopeptide (IPP)	*in vitro* degradation	N/A	12
Protac-5 (peptidic)	2004	AR	DHT	VHL	ALAPYIP-(d-$Arg)_8$-NH_2	cellular degradation	N/A	17
Protac-4 (peptidic)	2004	$FKBP12^{F36V}$	AP21998	VHL	ALAPYIP-(d-$Arg)_8$-NH_2	cellular degradation	N/A	17
PROTAC **14**	2008	AR	SARM	MDM2	nutlin	cellular degradation	N/A	19
SNIPER **4**	2010	CRABP-II	ATRA	cIAP1	MeBS	cellular degradation of both cIAP and CRABP-II at μM concentrations	N/A	24
SNIPER **6**	2011	CRABP-II	ATRA	cIAP1	MeBS	cellular degradation of both cIAP at μM concentrations	N/A	25,26
SNIPER(ER)-3	2013	ERα	4-OHT	cIAP1	Bestatin	cellular degradation at μM concentrations; induce necrotic cell death of MCF-7 cells	*N/A*	65
PROTAC_ERRα	2015	ERRα	thiazolidinedione derivative	VHL	hydroxyproline derivative	cellular degradation, DC_{50} = ~100 nM	broad tissue distribution and *in vivo* degradation;	3

PROTAC_RIPK2	2015	RIPK2	RIPK2 ligand	VHL	hydroxyproline derivative	cellular degradation, DC_{50} = 1.4 nM	N/A	[3]
dBET1	2015	BRD2/3/4	JQ1	CRBN	thalidomide derivative	cellular degradation, DC_{50} = 430 nM for BRD4; suppressed proliferation and induced apoptosis of AML cells	*in vivo* degradation; delayed leukemia progression in mice	[41]
ARV-825	2015	BRD2/3/4	OTX015	CRBN	pomalidomide	cellular degradation, DC_{50} < 1 nM for BRD4; suppressed proliferation and induced apoptosis of BL cells	N/A	[42]
MZ1	2015	BRD2/3/4	JQ1/I-BET762	VHL	VHL-1/VHL-2	cellular degradation, DC_{50} < 100 nM for BRD4;	N/A	[30]
dFKBP-1 dFKBP-2	2015	FKBP12	SLF	CRBN	thalidomide derivative	cellular degradation	N/A	[41]
HaloPROTAC-3	2015	HaloTag7 fusion proteins	chloroalkane	VHL	VH032	cellular degradation of fused protein target technology for biomedical research and drug discovery	N/A	[66]
ARV-771	2016	BRD2/3/4	JQ1	VHL	hydroxyproline derivative	cellular degradation, DC_{50} < 5 nM for BRD4; suppressed AR level and signaling;	*in vivo* degradation; induce regression of prostate tumor in mice	[32]

CLIPTACs	2016	Brd4, ERK1/2	JQ1-TCO Probe 1	CRBN	Tz-thalidomide	cellular self-assembly and degradation with DC_{50} < 1 μM	N/A	67
AT1	2017	BRD4	JQ1	VHL	hydroxyproline derivative	cellular selective degradation of BRD4	N/A	9
SNIPER(ER)-87	2017	ERα	4-OHT	XIAP	LCL161	cellular degradation, DC_{50} < 100 nM inhibited growth of MCF-7 and T47D with IC_{50} = 15.6 nM and 9.6 nM	*in vivo* degradation in mice; inhibit breast tumor growth in mice	27
SNIPERs	2017	BCR-ABL, BRD4, PDE4	Dasatinib,JQ-1, PDE4inhibitor	XIAP	LCL161	cellular degradation at nM concentrations	N/A	27
Homo-PROTAC CM11	2017	VHL	VH032	VHL	VH032	cellular degradation, 10 nM < DC_{50} < 100 nM for pVHL30	N/A	49
BETd-260	2018	BRD2/3/4	HJB97	CRBN	thalidomide	cellular degradation, DC_{50} < 1 nM for BRD4; inhibited growth of RS4:11 cell with IC_{50} = 51 pM	single dose caused durable *in vivo* degradation over 24 h in mice; induces leukemia tumor regression in mice	43
QCA570	2018	BRD2/3/4	QCA276	CRBN	thalidomide	cellular degradation, DC_{50} < 100 pM for BRD4; inhibited growth of RS4:11, MV4;11 and MOLM-13 cells with IC_{50} < 100 pM	*in vivo* degradation in mice; induces t complete and long-lasting leukemia tumor regression in mice	63
ZXH-3-26	2018	BRD4	JQ1	CRBN	Pomalidomide	cellular selective degradation of BRD4 with DC_{50} = 5 nM	N/A	48

MT802	2018	BTK^{C418S}	Ibrutinib derivative	CRBN	thalidomide derivative	cellular degradation	N/A	[68]
TD-PROTAC (peptidic)	2018	ERα	TD-PERM	VHL	HIF	cellular degradation at μM concentrations; inhibited growth of breast cancer cells with IC_{50} = ~30 μM	*in vivo* degradation in mice; inhibit breast tumor growth in mice	[69]
PROTAC-3	2018	Fak	Defactinib	VHL	hydroxyproline derivative	cellular degradation, DC_{50} = 3 nM inhibit downstream phosphorylation and cell migration invasion	N/A	[70]
PROTAC **12**	2018	Sirt2	SirReal **1b**	CRBN	thalidomide derivative	cellular degradation at μM concentrations	N/A	[45]
Degrader **9c**	2018	HDAC6	AB3	CRBN	pomalidomide	cellular degradation, DC_{50} = 34 nM for HDAC6	N/A	[71]
Homo-PROTAC CC15a	2018	CRBN	pomalidomide	CRBN	pomalidomide	cellular degradation, DC_{50} < 1 μM	N/A	[50]
dTAG13	2018	$FKBP12^{F36V}$ and fused proteins	AP1867	CRBN	thalidomide derivative	cellular degradation of fused protein target technology for biomedical research and drug discovery	N/A	[44]
ARD-69	2019	AR	enzalutamide derivative	VHL	VHL-d	cellular degradation, DC_{50} < 1 nM; inhibited growth of LNCaP, VCaP and 22Rvl cells with IC_{50} < 1 nM	single dose caused durable *in vivo* degradation over 48 h in mice;	[61]

MD-224	2019	MDM2	MI-1061	CRBN	thalidomide	cellular degradation, DC_{50} < 1 nM inhibited growth of RS4;11 cells with IC50 = 1.5 nM	*in vivo* degradation in mice; induces t complete and durable leukemia tumor regression in mice	62
ERD-308	2019	ERα	raloxifene derivative	VHL	VHL-1	cellular degradation, DC_{50} = 0.17 nM inhibited growth of MCF cells with IC_{50} = 0.77 nM and 57.5 % maximal inhibition	N/A	72
Degrader 32	2019	MDM2	Nutlin	CRBN	lenalidomide	cellular degradation, DC_{50} = 23 nM for MDM2 inhibit proliferation of RS4:11 leukemia cells	N/A	73
Degrader **12d**	2019	HDAC6	Nexturastat A	CRBN	pomalidomide	cellular degradation, DC_{50} = 1.6 nM for HDAC6 inhibited growth of MM1S cell with IC_{50} = 75 nM and 63% maximal inhibition	N/A	74
Hetero-PROTAC VHL-CRBN	2019	CRBN	pomalidomide	VHL	VH032	cellular degradation of CRBN over VHL, DC_{50} = 200 nM	N/A	52

1.3. PROTAC in Drug Discovery

It has been estimated that only 10% of proteome can be modulated by small-molecules and only half of the 10% are associated with diseases[75]. The term of "undruggable targets" are used to describe proteins that lack the enzymatic or receptor activity. These proteins usually function through PPI, such as transcriptional factor or scaffold proteins. Targeting undruggable disease-relevant proteins remained to be the frontier of many branches of life sciences. Rather than occupying the active site of enzymes by inhibitors or ligand binding domain of receptors, PROTAC induces the degradation of target by temporarily bringing the E3 ubiquitin ligase and POI into proximity. This degradation by PROTAC is event-driven and catalytic without requiring sustained occupation of the binding sites. PROTAC provides a novel strategy for treating diseases associated with abnormally expressed, mutated, or dysfunctional proteins.

PROTAC-based protein degraders exhibit unique features comparing with traditional inhibitors. PROTACs can often offer another level of selectivity. For example, although Foretinib promiscuously bound to 133 kinases, VHL- and CRBN-based PROTACs with the Foretinib motif bound to ~50 kinases and only led to efficient degradation of <15 kinases[33]. Another case was the development of the first HDAC6 degrader, which was created based on a pan-HDAC inhibitor that binds to all 11 HDACs[71]. The profiling of HDAC degradation showed only HDAC6 was affected by the degrader while other family members remained intact.

Meanwhile, potency and selectivity of inhibitors didn't necessarily benefit the degradation efficiency of PROTACs. For instance, the degradation efficiency of BET degraders was decreased when the "warhead" was converted from the less potent inhibitor JQ1 to the more potent inhibitor I-BET726[34]. During the development of Bruton's tyrosine kinase (BTK) PROTAC degraders[76], using irreversible-binding Ibrutinib as "warhead" resulted only limited degradation. Replacing Ibrutinib by a reversible-binding moiety in PROTAC enhanced BTK degradation efficiency.

The advantage of event-driven degradation over occupancy-driven inhibition was also revealed in multiple cases. For instance, PROTAC-mediated Fak degradation affected both kinase-dependent signaling (i.e. phosphorylation of downstream targets) and kinase-independent signaling including cell migration and invasion[70], which were not observed when the corresponding inhibitor was employed. This highlighted that the degradation of target by PROTAC exhibited additional outcomes in addition to inhibiting its activity. Moreover, depletion of receptor tyrosine kinases (RTK)[35] and BET proteins[77] by PROTACs resulted more potent and prolonged repression on downstream signaling than inhibition. Besides, RTK degrader provides a potential solution for kinome rewiring challenge due to receptor crosstalk generated resistance to kinase inhibitor[78].

In addition to genetic mutation, drug resistance can be generated by other mechanisms, such as activation of survival pathways, abnormal metabolism and target overexpression[79]. All of these are challenges we have to face during the development of chemotherapeutics for cancers. In recent studies, PROTACs were found to be effective to cancers that were resistant to traditional inhibitors, such as ibrutinib for chronic lymphocytic leukemia

(CLL)[68], ruxolitinib and quizatinib for acute myeloid leukemia (AML)[77,80] and proteasome inhibitors or IMiDs for multiple myeloma (MM)[81]. For example, BTK degrader MT-802 showed remarkable degradation effect for C481S mutant in patient cells and engaged fewer off-targets than covalent inhibitor ibrutinib[68].

Conversion of fms related tyrosine kinase 3 (FLT-3) inhibitor quizartinib into PROTAC degrader induced strong FLT-3 ITD mutant degradation and enhanced the antiproliferation towards AML cells[80]. BET degraders suppressed the viability in myeloma cells that were resistant to bortezomib, lenalidomide and pomalidomide and had synergistic effect with multidrug resistance protein 1 (MDR1) inhibitors verapamil[81]. In addition, BET degrader ARV-825 also showed synergism in combination with PI3K/mTOR inhibitor PQR209 in preclinical lymphomas model[82]. Those explorations in PROTAC-induced degradation along or in combination with other inhibitors underlined the promising future for advanced therapy innovation.

PROTACs are relatively large small molecules, generally with molecular weight of 700~1000 Da. There are concerns about solubility, cell permeability and other drug-like properties according to Lipinski's guidelines for oral drugs[83,84]. A number of strategies have been taken to overcome these challenges by modifying the linkers and affinity ligands. For example, early BET and AR degraders used polyethylene glycol (PEG) or alkyl linkers with moderate length and flexibility[41,85,86]. More recent degraders have short and rigid linkers, which are designed by structure-based rational optimization. Only two carbon units were used to tether JQ1 and pomalidomide to generated dBET57, which showed excellent degradation on Brd4 and Brd3 and left other members intact[48]. Through screening linkers

with various chemical and physical properties, ARD-69 was developed with soluble and rigid alkyne-piperidine-piperidine linker and exhibited potent AR degradation in cell and *in vivo*[61]. In addition, rather than engineering the molecular properties, Heightman and co-worker developed a strategy to couple tetrazine-tagged thalidomide derivative with trans-cyclo-octene tagged BET- or ERK1/2-ligand inside the cell to form complete PROTAC for targeted protein degradation[67]. They named this methodology as click-formed proteolysis targeting chimeras (CLIPTACs) and anticipated future exploration of it to overcome the cell penetration issue in developing PROTAC.

Last but not least, novel pharmacology of PROTAC provided new understanding of the potential of this strategy in drug discovery. Instead of continuously occupying the active sites, PROTAC is catalytic and it does not need to bind to its target all the time. The outcome of degradation instead of inhibition may also have a long-lasting effect when the protein re-synthesis rate is slow. In pre-clinical studies, efficacy of PROTAC in animal model benefited from these features. PROTAC degraders were administrated *in vivo* and showed strong and long-last degradation[27,43,61–63]. Some of the compounds had notable anti-tumor activity[27,43,62,63]. Limited studies were reported about the pharmacokinetic (PK) or pharmacodynamic (PD) of degraders in literature. Wang and co-workers performed parallel PK/PD study in mice bearing RS4;11 xenograft tumor and treated with BET degrader BETd-260[43]. Single dosed PROTAC induced both degradation and inhibited tumor growth inhibition over 24 h, while the concentration of degrader was undetectable at 24-h point. Although this outcome is also related to the turnover rate of BET proteins,

this finding supported the catalytic feature of PROTAC and underscored the significance of this strategy in preclinical and clinical development.

1.4. PROTAC in Chemical Biology

As the field of targeted protein degradation is flourishing, the improvement of our understanding of PROTAC and its detailed mode of action (MoA) will greatly facilitate the rational design of degraders. Theoretical, computational and experimental methods/platforms have been established to advance better understanding about PROTAC MoA.

1.4.1. Deciphering the Mechanism of PROTAC

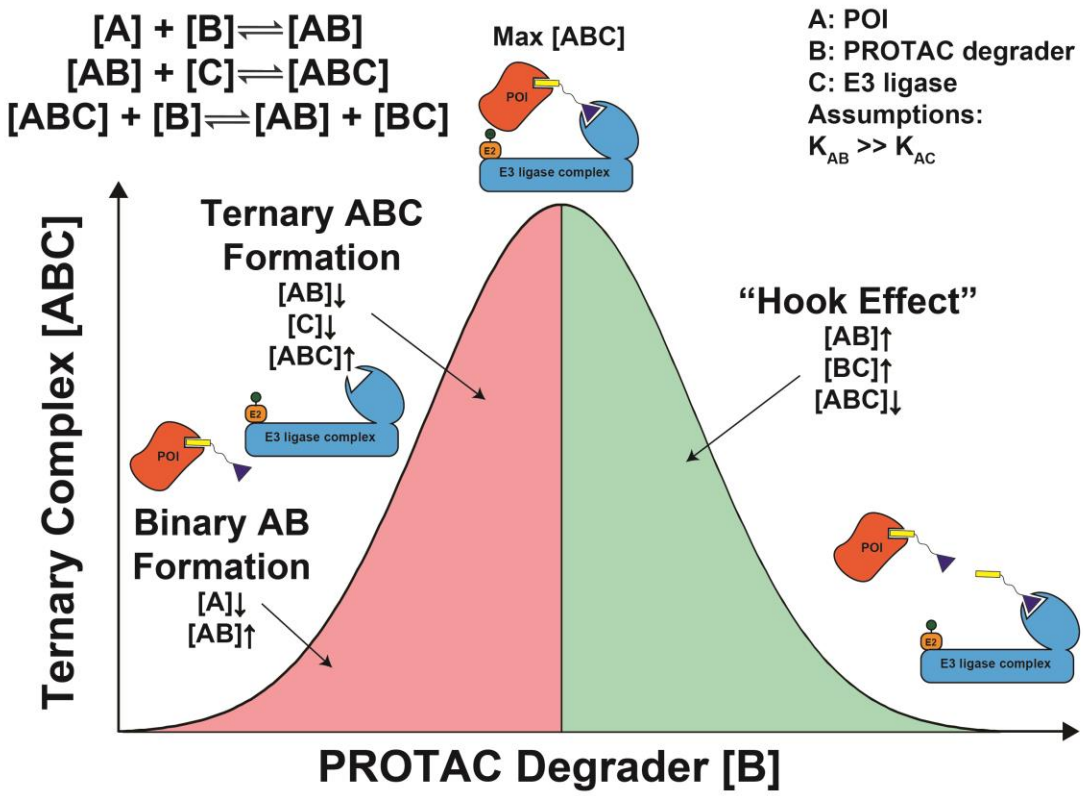

Figure 1.4.1.1. Illustration of Ternary Complex Formation

The degradation efficiency is highly dependent on the ternary complex formation[87]. To study the novel binding model of bifunctional molecules, multiple methods have been developed for the study of ternary complex formation. Co-immunoprecipitation (Co-IP) of E3 ligase and POI confirmed the their interactions induced by PROTACs[3,88]. The overdose of PROTAC would lead to favorable formation of binary complex and less degradation, which is generally described as "hook effects"[89]. Spiegel and co-workers established a mathematical model for analyzing this complex system[90]. The three-body equilibria were critical for PROTAC mechanism and is illustrated in **Figure 1.4.1.1**. Assuming the formation of AB was more favorable than BC ($K_{AB} > K_{BC}$), the [AB] and subsequent ternary complex [ABC] is increased as the PROTAC concertation [B] increases in a dose-dependent manner. When the majority of A is converted to AB or ABC complex, addition of extra B would lead to the formation of more binary complexes (BC and AB) , which consequentially diminished the degradation efficiency. The positive ($\alpha > 1$) or negative ($\alpha < 1$) cooperativity is defined by whether PROTAC favored or disfavored the formation of E3-PROTAC-POI ternary complex. Several critical values can be acquired from their model to evaluate the system, such like TF_{50} (Ternary Formation 50%) and TI_{50} (Ternary Inhibition 50%). Overall, they established a theoretical framework to conceptualize and analyze the ternary complex equilibria. Ciulli and co-workers adopted this model and implemented the data obtained from experiments for their mechanistic study of PROTAC. They used isothermal titration calorimetry (ITC) [9,34] or surface plasmon resonance (SPR)[91] or both to obtain the parameters in POI-ligand binding and E3-binary-complex binding.

Implementation of Spiegel's model allowed them to generate cooperativity α for proof of concept studies. Although the theoretical outcome did not perfectly match with what observed in experiment, their effort provided an example to learn how the cooperativity effect degradation efficiency.

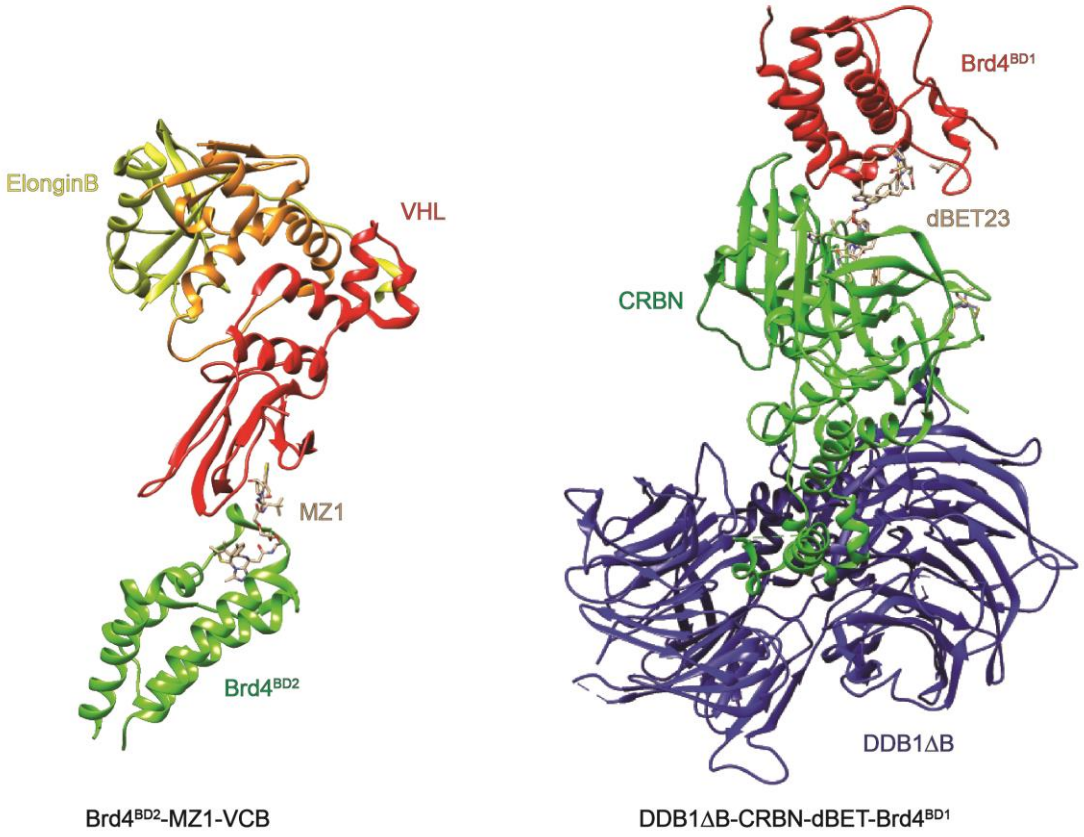

Figure 1.4.1.2. PROTAC crystal structure of $Brd4^{BD2}$-MZ1-VCB (PDB: 5T35) and DDB1ΔB-CRBN-dBET-$Brd4^{BD1}$ (PDB: 6BN7).

Structure elucidation is one of the straightforward methods to understand the drug-target action mode[92]. Up to now, crystal structures of complex recruited CRBN or VHL to Brd4 have been obtained (**Figure 1.4.1.2**). Ciulli and co-workers reported the first crystal

structure of ligases-PROTAC-target ternary complex, which facilitated the study of the structure reactivity and selectivity relationship (PDB: 5T35)[9]. The structure of $Brd4^{BD2}$-MZ1-VCB (VHL, EloinginC and ElonginB) clearly showed that the interaction between VHL and $Brd4^{BD2}$ generated a bowl-shaped hydrophobic interface where MZ1 is located to. MZ1 was one of the early VHL-based PROTAC tethering JQ1 and VH032. Beside expected binding modes of binary protein-ligand complex, the folding feature of PEG linker introduced additional interactions via van der Walls force and hydrogen bond. For example, they found that JQ1 interacted with the β4 region of VHL and VH032 contacted the ZA loop of $Brd4^{BD2}$. They then used reverse ITC together with surface mutagenesis and proximity to examine the isoform-specific PPI. With these insights, they moved forward to structure-based design of new PROTAC AT1 by replacing the *tert*-Leu group with penicillamine in VH032. This change increased the substrates discrimination and AT1 indeed showed better selectivity to Brd4 over other isoforms.

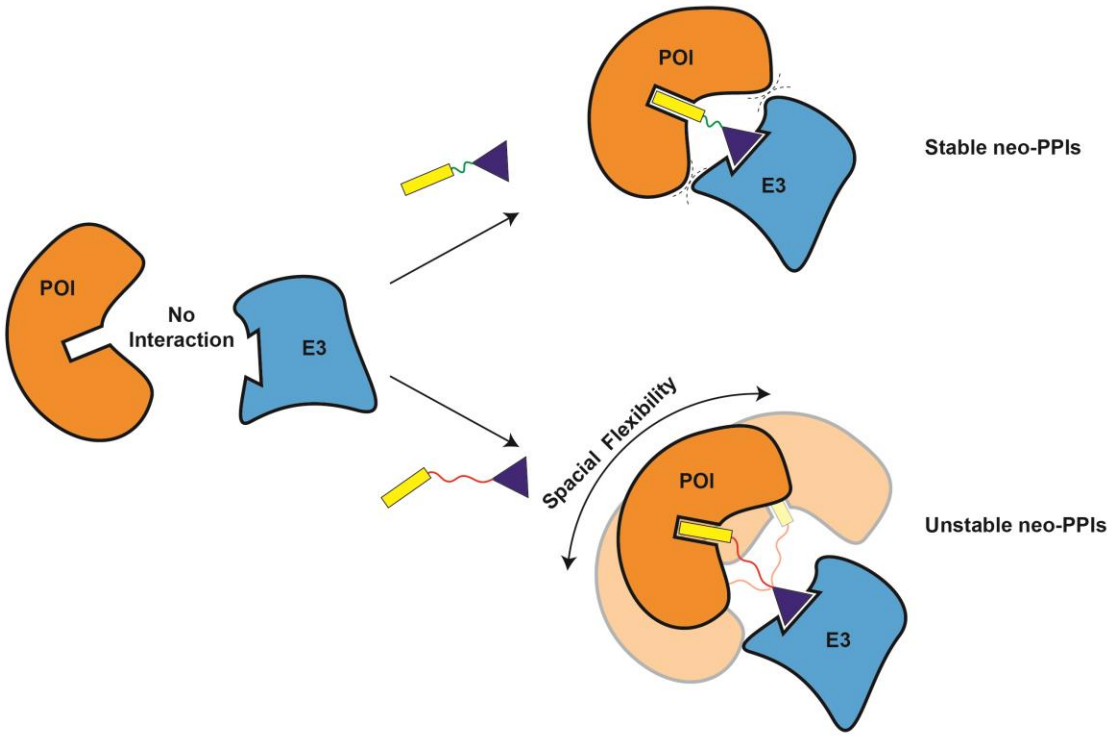

Figure1.4.1.3. PROTAC induced neo protein-protein interactions.

Fischer and his co-workers first solved the structure of CRBN-PROTAC-Brd4 complex formed by dBET series (PDB: 6BN7)[48]. The crystal structure of DDB1ΔB-CRBN-dBET-Brd4^{BD1} complex illustrated the hydrophobic interaction between the αC-helix of Brd4^{BD1} and two loops at the N-terminal domain (NTD) of CRBN. Together with other data, the plasticity of induced interaction between E3 ligase and targeted protein was revealed. The length and position of linkers were critical to PROTAC and led to distinct protein conformations and PPIs (**Figure 1.4.1.3**), which determined the selectivity of degraders. With the above information, ZXH-3-26 with relative shorter linker was rationally designed to be more "drug-like" by restricting the conformation to gain higher selectivity towards Brd4 over Brd2/3. These two case studies based on structures suggested 1) the

cooperativity are determined by the binding modes of each of the two binary complexes and the interaction between E3 ligase and "neo-substrate"; 2) degrader's efficiency and selectivity can be modulated by adjusting linker length and linking position to introduce more protein/protein "neo-interaction"; 3) structural analysis is extremely helpful for the rational design of PROTACs.

Along with structure elucidation, *in silico* modeling was also established. Drummond and Williams reported four different sampling methods to study the ternary complex formation mediated by PROTAC[93]. They utilized the existing crystal structure of POI-PROTAC-E3 complex discussed above. Each part was extracted as modeling component. Method 1 sampled all three components, POI, E3 and PROTAC, all at once. Method 2 sampled the PROTAC conformation first and then introduced the proteins to the sampled conformation. Method 3 sampled partial PROTAC (ligand with linker) in one protein first and then introduced another ligand-protein complex. Method 4 sampled each protein-ligand complex first and then docked the complex to the sampled PROTAC conformations in Method 2. A set of ternary complexes modeled by each method was collected. To minimize the complexity of the analysis, filters scoring those complexes were applied to remove ones far different from crystallographic observation. The resulting ternary complexes were then superposed to the crystalized structure and evaluated by Cα root-mean-dquare deviation (RMSD) for defining "crystal-like". "Hit rate", percentage of crystal-like poses in total, was then applied to evaluate which method is likely to succeed in generating ternary complexes similar to the experimentally obtained one. Method 4 was proved to be the most accurate one offering ~40% crystal-like geometries. Overall, their effort provided practical

computational method(s) for evaluating PROTAC-mediated ternary complexes, which may help *in silico* PROTAC design.

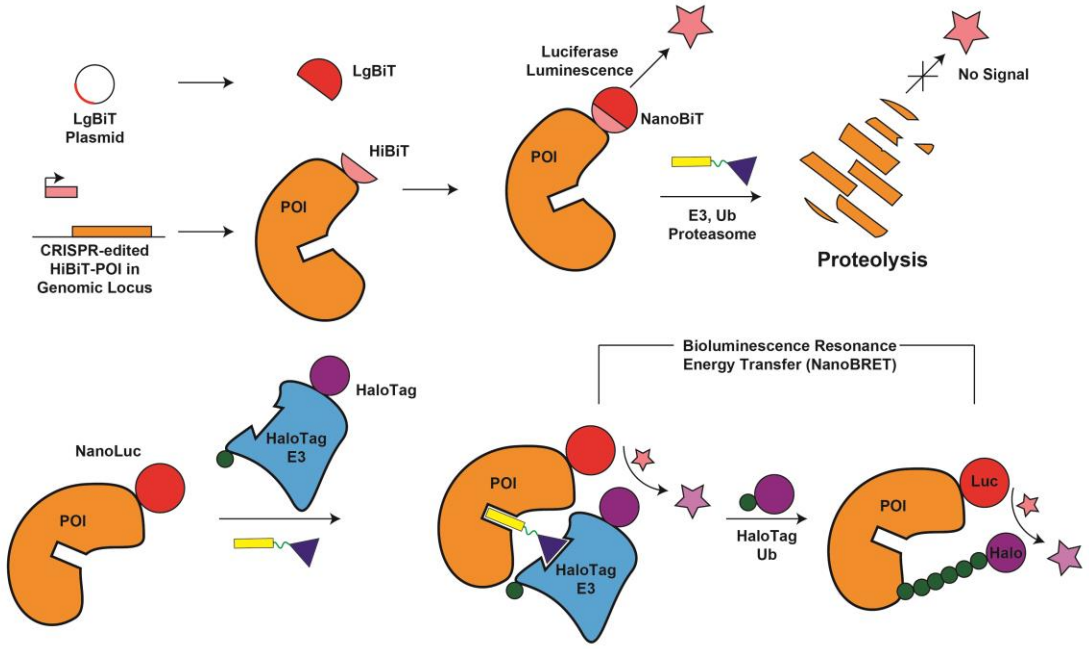

Figure1.4.1.4. NanoBiT and NanoBRET Technology for PROTAC Study

Several assays have also been developed to monitor the protein degradation and ternary complex formation. Promega Corporation developed quantitative real-time method to measure both ternary complex formation and target degradation[94]. The targeted protein was expressed in fusion with HiBiT, which was efficiently inserted by CRISPR/Cas9 technology. Fused POI-HiBiT bound to plasmid-expressed LgBiT to generate luminescence (NanoBiT luciferase) for monitoring the content of targeted protein in living cells. Real-time monitoring protein degradation allowed comprehensively and kinetically evaluate the degrader efficiency (degradation rate and time to reach D_{max}) and potency

(D_{max}[a], time at D_{max}[b], time of target recovery and DC_{50}[c]). By introducing HaloTag-E3 as acceptor, NanoLuc tagged protein donated energy to form bioluminescence resonance energy transfer (NanoBRET) signal for detecting the interaction between POI and E3. And their data also indicated that the signal of ternary complex was still very strong even after the protein degradation started, which supported that the ternary complex formation was a transient event in the catalytic cycle. Similar strategy was also established with HaloTag-Ubiquitin for real-time monitoring ubiquitination of targeted protein. In addition, Ciulli recently reported *in vitro* experimental model using surface plasmon resonance (SPR) to study the kinetic features of PROTAC-bridged ternary complexes formation[91]. A collection of these methods will advance the systematic analysis of PROTAC-mediated PPI, ubiquitination and degradation for understanding MOA.

1.4.2. Employing PROTAC as Powerful Chemical Tools for Biology Research

Figure 1.4.2.1. Chemical Tools Control Gene/Protein Expression in Biology

Knocking down or out gene(s) expression in biological pathways is an important method to study the cellular network. CRISPR-Cas9 and siRNA/shRNA technology has been used

[a] D_{max}: maximal degradation by degrader
[b] "Time at D_{max}": the duration of maximal degradation lasted after reaching a plateau.
[c] DC_{50}: concentration where half of maximal degradation is achieved

as the major methods in controlling protein expression in genome and transcriptome level[1,2] (**Figure 1.4.2.1**). However, several drawbacks are obvious: 1) unexpected downregulation of non-targeted genes known as off-targets; 2) transfection, colony selection and validation are time- and labor-consuming; 3) the genetic perturbation requires complicated multiple components; 4) irreversible knockdown or silencing increases difficulty in flexibly manipulating phenotypes. PTOTAC can be used as alternative tool of CRSPR or siRNA/shRNA to deplete functional proteins. Utilization of PROTAC as chemical tools allowed researchers to study important cellular pathways and validate potential targets for therapeutic development.

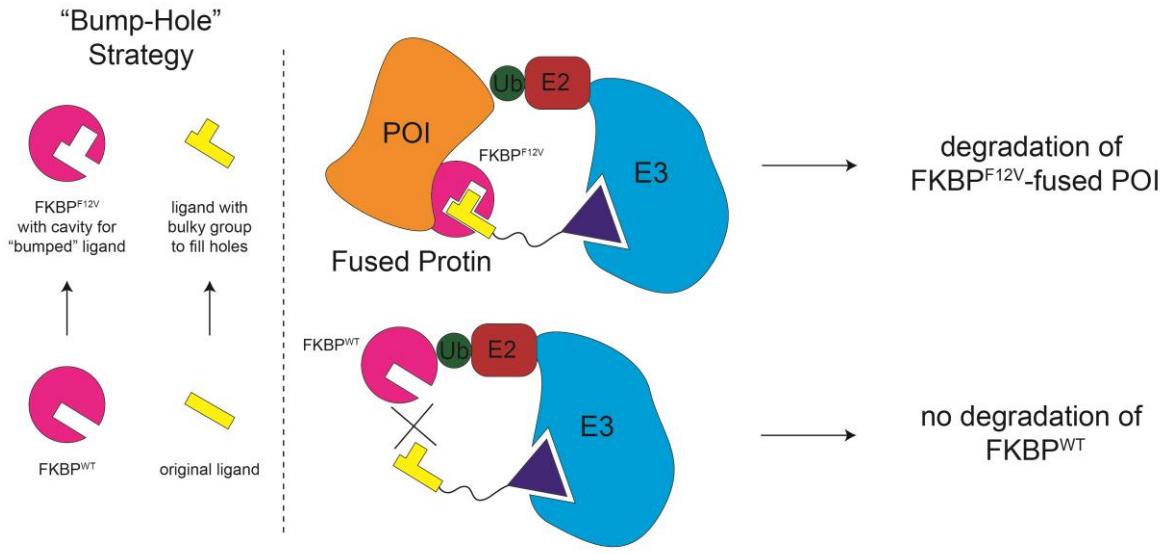

Figure 1.4.2.2. PROTAC dTAG system for fused target protein.

PROTAC-based specific target degradation system has been established to expand the scope of this technology to proteins not ligandable. HaloPROTACs was first introduced by Crews and co-workers to degraded fused green fluorescent protein (GFP) in 2015[66]. They

tethered chloroalkane to VHL ligand to form HaloPROTACs, which successfully degraded HaloTag7-fused GFP in cell-based assays. Later HaloPROTACs were constructed to degrade SGK3 and VPS34 for target validation. The introduction of HaloPROTAC highlighted PROTACs as chemical probes for controlling fused protein content. In 2018, Bradner and co-workers created dTAG platform based on a "bump-hole" approach for biological investigation and target validation in drug discovery[44]. They applied ligand AP1867, which selectively targets $FKBP12^{F36V}$ mutant, in conjugation with CRBN ligand. The dTAG molecules (dTAG-7 and dTAG-13) showed selective deletion of plasmid-expressed $FKBP12^{F36V}$ while only had limited effects on endogenously expressed $FKBP12^{WT}$. While the Brd4 is not the target of $FKBP12^{F36V}$ ligand, Brd4 in fusion with $FKBP12^{F36V}$ was degraded by dTAGs. This proved the principle and feasibility of dTAG system. The dTAG-induced degradation was then applied to more targets, including HDAC1, MYC, EXH2, PLK1 and $KRAS^{G12V}$. Through profiling the effects of depletion of those fusion proteins quickly and reversibly, they were able to study various biological events due to the loss of functional proteins. For instance, degrading pan-BET bromodomain had enhanced antiproliferation over selective degradation of Brd4 alone. They also showed that the loss of KRAS mutant G12V induced rapid downstream proteomic and transcriptional effects, which indicates that $KRAS^{G12V}$ degraders are promising novel therapeutics. They also used *in vivo* model to evaluate the potential application in living organisms. Overall, they created a platform of using fused proteins and PROTAC to modulate protein level and validate function of protein targets.

Cellular knockdown by degrader yielded different downstream effects comparing with inhibition. As discussed in previous sections, Fak degrader not only decreased the phosphorylation level of its substrate but also suppressed the cell motility, which was contributed to the kinase-independent function[70]. This result suggested that the degraders could be used to modulate important signaling pathways while the corresponding inhibitors were not able to do so. Moreover, the development of selective cyclin-dependent kinase 6 (CDK6) degraders[95] allowed the profiling of the relevant signaling pathways and genetic network, which revealed that AML cells were genetically dependent on CDK6 pathway. But CDK4/6 inhibitor failed to discriminate that dependency. In addition, Bantscheff and co-workers performed mass-spectrometry-based multiplexed proteome dynamic profiling (mPDP) to compare JQ1 with JQ1-teathered PROTACs[96]. Degradation of FYTTD1 was identified as one of the off-targets, which led to nuclei-accumulation of RNA and affected the protein synthesis. Meanwhile, the transmembrane protein SOAT1, an off-target of JQ1, was not depleted by JQ1-PROTAC. Cellular location of target was suggested as the source of selectivity for degraders. In brief, these studies exploited PROTACs as chemical tools to tune protein homeostasis and signaling pathways, which contributed to the understanding of novel cellular biology and underscored versatility of PROTAC degraders.

1.5. Conclusion

Many cell permeable small molecule PROTACs with potent cellular and even in-vivo activity have been published since 2015. These PROTACs can induce rapid and robust

protein degradation in cells and in animals. By controlling the lifetime of protein, the PROTAC technology has remarkable therapeutic potential and is also a valuable tool for basic biology research. This review chapter briefly summarized the history of PROTAC and focused more on parameters in PROTAC design and methods to study the mechanism of action. It is my hope that further understanding of the mechanistic details of how PROTAC work will facilitate the process of exploiting the full therapeutic potential of this novel technology. I hope we can systematically and rationally design small molecule PROTACs to target any intracellular proteins in the future.

2. Development of Potent HDAC6 Degraders by Recruiting CRBN E3 Ligase

2.1. Introduction

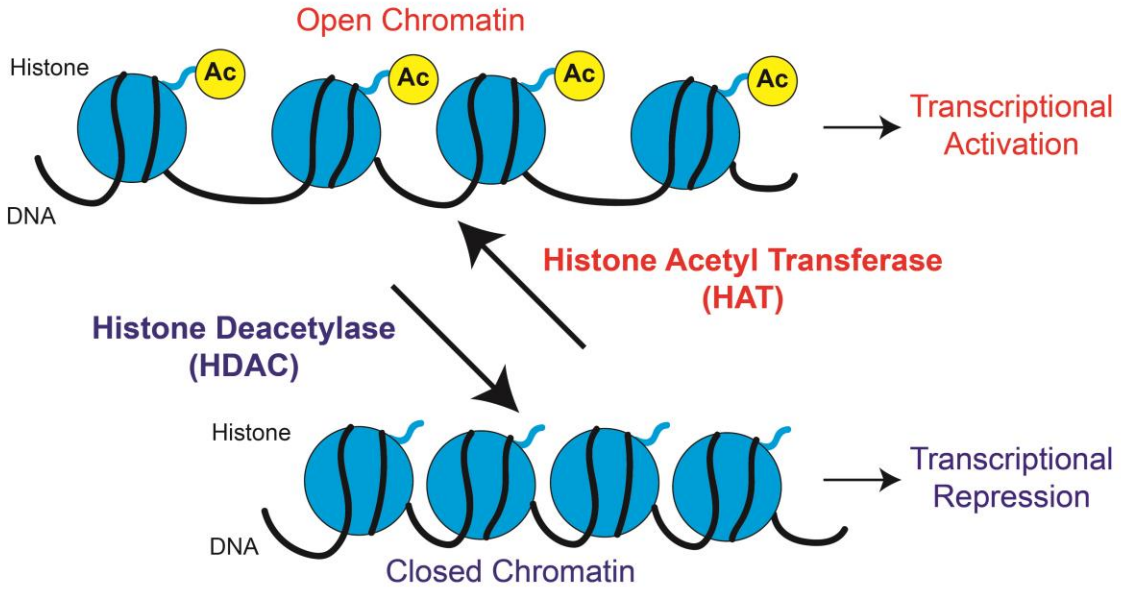

Figure 2.1.1. Most histone deacetylases control the chromatin structure and gene transcription

Post translational modification of proteins is essential in all cellular pathways[97]. Among them, lysine acetylation is regulated by histone acetyltransferases (HATs) and histone deacetylases (HDACs). Most members of HDACs serve as epigenetic "eraser" to remove the acetyl group of lysine residue of histone tails and promote chromatin condensation in nucleus and gene suppression[98,99]. There are 11 zinc-dependent HDACs and 7 nicotinamide adenine dinucleotide (NAD^+) dependent deacetylase sirtuins (SIRTs) in HDAC

superfamily. HDACs can act on both histones and non-histone proteins, such as DNA binding proteins, transcriptional regulators, chaperone proteins, and structural proteins[100]. Abnormal changes in HDACs expression have been implicated in many types of cancers.[101]

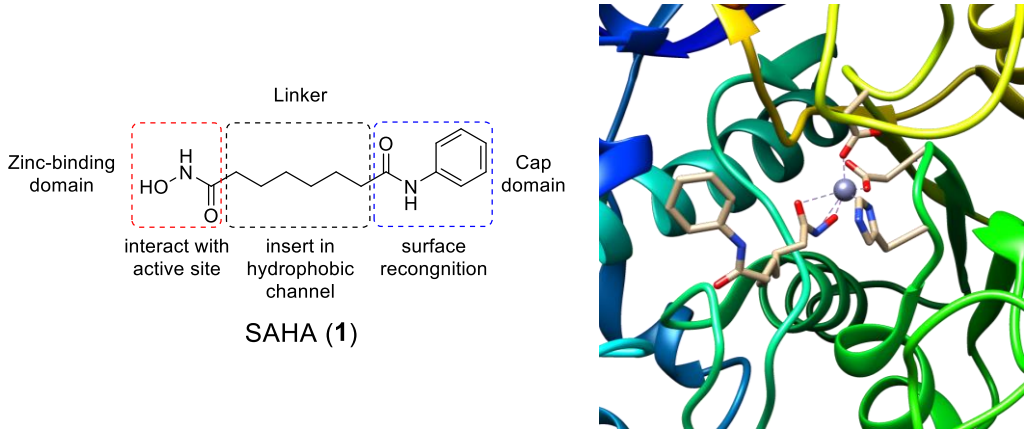

Figure 2.1.2. Structural characteristics of pan-HDAC inhibitor SAHA and the structure illustration of the binding mode (PDB: 1C3S)

HDAC inhibitors (HDACis) can inhibit HDAC activity and re-activate the transcription of important genes including tumor suppressors[98]. SAHA (Vorinostat, **1**, **Figure 2.1.2**) is one of the FDA-approved HDAC inhibitors for the treatment of advanced primary cutaneous T-cell lymphoma. SAHA has potent inhibitory potency against HDAC1, HDAC2, HDAC3 and HDAC6.[102,103] Taking SAHA as an example, classical HDAC inhibitors are generally composed of three components: zinc-binding domain, linker and surface recognition domain (or cap domain)[104]. Its binding mode was illustrated in **Figure 2.1.2** (PDB: 1C3S)[105]. The hydroxamic acid interact with the active site through hydrogen bond to residues and chelation with the zinc cofactor. The linker occupies the channel from surface to active site of binding pocket. The cap domain is general hydrophobic for recognition of

surface residues and determines the selectivity of inhibitor. Beside using hydroxamic acid as metal binding moiety, other metal binding groups in HDACi include thiols, benzamides and aliphatic acids[106]. HDAC inhibitors have shown antitumor activity in many pre-clinical and clinical models. In addition to SAHA, several other HDAC inhibitors such as Romidepsin (FK288) and Belinostat (PXD101) have been approved for the treatment of cancers.[98,99,106] All of the approved HDAC inhibitors, however, non-selectively target various HDACs and exhibit significant toxicity.[102] Development of selective HDAC inhibitors is one of the current focuses to reduce the toxicity and achieve wider therapeutic indexes for a variety of cancers.[107] Various bifunctional HDAC inhibitors have also been developed for more targeted therapy by conjugating HDAC inhibitors with other functional molecules, such as estrogen receptor ligands,[108] androgen receptor ligands,[109] topoisomerase inhibitors,[110] and others.[111–117]

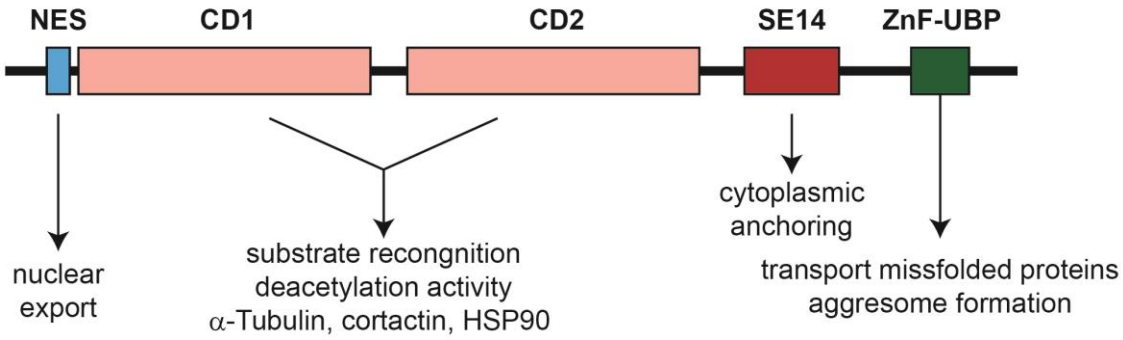

Figure 2.1.3. Functional domains of HDAC6

Among HDAC family, HDAC6 is a unique member of class IIb HDACs and has several domains (**Figure 2.1.3**). The nuclear export signal (NES) is responsible for translocation of HDAC6 from nuclei to cytoplasm[118,119], which makes HDAC6 distinct from other

HDACs that are primarily localized in nuclei. HDAC6 has two tandem catalytic domains, CD1 and CD2, which are highly homologoues[118]. HDAC6 has a number of non-histone substrates such as α-tubulin[120], cortactin[121] and HSP90[119]. HDAC6 is responsible for regulating diverse cellular functions such like cell motility[121,122], immunoregulation[123,124], and aggresome formation[125,126]. Abnormal expression of HDAC6 has been observed in cancers such as oral squamous cell carcinoma, acute myeloid leukemia, ovarian cancer, and hepatocellular carcinomas[127–130].

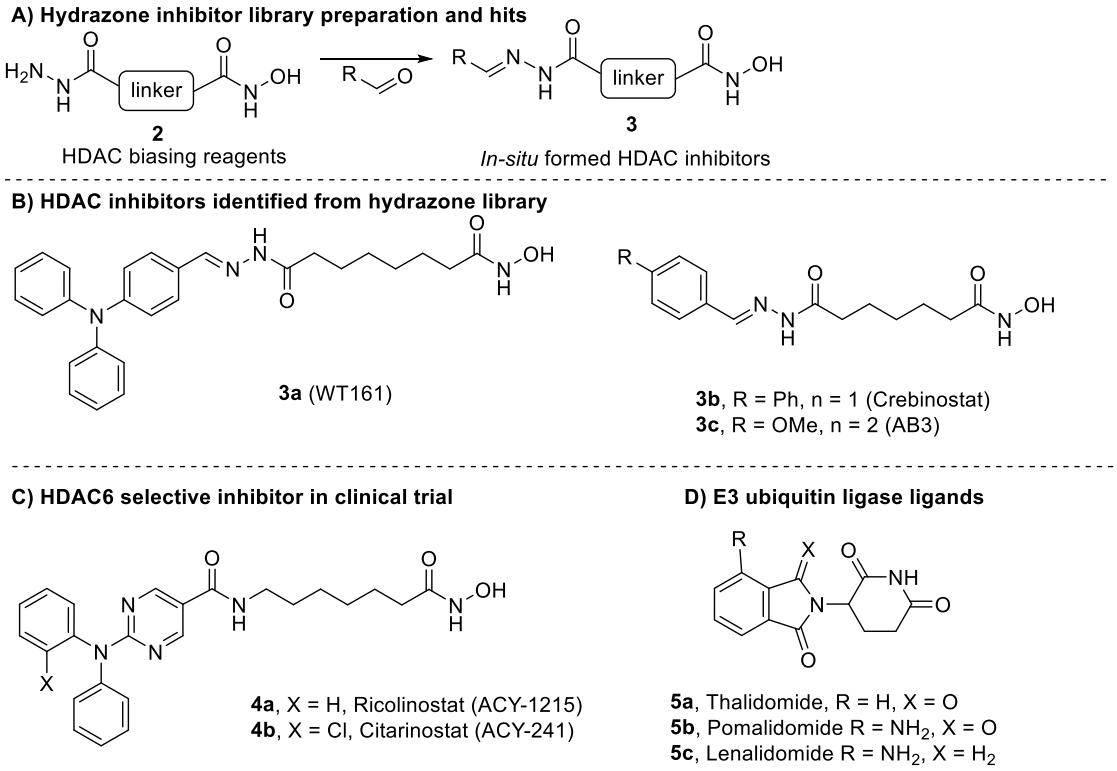

Figure 2.1.4 Strategy for the generation of diverse HDAC inhibitors and E3 ligase ligands

HDAC6 selective inhibitors have been developed and emerged as promising therapeutic agents for cancer treatment[127,131]. We previously developed a strategy that can provide

quick access to a library of diverse HDAC inhibitors, as shown in **Figure 2.1.3**[132]. A series of HDAC biasing reagents **2** was prepared and coupled with a diverse range of aldehydes to generate a large collection of acylhydrazone-linked HDAC inhibitors **3**. The resulting products have sufficient purity and can be directly tested in relevant biological assays. This strategy has yielded a number of useful chemical probes. For example, compound **3a** (WT161), one member of the library, is a highly selective HDAC6 inhibitor and is very effective for the treatment of bortezomib-resistant multiple myeloma (MM) in cells and mouse models, when it is combined with bortezomib[133]. Structurally related analogues such as **4a** and **4b** are currently in human clinical trials for the treatment of various cancers[134–136]. Within these trials **4a** and **4b** are combined with other therapeutics, such as thalidomide and its analogues (e.g. **5a**-**5c**), which are ligands of the CRL^{CRBN} E3 ubiquitin ligase[10,38–40,137]. Other members of the library have also shown promising results. Compound **3b** increased the density of synapsin-1 puncta along dendrites in cultured neurons and enhanced memory in mouse models,[138] and compound **3c** suppressed aggressive thyroid cancer in cells and in animal models.[139,140]

The degradation of Sirt2 by PROTACs was the first published example of degraders for epigenetic "erasers"[45]. There are several potential advantages for enzyme degraders over enzyme inhibitors.[8] First, inhibition of certain cellular pathways often increases the expression of the target protein, which is mediated by a feedback mechanism, and this often leads to pharmacological insufficiency. The degradation activity can then negate the effects of protein overexpression. Second, the phenotype, or very often the cause, of the diseases is the overexpression of the target protein. The more appropriate correction of the disease

state is to tune down the level of this protein until it reaches its physiological level instead of inhibiting the enzymatic functions. Finally, inhibitors require stoichiometric drug binding to the target in order to modulate the protein function. In contrast, TPD by small molecule degraders is catalytic, providing favorable pharmacology.

We developed the first small molecule HDAC degraders by conjugating non-selective HDAC inhibitors with E3 ubiquitin ligase ligands[71]. Through screening the expression of HDACs, we find the non-selective HDAC inhibitor was converted to HDAC6 selective degrader after tethering it with E3 ligand Pomalidomide. Mechanistic study illustrated the critical role of CRBN E3 ligases and the ubiquitination-proteasome system in HDAC6-targeting degradation. Later, we developed the second generation of HDAC6 degraders by using selective HDAC6 inhibitor as the "warhead". The novel degraders exhibited improved potency and selectivity. After further optimizing the linker length and linking positions, we have discovered potent degraders with nanomolar DC_{50} that exhibit promising anti-proliferation activity in multiple myeloma (MM) cells. HDAC6 degraders have the potential to be developed into anti-cancer agents.

2.2. First-generation Degraders Using Pan-HDAC6 Inhibitor as "Warhead"

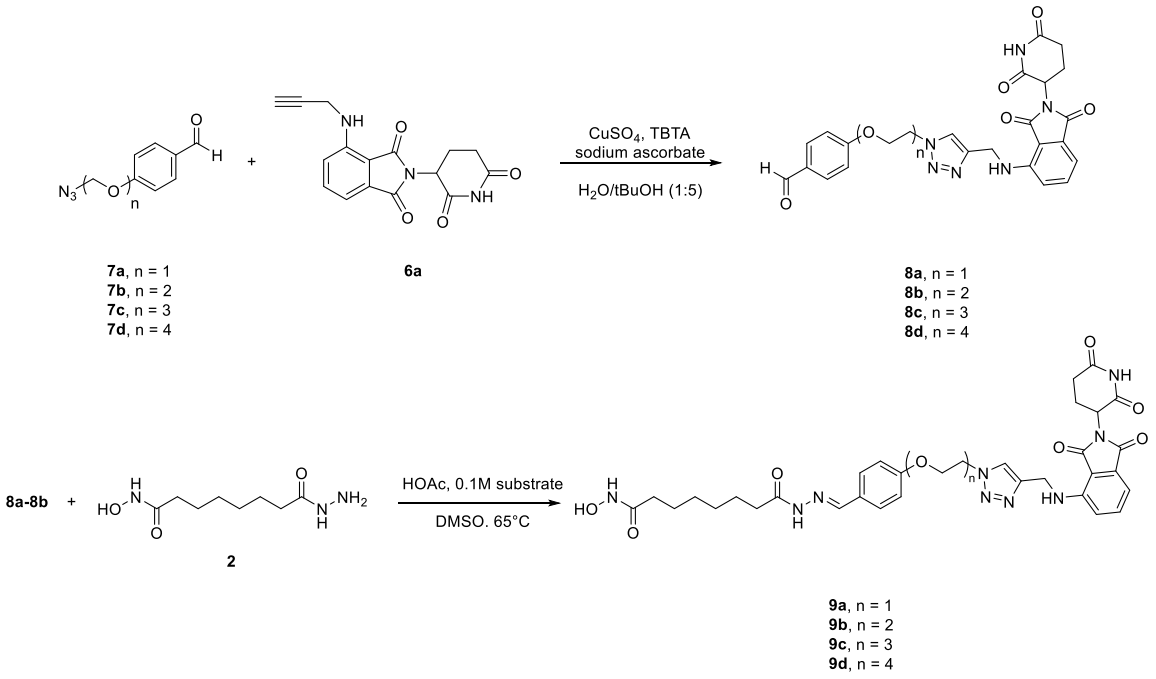

Scheme 2.2.1 Synthetic route to PROTAC degraders targeting HDAC.

We envisioned that our HDACi library preparation strategy could also facilitate the development of various small molecule HDAC degraders. For the first series of acylhydrazone-linked HDAC degraders, we conjugated non-selective HDAC inhibitor **3c**, derived from our previous strategy, to a thalidomide-type E3 ligase ligand with various linkers. The synthesis of our HDAC degraders is summarized in **Scheme 2.2.1**. Aldehydes **7a-7d** containing an azide functional group and one to several polyethylene glycol units were prepared according to literature methods.[141,142] An alkyne functional group was introduced to pomalidomide to afford analogue **6a** by a S_NAr reaction between known fluoro-thalidomide and propargyl amine according to literature procedures.[43] A copper-catalyzed cycloaddition between alkyne **6a** and azides **7a-7d** afforded the corresponding

pomalidomide-conjugated azides **8a**-**8d** with varying linker lengths. Condensation of **8a**-**8d** with HDAC-biasing reagent **2a**[132] in DMSO yielded products **9a**-**9d** as the bifunctional molecules. The resulting DMSO solutions were analyzed by LC-MS and determined to be of sufficient purity for further biological evaluations.

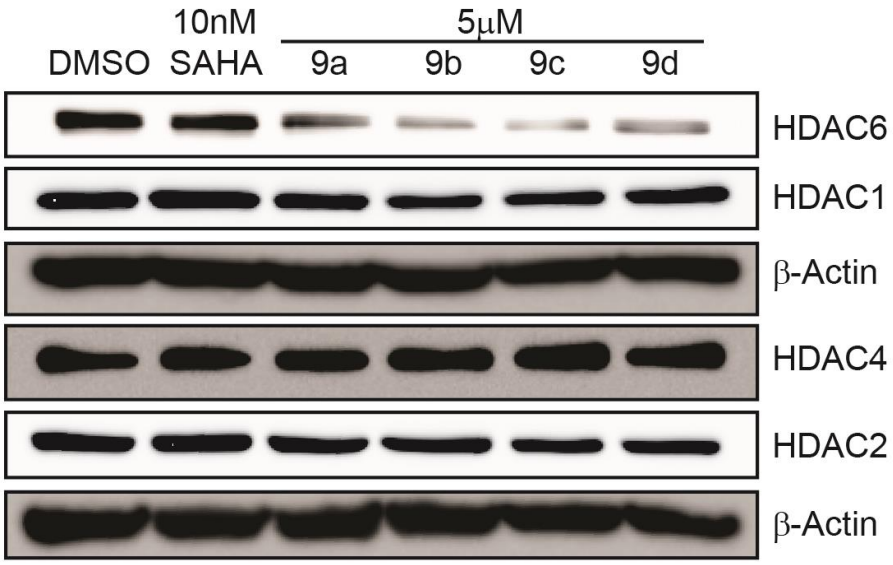

Figure 2.2.1 Profiling HDAC expression under treatment of degraders

We first incubated bifunctional molecules **9a**-**9d** at 5 μM in MCF-7 cells. After 12 h, the whole cell lysate was generated for SDS-PAGE and immunoblot. By examining the amount of HDAC1, HDAC2, HDAC4 and HDAC6 protein, we observed a considerably lower level of HDAC6 compared to others (**Figure 2.2.1**). HDAC1 protein was slightly suppressed by these probes. Meanwhile, the amount of HDAC proteins remained the same using the SAHA treatment. We were encouraged by the fact that these bifunctional molecules, with relatively high molecular weights, were able to cross the cell membrane to degrade certain HDAC members. Among the four bifunctional molecules with various

linker lengths, compound **9c** showed higher activity for the degradation of HDAC6 than the other three compounds at a 5 μM concentration. This data indicated that the linker length has significant impact on the efficiency of TPD, which is consistent with previous reports for the PROTAC-mediated degradation of other proteins.[43,9] The selective degradation of HDAC6 over other HDACs is unexpected, but not surprising, because it has been reported that highly selective kinase degraders can be developed by tethering a relatively non-selective kinase inhibitors with a E3 ubiquitin ligase ligand.[33]

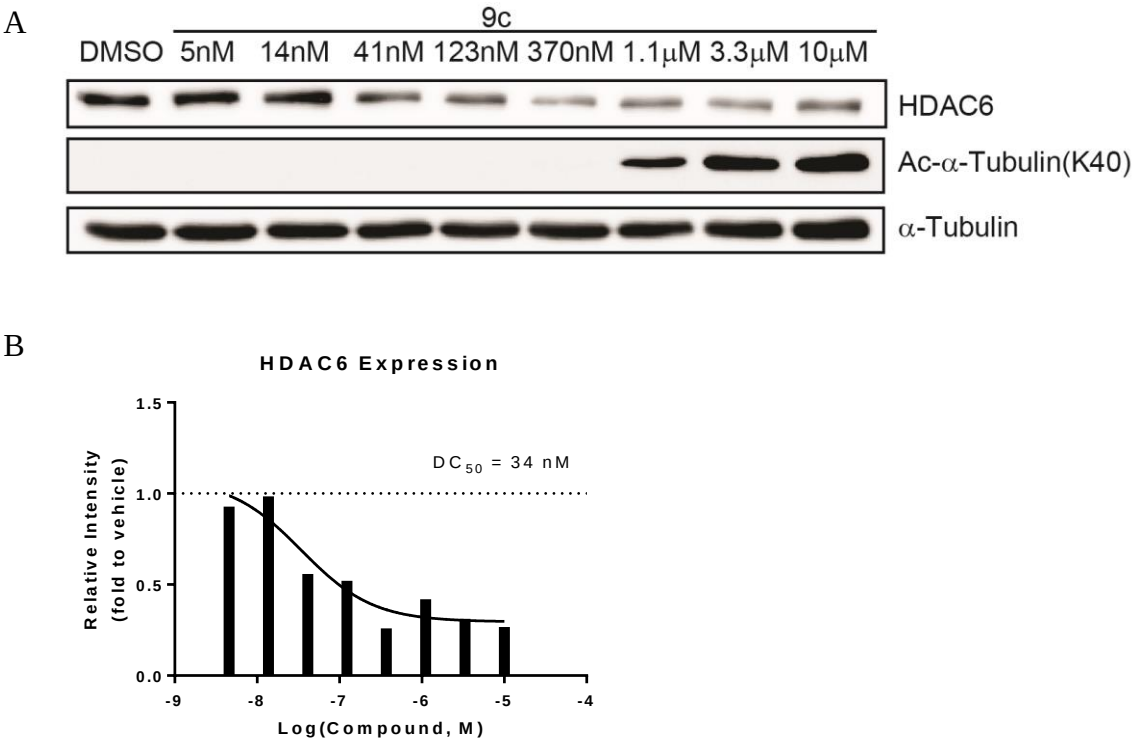

Figure 2.2.2 Dose response of HDAC6 degrader **9c** in MCF-7

To probe the effective concentration range, incubation of cells with 5 nM to 10 μM of **9c** resulted in the degradation of HDAC6 in a dose dependent manner. (**Figure 2.2.2 A**) The degradation occurred at concentrations as low as 41 nM and reached the maximal effect

between 123 nM and 370 nM. No obvious "Hook effect" was observed at higher concentration.[90] The concentration at which half-maximal degradation was achieved (DC_{50}) and the maximum percentage of degradation (D_{max}) are 34 nM and 70.5% respectively, based on the blot intensity (**Figure 2.2.2 B**). It has been established that HDAC6 regulates the acetylation of α-tubulin[120]. Knockdown of HDAC6 by siRNA or inhibition by small molecule HDAC6 inhibitors can upregulate the level of acetylated α-tubulin.[122,133] Indeed, increased acetylated α-tubulin levels were observed at 1.1 μM and above (**Figure 2.2.2 A**). The increased acetylated α-tubulin level should be the result of inhibition and degradation of HDAC6.

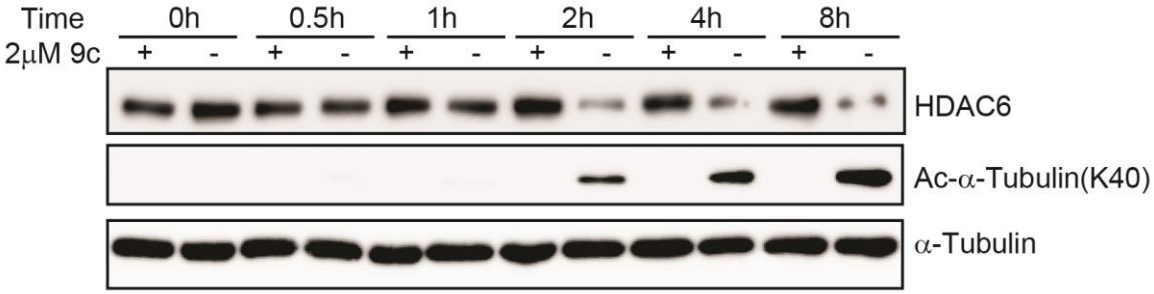

Figure 2.2.3 Time-course study of HDAC6 degrader **9c** in MCF-7

To further study the mechanism of action of our HDAC6 selective degraders, we conducted a series of experiments. A time-course experiment revealed that significant degradation of HDAC6 and upregulation of tubulin acetylation occurred around 2 h after treating MCF-7 cells with 2 μM of compound **9c** (**Figure 2.2.3**), which suggested the high efficiency of TPD of HDAC6 protein.

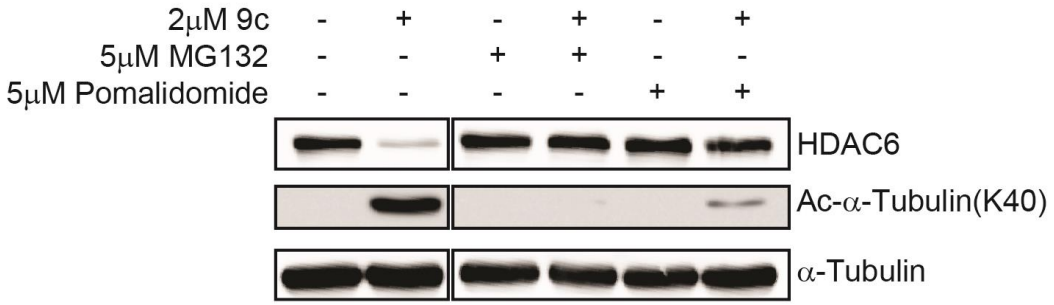

Figure 2.2.4 Co-treatment of MG132 or Pomalidomide with degrader **9c** in MCF-7

Co-treatment of 2 μM of compound **9c** with either 5 μM MG132, a known proteasome inhibitor, or 5 μM pomalidomide, the CRBN ligand, abolished the effect of compound **9c** for the degradation of HDAC6 (**Figure 2.2.4**). The tubulin acetylation level was also almost recued in these cases. These results indicated the essential role of the ubiquitin-proteasome pathway for the TPD of compound **9c**. First of all, proteasome activity was required for compound **9c** mediated HDAC6 turnover since the inhibition of the proteasome by MG132 abolished the effect of compound **9c**. Second, the recruitment of the CRBN E3 ligase was also critical for compound **9c** mediated degradation of HDAC6 because the competitive binding of pomalidomide to CRBN and abolished the effect of compound **9c**. In addition, the significantly different levels of acetylated tubulin by the treatment with **9c** alone and by **9c**-pomalidomide co-treatment suggested that HDAC6 degradation by **9c** was primarily responsible for raising the level of acetylated α-tubulin, at least in the case of the 12 h treatment. Furthermore, the residual level of acetylated tubulin after the **9c**-pomalidomide co-treatment indicated that compound **9c** continually served as a HDAC6 inhibitor after its degradation ability is disabled by pomalidomide.

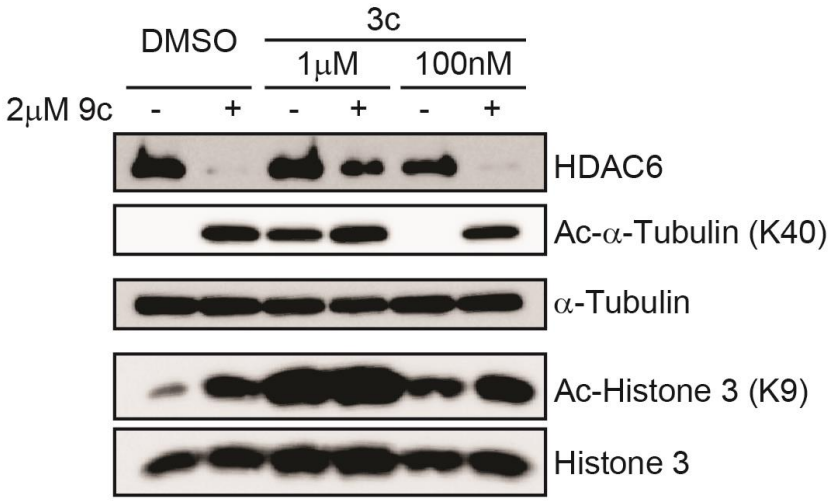

Figure 2.2.5 Co-treatment of pan-HDAC inhibitor **2c** with degrader **9c** in MCF-7

A similar effect was also observed when pan-HDAC inhibitor **2c**, the "warhead" of HDAC6 degrader **9c**, was used as the competitive ligand for HDACs (**Figure 2.2.5**). In the presence of 2 μM of compound **9c**, the addition of 1 μM of **2c** is sufficient to rescue HDAC6 from TPD. Lowering the concentration of **2c** to 100 nM, however, is not sufficient to abolish compound **9c**-mediated degradation of HDAC6. On the other hand, a large degree of tubulin acetylation by compound **9c** was still observed. In addition to the level of acetylated tubulin, we also examined the level of acetylated histone 3 (H3) to evaluate the selectivity of compound **9c**. Compound **9c** at a 2 μM concentration clearly exhibited less of an effect than compound **2c** alone at the same concentration for the increase of acetylated H3. The effect of compound **9c** alone for the increased of acetylated H3 is likely due to direct inhibition of class I HDAC(s) in the nucleus instead of insignificant degradation of HDAC1. Our results indicate that bifunctional molecule **9c** has dual functions: selective degradation of HDAC6 and inhibition of HDACs.

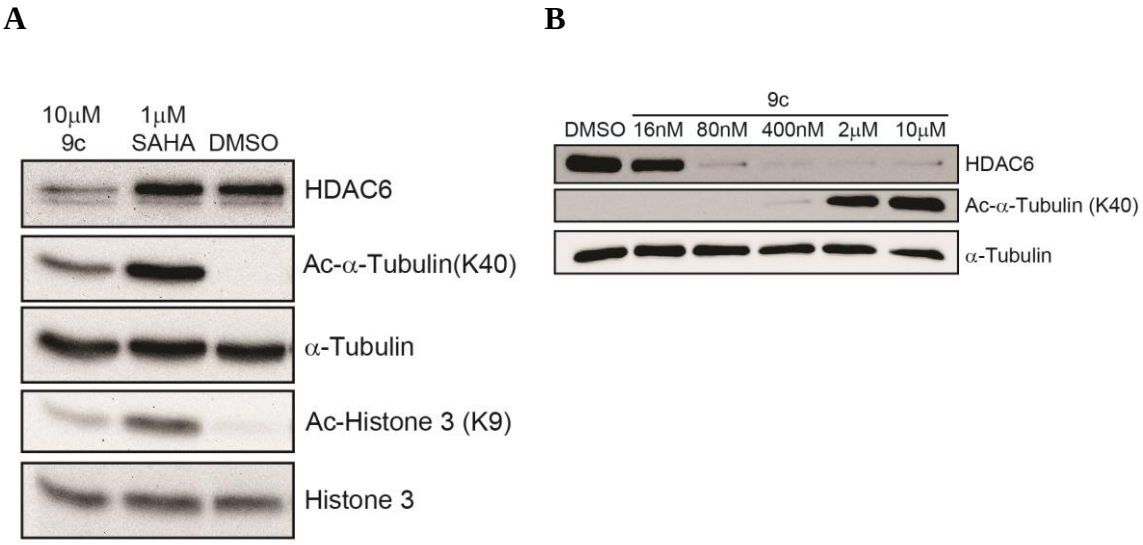

Figure 2.2.6 Bioactivity test of HDAC inhibitor or degrader in HeLa (A) and MM.1S (B) cells

To examine the scope, we also tested SAHA or degrader **9c** in HeLa and MM.1S cells. The HeLa cells treated with SAHA for 12 h didn't affect the HDAC6 level while degrader **9c** induced obvious degradation (**Figure 2.2.6 A**). SAHA increased significant acetylation level of Tubulin and Histone 3 in comparison of **9c**. It suggested the degrader with non-selective "warhead" cause less potent downstream effects in this type of cells. We also tested compound **9c** in the MM.1S cell line, a type of multiple myeloma (MM). After a 6 h treatment, the maximal effect of HDAC6 degradation was observed at 80 nM or higher concentrations (**Figure 2.2.6**). The increase in acetylated tubulin was observed at higher concentrations of compound **9c** in MM.1S cells, which is similar to what was observed in MCF-7 cells. The MM.1S cell line appeared to be more sensitive to compound **9c** for the degradation of HDAC6.

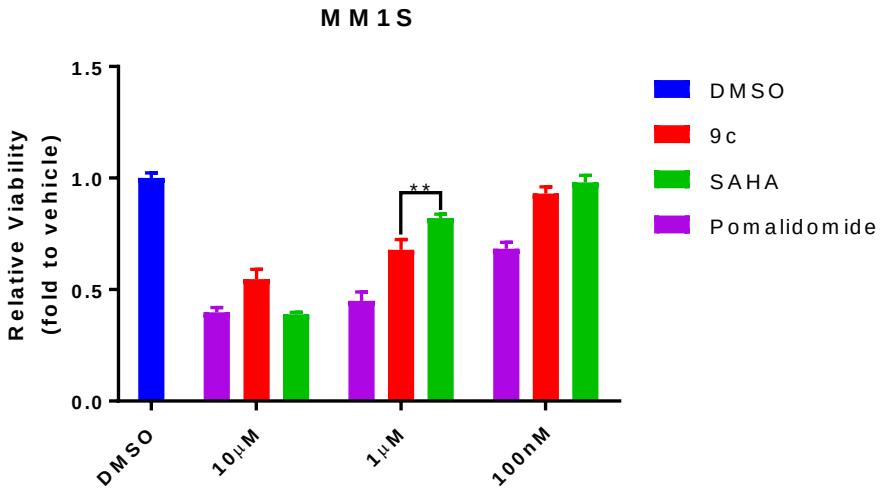

Figure 2.2.7 Antiproliferation of **9c** in MM1S

Pomalidomide inhibits the growth of MM cells via CRBN and showed synergy with HDAC inhibitors for treating myeloma[38,143]. Since our HDAC6 degrade bearing Pomalidomide, we hypothesize there may be some synergy between HDAC6 degradation and Pomalidomide-induced anti-proliferation. To examine the functionality of HDAC6 degrader in MM cells, we treated MM.1S cells with degrader 9c, SAHA and Pomalidomide for 48 h (**Figure 2.2.7**). SAHA and **9c** at 100 nM didn't affect the proliferation of MM cells while Pomalidomide suppressed ~30% cell growth. At 1 μM, Pomalidomide and **9c** achieved over 50% and ~30% inhibition, respectively. In comparison, SAHA only showed less than 20% growth inhibition. These results indicated the advantage of using Pomalidomide-based HDAC6 degrader over pan-HDAC inhibitor. However, **9c** turned out to be weaker than SAHA at 10 μM, where both SAHA and Pomalidomide inhibited over 40% cell proliferation.

2.3. Second-generation Degrader Using HDAC6 Selective Inhibitor as "Warhead" with Anti-myeloma Activity

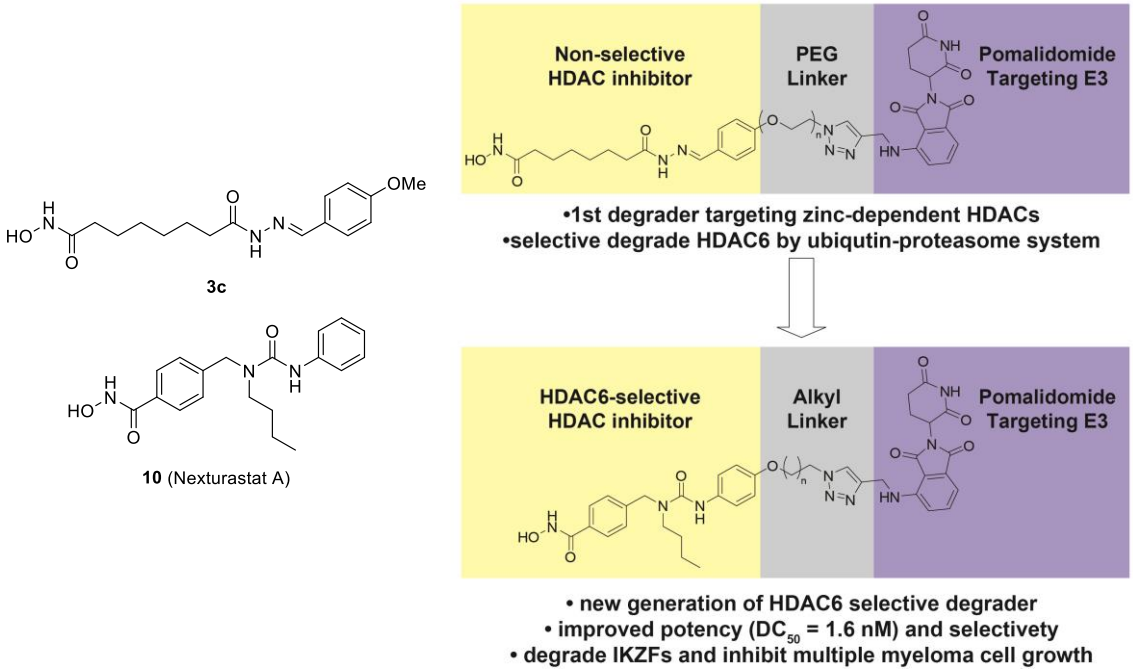

Figure 2.3.1 Structure of HDAC6 degraders and "warhead" inhibitors

First-generation degrader **9c** used non-selective inhibitor **3c** as the "warhead". It selectively degraded HDAC6 and accounted for limited growth inhibition of multiple myelomas. However, other members of HDACs are still inhibited by the pan-inhibitor "warhead" as demonstrated by the elevated level of acetylated histones (**Figure 2.2.6** and **Figure 2.2.7 A**). Clearly, the selectivity and potency of HDAC6 degraders need to be improved by using a completely different scaffold for further biological and pharmacological studies. We therefore designed a new generation of selective HDAC6 degraders by attaching E3 ligase ligand to the aniline group of HDAC6 selective inhibitor Nexturastat A[144] (Next-A, **10**, **Figure 2.3.1**). During our investigation of the new generation HDAC6 selective degraders,

Rao's group reported a class of PROTACs in 2019 by attaching a E3 ligase ligand to the alkyl chain of Next-A.[5] However, their PROTACs did now show any improved anti-proliferation activity over the parent HDAC6 inhibitor Next-A.

Despite the revolution in myeloma therapy in the last two decades, many patients are resistant to currently approved agents[145]. HDAC6 selective inhibitors have been used in combination with proteasome inhibitor[134,146], immunomodulatory drugs (e.g. **5a-c**)[143] and anti-PD-L1 antibody[147] in anti-myeloma therapeutic development. HDAC6 selective inhibitors showed synergy with IMiDs for the treatment of multiple myeloma in animal models and human clinical trials. Upon binding to CRBN, pomalidomide analogues are known to activate CRBN's E3 ligase activity towards IKZFs and promote their ubiquitination and subsequent degradation[40,137,148]. IKZFs become the neo-substrates of ligand-bound CRBN. The induced degradation of IKZFs by pomalidomide and its analogues are believed to be responsible for their significant anti-proliferation effect in multiple myeloma. Interestingly, PROTACs with IKZF degradation activity have also been reported in a number of cases when pomalidomide was employed as the ligand for CRBN E3 ligase[44,46–48]. The degradation of IKZFs is often considered as undesired during the development of PROTACs. We hypothesize that multifunctional HDAC6 degraders that retain the degradation activity of IKZFs would have enhanced anti-myeloma activity. We then developed a new generation of HDAC6 selective degraders with distinct advantages in degradation efficiency and selectivity over our previous compounds. Our new HDAC6 degraders are also significantly more potent than HDAC6 inhibitor Next-A for the anti-proliferation of multiple myeloma cancer cell lines.

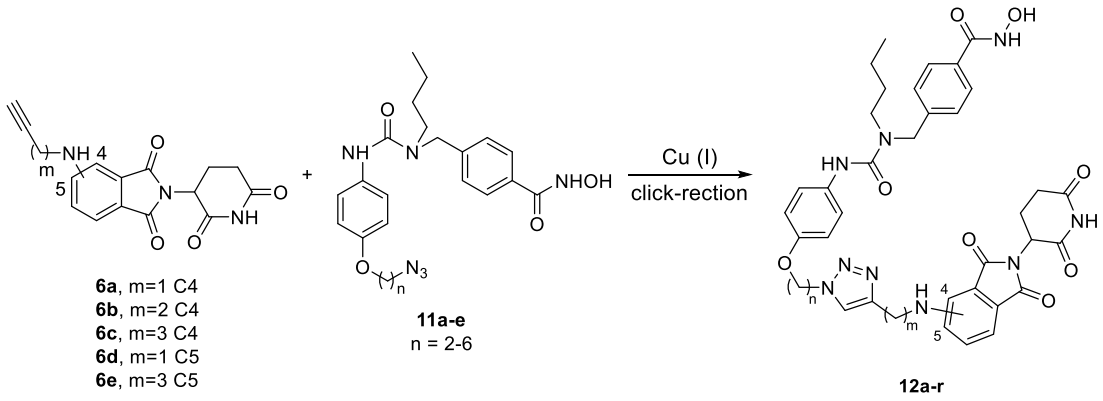

Scheme 2.3.1 "Click" synthesis of PROTAC degraders

To increase the selectivity and potency of HDAC6 degrader, we synthesized 18 degraders by tethering HDAC6-selective inhibitor Next-A (**10**) with CRBN E3 ligand Pomalidomide. Azides (**11a**-**e**) bearing Next-A moiety were "clicked" with pomalidomide linked alkynes to afford PROTAC **12a**-**r** with varying linkers (**Scheme 2.3.1**). These degraders are divided into to two series based on their linking position of the amino group on the phthalimide ring of Pomalidomide: C4- or C5-linked series (**Table 2.3.1**). Within each series, the degraders are different from each other by the numbers of carbon atoms between Next-A and the triazole ring (n) or between Pomalidomide and the triazole ring (m). It is known that both C-4 and C-5 positions of Pomalidomide are exposed to solvent and can be the position to place the linker for PROTACs [148,149]. The para position of the aniline in Next-A was chosen to place the linker because it is well known that the aromatic ring "cap" of HDAC inhibitors is exposed to the solvent [105,150].

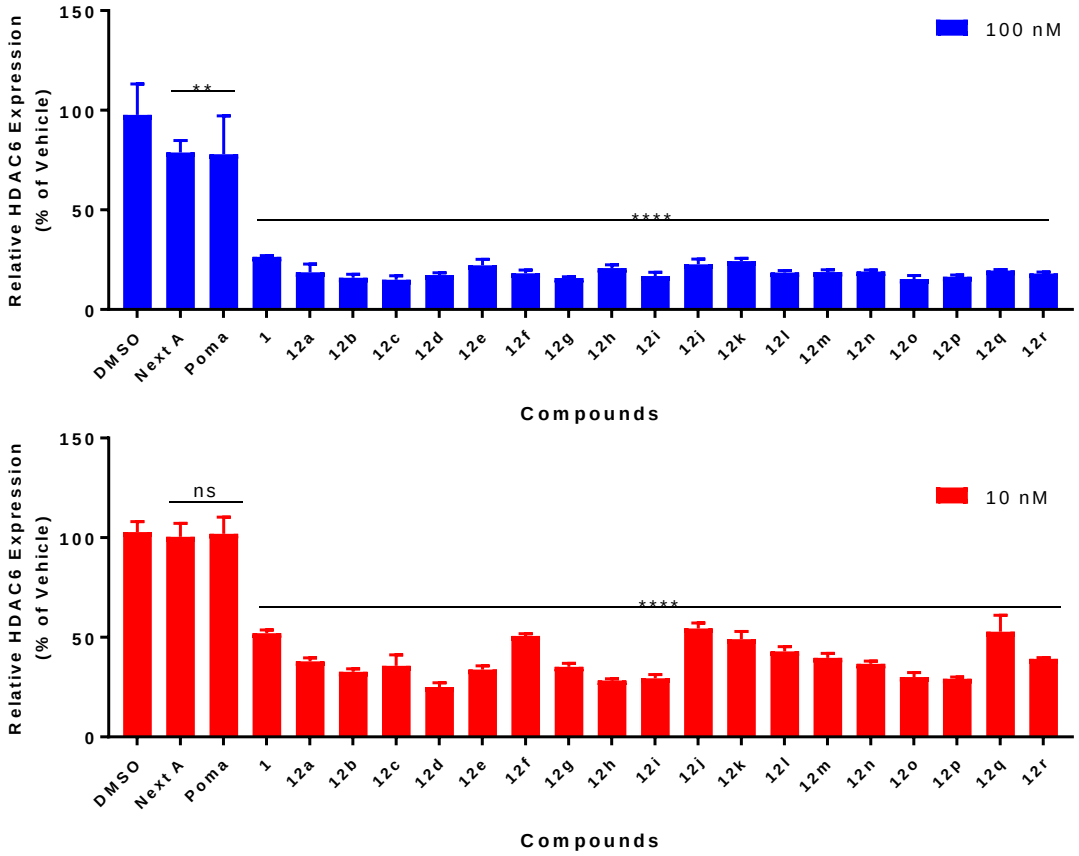

Figure 2.3.2 Screening of Compounds for HDAC6 degradation by in-cell ELISA

To screen the new series of degraders, we first developed and validated an in-cell ELISA assay (see **Chapter 3** for details). We treated the compounds at 100 nM and 10 nM in MM1S cells for 6 h. Resulting cells were then fixed and analyzed by in-cell ELISA (**Figure 2.3.2**). Comparing with vehicle, Next-A and Pomalidomide didn't affect the expression of HDAC6 at 10 nM and had very minimal effects at 100 nM. At both concentrations, all degraders remarkably decreased the amount of HDAC6 protein. The degradation level was calculated and listed in **Table 2.3.1**.

Table 2.3.1. Screening of compounds for HDAC6 degradation activity

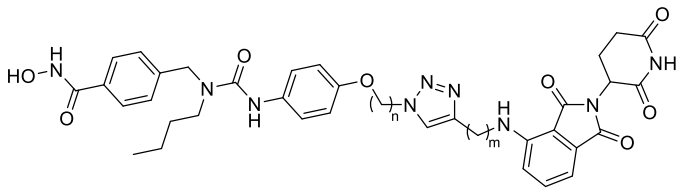

C4-linked-series

Cpd	n	m	Degradation (%)[a]	
			100 nM	10 nM
9c	N/A		73.5 ± 0.3	47.9 ± 0.9
12a	2	1	81.3 ± 2.3	62.1 ± 1.0
12b	3	1	84.1 1.0	67.3 ± 0.8
12c	4	1	85.0 ± 1.2	64.3 ± 3.2
12d	5	1	82.7 ± 1.7	74.9 ± 1.2
12e	6	1	77.8 ± 1.7	66.1 ± 1.1
12f	2	2	81.8 ± 0.9	49.3 ± 0.6
12g	3	2	84.2 ± 0.4	64.8 ± 1.0
12h	4	2	79.2 ± 0.9	71.7 ± 0.5
12i	2	3	83.1 ± 1.0	70.6 ± 1.1
12j	3	3	77.3 ± 1.5	45.6 ± 1.6
12k	4	3	75.7 ± 0.8	50.9 ± 2.2

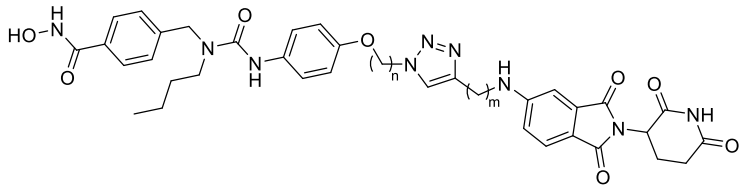

C5-linked-series

Cpd	n	m	Degradation (%)[a]	
			100 nM	10 nM
12l	2	1	81.4 ± 0.6	57.1 ± 1.4
12m	3	1	81.2 ± 0.6	60.3 ± 1.3
12n	4	1	80.9 ± 0.4	63.3 ± 0.8
12o	5	1	84.7 ± 1.0	69.9 ± 1.3
12p	6	1	83.5 ± 0.5	70.8 ± 0.4
12q	2	3	80.4 ± 0.3	47.2 ± 4.8
12r	3	3	81.9 ± 0.4	60.9 ± 0.4

[a]Degradation percentage calculated from **Figure 2.3.2**. Degradation percentage represents [100% - mean (± SD) of HDAC6 relative expression of biological replicates (n = 3)].

At 100 nM concentrations, compounds including **9c** degraded 73.5% to 85.0% of HDAC6 with minor difference. At 10 nM concentration of compounds, obvious structure-activity-relationship was observed. While only 47.9% of HDAC6 expression was suppressed by our previously reported degrader **9c**, several new degraders are much more potent. For example, **12d**, **12h**, **12i**, **12o** and **12p** all achieved about 70% degradation. Among the C4-linked series, **12d** with medium length linker (5 + 1) achieved most degradation in sub-series **12a-e** (m = 1). For sub-series **12f-h** (m = 2), the degradation potency increased when linkers were elongated and **12h** (4 + 2) was the best. Within sub-series **12i-k** (m = 3), **12i** with the shortest linker (2 + 3) turned out to be the most potent degrader. Among C5-linked series, the potency of sub-series **12l-p** (m = 1) increased with the linker length. Compounds **12o** (5 + 1) and **12p** (6 + 1) have the similar potency for the degradation of HDAC6. Sub-series **12q-r** (m = 3) showed relative low effects for the degradation of HDAC6. The above results suggest that the optimal total number of methylene units in the linker is about 6 and the C4-linked series are slightly more potent than the C5-series, which might relate to the accessibility of the degrader-recruited E3 ligase to the available ubiquitination site(s) of HDAC6. It appeared that both the distance and linking positions contributed to the degradation efficiency.

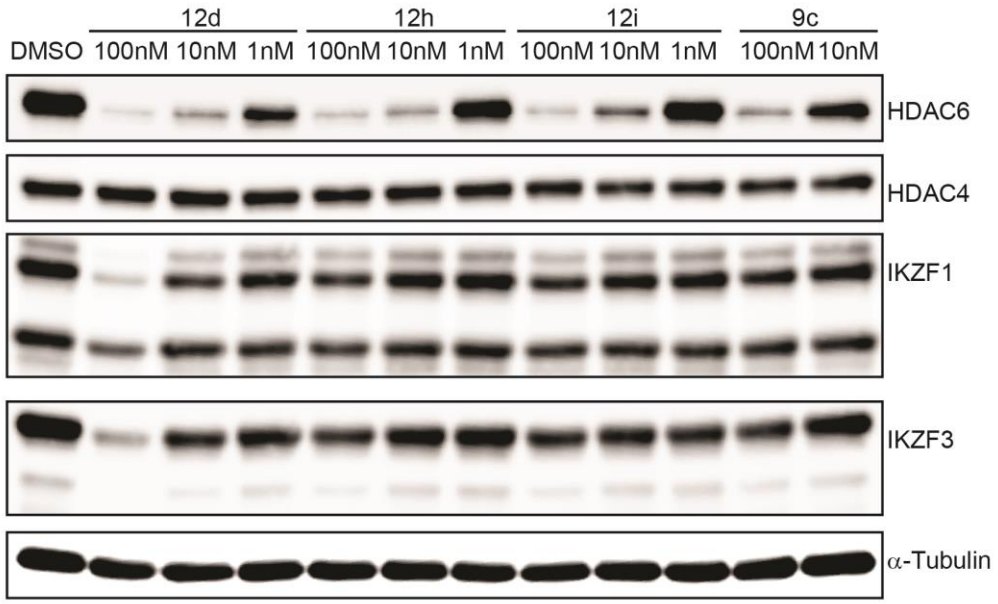

Figure 2.3.3. MM1S cells treated with selected candidates from C4-lined series

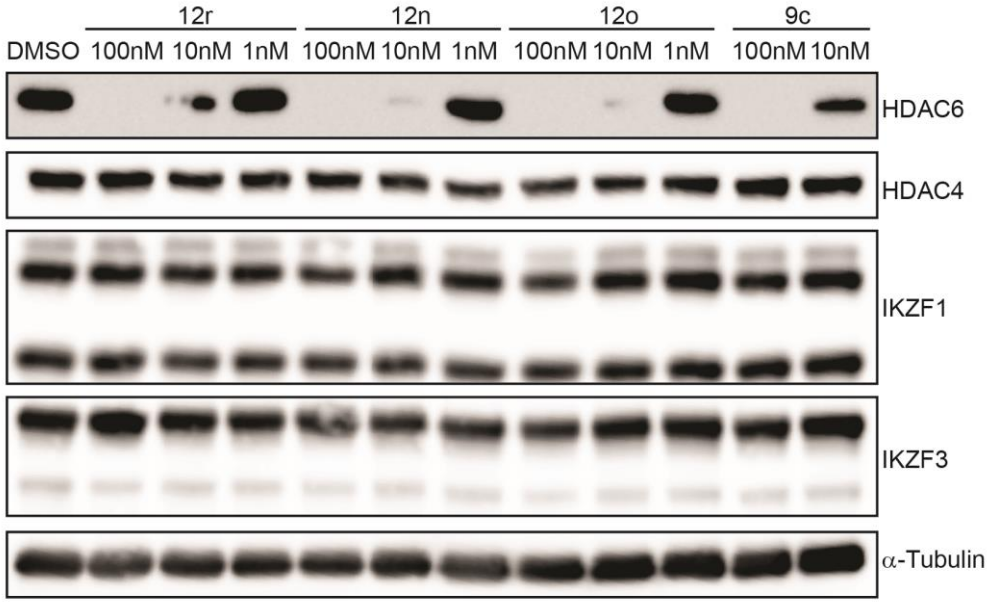

Figure 2.3.4. MM1S cells treated with selected candidates from C5-lined series

After the identification of the most potent candidates from each sub-series, we incubated selected compounds at 100 nM, 10 nM and 1 nM for western blot analysis (**Figure 2.3.4**) to confirm the ELISA results. Class II HDAC4 was selected for comparison. For selected compounds from C4- or C5-linked series, all of them presented maximal effects at 100 nM and degraded significant amount of HDAC6 at 10 nM. Clearly, our previous HDAC6 degrader **9c** degraded much less HDAC6 at 10 nM concentration. The results from Western blot are consistent with the screening results by ELISA.

As discussed before, pomalidomide and its analogues are known to modulate CRBN's E3 ligase activity and lead to the degradation of neosubstrates IKZFs. Interestingly, among the candidates we examined, only **12d** retained the induced degradation of IKZF1/3 by pomalidomide moiety at 100 nM. IKZFs regulate the expression of interferon regulatory factor 4 (IRF4) and c-Myc to affect the proliferation of multiple myeloma (MM)[137]. The downregulation of IKZF 1 and 3 by pomalidomide and its analogues are believed to be responsible for their significant anti-proliferation effect in multiple myeloma. PROTACs with IKZF degradation activity have been reported in a number of cases[44,46–48] and the IKZFs are often considered as "off-targets" during the development of these PROTACs. Our results indicate that the IKZF degradation activity can be impacted by the linker position and the functional group next to the phthalimide ring. In our studies, the triazole ring linked to C4 position likely contributed to the induced interaction between CRBN and IKZFs.

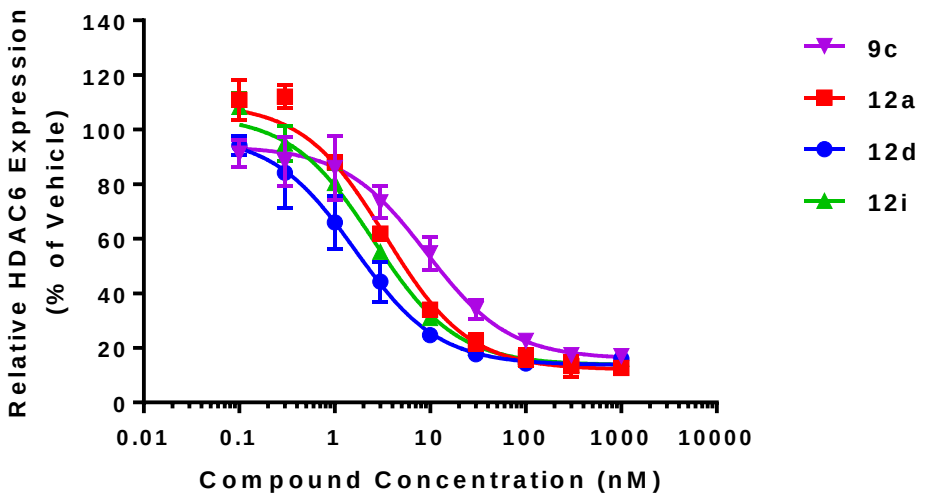

Figure 2.3.5. In-cell ELISA of MM1S cells treated with degraders for 6 hours

Table 2.3.2 DC_{50} and D_{max} of Selected Degraders

Cpd	DC_{50}[a] (nM)	D_{max}[b] (Vehicle%)
1	9.12 ± 1.64	84.07 ± 2.41
12a	3.41 ± 0.52	88.01 ± 2.23
12d	1.64 ± 0.24	86.26 ± 1.70
12i	2.54 ± 0.32	86.30 ± 1.67

[a]The concentration at which half-maximal degradation was achieved. [b]The maximum percentage of degradation. [a,b]Values with ± SD obtained from nonlinear fitted data in **Figure 2.3.5**.

To examine the potency of the selected candidates, we used in-cell ELISA to analyze the HDAC6 content in MM1S cells treated with **12a**, **12d** and **12i** and compared them with

degrader **9c**. We measured the amount of cellular HDAC6 in response to concentrations of compounds from 0.1 nM to 1 μM (**Figure 2.3.5.**). DC_{50} and D_{max} were calculated and listed in **Table 2.3.2**. All degraders achieved 84-88% maximal degradation and no "hook effects" [90] was observed at ≤ 1 μM. Our new degraders had single-digit nanomolar DC_{50}, which was about 3- to 5-fold of improvement from 9.12 nM of degrader **9c**. Among these degraders, **12d** showed excellent potency with a DC_{50} at 1.64 nM. As discussed above, most PROTACs were designed to avoid degrading other proteins except the targeted POIs. However, in our study, we hypothesized that HDAC6 degraders with IKZF degradation will have enhanced anti-proliferation effect for MM1S cells. Since compound **12d** showed promising IKZF degradation activity (**Figure 2.3.3**), we further characterized its activity and mechanism of action.

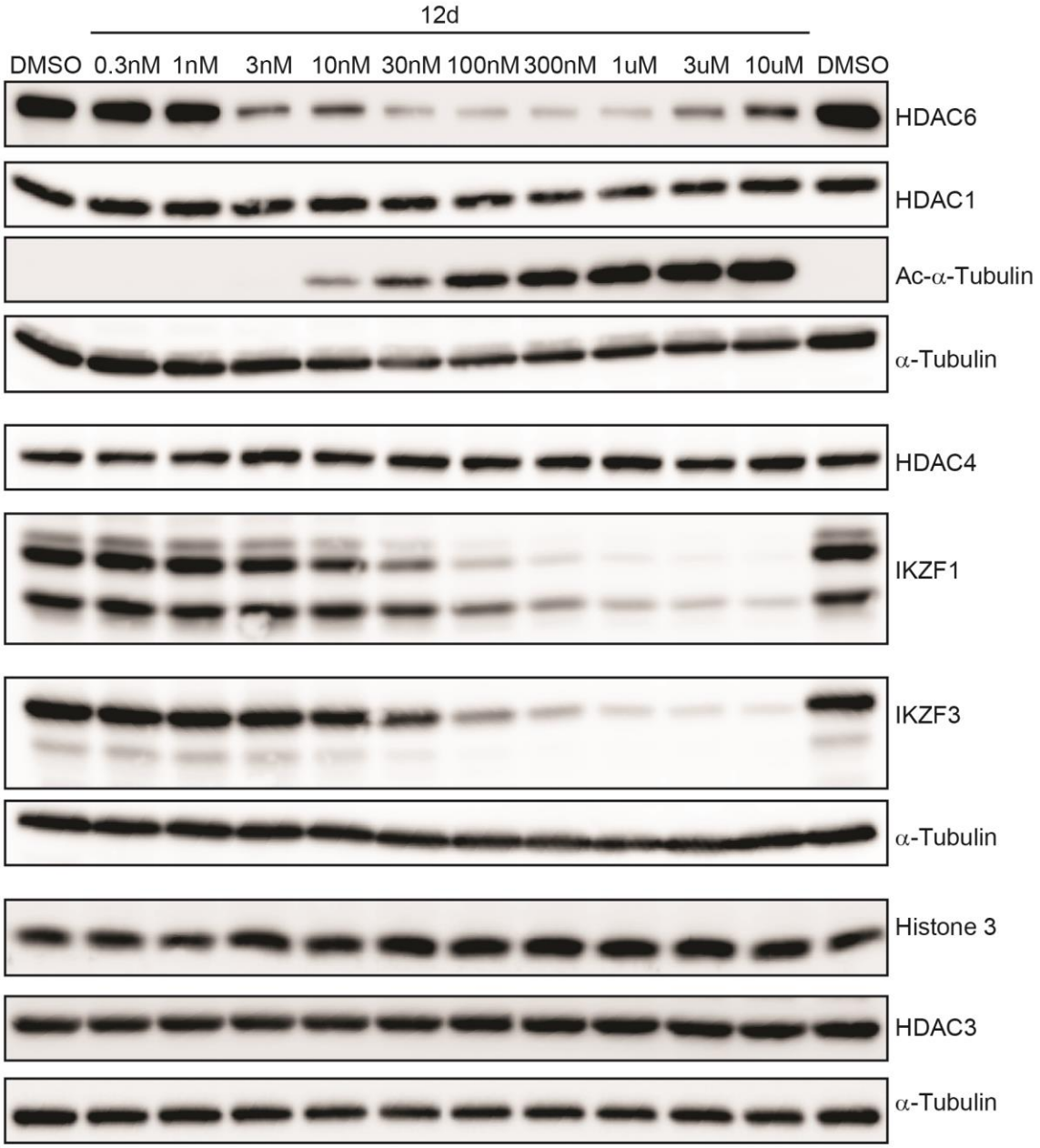

Figure 2.3.6. Profiling of different protein expression in dose response of **12d** in MM1S

To evaluate the activity and selectivity of 1**2d**, we first performed a full dose response experiment with compound concentrations ranging from 0.3 nM to 10 μM in MM1S cells (**Figure 2.3.6**) for several HDACs, IKZFs, and Ac-tubulin. The results indicated that only

the expression of HDAC6 was affected among the HDACs we examined. Degrader **12d** reduced HDAC6 protein content at as low as 3 nM and achieved maximal effects around 30 nM. The "Hook effect" was observed at 3 μM or above due to the formation of binary complexes[90]. The degradation of IKZFs started from 30 nM and was dose-dependent. It is interesting to see the more efficient degradation of HDAC6, which requires the binding of both ligands to their protein targets, than that of IKZFs, which only requires the binding of pomalidomide motif to CRBN. In addition to the distinct mechanism, the different turnover rates of HDAC6 and IKZFs may also contribute to the observed results. The acetylated tubulin level was also dose-dependent. At higher concentrations (3 μM and 10 μM), tubulin acetylation was not decreased in response to recovered HDAC6 expression by "hook effect". The elevated tubulin acetylation at higher concentrations was likely due to the more significant HDAC6 inhibition since the degrader has the inhibitory motif.

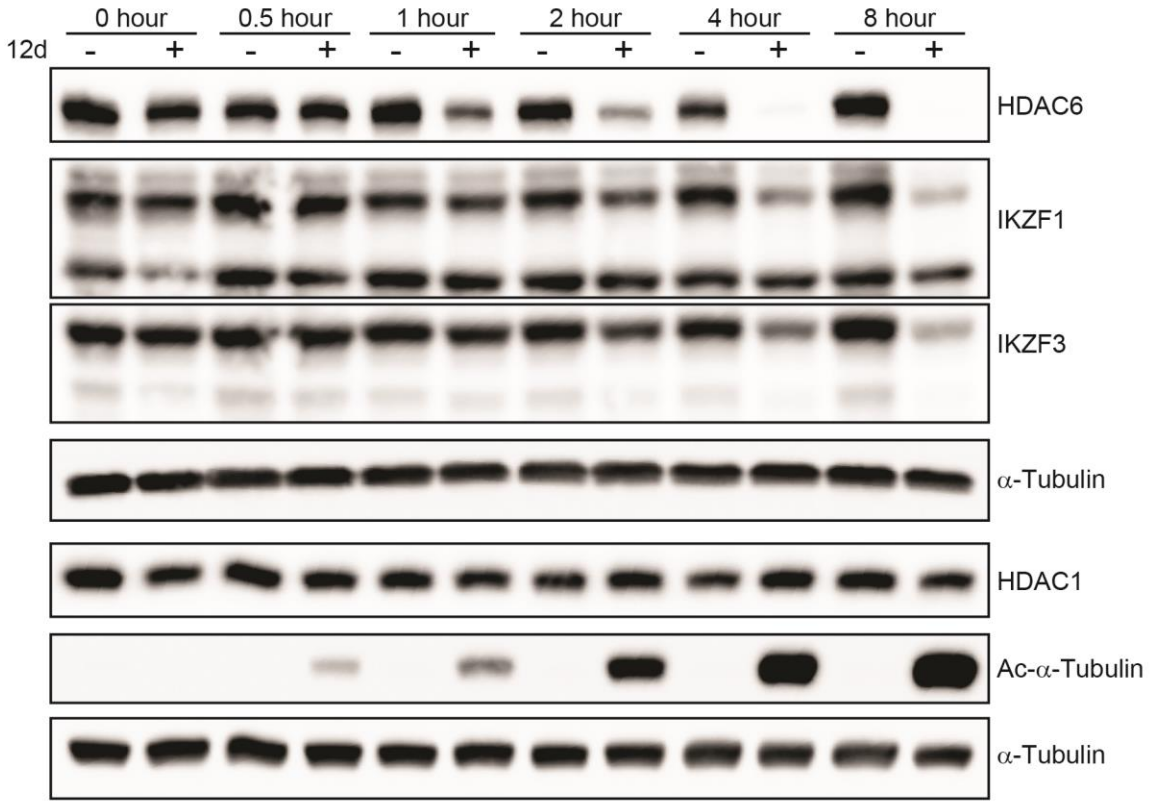

Figure 2.3.7. Time-course study of degrader **12d** in MM1S cells

To probe the efficiency of **12d**, we treated MM1S with 100 nM **12d** and monitored the change of HDAC6 protein level by time (**Figure 2.3.7**). The HDAC6 degradation started around 1 h and reached maximal degradation effect at 4 h. The degradation of IKZFs was only observed after 4 h. Meanwhile, HDAC1 was not affected and the acetylation of tubulin was accumulated by time.

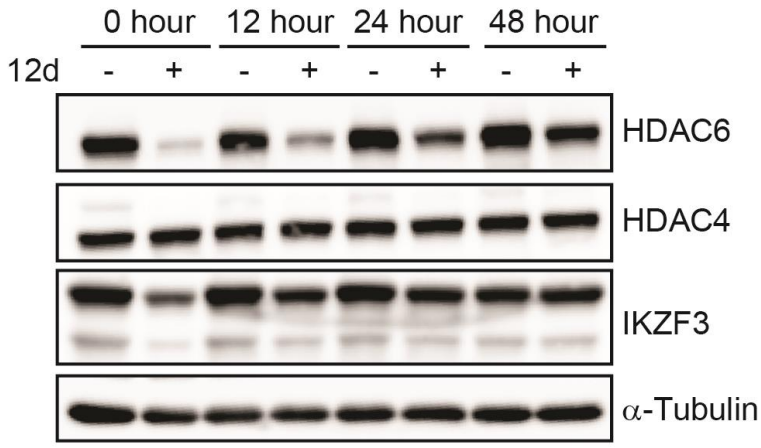

Figure 2.3.8. "Wash-out" experiment in MM1S cells

To study the re-synthesis rate of HDAC6 after degradation, we performed "wash-out" experiment (**Figure 2.3.8**). Cells were treated with 100 nM of **12d** for 6 h and then washed with PBS to remove remaining degraders. HDAC6 expression was monitored for 48 h. HDAC6 was not fully recovered within 48 h, suggesting the slow turnover rate of HDAC6. Interestingly, IKZF3 was quickly recovered after 12 h, indicating the fast re-synthesis rate of IKZFs, which might be one of the reasons for the requirement of higher concentrations of compounds for the degradation of IKZF.

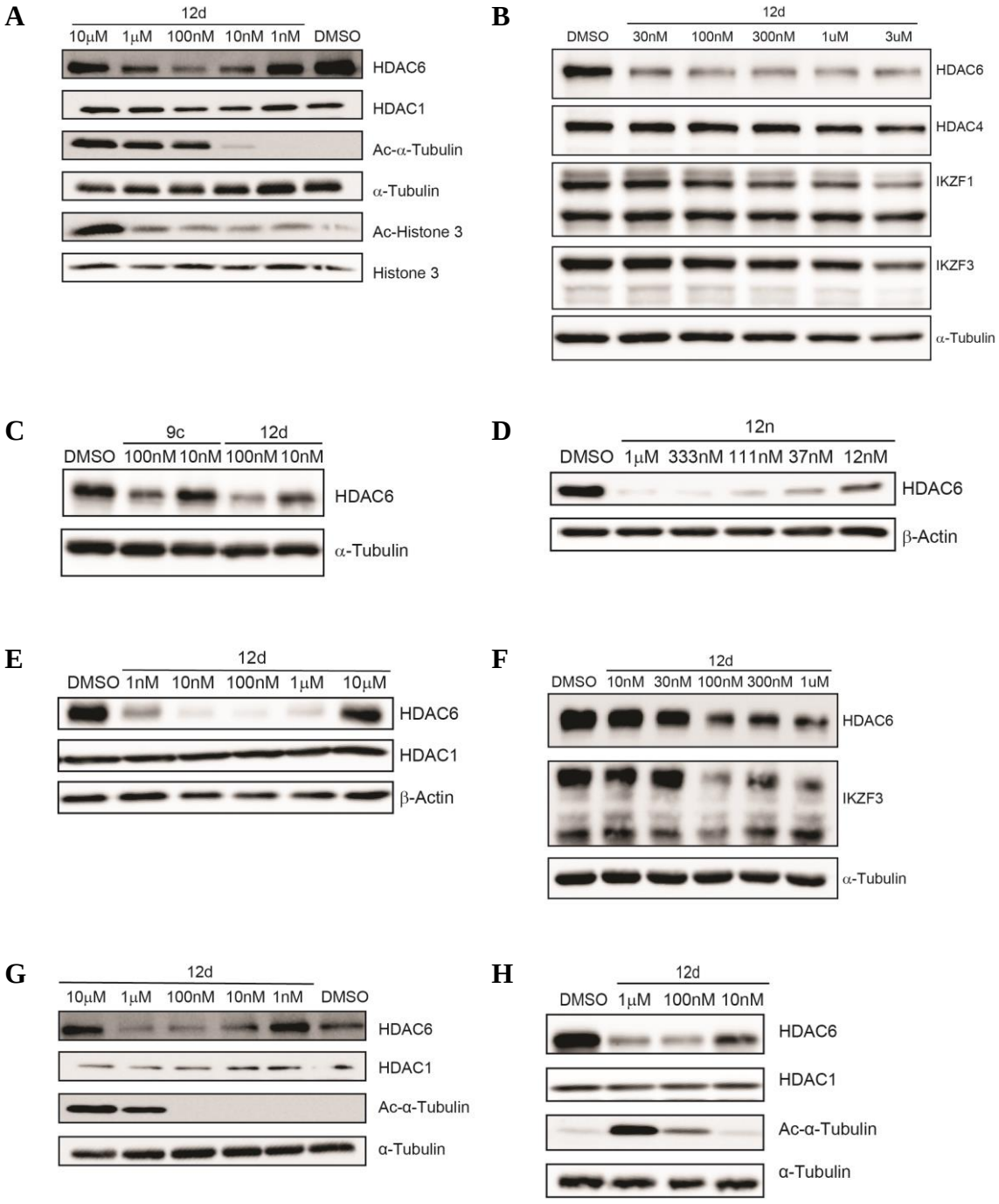

Figure 2.3.9. Western blot analysis of degraders in other cell lines

To examine the correlation between degradation efficiency and cell types, we also tested selected degraders in other cell lines. **Figure 2.3.9 A-H** represent results from A431 (6 h), RPMI-8226 (12 h), Jurkat (6h), HepG2 (6h), RS4;11 (6h), A375 (6h), Hela (6h) and MCF-7 (6h) respectively. Overall, the HDAC6 degrader is effective for the degradation of HDAC6 among all tested cancer cell lines.

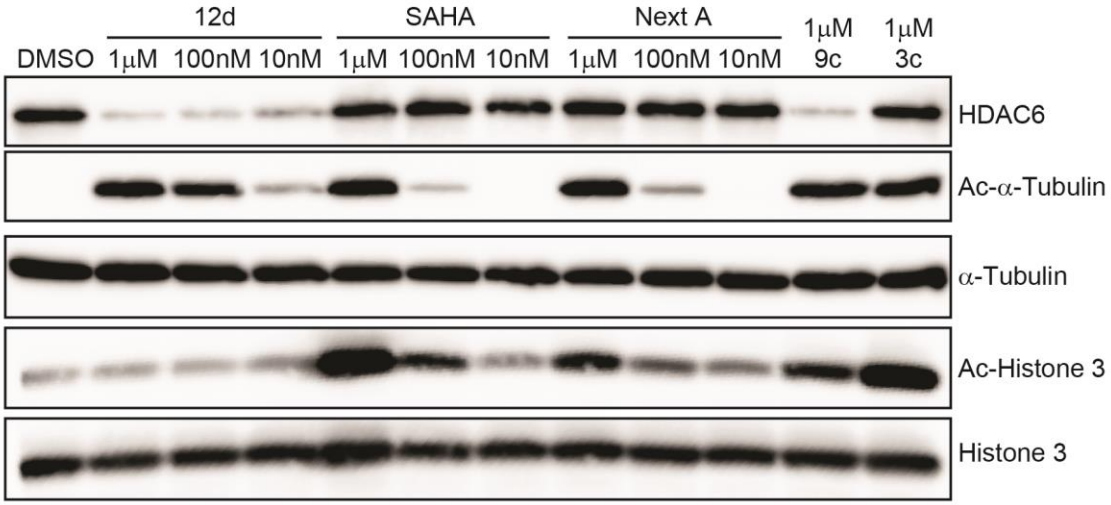

Figure 2.3.10. HDAC6 degrader selectively targeted HDAC6 over others

To further examine the selectivity of our new generation of HDAC6 degraders, we compared compound **12d** with SAHA, Next-A, degrader **9c** and pan-inhibitor **3c** for change of acetylated α-tubulin and acetylated histone H3 (**Figure 2.3.10**). Compound **12d** increased the acetylated tubulin at 100 nM while SAHA and Next-A didn't, indicating that the elevated acetylated tubulin was primarily due to HDAC6 degradation rather than the inhibition by "warhead" Next-A. We didn't observe any increase of acetylated histone H3 by the treatment **12d**, which is in sharp contrast to the strong acetylated histone H3 signal induced by SAHA, suggesting high selectivity of the degrader. Compared to our previously

developed degrader **9c**, compound **12d** also showed significantly improved selectivity for increasing the level of acetylated tubulin over acetylated histone H3, indicating the advantage of replacing a pan-HDAC inhibitor by HDAC6 selective inhibitor as the ligand of HDAC6 for PROTACs.

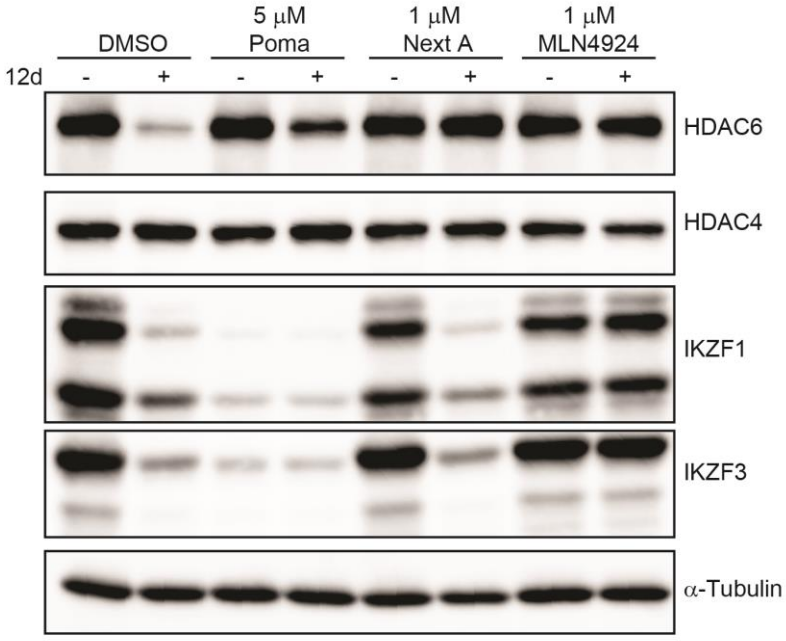

Figure 2.3.11. Mechanism study by co-treatment of the degrader with E3/POI ligands and NAE inhibitor

To support the involvement of ubiquitination-proteasome system for the decrease of HDAC6 protein level, we co-treated the degrader with binding competitors or pathway blockers (**Figure 2.3.11**). The co-treatment of degrader with Pomalidomide (Poma) or Next-A recovered HDAC6 level while the degradation of IKZFs was preserved, indicating that the binding of the degrader to both HDAC6 and CRBN E3 ligase are required for induced protein degradation. Moreover, it also confirmed the role of Pomalidomide moiety

in modulating IKZFs. Neddylation of cullin RING ligase (CRL) by NEDD8-Activating Enzyme (NAE) regulated CRL's activity as a E3 ligase[41,151]. Inhibiting neddylation by NAE inhibitor MLN4924 resulted in abolishing the degradation of both HDAC6 and IKZFs (**Figure 2.3.11**).

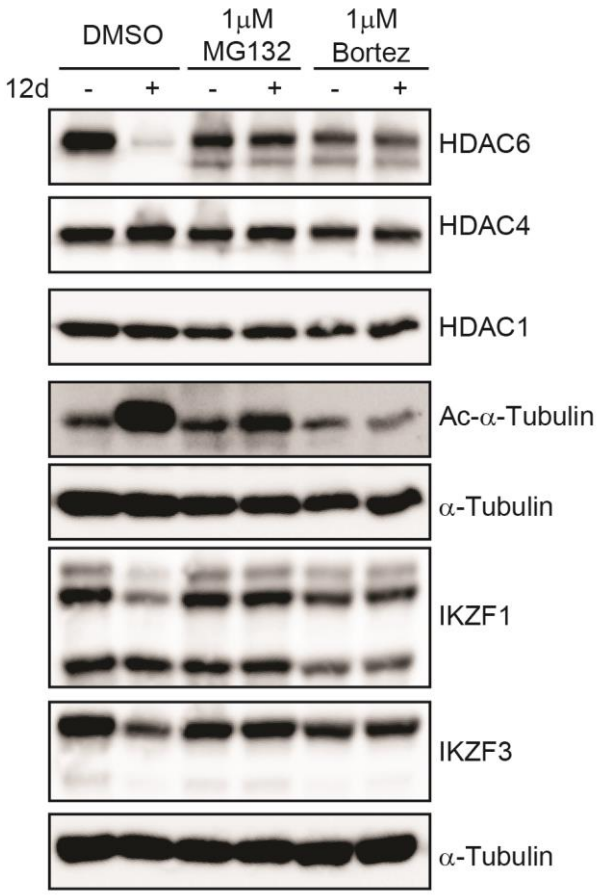

Figure 2.3.12. Mechanism study prove PROTAC-induced degradation by proteasome

We also used proteasome inhibitor MG132 and Bortezomib (Bortez) to block the down-stream proteasome degradation (**Figure 2.3.12**). Under the co-treatment of both inhibitors, no degradation of HDAC6 or of other HDACs was observed. Acetylated tubulin level was

suppressed as well. This confirms that HDAC6 degradation is primarily responsible for the acetylation of its substrates rather than inhibition by the “warhead” moiety.

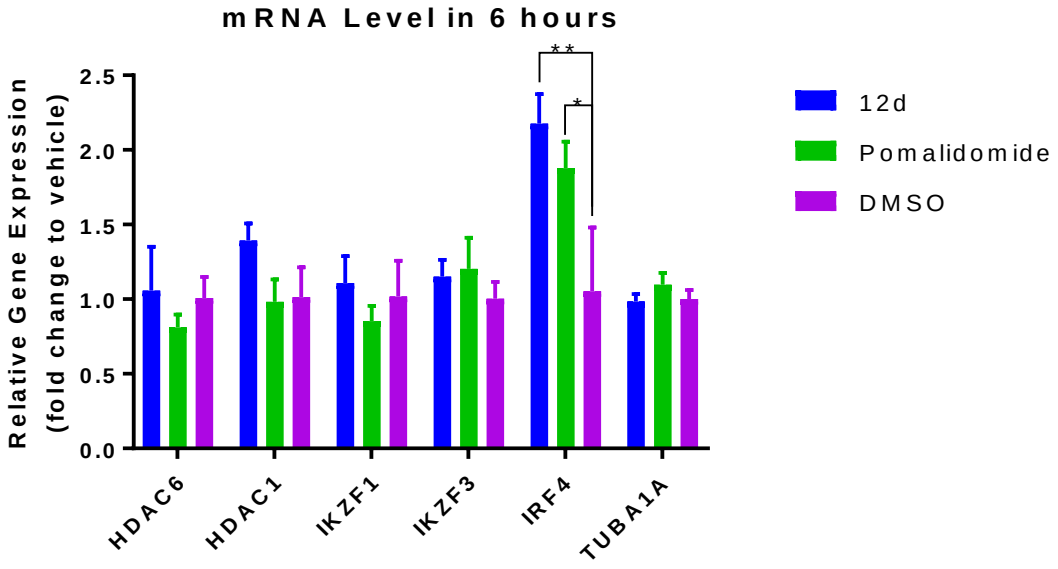

Figure 2.3.13. Transcriptional effects under treatment of degrader and Pomalidomide

To exclude the possible transcriptional impact by degraders, we used qRT-PCR to examine the mRNA level of HDAC6 and related genes (**Figure 2.3.13**). We observed little effects on HDACs and IKZFs after 6 h treatment of degrader **12d**. It is consistent with the hypothesis that the cellular knockdown of HDAC6 is due to direct protein degradation, not by transcriptional downregulation. However, in this relative short treatment time, both degrader and Pomalidomide increased the mRNA level of IRF4. IRF4 is a crucial gene for multiple myeloma growth. IRF4 was downregulated by IMiDs in both protein level and transcription level for longer treatment time (24 - 48 hours). [152,153]

Our HDAC6 degrader **12d** thus has three functions: inhibition of HDAC6 by the Next-A motif, degradation of IKZFs by the pomalidomide moiety, and the degradation of HDAC6 through the formation of the ternary complex. The former two functions can be achieved by the combination of HDAC6 selective inhibitor and pomalidomide. The third function is unique for HDAC6 degraders. Since HDAC6 selective inhibitors showed synergy with pomalidomide and its related analogues for the treatment of multiple myeloma in animal models and human clinical trials[136,143,154], we envision that HDAC6 degrader **12d** would have enhanced anti-myeloma activity over the combination of HDAC6 selective inhibitor and pomalidomide.

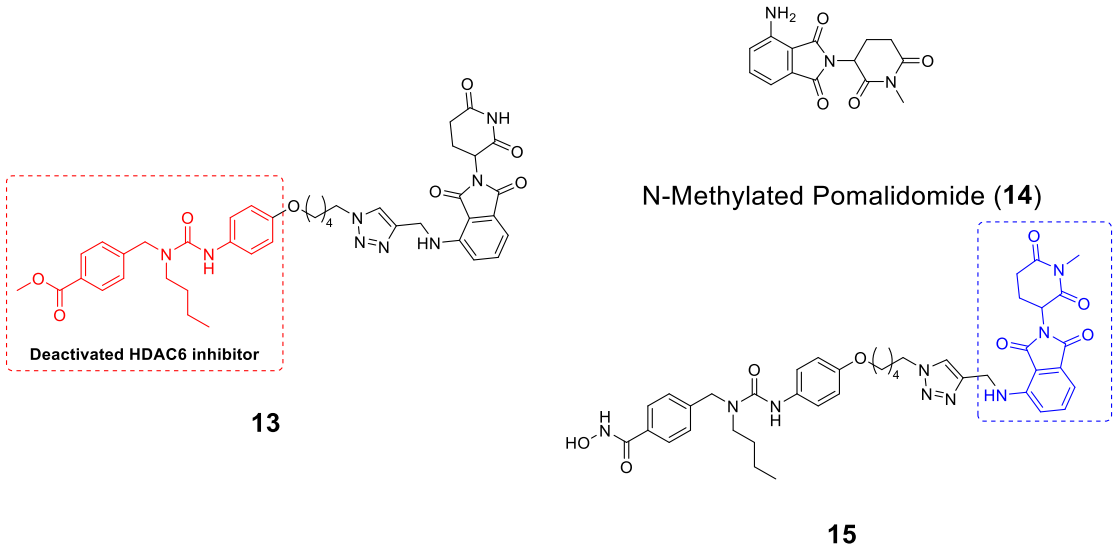

Figure 2.3.14. Structure of deactivated degraders and N-methylated pomalidomide

To rule out the potential cell-permeability issue, we synthesized deactivated degraders (**Figure 2.3.14**), which have similar molecular weight and size comparing to **12d**, for better comparison. We blocked the binding of **13** to HDAC6 by replacing the hydroxamic acid

zinc binding moiety with a methyl ester. The *N*-methylated Pomalidomide (**14**) moiety was used as the negative control for Pomalidomide-based PROTACs[42]. The binding of **15** to CRBN is blocked by attaching a methyl group to the key imide NH.

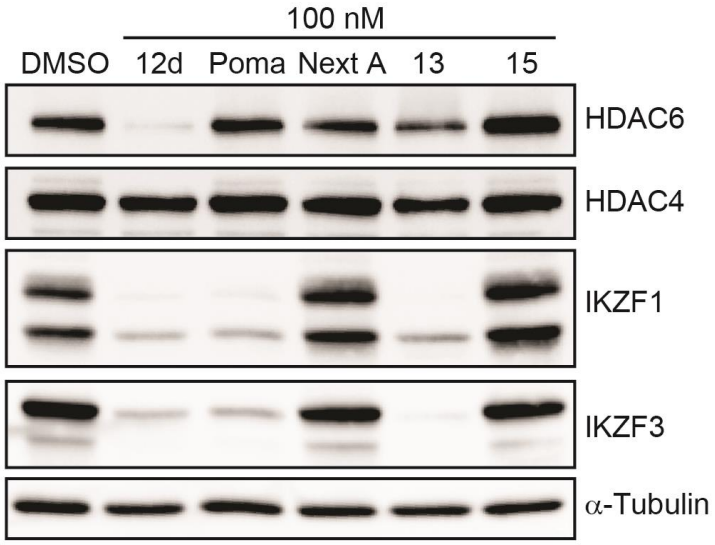

Figure 2.3.15. Western blot analysis of deactivated degraders

Western blot analysis proved that both compounds **13** and **15** are inactive in MM1S (**Figure 2.3.15**). Compound **13** induced limited HDAC6 degradation and this might be due to hydrolysis of carboxylic ester to carboxylic acid, which is a weak ligand for zinc ion. This observation may be worth to follow up since carboxylic acid is generally much less toxic than hydroxamic acid and a more optimized carboxylic acid-based degrader may provide a wider therapeutic window.

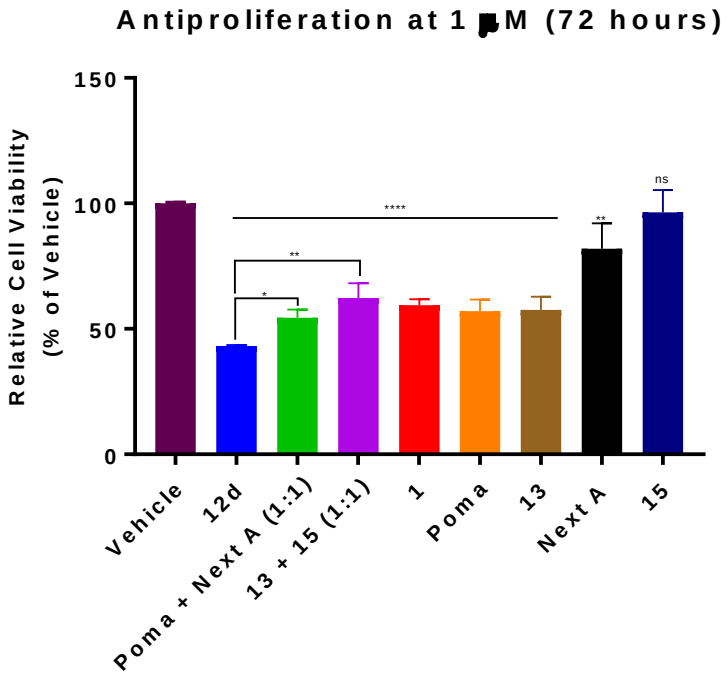

Figure 2.3.16. Proliferation of MM1S cells

We performed single treatment or co-treatment as combined therapy (1 μM) for 72 h in MM1S cells (**Figure 2.3.16**). Next-A had minor effects on cell growth while **15** was totally inactive. Pomalidomide, **13** and degrader **9c** shared similar antiproliferation effects at this concentration. We didn't observe statistically significant synergy of dual treatment with **13** + **15** (1:1) or dual treatment with Pomalidomide + Next-A (1:1) comparing with single treatment of **13** or Pomalidomide ($P > 0.05$). The dual treatment of Pomalidomide + Next-A (1:1) is slightly more potent than that of **13** + **15** (1:1). However, the single treatment of **12d** improved about 19% ($P = 0.0017$) and 11% ($P = 0.0213$) growth inhibition comparing with the combination sets of **13** + **15** (1:1) and Pomalidomide + Next-A (1:1), respectively.

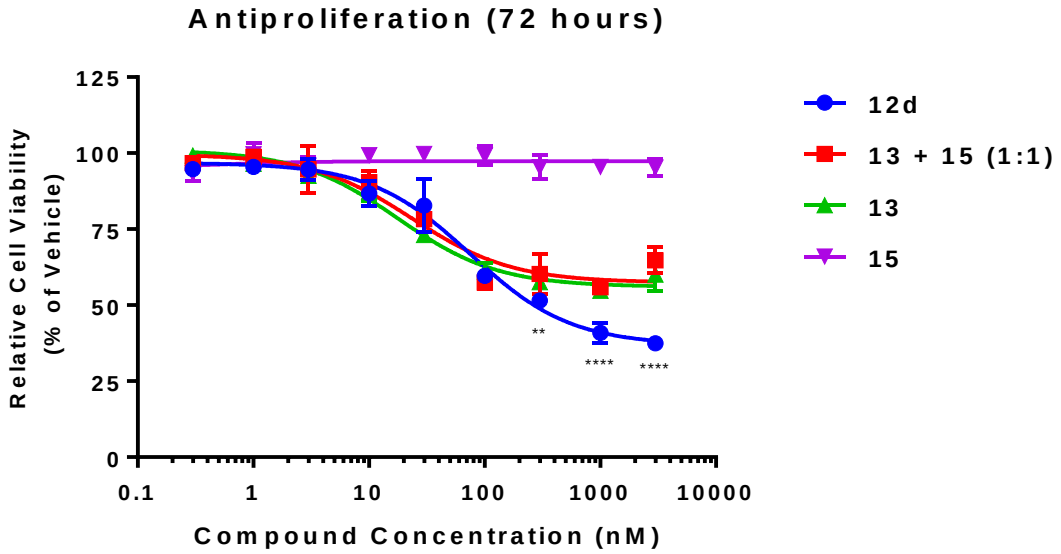

Figure 2.3.17. Dose response of antiproliferation in MM1S cells

Table 2.3.3. IC_{50} of Antiproliferation in MM1S

	IC_{50} (nM) [a]	**Maximal Inhibition (%) [b]**
12d	74.92 ± 11.35	63.15 ± 1.82
13 + **15 (1:1)**	23.50 ± 6.26	42.57 ± 1.88
13	17.72 ± 2.84	43.96 ± 1.16

[a]The concentration at which half-maximal growth inhibition was achieved. [b]The maximum percentage of growth inhibition. [a,b]Values with ± SD obtained from nonlinear fitted data in **Figure 2.3.17**.

To further confirm the observed enhancement, we studied the anti-proliferation in response to **12d** from 0.3 nM to 3 μM (**Figure 2.3.17**). We compared this single treatment with dual

treatment of **13** and **15** to rule out the potential complication derived from cell permeability issue. The resulting EC_{50}[d] and maximal inhibition was listed in **Table 2.3.3** and the Statistical significance was listed in **Table 2.3.4**. Degrader **12d** lowered the bottom line (minimal proliferation) of curve over 20% although its EC_{50} was decreased consequentially. The combination of **13** and **15** failed to work synergistically, indicating the HDAC6 degradation, other than inhibition, was crucial for the enhanced antiproliferation by degrader **12d**.

Although the EC_{50} of **12d** (74.9 ± 11.3) appeared higher than the combination of **13**+**15** (23.5 ± 6.3) or **13** (17.7 ± 2.8) alone, it is clear that the relatively higher EC_{50} for **12d** is due to its lower bottom or the higher maximal growth inhibition. The three curves almost overlap at concentrations lower than 100 nM. At concentrations higher than 100 nM, degrader **12d** starts to inhibit the growth of the cell much more significantly than **13** alone or the combination of **13** and **15**. The maximal inhibition of **12d** (63.1 ± 1.8) is much higher than that of the combination of **13** and **15** (42.6 ± 1.9) or **13** alone (44.0 ± 1.2).

[d] EC_{50}: concentration of compound that gives half-maximal response

Table 2.3.4. Statistical Significance of Figure

Concentrations	**12d** *v.s.* **13** + **15 (1:1)**	**12d** *v.s.* **13**	**12d** *v.s.* **15**
3 μM	****	****	****
1 μM	****	****	****
300 nM	**	ns	****
100 nM	ns	ns	****
30 nM	ns	**	****
10 nM	ns	ns	****
3 nM	ns	ns	ns
1 nM	ns	ns	ns
0.3 nM	ns	ns	ns

Statistical significance was analyzed by Two-way RM ANOVA using Dunnett's multiple comparisons test for **Figure 7B** in main article. Table showed the multiple comparison using "**12d**" as control column. Not significant (ns) $P > 0.05$, *$P \leqslant 0.05$, **$P \leqslant 0.01$, ***$P \leqslant 0.001$, ****$P \leqslant 0.0001$.

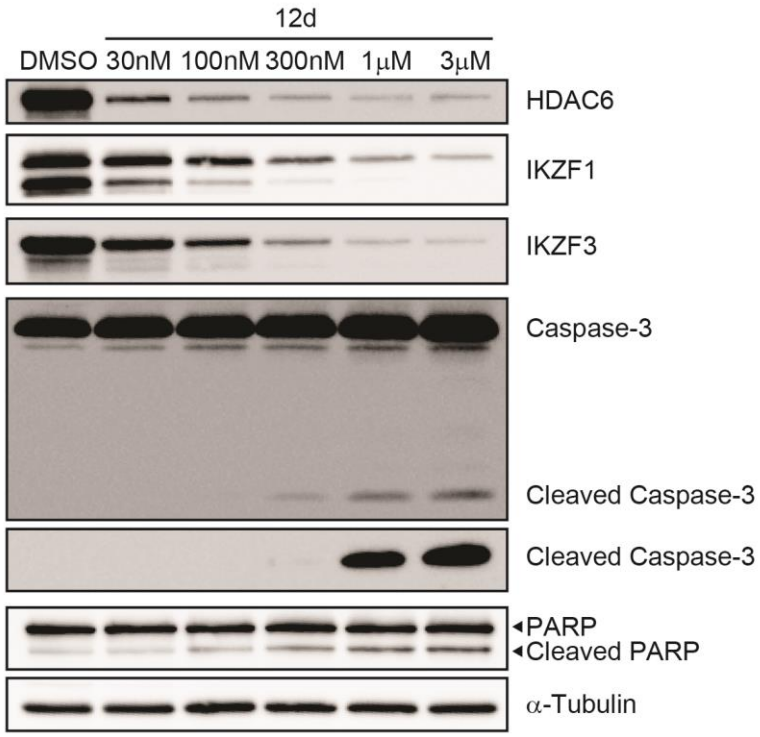

Figure 2.3.18. Profiling of apoptosis markers

Hence, we concluded that the HDAC6 degradation and IKZF degradation had synergistic effects at higher concentration (≥ 300 nM) of the degrader. For 48 h treatment of **12d** in MM1S, we observed the cleavages of Caspase-3 and poly ADP ribose polymerase (PARP) in dose dependent manner (**Figure 2.3.18**), suggesting that the synergy was derived from degrader-promoted cell apoptosis.

2.4. Summary and Perspectives

In summary, we have developed the first-in-class small molecule degraders for zinc-dependent HDACs by conjugating a pan-HDAC inhibitor with thalidomide analogues.

Cell-based assays indicated that these HDAC degraders could selectively degrade HDAC6 over other HDACs. Our mechanistic investigations indicate that the CRBN E3 ligase and proteasome are responsible for the degradation of HDAC6. The HDAC degraders derived from pan HDAC inhibitors also inhibit other HDACs, as indicated by the increased acetylated histone level. We then developed more selective HDAC6 degraders by tethering Pomalidomide and HDAC6 selective inhibitor Next-A. By varying the linker length and linking positon, we discovered potent and selective HDAC6 degrader **12d** that retains the degradation activity of IKZFs. Further investigation confirmed its mechanism of action. The antiproliferation study demonstrated the advantage of our HDAC6 degraders over HDAC6 inhibitor alone, IMiD alone, or its combination, presumably because of the multi-function of the degrader. Our results highlighted the utility of PROTACs as a novel strategy for the development of therapeutics against multiple myeloma.

Development of HDAC6 degrader is a promising strategy in drug discovery. For future work, we propose to investigate the potential of HDAC6 selective degraders in immunotherapy. Programmed cell death ligand 1 (PD-L1)/ programmed cell death protein 1 (PD-1) were negative co-stimulatory factors that can regulate tolerance and autoimmunity[155,156]. HDAC6 was shown to regulate PD-L1 expression via STAT3 signaling pathway in melanoma[124], osteosarcoma[123] and glioblastoma[157]. HDAC6 inhibition or silencing suppressed the phosphorylation of STAT3 and sequentially affect the PD-L1 expression. Combination of HDAC6 inhibitor and anti-PD-1 antibody worked synergistically for treating multiple myeloma[147]. IMiDs, such as Lenalidomide, enhanced the anti-myeloma immune response by PD-1/PD-L1 blockade. These results from literature

suggest that HDAC6 degraders might suppress PD-L1 expression more efficiently in cancer cells and enhance their sensitivity towards immunotherapy. In addition, we also plan to explore the combination therapy of HDAC6 degrader with other therapeutic reagents. For example, BET inhibitor JQ1 induced the HDAC6 expression in multiple myeloma and co-targeting BET proteins and HDAC6 yielded enhanced antiproliferation in mice model bearing human MM cells[158]. Thus, HDAC6 degrader might overcome the unexpected induction of HDAC6 expression by BET inhibitor. Synergistic treatment of HDAC6 degrader and BET inhibitor or degrader would be a rational option for future anti-myeloma therapy.

HDAC6 is a unique deacetylase that is involved in multiple cellular processes, such as protein degradation, inflammation, angiogenesis, cell motility[159]. In quantitative proteomic analysis of HDAC6-knockout mice, Zhou and co-workers identified many proteins with elevated acetylation and several candidates were validated as novel substrates of HDAC6[160]. Selective HDAC6 degraders can regulate HDAC6 level reversibly with great temporal and spatial control. HDAC6 selective degraders may serve as a powerful tool for studying the HDAC6 related biology, especially the non-enzymatic activity of HDAC6.

2.5. Experimental Procedures

General Information in Synthetic Chemistry.

All reactions were conducted under a positive pressure of dry argon in glassware that had been oven dried prior to use. Anhydrous solutions of reaction mixtures were transferred

via an oven dried syringe or cannula. All solvents were dried prior to use unless noted otherwise. Thin layer chromatography (TLC) was performed using precoated silica gel plates. Flash column chromatography was performed with silica gel. ^{1}H and ^{13}C nuclear magnetic resonance (NMR) spectra were recorded on Bruker 400 MHz and 500 MHz spectrometers. ^{1}H NMR spectra were reported in parts per million (ppm) referenced to 7.26 ppm of $CDCl_3$ or referenced to the center line of a septet at 2.50 ppm of DMSO-d_6. Signal splitting patterns were described as singlet (s), doublet (d), triplet (t), quartet (q), quintet (quint), or multiplet (m), with coupling constants (*J*) in hertz. High resolution mass spectra (HRMS) were performed on an Electron Spray Injection (ESI) TOF mass spectrometer. The liquid chromatography mass spectrometry LC-MS analysis of final products was processed on Agilent 1290 Infinity II LC system using Poroshell 120 EC-C18 column (5 cm × 2.1 mm, 1.9 μm) for chromatographic separation. Agilent 6120 Quadrupole LC/MS with multimode electrospray ionization plus atmospheric pressure chemical ionization (MM-ES+APCI) was used for detection. The mobile phases were 5.0% methanol and 0.1% formic acid in purified water (A) and 0.1% formic acid in methanol (B). The gradient was held at 35% (0-0.2 min), increased to 100% at 2.5 min, then held at isocratic 95% B for 0.4 min and then immediately stepped back down to 35% for 0.1 min re-equilibration. The flow rate was set at 0.8 mL/min. See Supporting Information for ^{1}H and ^{13}C NMR spectrums and LC-MS purity analysis of compounds.

Synthesis of Intermediates in **Section 2.2**

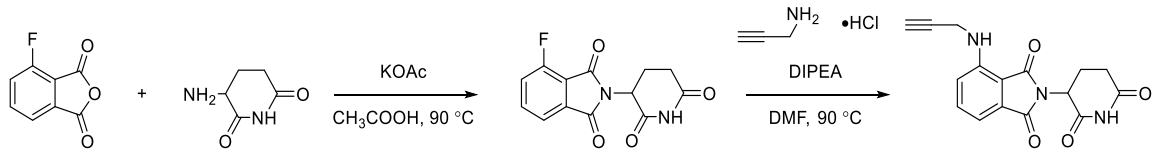

6

A mixture of 3-fluorophthalic anhydride (500 mg, 3.00 mmol), potassium acetate (911.4 mg, 9.44 mmol) and 3-aminopiperidine-2,6-dione hydrochloride (543 mg, 3.30 mmol) in acetic acid (10.0 mL, 0.3 M) was heated to 90℃ for overnight. The black reaction mixture was cooled to room temperature and diluted to 20 mL by water and extracted with ethyl acetate (30 mL x3). The combined organic phases were washed with water (50 mL) and brine (50 mL), dried over anhydrous sodium sulfate, and concentrated under reduced pressure. The residue was purified by silica gel flash column chromatography (eluted with 50% ethyl acetate in hexanes) to afford fluoro-thalidomide 2-(2,6-Dioxopiperidin-3-yl)-4-fluoro-2,3-dihydro-1H-isoindole-1,3-dione (704.4 mg, 85% yield) as a white solid.

A mixture of Propargylamine hydrochloride (91.5mg, 1.0 mmol), fluoro-thalidomide afforded above (276.2 mg, 1.0 mmol) and N-ethyl-N-isopropylpropan-2-amine (0.52 ml, 3.0 mmol) in dry N,N-dimethylformamide (4 mL) was stirred at 90℃ for 12 h. The mixture was cooled to room temperature, poured into water (20 mL) and extracted with ethyl acetate (35 mL x 2). The combined organic phases were washed with water (30mL) and brine (30 mL), dried over anhydrous sodium sulfate, and concentrated under reduced pressure. The crude residue was purified by silica gel flash column chromatography (eluted with 20% ethyl acetate in hexanes) to afford 2-(2,6-Dioxopiperidin-3-yl)-4-Propargylamino-2,3-dihydro-1H-isoindole-1,3-dione (**6**) (93.3 mg, 30% yield) as a yellow

oil. ^{1}H NMR (500 MHz, $CDCl_3$): δ 2.12-2.16 (m, 1H), 2.27 (t, *J* = 2.3 Hz 1H), 2.70-2.93 (m, 3H), 4.10 (dd, *J* = 6.1, 2.4 Hz, 2H), 4.92 (dd, *J* = 12.3, 5.4 Hz, 1H), 6.45 (t, *J* = 5.8 Hz, 1H), 7.03 (d, *J* = 8.5 Hz, 1H), 7.20 (d, *J* = 7.2 Hz, 1H), 7.56-7.59 (m, 1H), 7.97 (s, 1H). ^{13}C NMR (126 MHz, DMSO) δ 22.74, 31.61, 32.25, 49.03, 72.49, 79.67, 111.26, 112.20, 117.39, 132.46, 136.04, 145.54, 167.55, 169.17, 169.43, 172.34. HRMS (EI) calcd. for $[C_{16}H_{13}N_3O_4]$ $(M + H)^+$ 312.0979, found 312.0981.

7a was synthesized according to literature method.[141] **7b-d** was synthesized via the same route according to literature method.[142]

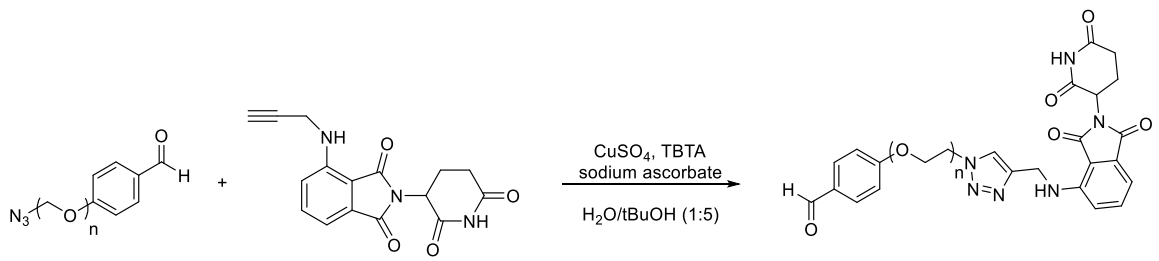

7a, n = 1
7b, n = 2
7c, n = 3
7d, n = 4

6a

8a, n = 1
8b, n = 2
8c, n = 3
8d, n = 4

A mixture of **7** (1.0 mmol) and compound **6** (1.0 mmol), tris[(1-benzyl-1H-1,2,3-triazol-4-yl)methyl]amine (0.1 mmol), $CuSO_4$ (0.1 mmol), sodium ascorbate (1.0 mmol) in *t*-BuOH:H_2O (1:5) (10 mL) was stirred at room temperature for 16 h. The reaction mixture was then quenched with water (20 mL) and extracted with dichloromethane (30 mL x 3). The combined organic phases were washed with water (50 mL) and brine (50 mL), dried over anhydrous sodium sulfate, and concentrated under reduced pressure. The residue was purified by silica gel flash column chromatography (eluted with 25-50% ethyl acetate in hexane) to afford the corresponding aldehyde **8a-8d** as yellow oil (60-70% yield).

8a: ^{1}H NMR (400 MHz, DMSO): δ 1.99- 2.03 (m, 1H), 2.54- 2.61 (m, 2H), 2.85-2.93 (m, 1H), 4.50 (t, J = 5.1 Hz, 2H), 4.60 (d, J = 5.8 Hz, 2H), 4.77 (t, J = 5.1 Hz, 2H), 5.03-5.08 (m, 1H), 7.04-7.09 (m, 4H), 7.16 (d, J = 8.6 Hz, 1H), 7.55 (m, 1H), 7.83 (d, J = 8.4 Hz, 2H), 8.10 (s, 1H), 9.85 (s, 1H), 11.09 (s, 1H). ^{13}C NMR (100 MHz, DMSO): δ 22.61, 31.45, 38.04, 49.03, 49.28, 67.03, 110.16, 111.41, 115.50, 118.11, 124.00, 130.48, 132.24, 132.60, 136.60, 145.12, 146.28, 163.17, 167.75, 169.23, 170.54, 173.29, 191.82. HRMS (EI) calcd. for $[C_{25}H_{22}N_6O_6]$ $(M + H)^+$ 503.1674, found 503.1654.

8b: ^{1}H NMR (400 MHz, $CDCl_3$): δ 2.08-2.13 (m, 1H), 2.71-2.89 (m, 3H), 3.79-3.81 (m, 2H), 3.93 (t, J = 5.0 Hz, 2H), 4.09-4.14 (m, 2H), 4.53- 4.56 (m, 4H), 4.88-4.93 (m, 1H), 6.63 (t, J = 5.6 Hz, 1H), 6.95-6.98 (m, 3H), 7.11 (d, J = 7.1 Hz, 1H), 7.46 (dd, J = 8.3, 7.3 Hz, 1H), 7.62 (s, 1H), 7.81 (d, J = 8.8 Hz, 2H), 8.28 (s, 1H), 9.86 (s, 1H). ^{13}C NMR (100 MHz, $CDCl_3$): δ 22.77, 31.41, 38.73, 48.95, 50.39, 67.48, 69.47, 69.66, 110.80, 112.30, 114.77, 117.14, 122.89, 130.25, 132.04, 132.40, 136.20, 146.19, 163.51, 167.46, 168.37, 169.35, 171.05, 190.80. HRMS (EI) calcd. for $[C_{27}H_{26}N_6O_7]$ $(M + H)^+$ 547.1936, found 547.1911.

8c: ^{1}H NMR (500 MHz, $CDCl_3$): 2.11-2.14 (m, 1H), 2.68-2.92 (m, 3H), 3.60-3.66 (m, 4H), 3.81 (dd, *J* = 5.5, 3.7 Hz, 2H), 3.87 (t, *J* = 5.0 Hz, 2H), 4.17 (dd, *J* = 5.6, 3.7 Hz, 2H), 4.52 (t, *J* = 5.0 Hz, 2H), 4.57 (d, *J* = 5.9 Hz, 2H), 4.87-4.94 (m, 1H), 6.63 (t, *J* = 5.8 Hz, 1H), 6.95-7.02 (m, 3H), 7.13 (d, *J* = 7.1 Hz, 1H), 7.46-7.48 (m, 1H), 7.68 (s, 1H), 7.81 (d, *J* = 8.7 Hz 2H), 8.09 (s, 1H), 9.87 (s, 1H). ^{13}C NMR (100 MHz, $CDCl_3$): δ 22.87, 31.52, 38.79, 49.04, 50.48, 67.83, 69.52, 69.55, 70.61, 70.81, 110.82, 112.35, 114.93, 117.28, 123.05,

130.23, 132.10, 132.48, 136.30, 144.89, 146.28, 163.80, 167.58, 168.54, 169.45, 171.25, 190.90. HRMS (EI) calcd. for $[C_{29}H_{30}N_6O_8]$ $(M + H)^+$ 591.2198, found 591.2202.

8d: ^{1}H NMR (400 MHz, $CDCl_3$): δ 2.08-2.14 (m, 1H), 2.67-2.89 (m, 3H), 3.57 (s, 4H), 3.59-3.62 (m, 2H), 3.68-3.70(m, 2H), 3.83-3.86 (m, 4H), 4.17-4.20 (m, 2H), 4.50 (t, J = 5.0 Hz, 2H), 4.60 (d, J = 5.7 Hz, 2H), 4.87-4.92 (m, 1H), 6.66 (t, J = 5.9 Hz, 1H), 6.97-7.03 (m, 3H), 7.12 (d, J = 7.1 Hz, 1H), 7.48 (dd, J = 8.5, 7.1 Hz, 1H), 7.70 (s, 1H) 7.81 (d, J = 8.7 Hz, 2H), 8.30 (s, 1H)., 9.87 (s, 1H). ^{13}C NMR (101 MHz, $CDCl_3$): δ, 22.77, 31.41, 38.69, 48.92, 50.38, 67.73, 69.38, 69.46, 70.50, 70.51, 70.52, 70.88, 99.99, 110.73, 112.24, 114.83, 117.19, 123.00, 130.09, 131.97, 132.39, 136.20, 146.21, 163.73, 167.47, 168.33, 169.32, 171.04, 190.81. HRMS (EI) calcd. for $[C_{31}H_{34}N_6O_9]$ $(M + Na)^+$ 657.2279, found 657.2247.

General Synthesis of Arylhydrazone PROTAC in **Section 2.2**

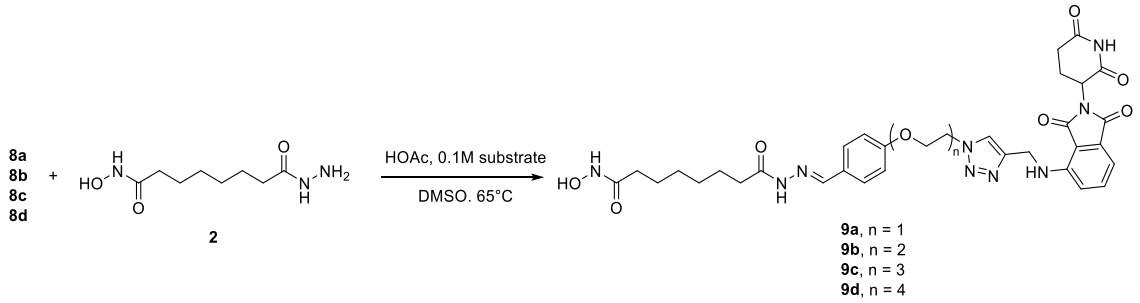

In-situ formation of HDAC degraders by coupling acylhydrazide **1** with aldehydes **8a**, **8b**, **8c**, or **8d**.

To a solution of aldehyde (**8a-8d**) in DMSO (25 μL, 0.2M) was added into 25 μL of hydrazide **2** solution (0.2 M in DMSO). The mixture was diluted with 0.45 mL DMSO

after heating at 75°C for 12h. The resulting solution (10 mM) was heated again at 75°C for 12h. The purity of the acylhydrazone was analyzed by LCMS and predominantly one peak was observed for all compounds (see S3 for purity analysis). The in-situ formed HDAC degraders were directly tested in a cell-based assay for activity.

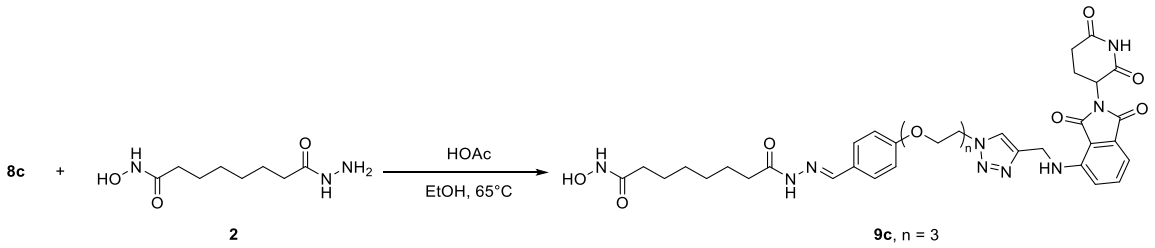

The most active compound **9c** was resynthesized.

To a mixture of aldehydes **8c** (59.06 mg, 0.10 mmol) and acylhydrazide **2** (44.71 mg, 0.22 mmol) in ethanol (1mL) was added 10uL of AcOH. The reaction mixture was stirred and heated at 65 °C for overnight. Precipitate appeared after the solution was cooled to 0 °C. The solid product was collected by filtration and washed by cold ethanol and water to yield 73.7 mg of product (95% yield).

9c: mixture of cis- and trans- (1:1) product. ^{1}H NMR (400 MHz, $CDCl_3$): δ 1.23-1.27 (m, 4H), 1.46-1.55 (m, 4H), 1.93 (t, J = 7.4 Hz, 2H), 1.99-2.02 (m, 1H), 2.16 (t, J = 7.4 Hz, 1H), 2.54-2.59 (m, 3H), 2.83-2.92 (m, 1H), 3.51 (s, 4H), 3.66-3.68 (m, 2H), 3.79 (t, J = 5.2 Hz, 2H), 4.05-4.08 (m, 2H) 4.49 (t, J = 5.2 Hz, 2H), 4.56 (d, J = 6.0 Hz, 2H), 5.02-5.07 (m, 1H), 6.94-6.97 (m, 2H), 7.04 (d, J = 6.9 Hz, 2H), 7.15 (d, J = 8.6 Hz, 1H), 7.53-7.59 (m, 3H), 7.89 (s, 0.5H), 7.99 (s, 1H), 8.08 (s, 0.5H), 8.65 (s, 1H), 10.33 (s, 1H), 11.04 (s, 0.5H), 11.09 (s, 1H), 11.18 (s, 0.5H). ^{13}C NMR (101 MHz, $CDCl_3$): δ 22.15, 24.16, 24.99,

25.04, 28.38, 28.43, 28.43, 28.54, 30.98, 31.88, 32.25, 37.63, 48.57, 49.40, 67.24, 68.73, 68.81, 69.56, 69.75, 109.68, 110.94, 114.72, 114.76, 117.63, 123.27, 127.00, 128.11, 128.49, 132.10, 136.13, 144.31, 145.82, 159.64, 167.26, 168.39, 168.77, 169.11, 170.05, 172.80, 174.12. HRMS (EI) calcd. for $[C_{31}H_{34}N_6O_9]$ $(M + Na)^+$ 798.3182, found 798.3186.

All other PROTAC degraders or inactivated degraders in **Section 2.3** was synthesized by Dr Hao Wu. Refer to future literature(s) for details.

Biochemical Reagent and Antibodies

MTT (M5655), Janus Green B (201677), Resazurin sodium salt (R7017), N-Methylated pomalidomide (901494) were purchased from Sigma-Aldrich. Pomalidomide (S1567), Thalidomide (S1193), Lenalidomide (S1029), MG132 (S2619), Bortezomib (S1013) were purchased from Selleckchem**.** SAHA (10009929) was purchased from Cayman Chemical.

Antibodies against HDACs, IKZF1, IKZF3, Ac-α-Tubulin (K40), Histone-3, Ac-Histone-3 (K9), Caspase-3, PARP and anti-mouse- and anti-rabbit HRP-linked antibodies were purchased from Cell Signaling Technology (CST). Antibodies against α-Tubulin and β-Actin were purchased from R&D system.

Cell lines and culture methods

Hela and HepG2 cells were cultured in DMEM medium (Corning, 1g/L glucose) supplemented with 10% FBS and 1% Penicillin/Streptomycin. A375, A431 and MCF-7 cells were cultured in DMEM medium (Corning, 4.5g/L glucose) supplemented with 10% FBS and 1% Penicillin/Streptomycin. MM1S, RPMI8226, A375, RS4;11 and Jurkat cells were cultured in RPMI-1640 medium (Corning) supplemented with 10% FBS, 1% Sodium

Pyruvate, and 1% Penicillin/Streptomycin, 10mM HEPES. All cell lines were grown at 37°C in a humidified 5% CO_2 atmosphere.

Immunoblot

When the cells reached 90% confluence, they were harvested and plated $1x10^6$ cells per well in 6-well plate. After overnight seeding, the cells were treated with a solution of compounds or vehicle in culture medium. The culture medium was removed after treatment and then washed twice with cold PBS. To obtain whole cell lysate, all cells were treated with RIPA lysis buffer (25mM Tris, pH 7-8, 150 mM NaCl, 0.1% SDS, 0.5% sodium deoxycholate, 1% Triton X-100, protease inhibitor cocktail (Roche, 1 tablet per 10 mL) and 1mM PMSF) on ice for 10 minutes. Supernatant was collected after spinning down at 16,000g at 4 °C for 15 minutes. Protein concentration was measured by using the Pierce BCA protein assay (Thermo Fisher Scientific). About 10-40 μg of total protein was mixed with 4X Laemmli Loading Dye (250 mM Tris, pH 6.8, 40% glycerol, 5% SDS, 0.005% bromophenol blue, 4% BME) and heated at 95-100°C for 5 minutes. The heated sample was then subjected to 7.5-12% SDS-PAGE and transferred to PVDF membrane (Bio-Rad). The membrane was blocked in 5% non-fat milk (Bio-Rad) in TBS-T washing buffer (137 mM NaCl, 20 mM Tris, 0.1% Tween) and then incubated with primary antibodies at 4 °C overnight. The membrane was washed 3 times with TBS-T, incubated with secondary horseradish peroxidase (HRP) linked antibodies for 1 hour, then washed 3 more times with TBS-T. Clarity ECL substrate (Bio-Rad) was incubated with membrane for 5 minutes. The Immunoblot was generated by ChemiDoc MP Imaging Systems (Bio-Rad) and analyzed

by Image J software. A band intensity bar graph was generated, and the curve was fitted using “log(inhibitor) vs. response (three parameters)” by GraphPad Prism.

In-cell ELISA assay.

Refer to **Chapter 3 Section 3.5** for detail procedures.

Cell Viability Assays.

For MTT assay, when reach 90% confluence, cells were harvested and plated 1 x 10^4 cells per well in 96-well plate. After overnight settle-down, the culture medium was removed. 200 uL of dose medium contain compounds or vehicle in desired compound was added to each well. After 24 hours, 200uL of medium containing 0.5mg/mL MTT was added and incubate for 2 hours. Then, the MTT medium was removed without any wash. Finally, 200uL of solubilization solution (10% Triton-X100 in isopropanol with HCl) was added to each well followed by gently mixing. The optical density was read at wavelength of 570nm and background absorbance at 690nm. Measure the optical density (OD) of each well by subtract absorbance at 690nm from absorbance at 570nm. Relative viability (RV) was calculated by following formula:

$$RV = \frac{OD_{570}\ of\ sample\ - OD_{690}\ of\ sample}{OD_{570}\ of\ vehicle\ - OD_{690}\ of\ vehicle}$$

Normalized data was graphed as bar graph representing as mean of relative viability (n = 3) with ± SD as error bar.

For alamarblue assay, MM1S cells were harvested and plated with 1x10^4 cells in 100µL media per well in 96-well plate. After overnight seeding, 25 µL media containing 5X

dosing concentration of the compounds or vehicle was added to each well. After 72-hour treatment at 37°C in a humidified 5% CO_2 atmosphere, 12.5 µL 10X resazurin solution (1 mg/mL) was added to each well. Then cells were incubated at 37°C overnight. The optical density was read at 570 nm and 600 nm by platereader. The relative viability (RV) was measured by followed formula:

$$RV = \frac{117216 \times OD_{570}\ of\ sample\ - 80586 \times OD_{600}\ of\ sample}{117216 \times OD_{570}\ of\ vehicle\ - 80586 \times OD_{600}\ of\ vehicle}$$

Normalized data was graphed as bar graph or dot plot representing as mean of relative viability (n = 3) with ± SD as error bar. For dose response curve, nonlinear fitting of [Inhibitor] vs. response (three parameters) was generated by GraphPad Prism with R^2 over 0.92.

Real-Time Quantitative Reverse Transcription PCR.

After treatment, cells were harvested and washed with cold PBS twice. Total RNA was extracted by GeneJET RNA Purification Kit (Thermo Scientific, K0731) following manufacture protocol. The concentration of RNA was measured by Plate Reader. Total RNA at normalized concentration was subjected to reverse transcription to generate cDNA library by High-Capacity cDNA Reverse Transcription Kit (Applied Biosystems, 4368814). 10 ng cDNA was mixed with primer sets and PowerUP SYBR Green Master Mix (Applied Biosystems, A25780) in 96-well optical PCR plate. Real-time PCR and fluorescent signal were processed by QuantStudio 7 Flex Real-Time PCR System. Fast cycling mode (50 °C, 2 minutes, hold; 95 °C, 2 minutes, hold; 95 °C, 1 second, then, 60 °C, 30 seconds, 40 cycles) was performed and followed with melt curve stage (1.6 °C/second to 95°C, 15 seconds;

1.6 °C/second to 60°C, 1 minute; 0.15 °C/second to 95°C, 15 seconds). C_t value at automatically selected threshold was reported and calculated by $2^{-\Delta\Delta Ct}$ method.[161] The bar graph was generated and by GraphPad Prism. Normalized data was graphed as bar graph representing as mean of relative viability (n = 3) with ± SD as error bar.

List of Primers for qRT-PCR

Gene Name	**Forward Primer**	**Reverse Primer**
HDAC6	AAGTAGGCAGAACCCCCAGT	GTGCTTCAGCCTCAAGGTTC
HDAC1	GGAAATCTATCGCCCTCACA	CTCGGACTTCTTTGCATGGT
IKZF1	CCCCTGTAAGCGATACTCCA	TGGGAGCCATTCATTTTCTC
IKZF3	TCGGAGATGGTTCCAGTTATCA	ATTCTGGCGTTCTTCATGGTT
IRF4	GCGGTGCGCTTTGAACAAG	ACACTTTGTACGGGTCTGAGA
GAPDH	CTCCTCTGACTTCAACAGCGACAC	TGCTGTAGCCAAATTCGTTGTCAT
TUBA1A	CGGGCAGTGTTTGTAGACTTGG	CTCCTTGCCAATGGTGTAGTGC

Statistical Analysis.

All statistical analysis was done by GraphPad Prism. Statistical significance was analyzed by performing t-test, one-way ANOVA or two-way ANOVA analysis of variance. For ANOVA analysis, multiple group comparisons were performed with vehicle or compound-treated group were followed Dunnett correction. Not significant (ns) $P > 0.05$, $^{*}P \leq 0.05$, $^{**}P \leq 0.01$, $^{****}P \leq 0.001$, $^{****}P \leq 0.0001$.

3. Development of In-cell ELISA Assay

3.1. Introduction

As an emerging technology, PROTAC has been studied by various methods. I have discussed several methods for investigating the mechanism of action or high-throughput screening in **Chapter 1 Section 1.4**. For example, Promega Corp. combined their NanoBit and NanoBRET technology to develop a platform for quantitative real-time measurement of both ternary complex formation and target degradation[94]. For the further development of protein degraders, larger number of compounds need to be prepared and tested. The throughput of western blot cannot fulfil our need. It became more and more critical to develop a higher throughput screening method. I thus developed in-cell enzyme-linked immunosorbent assay (ELISA)[162] or cytoblot assay for measuring cellular content of target(s). As an immunocytochemistry method, it specifically detected the protein *in situ* in fixed cells. The sample capacity (96-well plate format) allowed us to test various compounds at multiple concentrations in minimal batches. This approach facilitated the development of PROTAC degraders.

3.2. Assay Condition Optimization and Method Scope

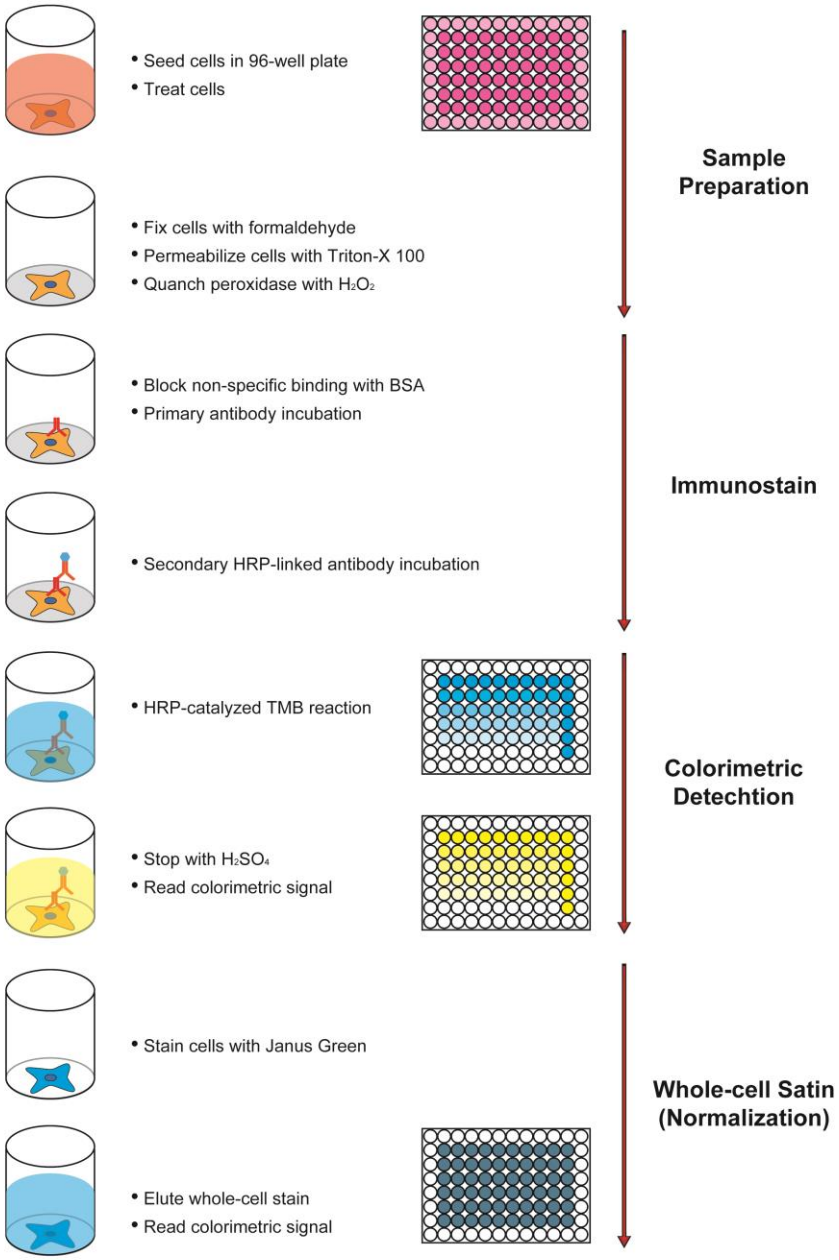

Figure 3.2.1. Workflow of in-cell ELISA

With previous experience on ELISA assay development, I combined the protocols from commercial in-cell ELISA kit (Thermo Scientific, 62200; R&D system, DY3888) and literatures[163,164]. The workflow was briefly illustrated in Figure **3.2.1**. The cells were first seeded in 96-well plate(s) overnight and treated after 6 h seeding or next day. Treatment time was generally 6 to 12 h. Then cells were fixed with formaldehyde solution and permeabilized with Triton-X. To minimize the background, endogenous peroxidases were quenched with hydrogen peroxide and potential promiscuous binding sites were blocked by bovine serum albumin (BSA). The primary anti-target antibody and horseradish-peroxidase (HRP) linked anti-specie secondary antibody were incubated sequentially. By using known TMB substrates set, HRP catalyzed the reaction between tetramethylbenzidine and hydrogen peroxide to generate product with blue colorimetric signal, which was quenched by sulfuric acid to generate endpoint yellow colorimetric signal. To normalize the signal by available cell population fixed in each well, cells were washed and stained with Janus Green Stain. Janus Green is a rapid whole cell stain for the determination of cell density[163,164].

To optimize the assay condition, I first screened HDAC6 antibodies from Cell Signaling Technology (CST, #7558, 1:500 dilution) and Santa Cruz Biotechnology (SCBT, sc-28386 and sc-28386 HRP, 1:100 dilution) in MCF-7 cells (**Figure 3.2.2. A**). I also included different dilution ratio of antibody for DMSO-treated control (**Figure 3.2.2. B and C**). The HRP-linked SCBT antibody failed to differentiate the difference between degrader-treated or vehicle-treated groups (data not shown). The maximal degradation achieved in 6 h was 50% and we observed “hook effects” at 10 μM. The CST antibody showed advantage in

both absolute signal and resolution over SCBT antibody. I repeated the method in MCF-7 once and obtained similar results (data not shown). We also found the dilution of primary antibody affected the relative signal. Although 1:1000 dilution of CST antibody yielded relatively less signal than 1:500, I found the resolution was slightly increased when comparing vehicle-treated with other conditions. Thus, I decided to use this dilution ratio for future assay optimizations and applications.

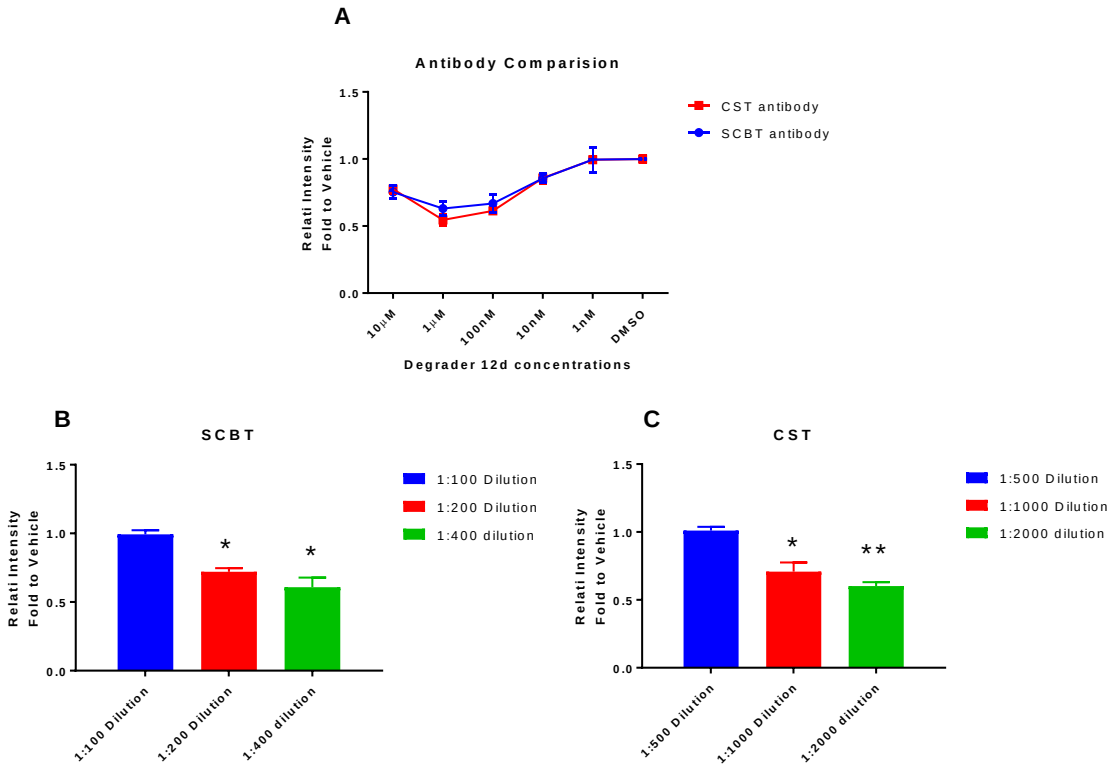

Figure 3.2.2. Condition optimization in MCF-7

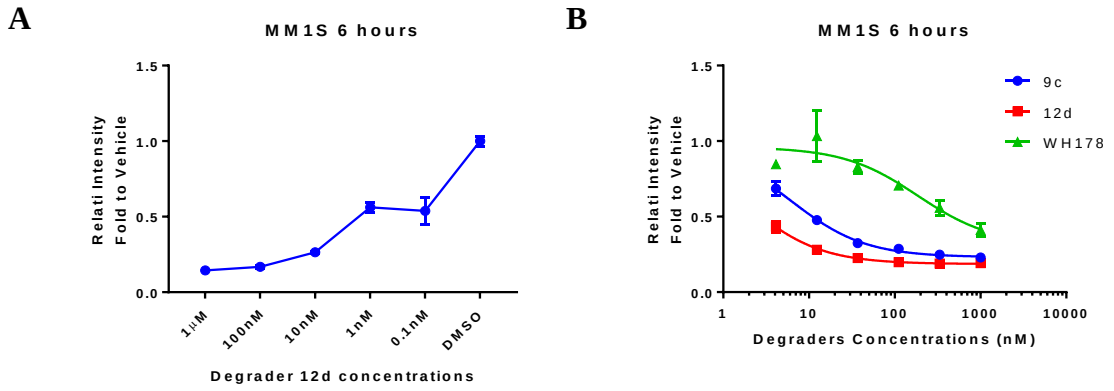

Figure 3.2.3. In-cell ELISA test of degraders in MM1S

Table 3.2.1 DC_{50} and D_{max} values calculated from Figure 3.2.3.

Cpd	DC_{50} (nM)	D_{max} (Vehicle%)
9c	6.11 ± 0.40	76.85 ± 0.73
12d	1.84 ± 0.11	81.40 ± 0.51
WH178	186.60 ± 89.15	68.56 ± 9.21

[a]The concentration at which half-maximal degradation was achieved. [b]The maximum percentage of degradation. [a,b]Values with ± SD obtained from nonlinear fitted data in **Figure 3.2.3**.

To extend the application to suspension cells, the method was tested in MM1S cells. As shown in **Figure 3.2.3**, more HDAC6 degradation was achieved in this cell line, which was consistent with previous western blot analysis of HDAC6 degraders[71]. The maximal degradation percentage at 1 μM was ~85%. No obvious hook effect was observed at this concentration range. I compared two CRBN-based degraders **9c**, **12d** and a VHL-based

degrader **WH178**, which will be discussed in **Chapter 4**, at six concentrations in MM1S. It clearly showed the dose response and the trend of potency (**12d** > **9c** > **WH178**) among degraders. The DC_{50} and D_{max} can be roughly calculated from limited data points and is shown in **Table 3.2.1**. Second-generation degrader **12d** showed a DC_{50} of ~1.8 nM and a Dmax of ~81.4%. Together with data from MCF-7 cells, these preliminary results validated the in-cell ELISA method for measuring HDAC6 expression in both adhesion and suspension cells. It provides a higher throughput method than western blot for the evaluation of the potency of HDAC6 degraders.

To further validate this method, we plated different cell numbers of MM1S or MCF-7 cells and then treated them with different concentrations of degrader **12d**. The validation in MM1S was done by collaboration with Zhongrui Zhang. We assumed the cellular HDAC6 protein content was proportional to cell number. For negative controls without any antibody, we only observed 1% to 4% signal (percentage of vehicle) in cell dependent manner (**Figure 3.2.4 A** and **Figure 3.2.5 A**), indicating that this assay only generated limited background signal. We plotted the ELISA signal by cell number, Janus Green Stain signal by cell number, ELISA signal by Janus Green Stain signal and fitted each plot with linear regression (**Figure 3.2.4 B-D** and **Figure 3.2.5 B-D**). All the linear fitting results were listed in **Table 3.2.2**. We also performed linear fitting for the raw ELISA signal by cell number and yield R^2 with a range from 0.97 to 0.99 in both cell lines. The slopes were in positive correlation with the HDAC6 expression without any normalization. The raw Janus Green Stain signal was also linear to cell number with R^2 over 0.96. Since this signal

was a direct marker of cell density, no obvious difference in slopes was observed suggesting minimal inconsistency caused by cell seeding or cytotoxicity of degraders.

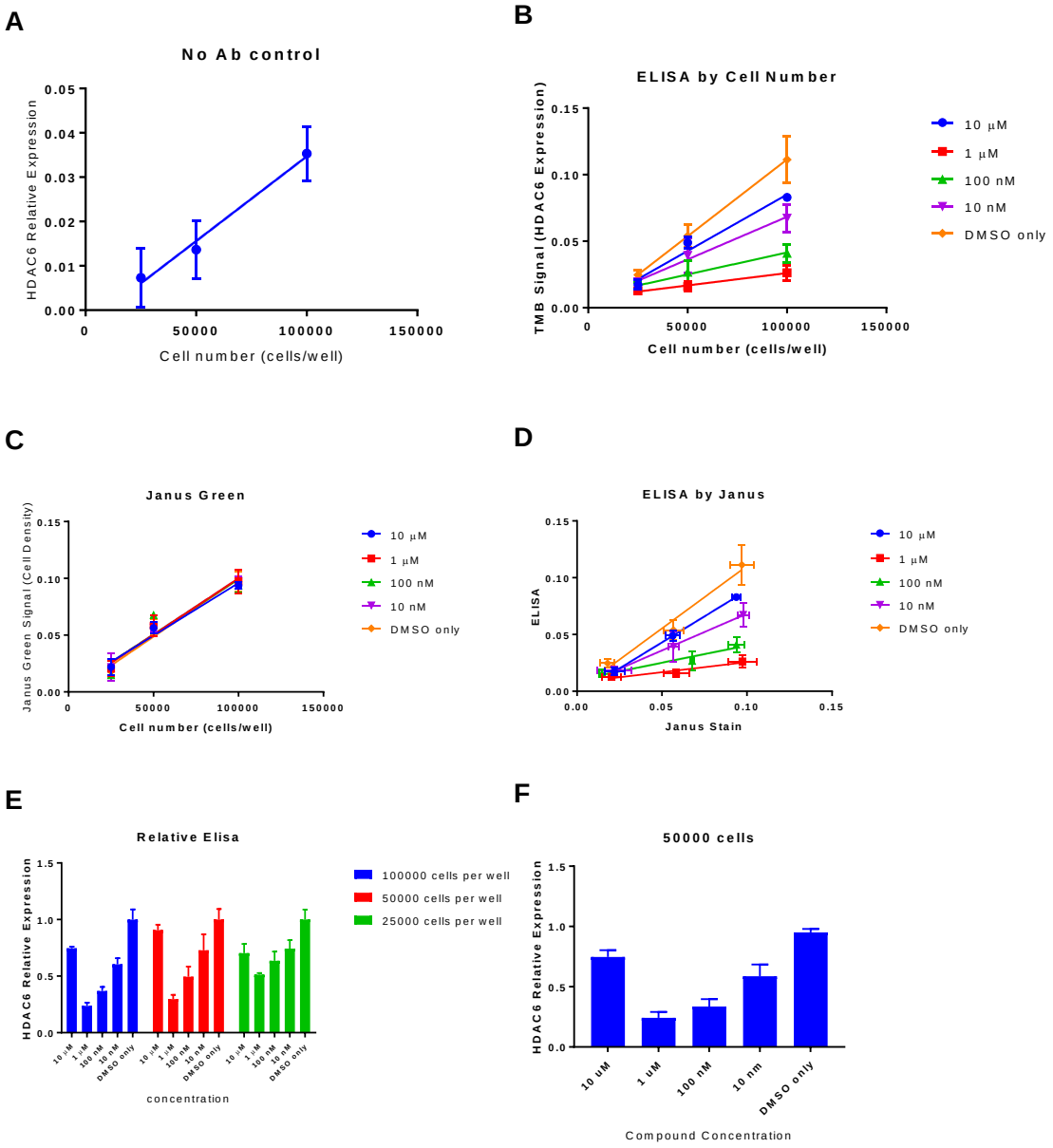

Figure 3.2.4. Validation in MM1S

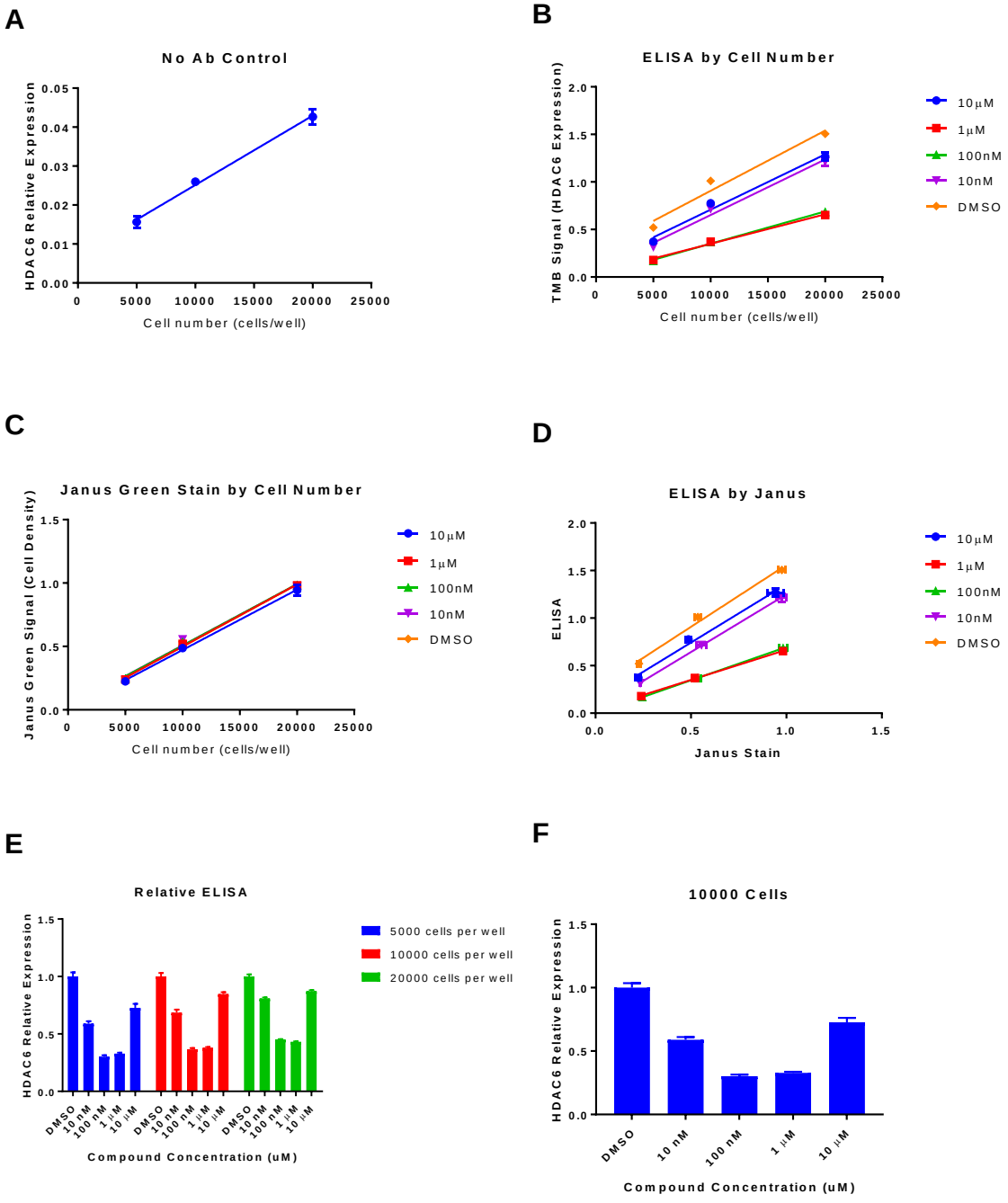

Figure 3.2.5. Validation in MCF-7

Table 3.2.2 Linear regression results of plots in **Figure 3.2.4** and **Figure 3.2.5**.

MM1S Plots in **Figure 3.2.4**						
Conditions		10 μM	1 μM	100 nM	10 nM	DMSO
ELISA	Slope ($*10^{-7}$)	8.5	1.9	3.3	6.4	11.5
by cell number	R^2	0.9715	0.9905	0.9870	0.9884	1.0000
Janus Green Stain	Slope ($*10^{-7}$)	9.3	9.9	9.8	9.8	10.2
by cell number	R^2	0.9727	0.9670	0.8590	0.9800	0.9687
ELISA	Slope	0.92	0.18	0.30	0.65	1.10
by Janus Green Stain	R^2	1.0000	0.9236	0.9285	0.9988	0.9706

MCF-7 Plots in **Figure 3.2.5**						
Conditions		10 μM	1 μM	100 nM	10 nM	DMSO
ELISA	Slope ($*10^{-5}$)	5.8	3.1	3.4	5.8	6.3
by cell number	R^2	0.9821	0.9934	0.9965	0.9836	0.9656
Janus Green Stain	Slope ($*10^{-5}$)	4.8	4.9	4.9	4.8	4.9
by cell number	R^2	0.9988	0.9974	0.9956	0.9870	0.9920
ELISA	Slope	1.23	0.63	0.70	1.21	1.30
by Janus Green Stain	R^2	0.9902	0.9991	1.0000	0.9998	0.9906

To assess the possibility of using Janus Green Stain signal (cell number) to normalize the ELISA signal, we plotted ELISA by Janus Green Stain (**Figure 3.3.4 D** and **Figure 3.3.5 D**). The R^2 obtained were all over 0.99 for MCF-7 cells. Signal obtained in 1 μM and 100 nM degrader treated MM1S likely reached the detection limit and yielded low R^2 but still above 0.92. We expected the slopes should be proportional to the HDAC6 expression. Although we also observed low HDAC6 signals by western blot for the 1 μM and 100 nM degrader treated MM1S cells (**Figure 2.3.6**), we obtained different slopes (0.18 and 0.30) for these two groups. This indicated the advantage of high sensitivity of in-cell ELISA, which could distinguish signals that are not distinguishable by western blot. However, it is difficult to use different cell numbers for actual screening. To find out the optimized cell number, we generated the final bar graph by concentrations (**Figure 3.3.4 E-F** and **Figure 3.3.5 E-F**). We found that 50,000 cells for MM1S and 10,000 cells for MCF-7 gave detectable signal and clear dose-dependent manner. Thus, we used these cell numbers for future applications in MM1S and MCF-7.

To evaluate the feasibility of high-throughput screening, I obtained the Z-factor in MM1S cells and analyzed them by the in-cell ELISA. The cells in a 96-well plate were treated with 100 nM **2d** (n = 30) or vehicle (DMSO, n = 30) for 6 h and then measured by in-cell ELISA assay. 15 samples of each treatment were added BSA-containing dilution buffer instead of primary antibody solution. These samples were considered as controls of minimal- or background-signal for corresponding treatment. Final data was normalized to vehicle (DMSO) treated group and bar graph represented as mean of relative expression (n = 15) with ± SD as error bar.

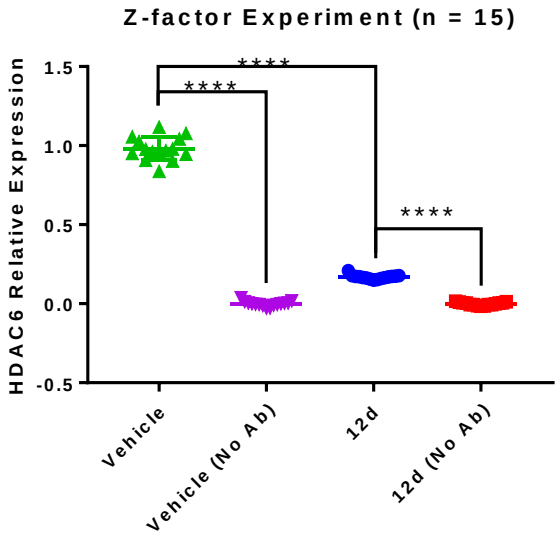

Figure 3.2.6. Evaluation for high-throughput screening

Through statistical analysis by unpaired t test, I observed significant difference of **12d** *v.s.* **12d** without primary Ab, vehicle *v.s.* vehicle without primary Ab and **12d** *v.s.* vehicle(****P $\leqslant$ 0.0001). It suggested that this assay can differentiate assay-signal *v.s.* background of all treatments. We also calculated several statistical parameters to evaluate the feasibility of this assay[165] (**Table 3.2.3**). For each treatment, the signal-to-noise ratios (S/Ns) were relatively high. There was a window or difference between the maximal degradation induced by **12d** and the corresponding no-Ab control (background), which can be regarded as the total amount of degraded HDAC6. This window indicates the sensitivity of this assay for detecting close-to-background signal. To analyze the window in each comparison set, we calculated screening window coefficient Z-factors and Z'-factor. All

factors were above 0.5 and suggested this assay would be feasible for high throughput screening, although the sample population was limited.

Table 3.2.3 Z-factors calculated from Figure 3.2.5

Comparisons	Z-Factor[a]	Signal Mean	Background Mean	S/N[b]
12d *v.s.* 1**2d** (No Ab control)	0.572	0.168673	-0.00041	16.91004
vehicle *v.s.* vehicle (No Ab control)	0.726	0.980581	-0.00127	59.55772
12d *v.s.* vehicle (**Z'-Factor**[c])	0.677		N/A	

[abc]See experimental section for details.

Using this in-cell ELISA, we screened our HDAC6 degraders discussed in **Chapter 2** and **Chapter 4** and their bioactivity were consistent with results from western blot. The successful development of potent HDAC6 degraders validated the utility of this approach.

To further expand the scope of the in-cell ELISA, I applied the same protocol to other targets by using antibodies against Ac-Tubulin, IKZF1 and IKZF3 from CST. I treated MM1S cells with different concentration of Pomalidomide (**4b**) for measuring IKZF1/3, which are neo substrates of CRBN by IMiDs[137]. I also performed the treatment of pan-HDAC inhibitor SAHA[102] and our potent HDAC6 degrader **12d** for monitor the acetylation level of Tubulin, which was the primary cytoplasmatic substrate of HDAC6[120].

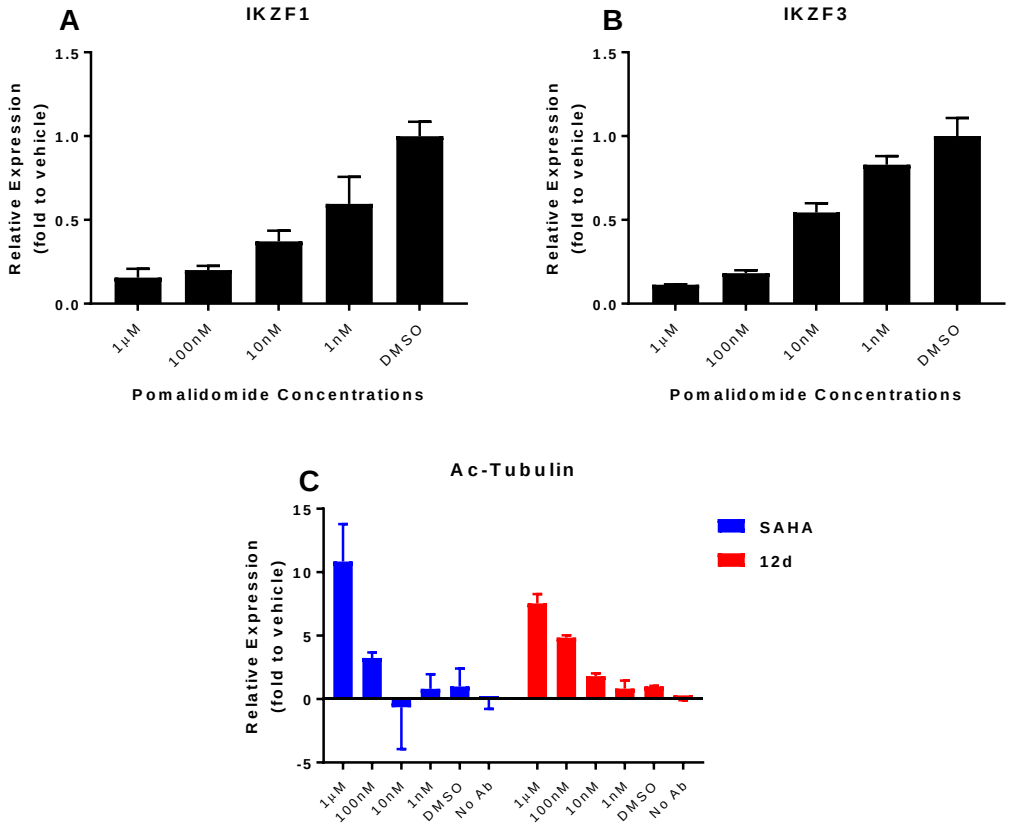

Figure 3.2.7. Application of in-cell ELISA for other protein targets

The raw ELISA data (not shown) showed strong IKZF3 signal, moderate IKZF1 signal and weak Ac-Tubulin signal, while the corresponding controls without any antibody yielded equal background signal. The different intensity of signals are primarily derived from the differences of the primary antibodies. The undesired signal intensity can be optimized in the future. For example, the strong signal of IKZF3 can be reduced by plating less cells or using less amount of primary antibodies. The weak signal of acetylated Tubulin can be increased by elongating the treatment time, adding additional amount of antibody or plating

more cells. The final normalized relative expression was showed in **Figure 3.2.7**. Although the exact conditions for each protein need further optimizations, I was still able to observe reduction of IKZF1/3 in dose-dependent manner by Pomalidomide. For tubulin acetylation, because of low overall signal and weak induction at low concentration of inhibitor or degrader, some negative values and large error bars were unexpectedly generated. But we believe this problem can be solved with further optimizations as discussed before.

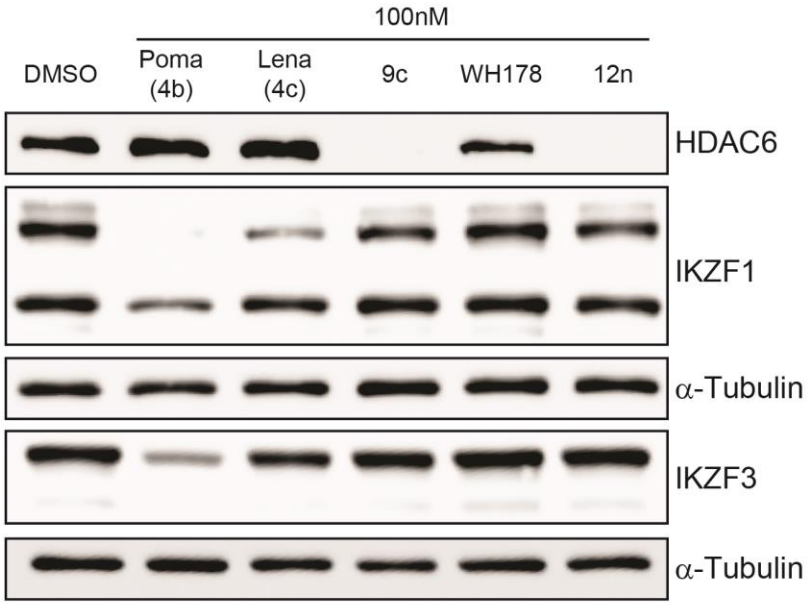

Figure 3.2.8. Western blot analysis of IKZFs after the treatment of IMiDs and degraders

To confirm the IKZF degradation observed in ELISA, we used western blot to analyze MM1S cells treated with Pomalidomide, Lenalidomide and three selected degraders (**Figure 3.2.8**). We observed more degradation by Pomalidomide than Lenalidomide at 100 nM. Degraders didn't induce IKZF1/3 degradation at this concentration, while **9c** and **12n**

showed notable degradation of HDAC6. This was consistent with previous results in **Figure 2.3.11**.

3.3. Using In-cell ELISA to Evaluate Binding Affinity for Cellular Target Engagement

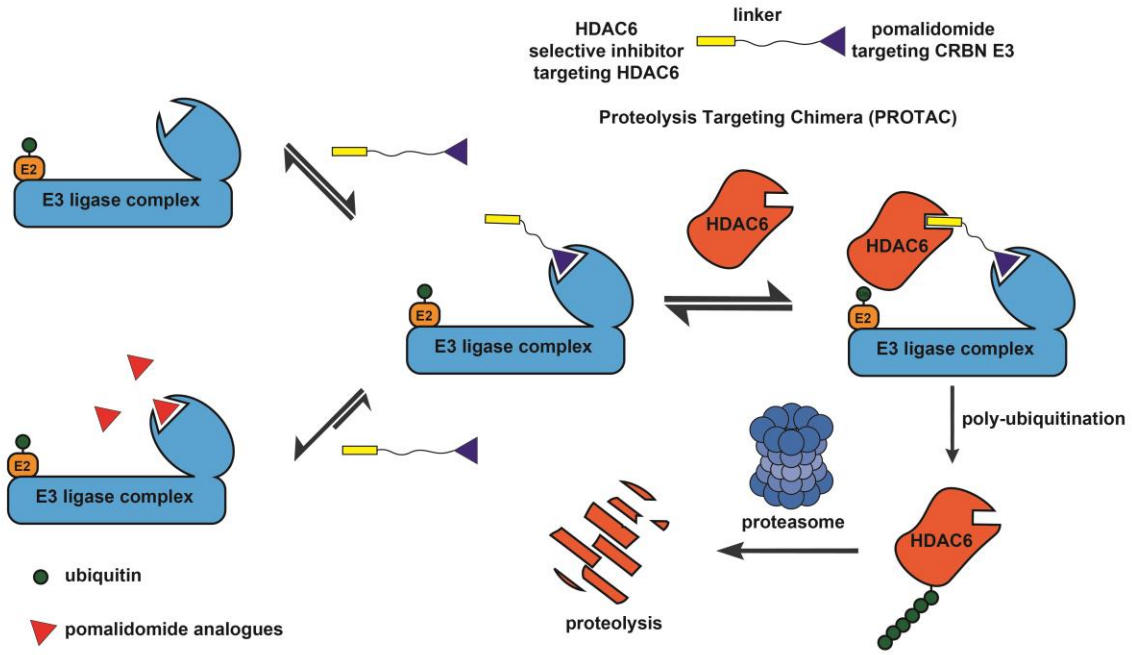

Figure 3.3.1. Illustration of target engagement study by degraders

Studying the target engagement is crucial in measuring drug efficacy and toxicity in drug discovery research[166]. Approaches to detect small molecule engaging its target has been established, such as resonance energy transfer (FRET-FILM, BRET), affinity-based chemical proteomics, ligand-directed protein labeling, enzyme fragment complementation assay and cellular shift assays[167]. For PROTAC strategy, methods to assess the degradation, ubiquitination and interactions among all participating partners have also been developed. For example, Promega designed and applied their NanoLuc technology to study the target

engagement for both targeted protein and E3 ligase[94]. To briefly describe this approach, the NanoLuc was fused ectopically with protein and served as BRET donor. Pre-occupied ligand conjugated with tracer accepted the fluorescence from NanoLuc and generated BRET signal. Any introduction of competitor ligands displaced the pre-occupied ligand and reduced the BRET signal. The fold of signal reduction was used as indicator of binding affinity of competitor ligands. However, drawbacks of this method were obvious, such like requirement of transfection/validation, limitation of targets and interference with endogenous targets. In addition, Jones and co-workers used pirin protein degrader to demonstrate the intracellular target engagement of pirin probes[168]. Through profiling different generations of probes, they discovered potent pirin degradation probe (PDP) with high affinity. We have developed potent HDAC6 degraders and in-cell ELISA for evaluating degradation efficiency. We then employed this method to develop a platform to measure binding affinity of thalidomide derivatives towards CRBN E3 ligase or inhibitor towards HDAC6 via cellular target engagement.

We showed in **Chapter 2 Section 2.2** and **Chapter 3 Section 3.2** that Pomalidomide or HDAC inhibitor "warhead" abolished the degradation effects by degraders. This was because those ligands compete with the degraders for the binding sites of either CRBN E3 or HDAC6. This competition led to less ternary complex formation after introduction of degraders as illustrated in **Figure 3.3.1**. However, in these co-treatment experiments, we had to use 5 μM Pomalidomide and 1 μM Next-A, which was 50 and 10 times the concentration of degrader, to observe notable recovery of HDAC6. We used these experiments to support the involvement of UPS in PROTAC induced HDAC6 degradation.

On the other hand, this assay also provides an opportunity to investigate the cellular engagement of targets by either ligand or bifunctional degraders. Ligands with higher affinity to their targets should compete the binding sites more effectively and abolish the effect of PROTAC degrader more effectively. We hypothesize that we can evaluate the binding affinity of a synthetic library of E3 ligase ligands using the in-cell ELISA assay.

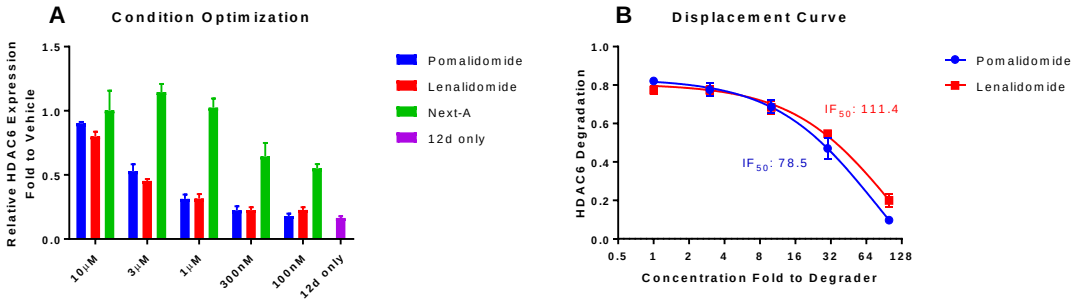

Figure 3.3.2. Assay condition optimization

To screen the conditions, I pre-treated MM1S cells with different concentrations of Pomalidomide, Lenalidomide and Next-A for 1 h and then added 100 nM degrader **12d** for 5-h treatment. The resulting cells were analyzed by in-cell ELISA (**Figure 3.3.2. A**). It showed the dose response of all three compounds. Next-A at 1 μM (10 times of degrader) or above almost completely abolished the degrader induced HDAC6 degradation. Even 100 nM Next-A was able to rescue HDAC6 to over 50%. This suggested the strong binding affinity of Next-A to HDAC6. Using this assay to develop advanced HDAC6 inhibitor will be discussed in future publication(s) beyond the scope of my work. On the other hand, Pomalidomide and Lenalidomide are less effective to abolish the effect of degraders for the E3 ligase binding site. With pre-treatment of 10 μM (100 times of degrader), there was

still 10-20% of HDAC6 remained. We chose 3 µM, where ~50% of HDAC6 were remained, as the condition for future application. This concentration provided us an ideal window to compare the thalidomide derivatives with the parent compound. A potent analogue at this concentration will inhibit more HDAC6 degradation and yield over 50% HDAC6 expression. A weaker ligand would recover less HDAC6. The HDAC6 relative expression was also correlated with concentration fold of compound to degrader (**Figure 3.3.2. B**). The IF_{50} is half maximal inhibitory fold or the folds of compound to degrader where HDAC6 degradation was abolished by half. Pomalidomide and Lenalidomide yielded IF_{50} with 78.5 folds and 111.4 folds respectively. It indicated Pomalidomide was the one with slightly higher affinity to CRBN E3.

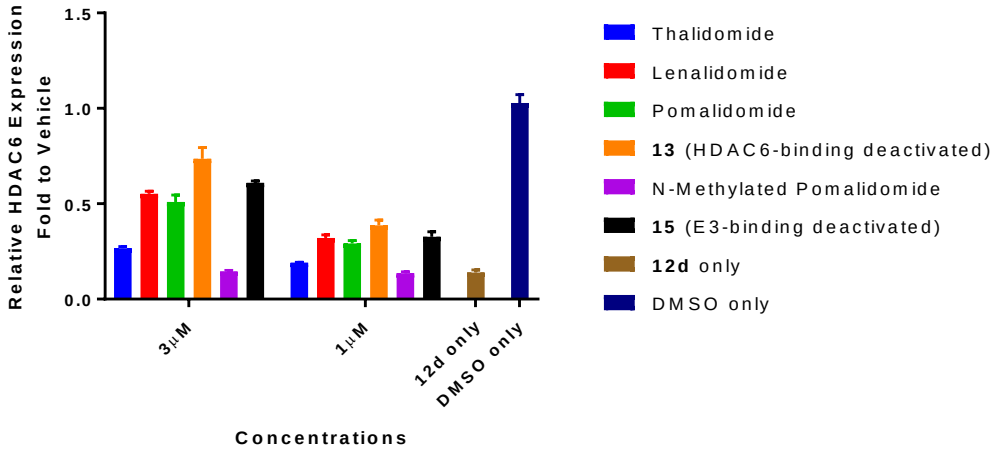

Figure 3.3.3. Proof of principle experiment

To further validate this target engagement assay, we compared three well-known IMiDs as well as degraders with or without deactivation (**Figure 3.3.3**). The binding affinity of Thalidomide, Pomalidomide and Lenalidomide to CRBN has been reported in

literatures[38,148,149,169]. Generally, Pomalidomide is slightly better than Lenalidomide while Thalidomide was the weakest. This potency order was also verified by our results. Thalidomide had the least HDAC6 recovery compared with the other two at both 3 μM and 1 μM. Our assay failed to distinguish the small difference between Pomalidomide and Lenalidomide. We also used a known negative control, *N*-Methylated Pomalidomide (**14**), which does not bind to CRBN E3 and should not lead to degradation of IKZF [42]. **14** was indeed not able to recover any HDAC6 as expected. Deactivated degrader **13** bearing carboxylic ester recovered ~50% and ~20% degraded HDAC6 at 3 μM and 1 μM respectively. The stronger effect for abolishing HDAC6 degradation by **13** than that of IMiDs might be the result of hydrolysis of the ester to carboxylic acid, a weak binding moiety for Zn^{2+} cofactor. This is consistent with previous western blot analysis showing moderate degradation of HDAC6 caused by **13** (**Figure 2.3.15**). Deactivated degrader **15** was based on **14**, which cannot bind to CRBN. **15** recovered ~45% and ~15% degraded HDAC6 and was weaker than Next-A, which might be due to lower cell permeability of **15** compared to Next-A. Overall, the above results indicated that the in-cell ELISA assay was able to differentiate the binding affinity of thalidomide derivatives through cellular target engagement.

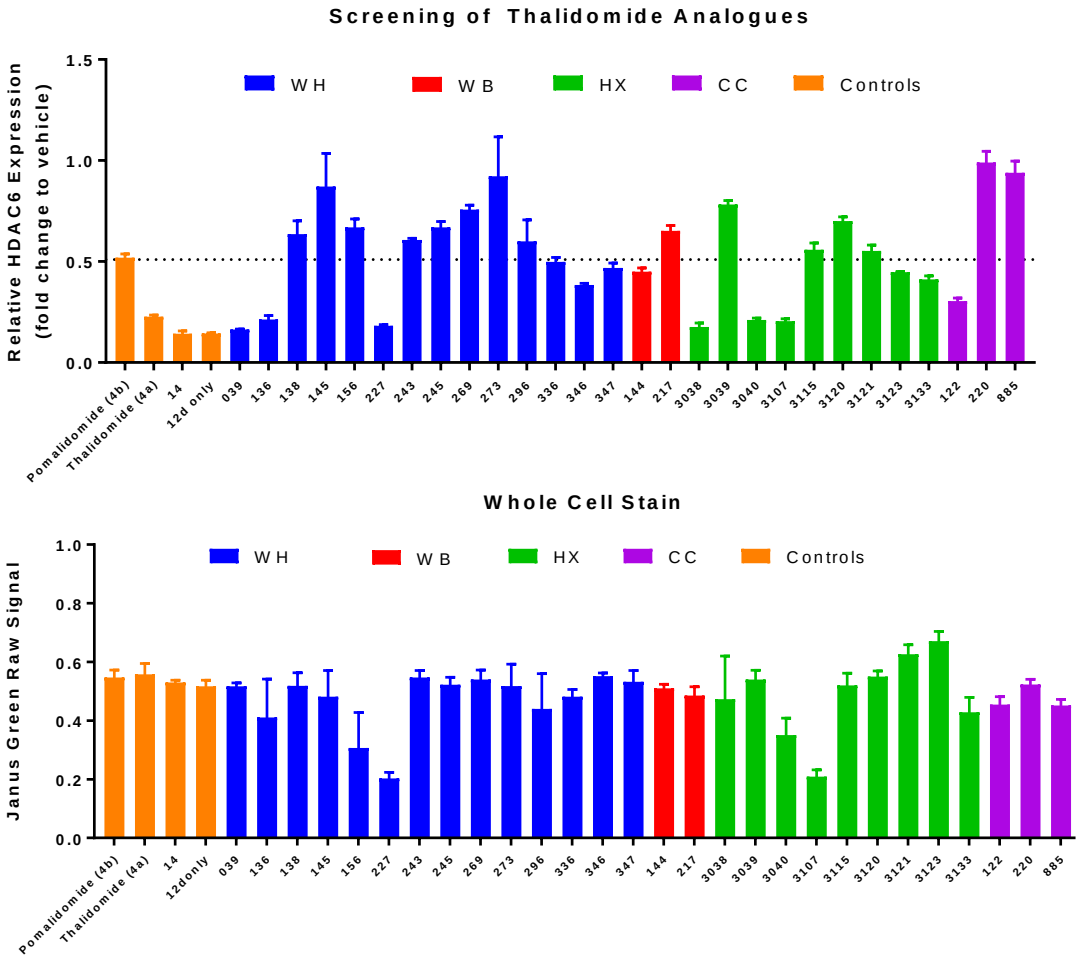

Figure 3.3.4. Screening of chemical intermediates towards PROTACs

After validating the assay, I started screening selected thalidomide analogues generated during the synthesis of PROTACs. Those compounds were divided into four series according to the chemists who made them, WHs from Dr. Hao Wu, WBs from Dr, Bo Wang, HXs from Dr Haibo Xie, and CCs from commercial vendors originally generated by Celgene Corporation. I used Pomalidomide and Thalidomide as positive controls and

N-Methylated Pomalidomide (**14**) as the negative control. The results are shown in **Figure 3.3.4**.

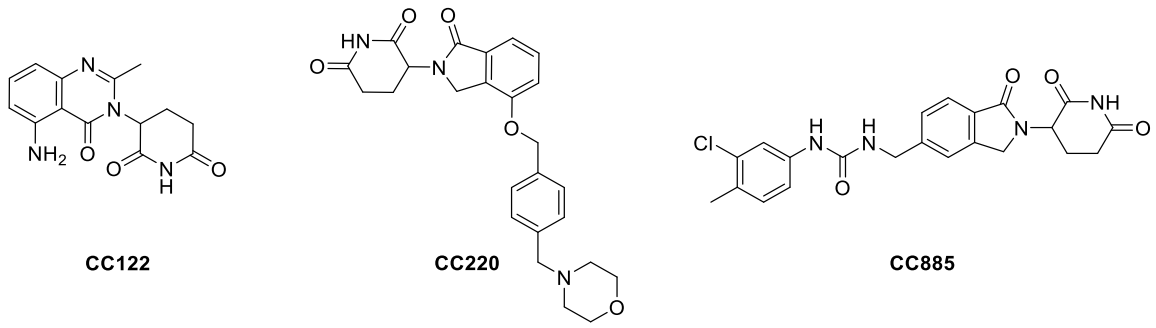

Figure 3.3.5. Structures of CC-122, CC-220 and CC-885

CC-122 (Avadomide)[170], CC-220 (Iberdomide)[171] and CC-885[46] are known IMiDs that bind to CRBN (**Figure 3.3.5**). CC-220 was tested for binding affinity towards CRBN by TR-FRET and had a IC_{50} of 60 nM, while the IC_{50}s for Pomalidomide and Lenalidomide are 1.2 μM and 1.5 μM, respectively[171]. We evaluated these three compounds in our cell-based assay. CC-122 was less potent than Pomalidomide. Both CC-220 and CC-885 remarkably reduced HDAC6 degradation, which are consistent with their high affinity to CRBN as reported in literature. However, CC-885 can recruit both IKZFs and GSPT1 as neo substrates to CRBN and promote their degradation[46,172]. This suggested using CC-885 as the ligand might introduce unexpected off-target effect for PROTAC degraders based on it. Further SAR studies may minimize this undesired effect. CC-220 is a promising candidate as a ligand of PROTACs.

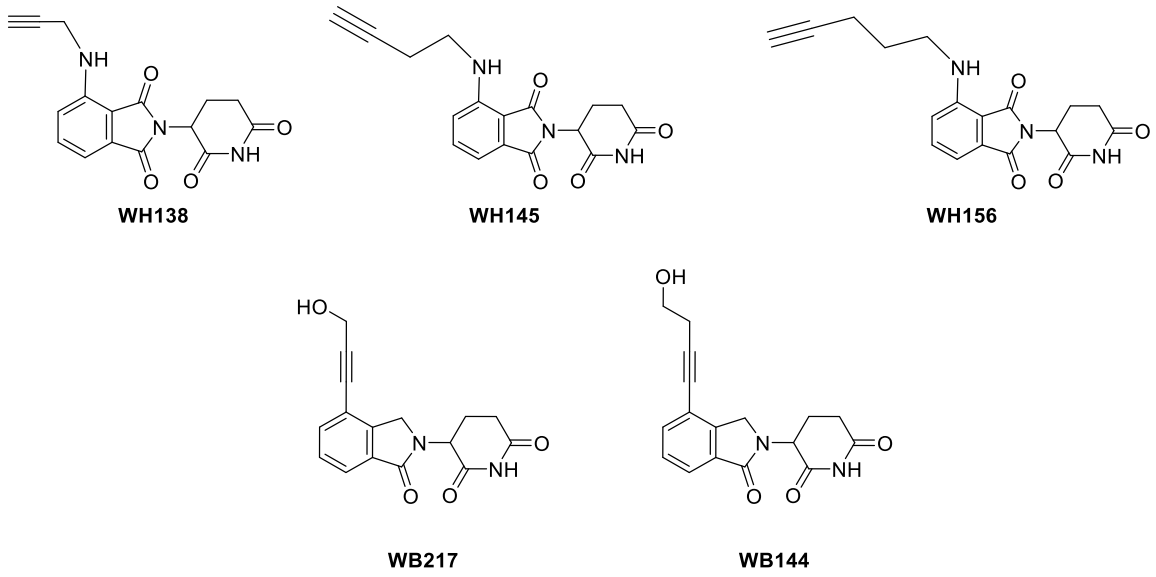

Figure 3.3.6. Structure of thalidomide derivatives with alkyne moiety.

Among the in-house-synthesized intermediates, we discovered that a series of thalidomide derivatives bearing alkyne moiety might be promising candidates as ligands of CRBN. WH138, WH145 and WH156 were pomalidomide derivatives linked with terminal alkynes via alkyl linkers of different lengths. All of them showed better affinity than Pomalidomide and WH145 with linker of two carbon units was the best. This SAR highlighted the importance of the terminal alkyne for this series compounds to bind to CRBN. PRTOAC(s) can be constructed based on WH145 in the future. WB217 is a thalidomide derivative with hydroxyl propyne and showed promising activity. But WB144, which is only one carbon different from WB217, showed weaker activity, suggesting that linker length plays an important role. Derivatives bearing hydroxyl propyne may be used for the development of novel PROTACs in the future. It is worth to point out that we observed less cells for some compounds, such WH156, WH227 and HX3107. It was suspected that these compounds

might cause cell death. However, no inhibition of cell growth was observed in the anti-proliferation assay using MM1S cells. Overall, the in-cell ELISA allowed us to identify several candidates as potential ligands to recruit E3 ubiquitin ligase for the development of PROTACs.

3.4. Discussion and Conclusion

There are several advantages for in-cell ELISA over the sandwich ELISA . The latter requires two distinct antibodies to recognize the antigen or targeted protein. These two antibodies need to recognize different sequences or domains of the target. One serves as the capture antibody (or primary antibody), which is immobilized on plate to bind to the antigen in the sample. The other one serves as the detection antibody (or secondary antibody), which is linked to an enzyme or a signal amplifying agent, and specifically binds to the target and generates colorimetric or fluorescent signals. The sandwich ELISA often takes significant amount of efforts to identify the proper antibody combinations and the optimal conditions, such as dilution ratio, incubation time and positive controls (protein standards). The in-cell ELISA is more flexible and we can often adopt the western-blot conditions, such as procedures, reagents and antibodies. We indeed used the same protocol to quantify HDAC6, IKZF1, IKZF3 and acetylated tubulin, though further optimization may be needed for some other targets.

Sandwich ELISA assays often have better detection limits than in-cell ELISA. For sandwich ELISA, the capture of antigens by primary antibody is also an enrichment of the antigen in samples, which increases the detection limit. For in-cell ELISA, the protein level

is directly associated with the number of cells seeded in plate. Without enriching antigen, it is more challenging to detect low abundant proteins in limited cell population.

To conclude, we developed cell-based ELISA assays for quantifying the protein expression in formaldehyde-fixed cells. We validated the signal linearity by cell numbers. We also validated this assay for high throughput screening (Z factor > 0.5). We screened several series of compounds using the in-cell ELISA assay. The results allowed us to analyze the structure activity relationship and provided insights for the development of new PROTACs. In addition to screening protein degraders, we also used the in-cell ELISA assays to quantify the binding affinity of thalidomide derivatives through cellular target engagement. HDAC6 degradation was used as readout to evaluate the potency of ligands to competitively occupy the binding pocket of E3 ligase. We validated the assay using known thalidomide analogues. After profiling the synthetic intermediates and other IMiDs, we identified several candidates with promising affinity. These CRBN ligands may be used as either candidates of anti-myeloma therapeutics or E3 recruiting ligands for PROTAC development.

3.5. Experimental Procedures

Cell Culture and Treatment

MM1S were cultured in RPMI-1640 medium (Corning) supplemented with 10% FBS, 1% Sodium Pyruvate, and 1% Penicillin/Streptomycin, 10mM HEPES. MCF-7 cells were cultured in DMEM medium (Corning, 4.5g/L glucose) supplemented with 10% FBS and

1% Penicillin/Streptomycin. Both cell lines were grown at 37°C in a humidified 5% CO_2 atmosphere.

MM1S cells were harvested and plated with $5x10^4$ cells in 100µL media per well 96-wells plate. After overnight seeding, 25 µL media containing 5X dosing concentration of the compounds or vehicle was added to each well. For target engagement experiment, 12.5 µL media containing 10X dosing concentration of the thalidomide derivative or vehicle was added to each well, followed by 1-hour incubation and then addition of 12.5 µL media containing 10X dosing concentration of WH181 (**12d**) or vehicle.

In-cell ELISA Assay.

After 5-hour treatment at 37°C in a humidified 5% CO_2 atmosphere, cells were fixed by adding 125 µL 8% formaldehyde in TBS buffer (137 mM NaCl, 25 mM Tris, 2.7 mM potassium chloride, pH 7.6). and incubated at room temperature (RT) for 15 minutes. Removal of fixing solution was followed by once rinse and twice washes with TBS-T washing buffer (137 mM NaCl, 20 mM Tris, 0.1% Tween, pH 7.6). Cells were then permeabilized by adding 100 µL 0.1% Triton-X in TBS and incubated at RT for 15 minutes. Removal of permeabilizing solution was followed by once rinse and once wash with TBS-T. Cellular endogenous peroxidases were quenched by adding 100 µL 1% H_2O_2 in TBS and incubation at RT for 20 minutes. Removal of quenching solution was followed by once rinse and once wash with TBS-T. Non-specific binding sites were blocked by adding 200 µL 5% BSA in TBS-T (with 0.02% NaN_3) and incubation at 4 °C overnight. Removal of blocking solution was followed by adding 50 µL primary antibody solution (HDAC6

Rabbit mAb, CST #7558, 1:1000 in 5% BSA in TBS-T with 0.02% NaN_3) and incubation at RT for 2 hours. Note: ELISA assay was also applied to other proteins by using antibodies against IKZF1 (#5443), IKZF3 (#15103) and Ac-α-Tubulin (K40, #5335) from CST. Two or more wells treated with DMSO or untreated were added blocking solution without antibody as background control. Removal of primary antibody solution was followed by once rinse and three times washes with TBS-T. Secondary antibody solution (Anti-rabbit IgG, HRP-linked Antibody, CST #7074, 1:2000 in 1% BSA in TBS-T) was added into cells and incubated at RT for 1 hour. Removal of secondary antibody solution was followed by once rinse and four times washes with TBS-T. TMB substrates (BioLegend #421101) were premixed, added into cells and incubated in dark at RT for 20 minutes. Stop solution (2N H_2SO_4 in ddH_2O) was added into reaction mixture and incubated at RT for 5 minutes with gentle shaking. The optical density (OD) of each well was read at 450 nm and 570 nm by FLUOstar Omega microplate reader (BMG LABTECH). ELISA OD was obtained by subtracting the OD_{570} from OD_{450}.

Janus Green Stain

Normalization of ELISA OD to cell number was processed by Janus Green Stain[163]. Removal of stop solution from last step was followed by once rinse and three times washes with TBS-T. 50 µL of 0.3% Janus Green B in TBS was added to cells and incubated for 5 minutes. Removal of stain solution was followed by twice rinses and three times washes with TBS-T. Cells were quickly rinsed with 100 µL 140 mM NaCl solution and then exposed to 0.5 M HCl in 100 µL 140 mM NaCl. Cells were incubated at RT for 5 minutes with medium shaking. The Janus Green OD of each well was read at 595 nm.

Calculation of Relative HDAC6 expression

The normalized signal (NS) was calculated by followed formula:

$$NS = \frac{ELISA\ OD\ of\ sample - ELISA\ OD\ of\ background\ control}{Janus\ Green\ OD}$$

The relative HDAC6 expression was calculated by divide NS of compound treated well by average NS of vehicle/DMSO treated wells and marked as "relative HDAC6 expression % of vehicle". Normalized data were generated bar graph or dot plot representing mean relative expression (n = 3) with ± SD as error bar. For dose response, nonlinear fitting of [Iinhibitor] vs. response (three parameters) was generated by GraphPad Prism with R^2 over 0.95.

Calculation of Statistical parameters

All parameters were calculated based on literature reported method[165]. To briefly described here. The signal-to-noise ratio (S/N) was calculated by followed formula:

$$S/N = \frac{Mean\ Signal - Mean\ Background\ Signal}{Standard\ Deviation\ of\ Background}$$

The Z-factors was calculated by followed formula:

$$\text{Z-factor} = 1 - \frac{(3\sigma_a + 3\sigma_b)}{|\mu_a - \mu_b|}$$

μ_a was the mean of assay signals; $\mu_b$was the mean of background signals (no Ab controls); σ_a was the standard deviation of assay signals; σ_b was the standard deviation of background signals (no Ab controls).

The Z'-factors was calculated by followed formula:

$$\text{Z'-factor} = 1 - \frac{(3\sigma_{c+} + 3\sigma_{c-})}{|\mu_{c+} - \mu_{c-}|}$$

Degrader 12d treated group was positive control (C+) and DMSO treated group was negative control (C-). μ_{c+} was the mean of signals of C+; $\mu_{c-}$was the mean of C-; σ_{c+} was the standard deviation of C+; σ_{c-} was the standard deviation of C-.

Calculated Z-factor or Z'-factor was evaluated as followed table:

Z-factor value	1	1 > Z ≥ 0.5	0.5 > Z > 0	0	< 0
Related to screening	An ideal assay	An excellent assay	A doable assay	A "yes/no" type assay	Screening essentially impossible

Statistical Analysis.

All statistical analysis was done by GraphPad Prism. Statistical significance was analyzed by performing two-tailed and unpaired t-test of variance. Not significant (ns) $P > 0.05$, $^{*}P \leq 0.05$, $^{**}P \leq 0.01$, $^{****}P \leq 0.001$, $^{****}P \leq 0.0001$.

4. Development of HDAC6 Degraders by Recruiting VHL E3 Ligase

4.1. Introduction

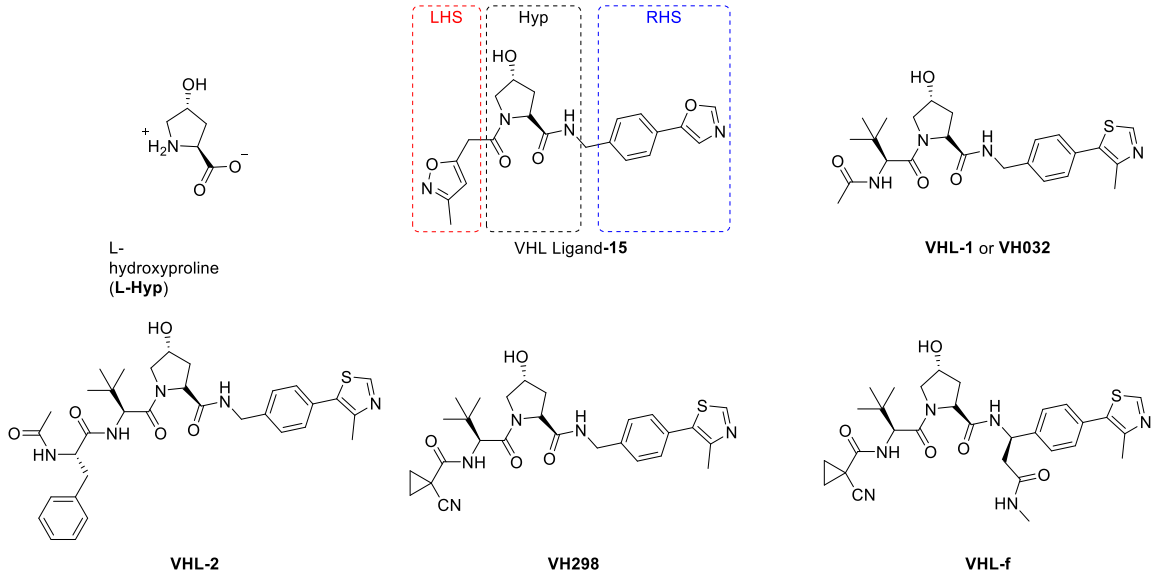

Figure 4.1.1 Structure of VHL ligand and featured VHL degraders

Von Hippel-Lindau tumor suppressor protein (VHL or pVHL) is part of the VBC E3 ubiquitin complex (VHL, elongins B and C, Cul2 and Rbx1)[173]. VHL recognizes hypoxia inducible factor 1α (HIF-1α), a transcriptional factor related to metabolism, angiogenesis and apoptosis, and the E3 complex drives HIF-1α for proteasomal proteolysis[174]. Early PRTOACs use small peptides or peptidomimetics to recruit E3 ligases for targeted protein degradation[12,17]. A seven amino acids sequence ALAPYIP was identified as the minimal domain of HIF-1 recognized by VHL[18]. Crews and co-workers employed this sequence and conjugated it with AP21998 and dihydrotestosterone (DHT) to create PROTAC

targeting $FKBP^{F36V}$ and AR, respectively[17]. Structural analysis indicated that the residue Hyp546 on HIF-1 was crucial for the interaction between HIF-1 and VHL[18,175]. Crews, Ciulli and their co-workers adopted the L-hydroxyproline (L-Hyp) as the core structure for the design and development of small-molecule VHL ligands (**Figure 4.1.1**). The most potent VHL ligand-15 ("15" as the compound number in original article) bearing phenyl chloride and oxazole moiety had a IC_{50} of 4.1 μM based fluorescent polarization assay and a K_d of 5.4 μM in ITC. In their later studies, the phenyl chloride part was defined as right hand side (RHS) and oxazole moiety was defined as left hand side (LHS) according to their positions to Hyp. Ciulli and co-workers optimized the ligand-15 to VHL-1/VH032, VHL-2 and VH298[29,176] with nanomolar K_ds. The novel ligands VHL-1 and VHL-2 were landmarks for PROTAC development. They showed that the carbonyl group on terminal amide of LHS formed water-bridged hydrogen bond with Asn67 and His115[29]. Thus, it allowed researchers to synthesize intermediates bearing a primary amine that can be linked to any ligand targeting protein of interest with a amide bond[3,9,30,32,49,52,72] without losing that hydrogen binding. Wang and co-workers also developed VHL-d, which could be linked from RHS region through a similar strategy[61].

We have developed two generation of CRBN-based HDAC6 degraders, which is discussed in **Chapter 2**. Candidate compounds, such as **12d**, showed promising anti-myeloma effects due to synergistic effects of HDAC6 degradation/inhibition and IKZFs degradation. However, IKZFs degradation is not always desired and the pomalidomide moiety has many other potential neo –substrates besides IKZFs[169]. To develop "cleaner" degraders with minimal off-targets, we designed the third-generation of HDAC6 degraders using

hydroxyproline ligand to recruit VHL E3 ligase. Dr Hao Wu synthesized all VHL-based degraders and ligands discussed in this section.

4.2. Degrader Design and Development

To explore the feasibility of recruiting VHL E3 ligase to HDAC6, we synthesized a series of degraders by tethering Next-A with VHL ligand VH032/VHL-1[32] via alkyl linkers of various length. The initially synthesized nine degraders include m + 2 (WH173, WH174, WH175), m + 3 (WH170, WH167, WH169) and m + 4 (WH185, WH177, WH178). Screening of these compounds in our established cell-based assays yielded functional and potent VHL-based HDAC6 degraders as discussed below. The structures of these degraders are summarized in **Table 4.2.1**.

Table 4.2.1 Structures of VHL-based HDAC6 degraders.

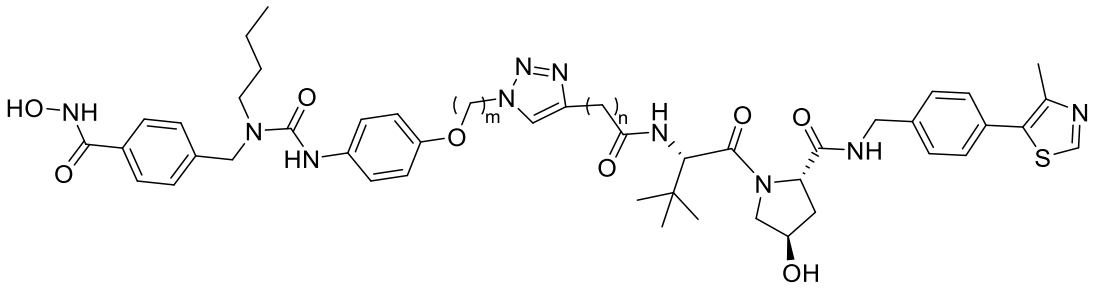

Cpd	WH173	WH174	WH175	WH170	WH167	WH169
m	2	3	4	2	3	4
n	2	2	2	3	3	3

Cpd	WH185	WH177	WH178	WH223	WH225	WH255
m	2	3	4	5	6	7
n	4	4	4	4	4	4

Cpd	WH256	WH258	WH315	WH316	WH317
m	8	9	10	11	12
n	4	4	4	4	4

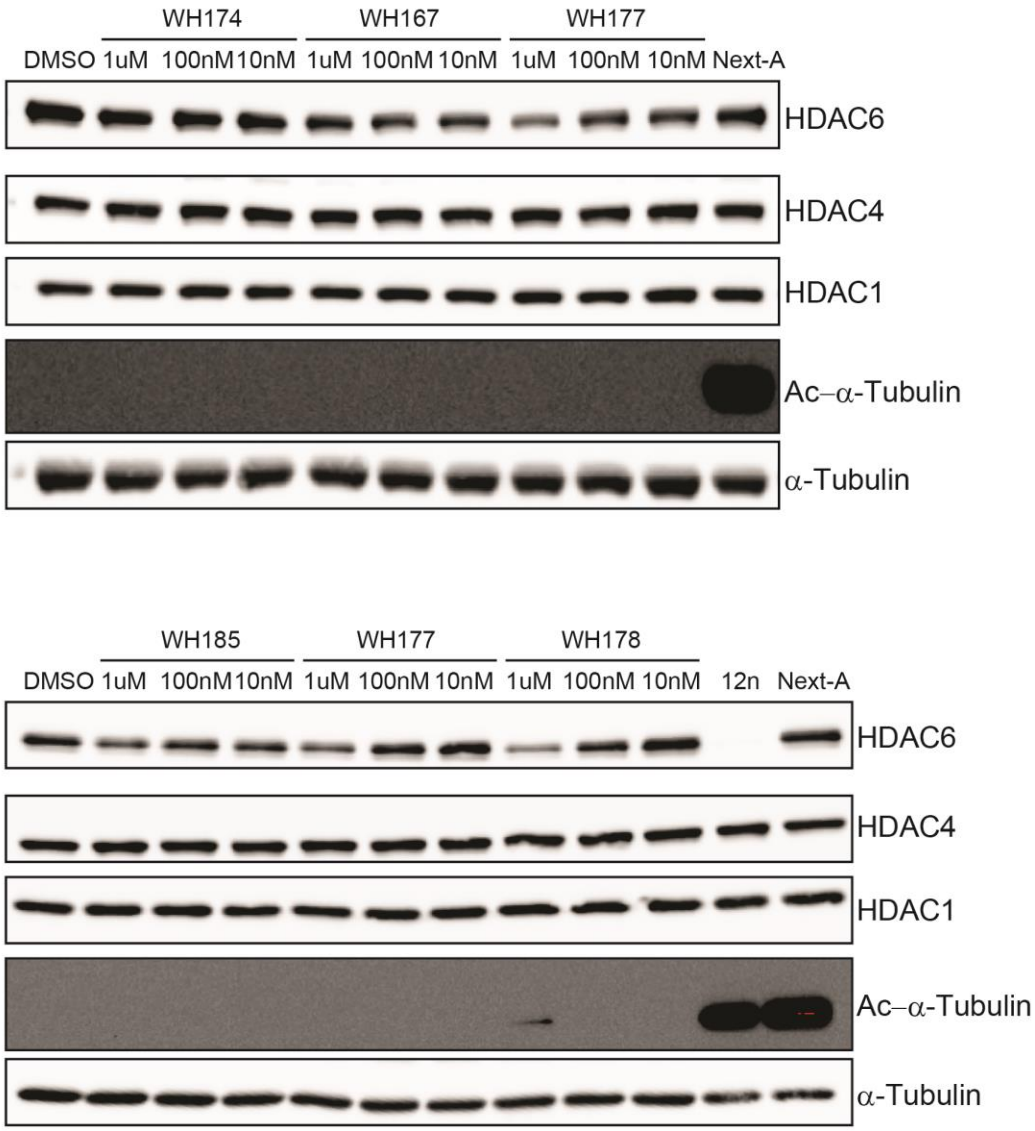

Figure 4.2.1. Western blot analysis of selected VHL degraders in MM1S

To examine the effect of the linkers, we tested WH174, WH167 and WH177 at three concentrations (1 μM, 100 nM and 10 nM) for their HDAC6 degradation activity in MM1S cells (**Figure 4.2.1**). All these three were the ones with medium lengths of linkers within each series. Only WH177 at 1 μM reduced the HDAC6 expression while the other two are

almost inactive. We then moved forward to test all three compounds in m + 4 series (Figure 4.2.2). WH178 induced significant degradation of HDAC6, while WH185 and WH177 were much less effective. Collectively, our results suggested that, at least for the initial set of PROTACs, compounds with longer linker could induce more degradation of HDAC6. In addition, we didn't observe any degradation of HDAC1 and HDAC4, indicating that the HDAC6 was selectively targeted and degraded. However, it is known that Next-A is a selective HDAC6 inhibitor based on biochemical assays. It is possible to develop degraders for other HDACs if we employ a nonselective HDAC inhibitor and a VHL ligand.

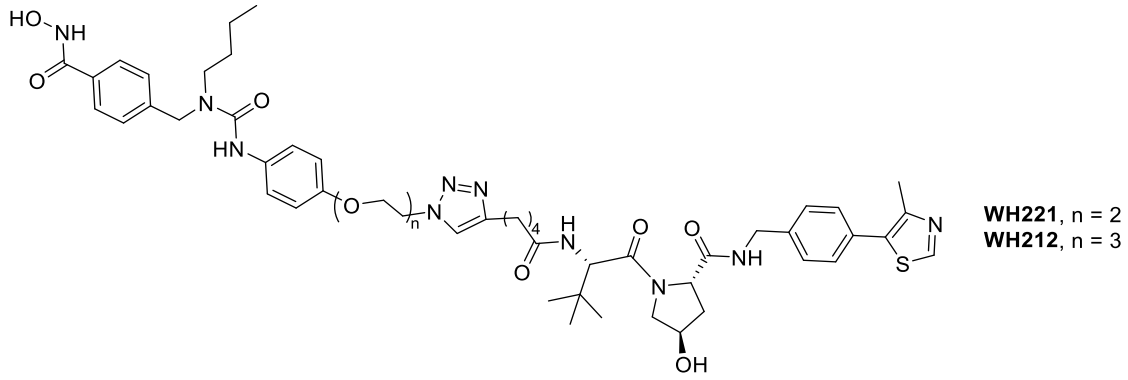

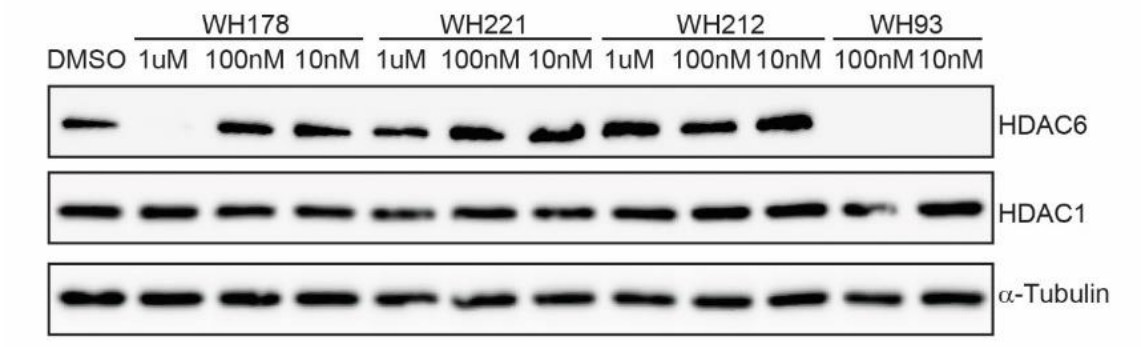

Figure 4.2.2. Western blot analysis of WH178 with PEG-linked VHL degraders.

Along with degraders with alkyl linkers, we also synthesized $(PEG)_n$ + 4 series degraders containing PEG units, such as WH221 and WH212. However, comparing with WH178, no obvious degradation of HDAC6 or HDAC1 was achieved by PEG degraders (**Figure 4.2.2**). These longer linkers with hydrophilic property didn't show any improved potency. It suggested PEG linker was unfavored for this type of degraders, though the reason is not clear.

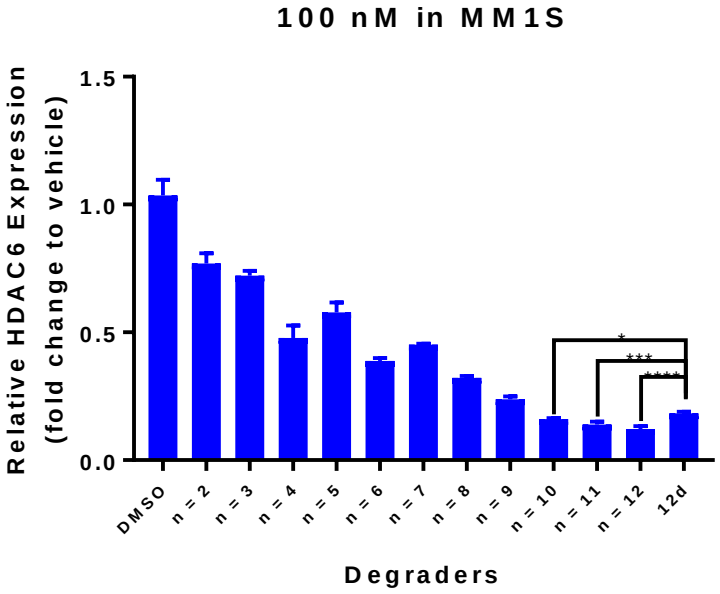

Figure 4.2.3. In-cell ELISA of m + 4 series and **12d** in MM1S.

To investigate the effect of linker lengths on the degradation efficiency of VHL degraders, we developed more compounds in m + 4 series as summarized in **Table 4.2.1**. The carbon units between HDACi moiety and triazole ring ranged from m = 2 to m = 12. We tested all 11 VHL degraders at 100 nM and compared them with CRBN degrader **12d** in MM1S. The resulting cells were analyzed for HDAC6 expression by in-cell ELISA (**Figure 4.2.3**).

We observed a clear trend of increased potency as the linker length increased from WH185 (m = 2) to WH317 (m = 12). The three most potent compounds, WH315, WH316 and WH317, induced slightly more degradation than **12d**. Statistical significance was analyzed by One-way ANOVA using Dunnett's multiple comparisons test and "**12d**" as the control **Figure 4.2.3**. (Not significant (ns) P > 0.05, *P ⩽ 0.05, ***P ⩽ 0.001, ****P ⩽ 0.0001.) It suggested that degraders based on VHL ligands depleted HDAC6 more efficiently at this concentration compared with degraders based on CRBN ligands.

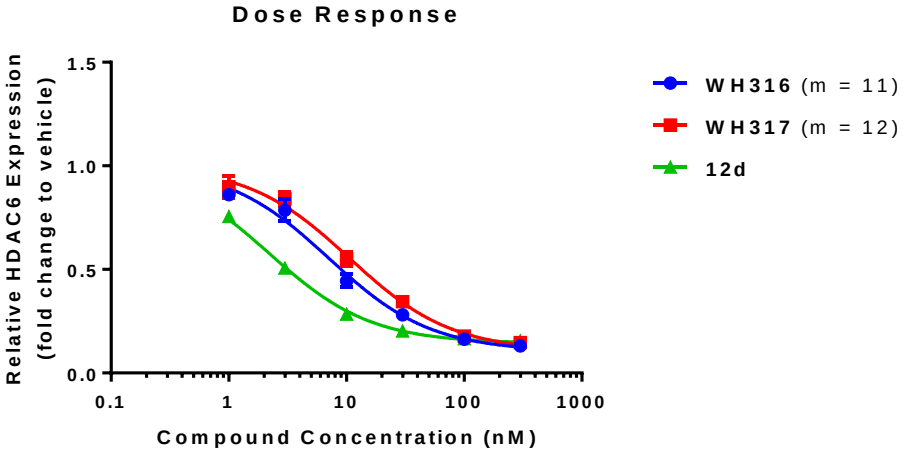

Figure 4.2.4. Dose response of selected candidates by In-cell ELISA.

Table 4.2.2 DC_{50} and D_{max} calculated from **Figure 4.2.4**.

Cpd	DC_{50} (nM)	D_{max} (Vehicle%)
12d	2.20 ± 0.12	85.69 ± 0.71
WH316	7.08 ± 0.75	89.53 ± 1.70
WH317	10.62 ± 1.04	89.48 ± 1.71

[a]The concentration at which half-maximal degradation was achieved. [b]The maximum percentage of degradation. [a,b]Values with ± SD obtained from nonlinear fitted data in **Figure 4.2.4**.

To differentiate the efficiency of degraders, we performed dose response study of WH316, WH317 and **12d** at concentrations ranging from 1 nM to 3 μM for 6 h in MM1S (**Figure 4.2.4**). The calculated DC_{50} and D_{max} from limited data points were listed in **Table 4.2.2**. The DC_{50} obtained for **12d** was 2.2 nM, which was similar to previous one (1.6 nM) from full dose response. WH316 and WH317 were less potent in terms of DC_{50}. However, both of them showed larger D_{max} (89.5%) than that of **12d** (85.6%). It requires more degraders based on VHL-ligands to achieve similar degradation of HDAC6 as degraders derived from CRBN ligands. But degraders based on VHL-ligand depleted more HDAC6 than degraders derived from CRBN ligands at higher concentrations.

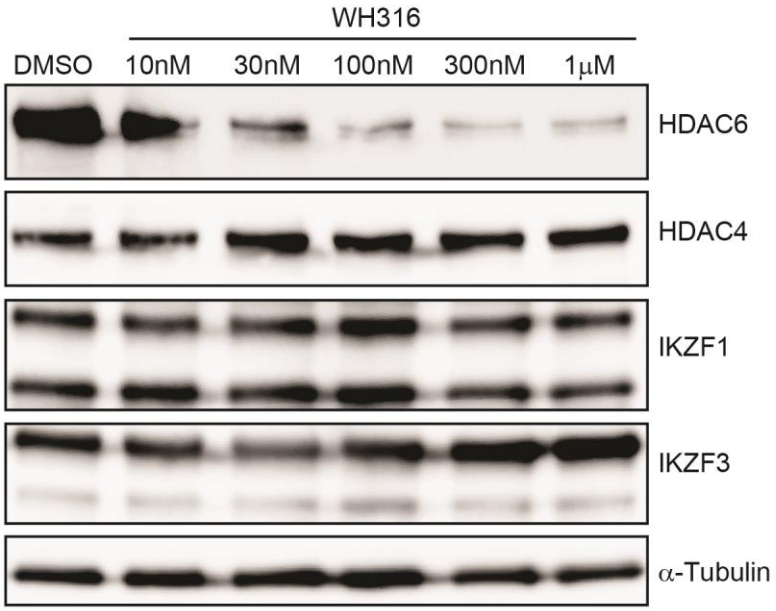

Figure 4.2.5. Dose response of WH316 by western blot.

To confirm the ELISA results, we used western blot to analyze the proteins expression under different concentrations of WH316 (**Figure 4.2.5**). As we expected, HDAC4, IKZF1 and IKZF3 were not affected by HDAC6 degraders derived from VHL ligands. HDAC6 was degraded remarkably at 30 nM of the degrader and the maximal effect was reached around 100 nM, which was consistent with in-cell ELSIA results. All of our data indicated that the HDAC6 degraders based on VHL ligands have high specificity, which are ideal chemical probe for future HDAC6-related research or potential therapeutic reagents in combination with other drugs for cancer treatment.

A

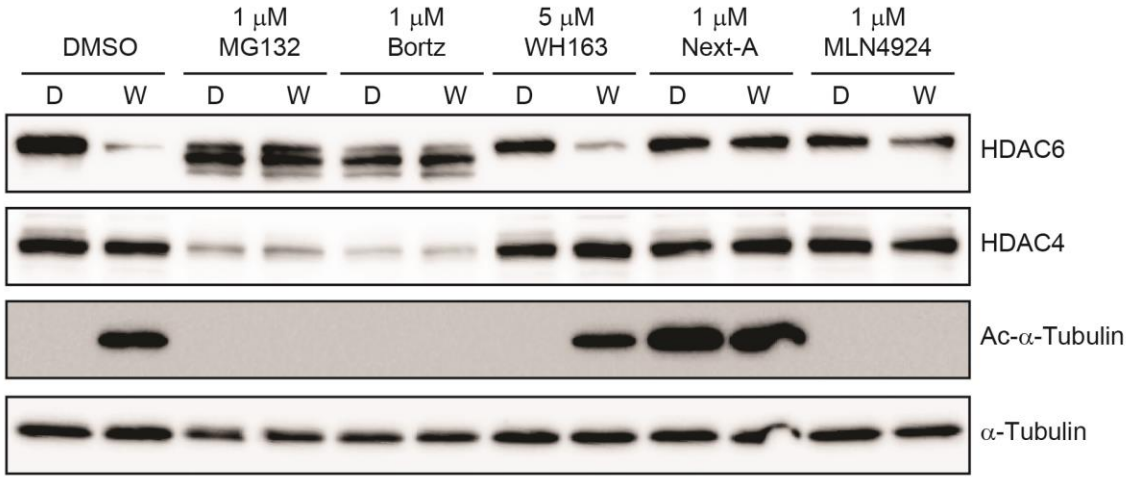

B

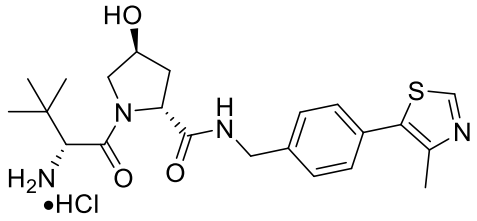

WH163

Figure 4.2.6. Mechanistic investigation of VHL degrader WH316.

To gain more evidence to support the hypothesis that the VHL-based degraders suppress HDAC6 expression via ubiquitination-proteasome pathway, we conducted a series of experiments by co-treating the HDAC6 degraders with competitive pathway inhibitors (**Figure 4.2.6**). MM1S cells pre-treated with proteasome inhibitor (MG132 and Bortezomib) showed no obvious HDAC6 degradation by WH316, supporting that the proteolysis of HDAC6 occurred in proteasome. Next-A abolished the effect of HDAC6

degradation by W316 by competitively binding to HDAC6 . NAE inhibitor MLN 4924 can deactivate the E3 ligase activity and abolish the WH316-induced degradation. It also indicated the neddylation and E3 were both required for VHL-based PROTACs. WH163 (**Figure 4.2.6 B**) is a hydrogen chloride salt, a synthetic intermediate towards VHL degraders. We though it could bind to VHL E3 ligase and block the ternary complex formation by degraders. However, we failed to observe any HDAC6 recovery by the pre-treatment of WH163, even though the ligand concentration used was 50-fold (5 μM) of the degrader (100 nM).

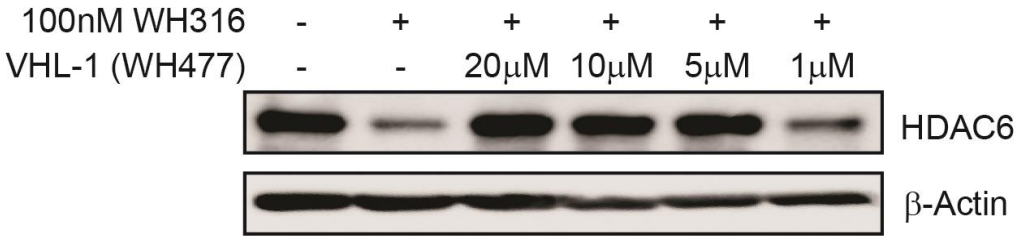

Figure 4.2.7. VHL binding is required for PROTAC-induced degradation.

After carefully examining the literature, we found that the reported VHL ligand VHL-1 (**Figure 4.1.1**) was the amide version of WH163. The carbonyl group of the terminal amide in VHL-1 played an important role in forming water-bridged hydrogen bonds[29]. All PROTAC molecules based on VHL ligands took advantage of the hydrogen bonds and used amide as the linking group[3,9,17,30,32,49]. This may explain why WH163 couldn't abolish the degradation effect. We thus acetylated the terminal amine of WH163 to yield VHL-1 (WH477). The VHL-1 completely recovered the HDAC6 expression at 5 μM or above

(**Figure 4.2.7** by Zhongrui Zhang), demonstrating that VHL E3 was required for efficient degradation by the VHL-ligand based degraders. In addition, this also confirmed the critical role of terminal amide for the interaction between VHL E3 ligase and its ligands.

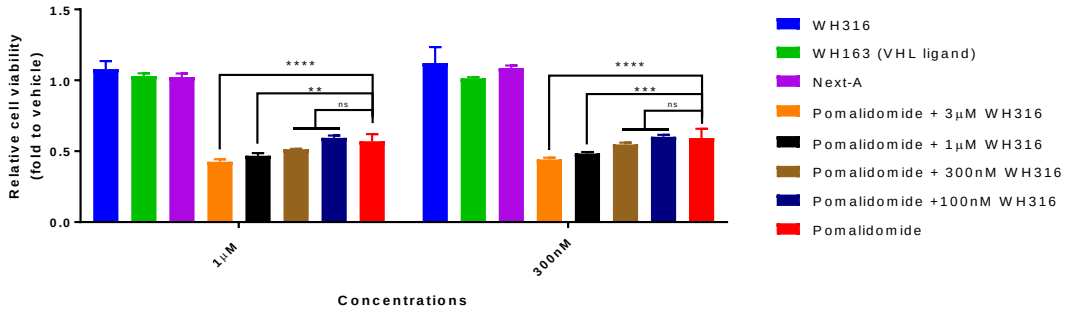

Figure 4.2.8. Combination of VHL HDAC6 degrader synergistically suppress MM1S proliferation.

To investigate the therapeutic potential of VHL-ligand based degraders, we examined the anti-proliferation effect of WH316 with or without other reagents for MM1S cells (**Figure 4.2.8**). At 1 μM, WH316, WH163 or Next-A alone did not cause any anti-proliferation effect for multiple myeloma. Pomalidomide suppressed ~50% proliferation at both concentrations, which was consistent with previous studies in **Chapter 2 Section 2.3**. In the presence of pomalidomide, the addition of 1 μM or 3 μM of WH316 further enhanced the anti-myeloma activity. Statistical significance was analyzed by Two-way RM ANOVA using Dunnett's multiple comparisons test and "Pomalidomide" as control for **Figure 4.2.7**. Together with previous studies on CRBN-ligand based second generation degraders, our results indicated that HDAC6 degradation and IKZF degradation worked synergistically to inhibit the growth of multiple myeloma cells.

4.3. Summary and Perspectives

In summary, we have developed the third-generation HDAC6 degraders by recruiting VHL instead of CRBN as the E3 ligase. We found a distinct SAR compared with the previously developed CRBN-ligand based degraders. Hydrophobic and long linkers are essential for the potency of VHL-ligand based degraders. We discovered WH316 as the most potent candidate among the new generation of degraders. It was less efficient at low concentrations but had higher maximal degradation at high concentrations. Mechanistic studies demonstrated that WH316 targeted HDAC6 for proteasomal degradation. WH316 didn't induce the degradation of IKZF1/3, which was often the target of previous CRBN-ligand based degraders. WH316 can serve as a more specific HDAC6 degrader for the study of HDAC6-related biological pathways. Without degradation of IKZFs, WH316 itself showed limited antiproliferation effects for multiple myeloma. The addition of WH316 enhanced the growth inhibition by Pomalidomide, indicating the synergistic effect of targeting IKZFs and HDAC6.

WH316 may also be applied to the in-cell ELISA to study the cellular target engagement of VHL ligands for the development of new types of PROTACs based on VHL-ligands. For example, it has been shown that the RHS in VHL-d can also be used to link with ligands of POI[61], suggesting that both RHS and LHS are exposed to solvents. We can use the in-cell ELISA to screen new VHL ligands with linkers on either RHS or LHS motif. It may also be possible to develop dimeric PROTACs with a short linker to further enhance the binding affinity and degradation efficiency.

4.4. Experimental Procedures

Refer to **Chapter 2 Section 2.5** for detail procedures.

5. Targeting PCSK9 Regulation Pathways with Novel Small Molecules

5.1. Introduction

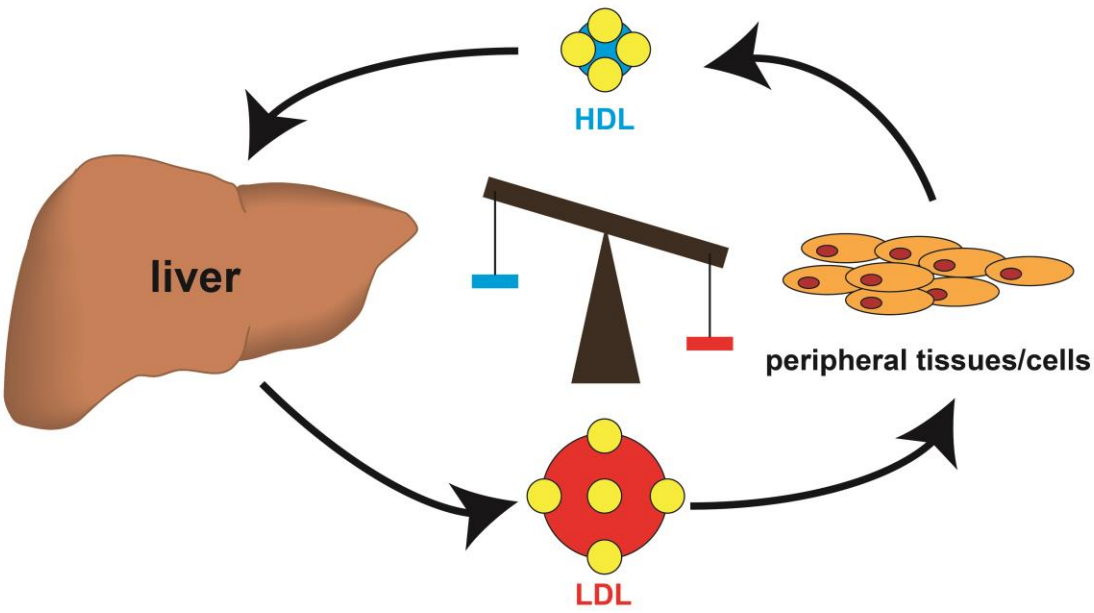

Figure 5.1.1 Cholesterol lipid transportation.

Cardiovascular diseases (CVDs) are one of the leading causes of death in United States and worldwide.[177] Dyslipidemia contributes to the risk of CVDs such as atherosclerosis[178]. High density lipoprotein (HDL) and low density lipoprotein (LDL) are responsible for most of lipid transportation and associated metabolism[179]. Over 70% of circulating lipid-cholesterol is delivered by LDL to peripheral tissues while HDL primarily transports cholesterol from peripheral tissues to liver for metabolic degradation[180] (**Figure 5.1.1**). High levels of LDL cholesterol in blood stream is clinically known as

hypercholesterolemia or hyperlipidemia[181]. The accumulation of vascular of LDL-c can initiate the formation of thrombosis plaque, which affects the blood flow and increases risk of atherogenesis[182]. In liver, low density lipoprotein receptor (LDLR) on the membrane can uptake LDL-c and promote its endocytosis and lysosomal degradation while LDLR itself can be recycled to back membrane surface for continuous uptake of LDL-c[183] (**Figure 5.1.1**). The LDLR is critical for the clearance of circulating LDL-c. Statin drugs are inhibitors of 3-hydroxy-3-methylglutaryl coenzyme A (HMG-CoA) reductase and serve as the main therapy for efficiently lowering LDL-c[184,185]. However, near 20% of patients failed in controlling cholesterol level by statin therapy[186]. Due to the side effect associated with statin drugs, the discontinue rate of statin therapy is more than 50%[184]. The mechanism of statin resistance is not fully clear and was implied with many factors, such as genetic mutation, disease and viral infection[187]. Alternatives of statin therapy and overcoming statin-resistance are major challenges for the discovery and development of novel cholesterol lowing therapeutics.

Proprotein Convertase Subtilisin/Kexin Type 9 (PCSK9), was first found to be the ninth member of proprotein convertases (PC) family and is mainly expressed and secreted in liver[188]. Later, PCSK9 was reported to target LDLR for degradation, revealing the important role of PCSK9 in cholesterol regulation and metabolism[189] (**Figure 5.1.1**). As a secreted protein, PCSK9 can bind to LDLR with or without uptaking LDL-c on cell membrane. PCSK9-LDLR complex is then transported to endosome, where LDLR is not able to disassociate with PCSK9. Unknown mechanism finally drives the complex of

PCSK9 and LDLR to lysosome for degradation. Disappearance of membrane LDLR decreases the clearance rate of circulating LDL-c and leads to hypercholesterolemia.

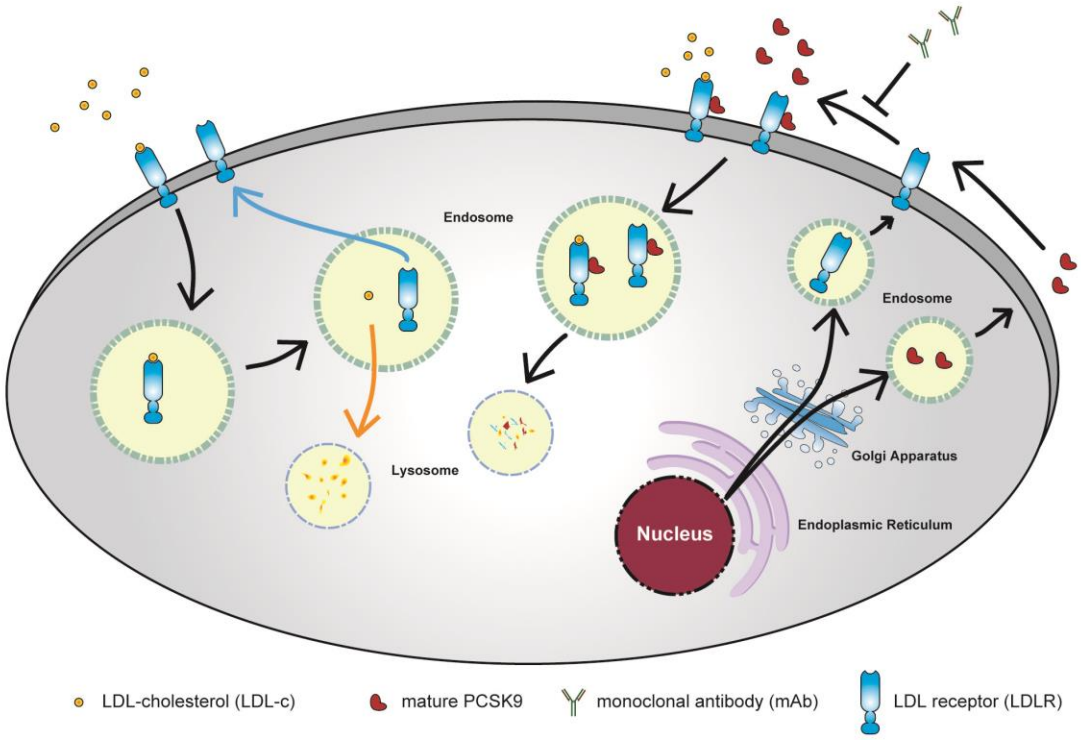

Figure 5.1.2 PCSK9 mediated lysosomal degradation of LDLR

After decades of investigation, PCSK9 has been validated as a therapeutic target to control LDL-c and reduce the risk of CVDs[190]. Evidence include genetic mutants found in disease-related population and transgenic mice for target validation, which are listed in **Table 5.1.2**. Loss-of-function (LOF) mutants which weaken the activity or expression of PCSK9 resulted in low cholesterol levels[188,191,192]. Gain-of-function (GOF) mutants yielded PCSK9 with enhanced activity or stability, which induced hypercholesterolemia[193–195]. Transgenic

animal models overexpressing PCKS9 or lacking PCSK9 were also created to verify the role of PCSK9 in circulating cholesterol level and CVDs[196,197]. These findings supported that PCSK9 was directly correlated to high cholesterol levels. Drug candidates inhibiting the function or expression of PCSK9 can serve as novel therapeutics for the treatment of hypercholesterolemia to lower the risk of CVDs.

Table 5.1.1 Examples validated PCSK9 as therapeutic target.

Type	Mutation & Function	Result	Ref
Loss-of-function mutants	C679X: incorrect folding of PCSK9 protein	Over 80% reduction in risk of CVD	191,192
	Q152H: prevent autocatalytic processing of proPCSK9	Reduce circulating level of PCSK9 (~80%) and LDL-C (~50%)	188
Gain-of-function mutants	D374Y: higher binding affinity to LDLR	Hypercholesterolemia in Utah pedigree substantiates	193,194
	R218S: decreased catabolism of PCSK9	Hypercholesterolemia	195
Transgenic mice	Tg(Apoe-PCSK9): overexpress PCSK9 under ApoE promoter	Complete depletion of LDLR, severely hypercholesterolemia	196
	Complete knockout of PCSK9 gene	Viable, fertile Severely hypocholesterolemia: reduced total cholesterol (~40%) and LDL-C (~80%)	197

One of the functions of statins is to enhance LDLR activity[198], but statin can also upregulate PCSK9 level though SRBP2 or NHF1α[199]. Thus, inhibitory agents against PCSK9 can be

combined with statin therapy for the treatment of CVDs. Several anti-PCSK9 monoclonal antibodies (mAb), such as Evolocumab and Alirocumab, have been approved by FDA[200,201]. These mAbs can prevent the interactions between LDLR and PCSK9, resulting the reduction of over 60% LDL-c in patients with statin-resistance. In addition, therapeutic siRNAs[202], peptides[203], vaccine[204] and CRISPR-Cas9[205] against PCSK9 are under either pre-clinical or clinical development.

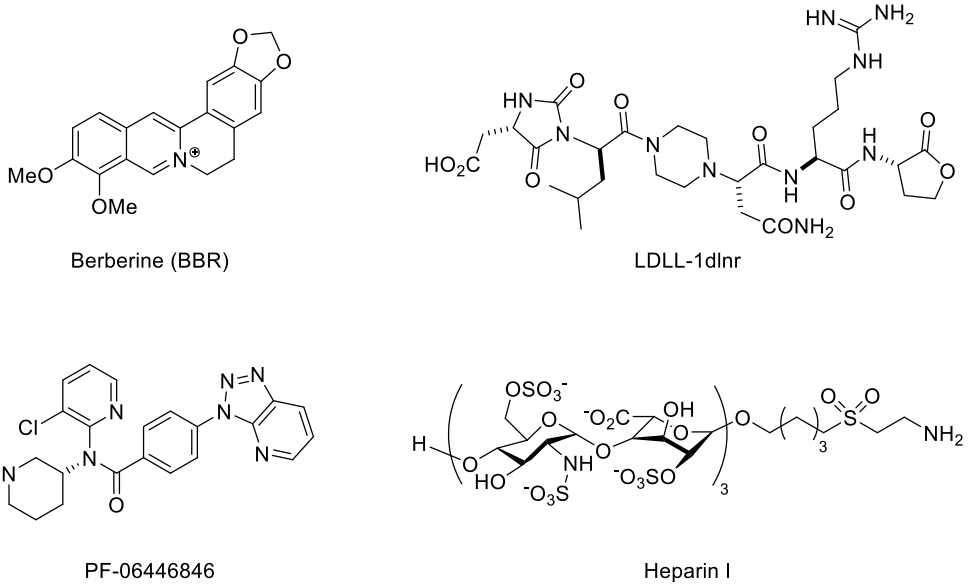

Figure 5.1.3 Featured PCSK9 small molecule modulators

Compared with macromolecular drugs, small-molecule drugs have several advantages such as ease of formulation and lower costs. To date, several small molecule inhibitors were reported, such as Berberine (BBR)[206], LDLL-1dlnr[207], PF-06446846[208] and heparin oligosaccharide[209] (**Figure 5.1.3**). They inhibit PCSK9 and lower the LDL-c through different mechanisms. For example, BBR suppresses the transcription of PCSK9 and stabilize LDLR mRNA[206]. LDLL-1dlnr disturbs the interaction between PCSK9 and

LDLR[207]. PF-06446846 specifically stall the translation of PCSK9 mRNA in ribosome[208] . Heparin oligosaccharide (e.g. Heparin I) prevents the recruitment of PCSK9 to LDLR via heparan sulfate proteoglycans (HSPG) on cell membrane[209]. However, all of them remain low potency, with micro-molar IC_{50}s when tested with immortalized hepatocytes. It requires significant efforts to develop these molecules as anti-PCSK9 agents for hyperlipidemia.

Our lab identified a class of heterocycle compounds that could reduce the PCSK9 level in a phenotypic assay[210,211]. By employing various synthetic methods and cell-based bioactivity tests, we have developed compounds with excellent potency against PCSK9. With these potent compounds in hand, we used their functional chemical probes to study the MoA and identify potential targets. Our efforts have revealed a novel transcriptional regulation pathway for PCSK9. This discovery may lead to new research directions on lipid regulation and the development of novel therapeutics.

5.2. Development of Novel Small-molecule PCSK9 Modulators

A) Methodology to generate diindolyl methane (DIIM) and indolyl cyclopropane

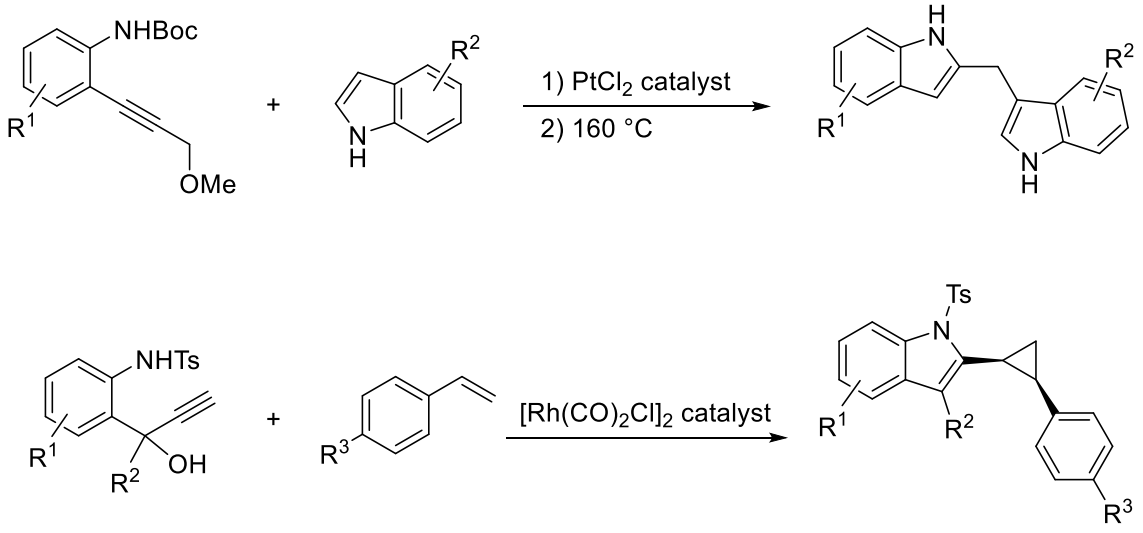

B) PCSK9 modulators hits identified in OIDD program

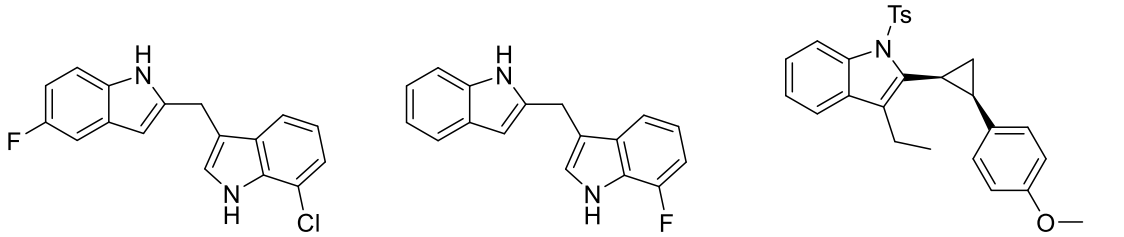

91553
PCSK9, IC_{50} = 0.25 μM
PCSK9 RPH IC_{50} = 30.1 μM

91565
PCSK9, IC_{50} = 0.3 μM
PCSK9 RPH IC_{50} 25.2 μM

7640
PCSK9, IC_{50} = 0.7 μM
PCSK9 RPH, at 100 μM, 60%

Scheme 5.2.1 Preparation of indole-containing heterocycles and hits identified in OIDD program

Our lab developed a series of synthetic methods for the preparation of various substituted indole-containing heterocycles, such as 2,3'-diindolyl methane (DIIM) and indolyl cyclopropane, through platinum- and rhodium-catalyzed reactions[212,213] (**Scheme 5.2.1 A**).

By collaborating with Eli Lilly's open innovation drug discovery (OIDD) program, we screened many of these indole-containing heterocycles in an AlphaLISA platform. To our delight, halogen substituted DIIMs (91553 and 91565) and cyclopropane 7640 were identified as novel modulators that can suppress PCSK9 expression with sub-micromolar IC_{50} and low cytotoxicity (**Scheme 5.2.1 B**).

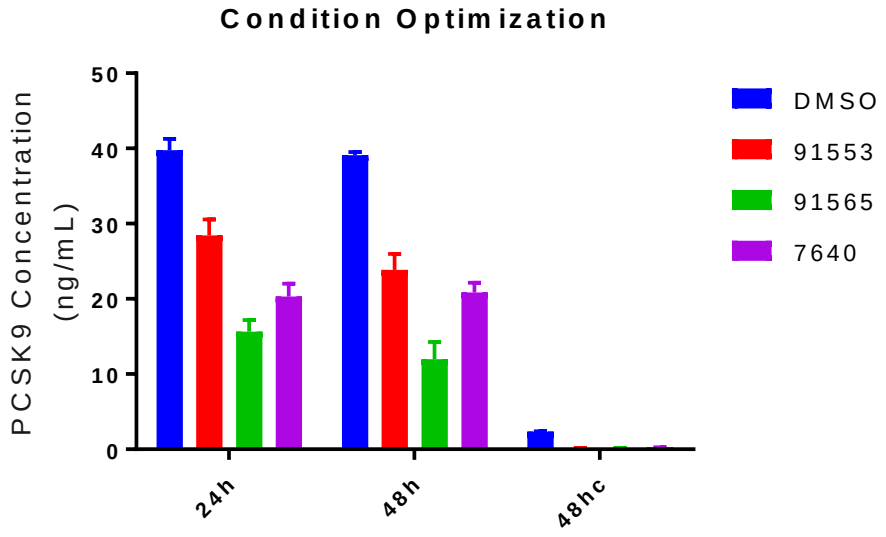

Figure 5.2.1 Optimization of assay conditions for screening

I joined the team on optimizing different parameters for the cell-based assay by working together with Dr. Gabrielle Winston-McPherson, a former graduate student in our group. With the above hits, we first developed a new phenotypic assay by using sandwich-ELISA to measure both intracellular and extracellular (secreted) PCSK9 content for the development of more potent and selective compounds. Using 91553, 91565 and 7640 as the positive control for modulating PCSK9, we treated HepG2 cells with 5 μM compounds dissolved in culture medium and incubated for certain time. At 24 h and 48 h time points,

we collected the medium sample to measure secreted PCSK9 and re-added freshly prepared medium with compounds. At the final endpoints, second medium sample was collected and cells were lysed to afford samples for probing intracellular PCSK9. The 91565 had the highest intracellular or extracellular potency by suppressing over 50% of extracellular PCSK9. The second medium sample (48h) gave more significant differences among compounds. Intracellular PCSK9 was remarkably affected by all compounds. Based on this result, we quickly focused on the synthesis of diindolylmethanes with halogen-substitution as 91565 analogues. For phenotypic screening conditions, we decide to choose 48 h treatment with refreshment of medium with compounds at 24 h. PCSK9 content in medium was the major indicator to determine the potency of compound.

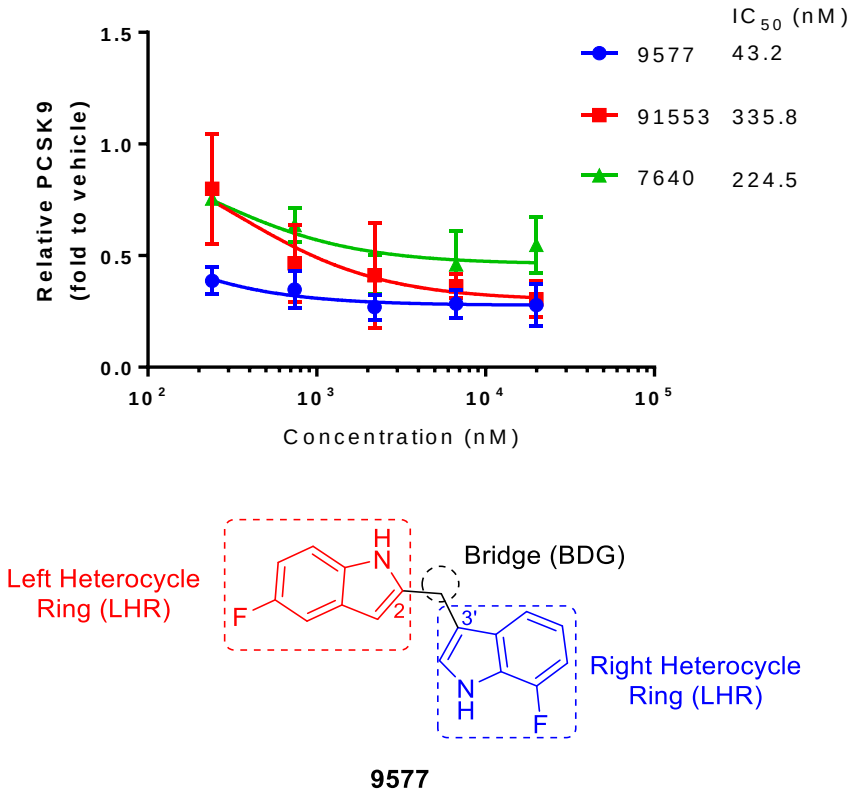

Figure 5.2.2 Dose response of novel PCSK9 modulators

We first synthesized difluoro-substituted DIIM 9577 and examined its dose-response at five concentrations and compared them with 91553 and 7640 (**Figure 5.2.2**). We found that 9577 had a IC_{50} at 43 nM, better than that of fluoro- and chloro-substituted 91553 (IC_{50} = 335.8 nM) and indolyl cyclopropane 7640 (IC_{50} = 224.5 nM). It suggested that the fluoro substitutions on both sides were critical for the potency. Later, Dr Haibo Xie prepared other DIIMs based on 9577 and all compounds discussed below in this chapter. To simplify the description, the 2-linked indole of 9577 was defined as the left heterocycle ring (LHR) and 3'-linked indole was designated as the right heterocycle ring (RHR).

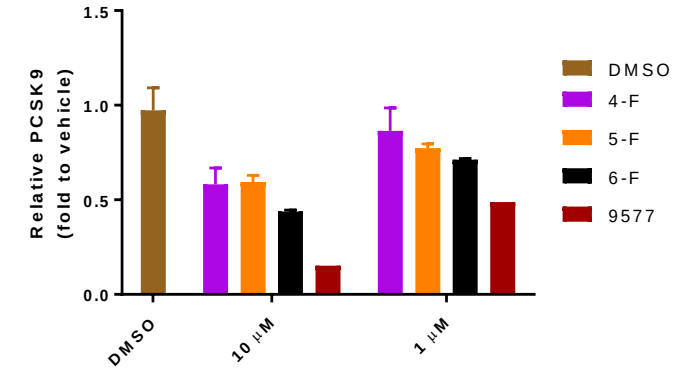

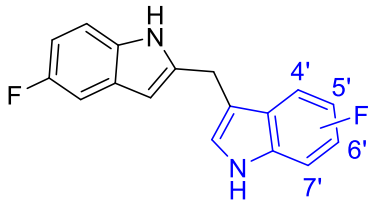

Cpd	Fluoro position
4-F	4'-
5-F	5'-
6-F	6'-
9577	7'-

Figure 5.2.3 Fluoro substitution on RHR of 9577

We then fixed the fluorine substituent on LHR and walked the fluorine substituent on RHR. The resulting compounds were tested at two concentrations (1 μM and 10 μM) in HepG2 cells (**Figure 5.2.3**). The potency was increased when the fluorine atom was moved from 4'- to 7'- position at both concentrations. 9577 with 7'-fluoro substitution was the best among these difluoro heterocycles.

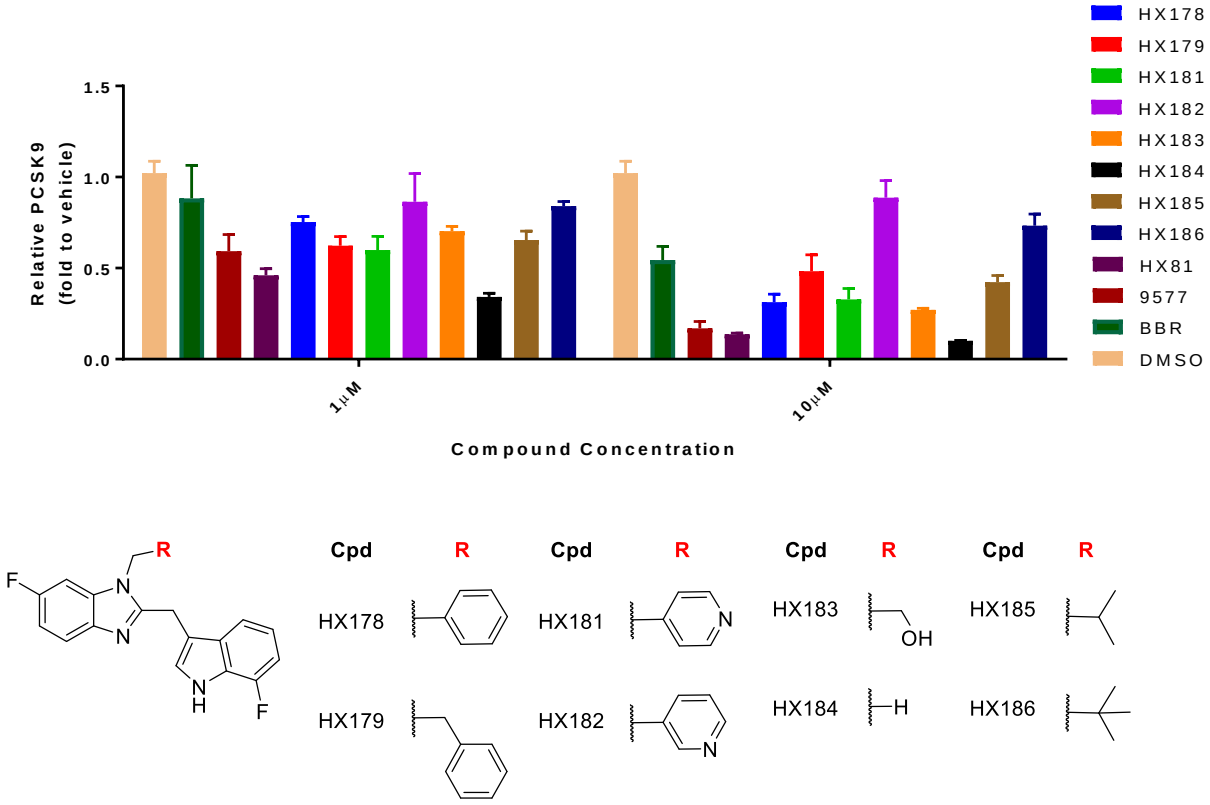

Figure 5.2.3 SAR for the LHR part of HX81

To improve the solubility, we synthesized benzimidazole-indolyl methanes (BIIMs) with different substituents on the nitrogen atom of LHR (**Figure 5.2.3**). We employed 9577 and BBR, a known PCSK9 mRNA suppressor[206], as positive controls. By testing these compounds, we identified two BIIMs, HX81 and HX184, which reduced more PCSK9 in than the positive controls. HX184 has an additional methyl substituent compared to HX81 and showed better potency. All other bulky groups, such as aryl and butyl groups, didn't improve the potency. This suggested the methyl group might serve a key hydrophobic interaction between our molecule and the target.

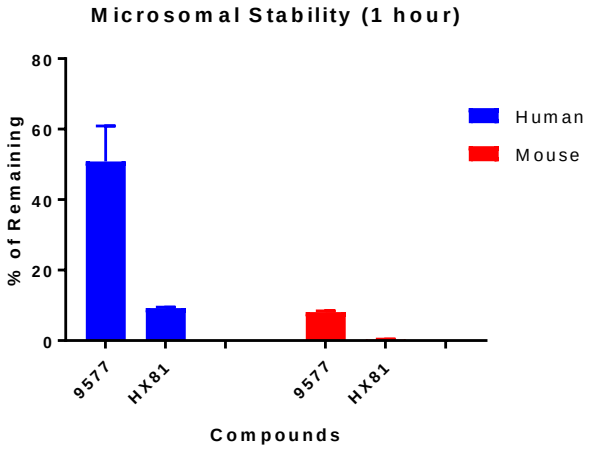

Figure 5.2.4 Microsomal stability of DIIM and BIIM

We next tested 9577 and HX81 for their microsomal stability[214] (**Figure 5.2.4**). It appeared that both compounds were metabolically unstable, less than 50% after 1h incubation with either human or mouse microsomes. Although DIIMs are generally more stable than BIIMs, HX81 has better solubility (data not showed) and is more potent.

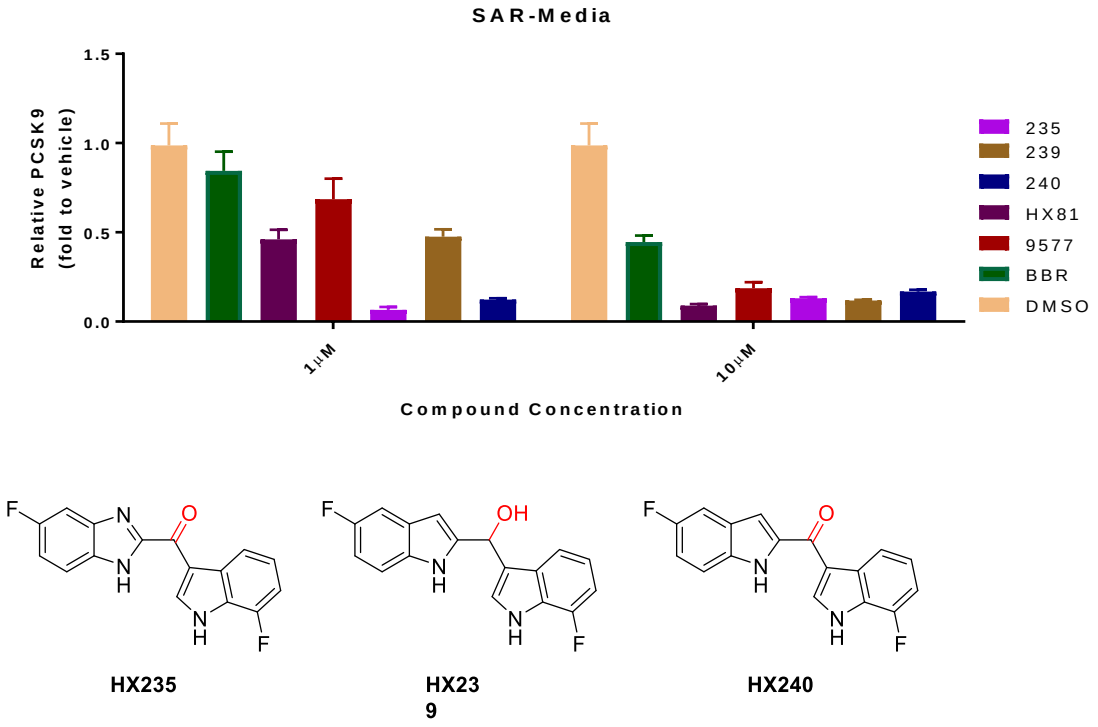

Figure 5.2.5 Putative oxidation product of 9577 and HX81

Based on the SAR and metabolic stability data, we hypothesized that the metabolites of 9577 and HX81 might preserve the bioactivity, because liver cells are known to oxidize metabolically labile compounds and our initial hits are relatively potent in HepG2 cells. The methylene bridge between the two aromatic rings is doubly activated by the two aromatic heterocycles and may be more labile towards cytochrome P450 (CYP) enzyme-mediated oxidation[215]. We thus synthesized the putative oxidation products of 9577 and HX81 (**Figure 5.2.5**). Ketones HX235 and HX240 suppressed over 85% PCSK9 expression. Hydroxylmethane HX239 only offered limited enhancement. Diindolyl ketone (DIIK) and Benzimidazole indolyl ketone (BIIK) were then chosen as new lead structures.

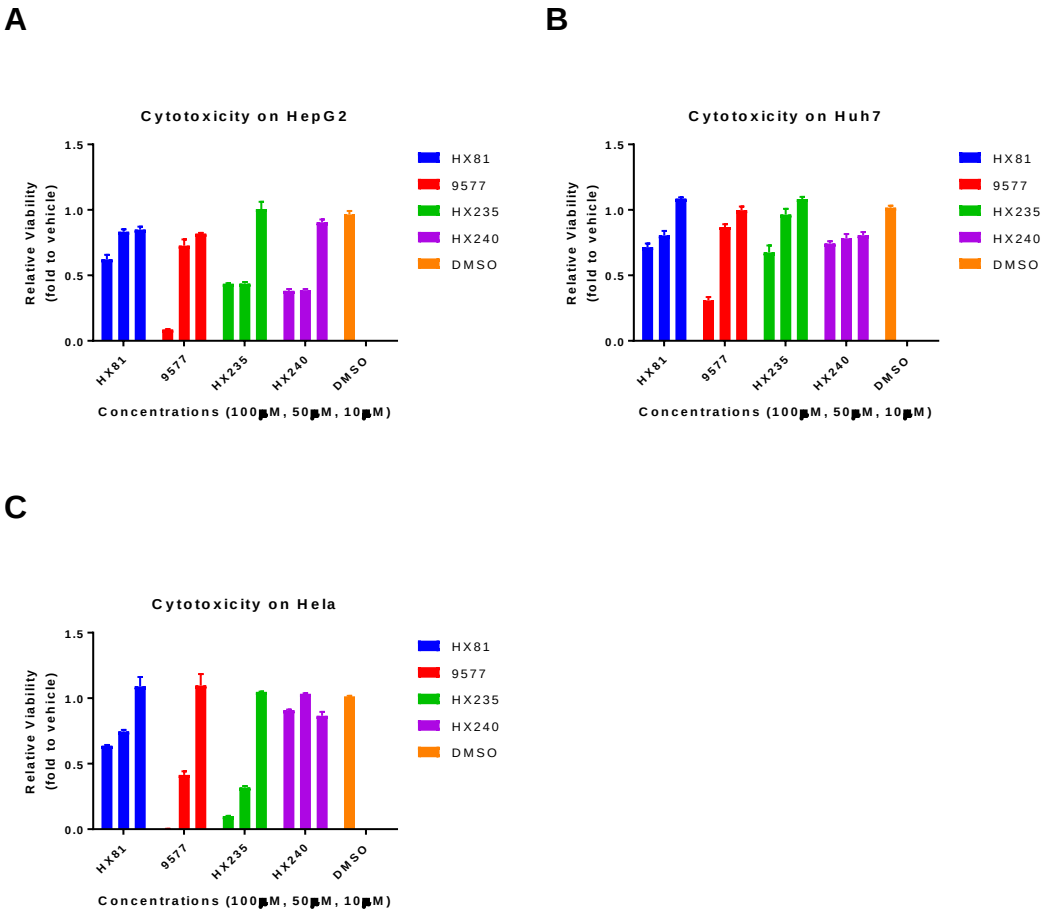

Figure 5.2.6 Cytotoxicity of DIIM, BIIM, DIIK and BIIK.

To exclude the possibility reduced PCSK9 level as a result of cytotoxicity, HepG2, Huh7 and HeLa cells were treated with 100 µM, 50 µM and 10 µM of compounds for 48 h. Cell viability was measured by MTT assay (**Figure 5.2.6**). No significant anti-proliferation effect was observed for all compounds at 10 µM. Some compounds such as 9577 and HX235 showed cytotoxicity at 100 µM and or 50 µM. It suggested the suppression of PCSK9 was not a result of reduced cell population.

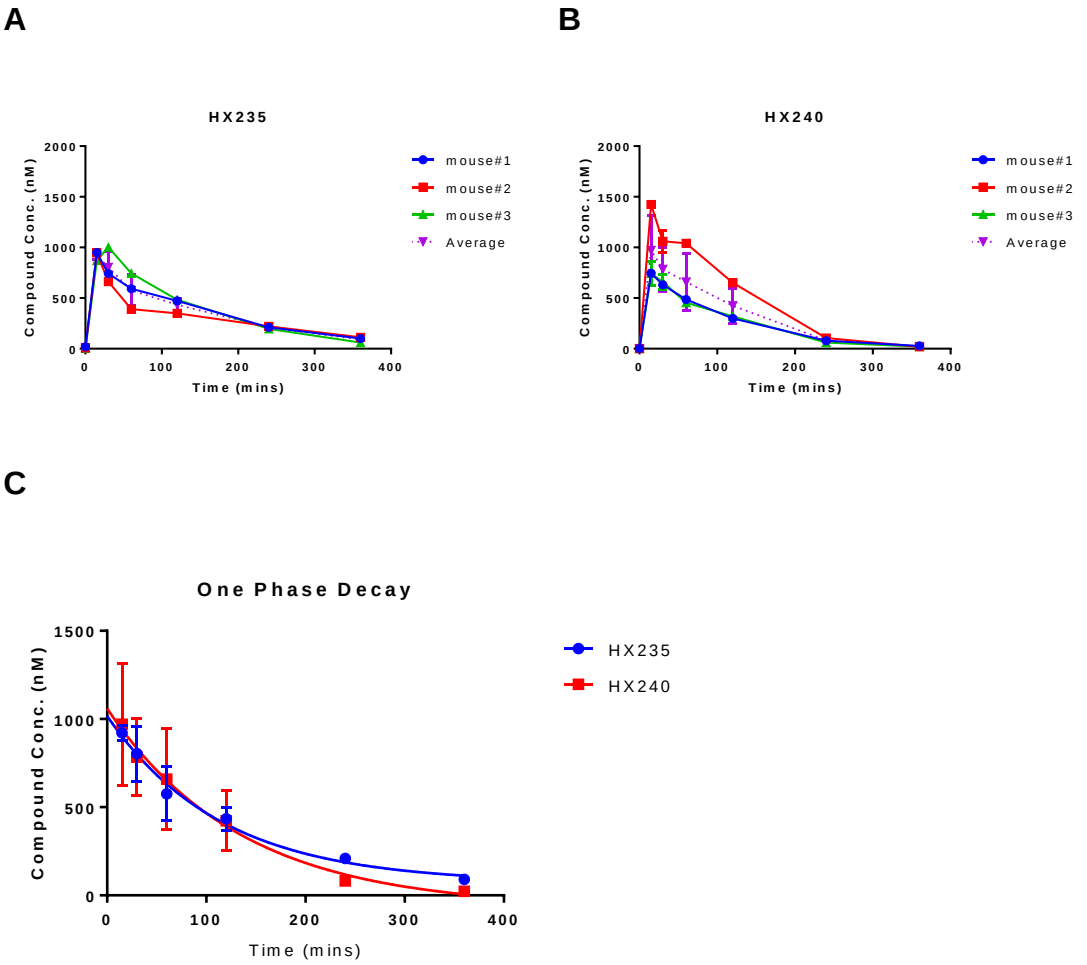

Figure 5.2.7 Preliminary pharmacokinetic study in mice

Table 5.2.1. List of calculated pharmacokinetic parameters[a]

Compounds	Peak (nM)	Plateau (nM)	$T_{1/2}$ (Mins)	R^2
HX235	1018 ± 40.21	70.87 ± 44.69	79.47	0.9069
HX240	1060 ± 82.48	-71.98 ± 82.48	93.26	0.7419

[a]Values with or without ± SD obtained from nonlinear fitted data in **Figure 5.2.7 C**

To prepare for *in vivo* study with our lead compounds HX235 and HX240, we examined their preliminary pharmacokinetic properties (**Figure 5.2.7**). Mice were handled by collaborators in Dr. Alan Attie's Lab. Mice were intraperitoneally injected with 2 mM formulated solution of compounds. Plasma samples were collected and stored. We measured the concentration of compounds by LC-MS/MS at Analytical Instrument Center (AIC) in the School of Pharmacy. Both compounds reached their peak concentrations at 15 min after injection (**Figure 5.2.7 A** and **B**). The peak concentration of both compounds was ~950 nM. At 6 h, the concentration of HX235 decreased to 91 nM, while only 23 nM of HX240 was remained. It suggested that HX235 had higher stability in mice. We performed one-phase-decay nonlinear fitting of all biological and technical replicates and obtained the plasma half-life ($T_{1/2}$) and other parameters of these compounds (**Figure 5.2.7 C** and **Table 5.2.1**). The peak value and plateau value were consisting with non-fitted data. The $T_{1/2}$s of HX235 and HX240 were 79.47 minutes and 93.26 minutes, respectively. The value of R^2 indicated a satisfactory fitting. Overall, these results provide valuable preliminary data for *further in-vivo* studies.

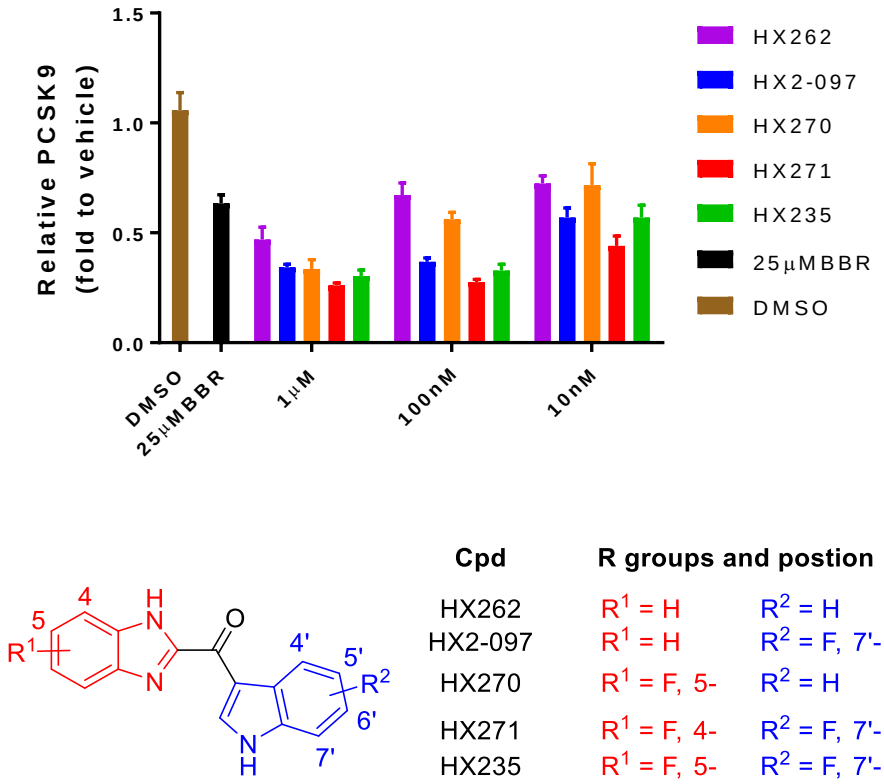

Figure 5.2.8 Fluoro Substitution of BIIK HX235

To optimize the lead compounds, we first synthesized fluorine-substituted BIIKs and none-substituted HX262 (**Figure 5.2.8**). Because BIIKs are potent PCSK9 modulators, we lowered our screening concentrations down to 100nM and 10 nM in HepG2 cells. Compared to HX262, we found that compounds without any fluorine substituent (e.g. HX2-097 and HX270) had lower activity. HX235 and HX271 bearing two fluorine substituents showed promising potency. These results indicate that the activity of BIIK was highly dependent on the fluorine substituents. The fact that HX271 was more potent than HX235 suggested that the potency can be tuned by changing the position of fluorine.

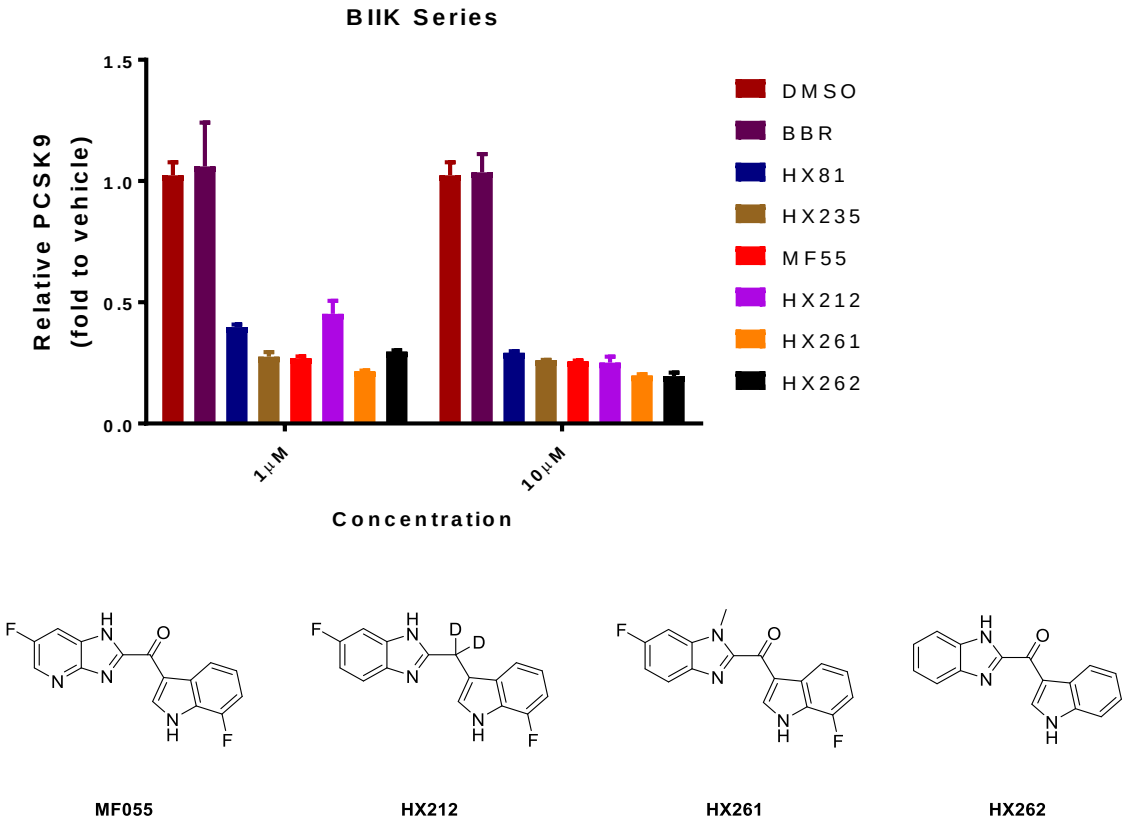

Figure 5.2.9 SAR for Derivatives of HX235

We then synthesized several derivatives from HX81 and HX235 (**Figure 5.2.9**). We prepared MF055 by using pyridoimidazole instead of benzimidazole. We replaced the hydrogen on the bridging methylene by deuterium in HX212 to improve the metabolic stability[216]. We prepared HX261 because the *N*-methyl group improved the potency previously (e.g. HX184 vs HX81). To our delight, HX261 inhibited more expression of PCKS9 than HX235, while MF55 or HX212 didn't show any improvement.

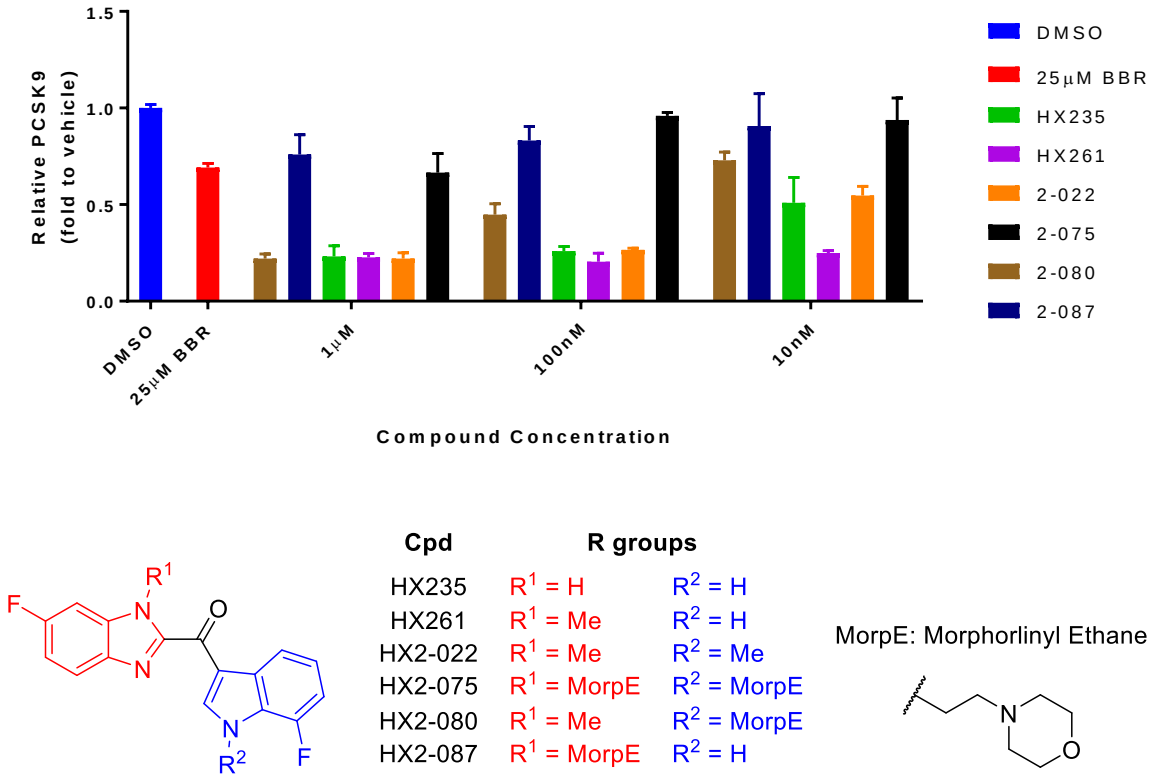

Figure 5.2.10 SAR for Analogues of HX235

Since the methyl group was also critical for the potency of BIIK series of compounds, we examined different substitution on the nitrogen atom of both rings (**Figure 5.2.10**). The substituents included methyl group and morpholinyl ethane (MorpE). The latter might enhance the solubility. However, the mono-methyl substituted HX261 remained as the most potent compound. Any substitution of MorpE or substitution on indole ring decreased the activity.

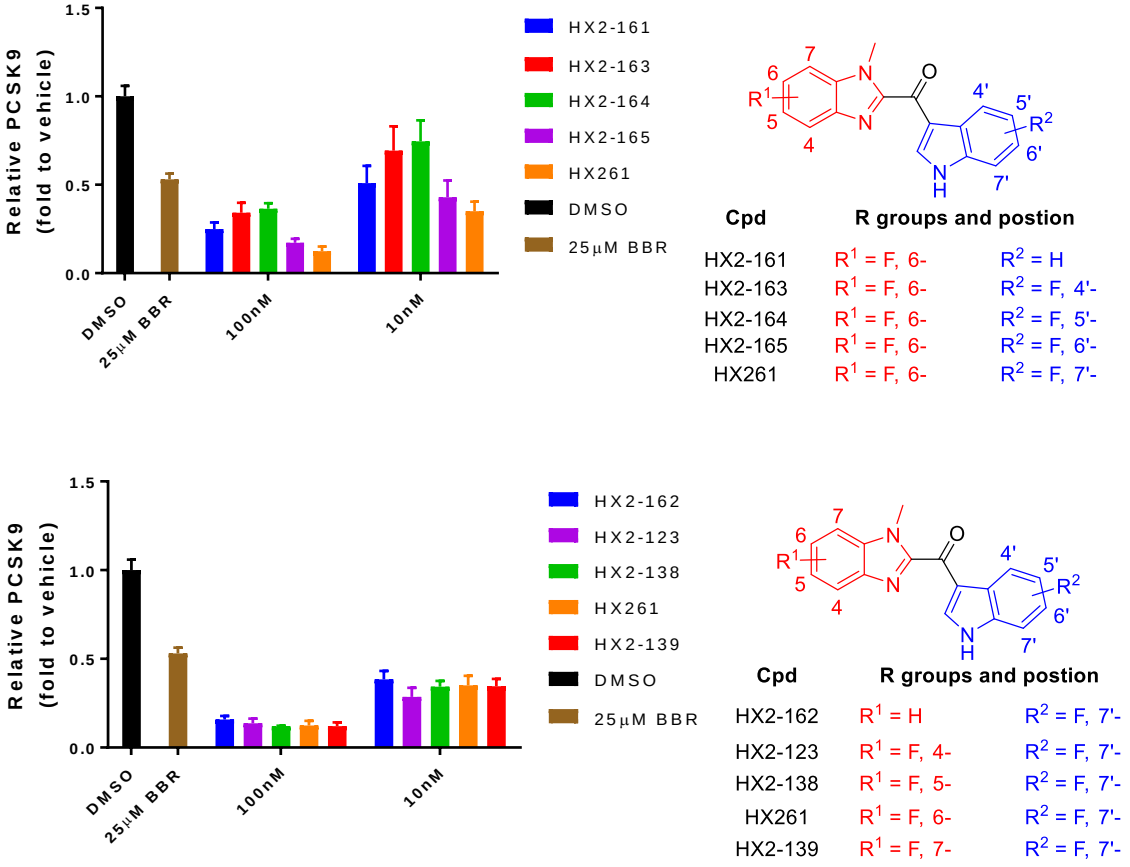

Figure 5.2.11 Fluoro substitution on LHR of HX81

To examine the effect of fluorine substituent on both LHR and RHR, we walked the fluorine atom on one ring while fixing it on the other ring (**Figure 5.2.11**). For RHR, having a fluorine on the 7'- position showed the best activity. A bell-shape response was observed when the fluorine atom was moved from 4'- to 7'-position. For LHR, the position of fluorine atom didn't obviously affect the activity. All of our results indicated HX261 was the most potent compound, which had several structural features: benzimidazole ring, methyl group on the nitrogen atom of LHR and having 7'-fluoro substituent on the right indole ring.

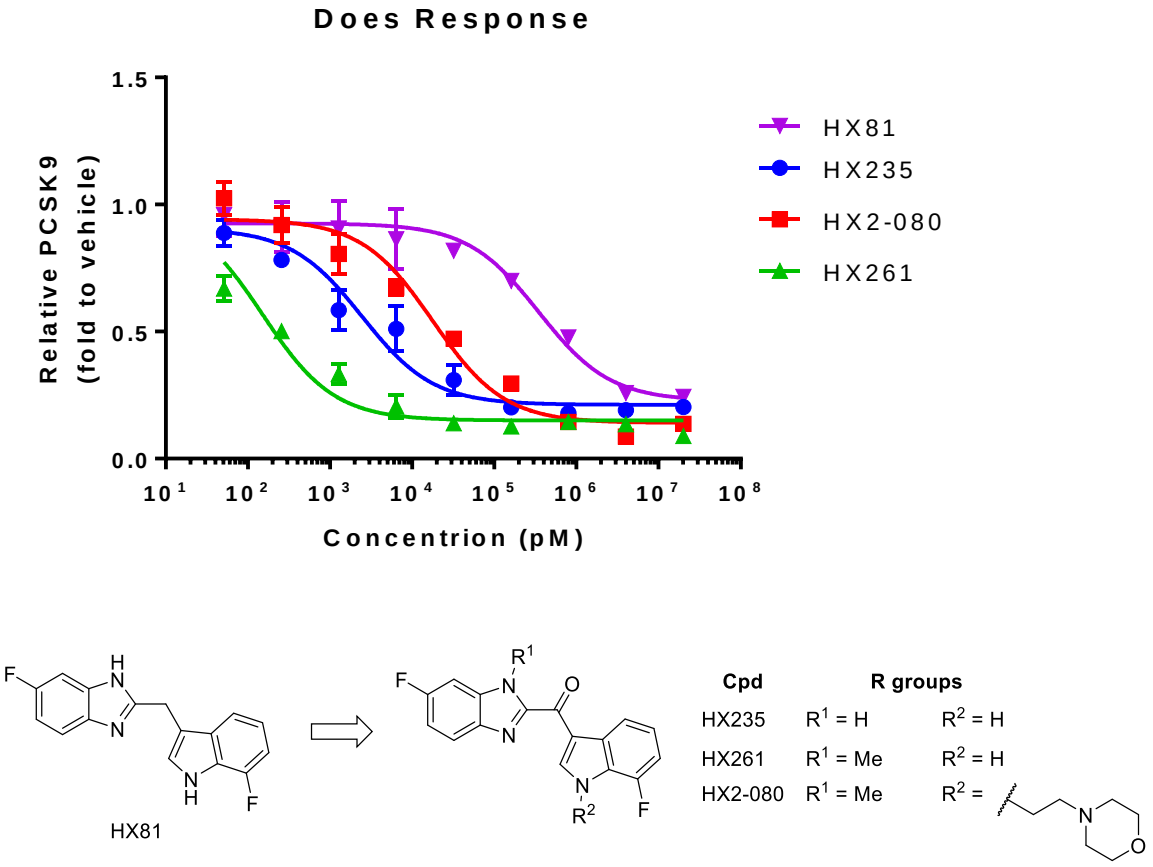

Figure 5.2.12 Dose response of benzimidazole-indolyl compounds.

To examine the potency of selected compounds generated during our SAR study, we treated HepG2 cells with HX81, HX235, HX2-080 and HX261 at 10 concentrations including vehicle (DMSO). The dose response curves are shown in **Figure 5.2.12** and the calculated IC_{50}s are listed in **Table 5.2.12**. HX261 had IC_{50} of 0.15 nM, which was over 2000-fold change from the parent compound HX81, which had a IC_{50} of 348.34 nM. The IC_{50}s for compounds HX235 and HX2-080 are 2.46 and 17.87 nM, respectively. Although less potent, HX2-080 was more soluble than HX261 (data not shown) and may be better suited for *in-vivo* study.

Table 5.2.2. List of IC_{50} and maximal inhibition of PCSK9 expression by compounds

Compounds	IC_{50} (nM) [a]	Maximal Inhibition (Vehicle%)[b]
HX81	348.34 ± 104.68	77.28 ± 4.07
HX235	2.46 ± 0.63	78.80 ± 2.11
HX2-080	17.87 ± 3.79	85.95 ± 2.39
HX235	0.15 ± 0.03	84.97 ± 1.58

[a]The concentration at which half-maximal degradation was achieved. [b]The maximum percentage of inhibition of PCSK9 expression. [a,b]Values with ± SD obtained from nonlinear fitted data in **Figure 5.2.11**

To probe the downstream effects of our PCSK9 modulators, we analyzed the abundance of several proteins in lysates of HepG2 cells treated with HX261 and controls by western blot. When we optimized the conditions, we found routinely used culture medium supplemented with full-formula fetal bovine serum (FBS) unexpectedly suppressed the LDLR expression (data not shown). The lipoproteins, especially LDL particles, in FBS was suspected to be the source for this unexpected change of LDLR, because it has been reported that they affect the cholesterol biosynthesis[217] and LDLR[218]. We thus had to use medium without FBS or with lipoprotein-deficient fetal bovine serum (LDPS) to examine the expression of LDLR after the treatment of compounds. In the first experiment, HepG2 cells were treated in regular medium for 24 h and then in FBS-free medium for another 24 h. In the second experiment, we used LDPS medium for both treatments (24 h).

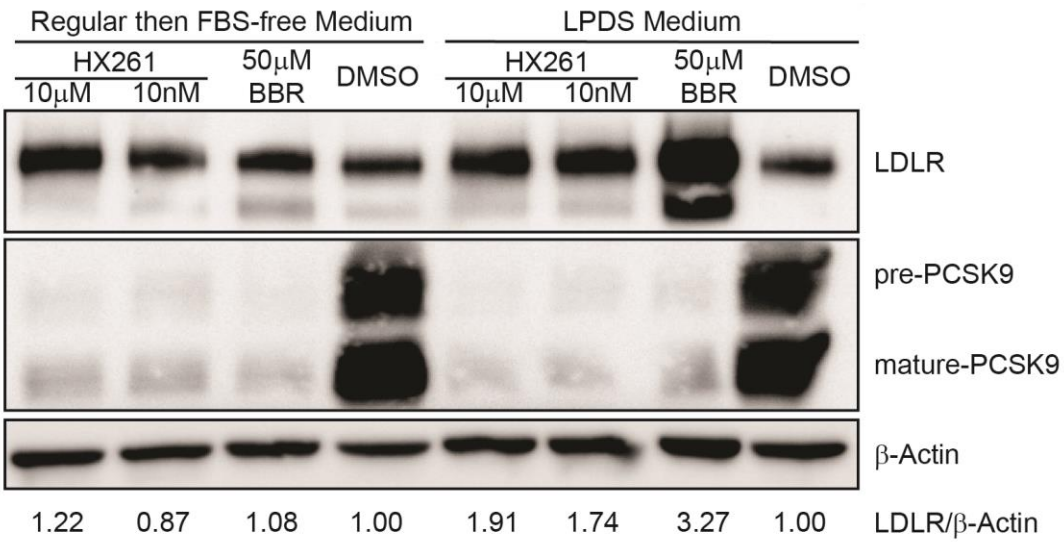

Figure 5.2.13 HX261 induced LDLR expression

Cells were then lysed and the lysates were subjected to western blot analysis (**Figure 5.2.13**). When LDPS was used, we observed a significant induction of LDLR by BBR (3 fold to vehicle) and HX261 (~2 fold at 10 μM), while intracellular PCSK9 was significantly suppressed. The FBS-free medium diminished the induction of LDLR by both BBR and HX261, suggesting that the absence of FBS may affect related modulatory process.

In summary, we established phenotypic assays for the development of PCSK9 modulators. Through several rounds of SAR studies, we discovered potent PCSK9 modulator HX261, which could inhibit PCSK9 expression with a IC_{50} in the picomolar range.

5.3. Investigation of the mechanism of action our PCSK9 modulators

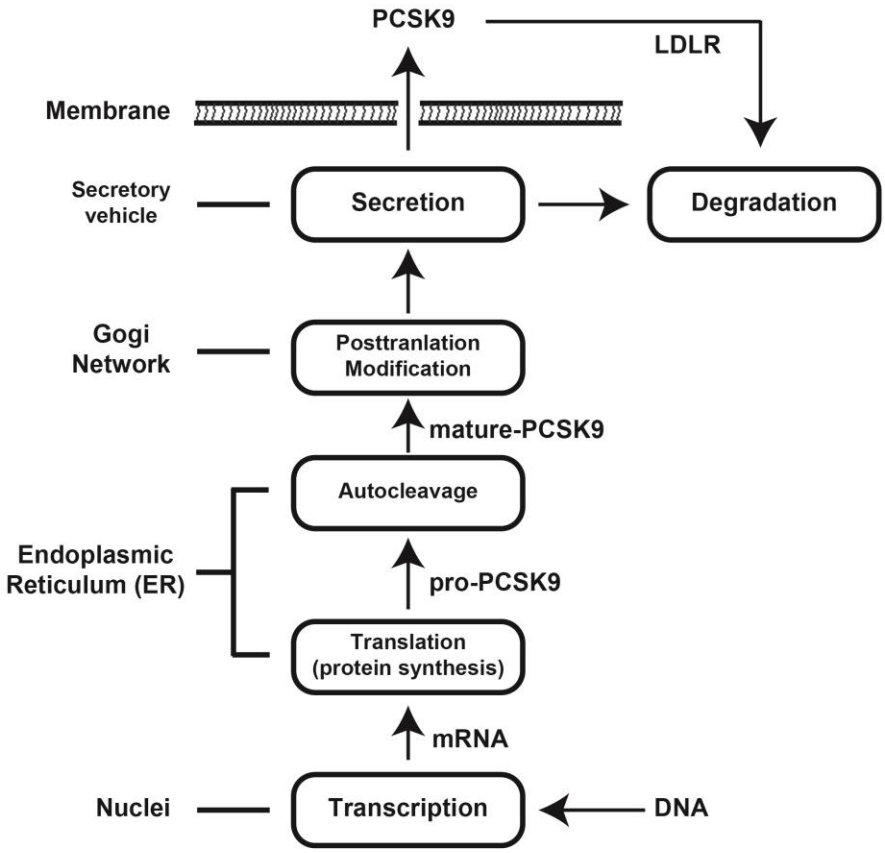

Figure 5.3.1 Life span of PCSK9 as a secreted protein.

With several potent and non-toxic PCSK9 modulators in hand, we proceeded to investigate the possible MoA for these small molecules. PCSK9 is a secreted protein and the small molecule modulator can interfere with many steps shown in **Figure 5.3.1**, including transcription from DNA to mRNA, translation from mRNA to pro-PCSK9 in ribosome, translocation to ER, where pro-PCSK9 undergoes autocleavage of its pro-segment to become mature-PCSK9, post-translational modification (PTM), translocation of mature-PCSK9 through trans-Golgi network, and finally secretion.

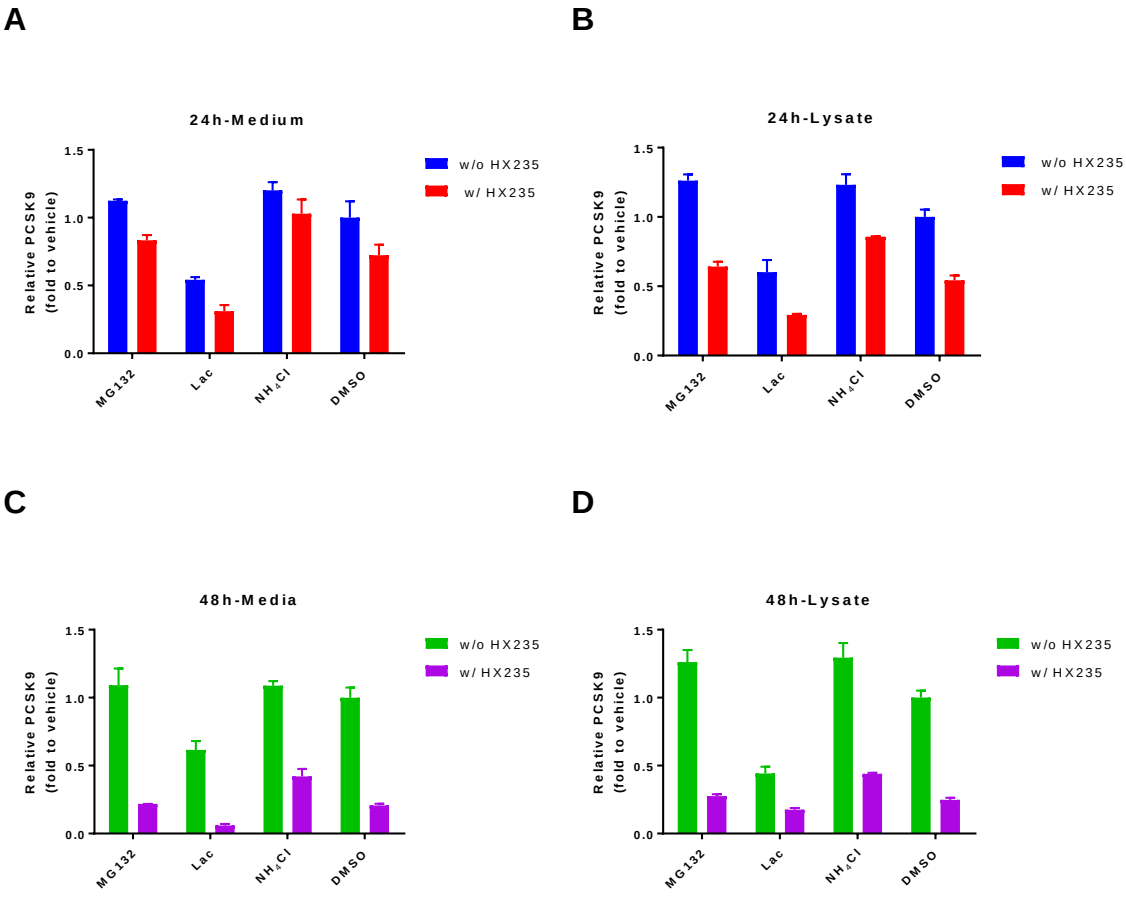

Figure 5.3.2 Study on protein degradation pathways.

We first co-treated our PCSK9 modulators with some pathway blockers, such proteasome inhibitor MG132, protease inhibitor lactacystin (Lac) and lysosome inhibitor ammonium chloride (NH_4Cl). HepG2 cells were treated with blockers or vehicle for 1 h. Compounds HX235 were then added to the cells, which were incubated for 24 and 48 h (**Figure 5.3.2**). Without HX235, PCSK9 was decreased by LAC and increased by MG132 or NH_4Cl as reported in literature[219,220]. However, the addition of HX235 still downregulated PCSK9. If our compounds act on these pathways, the effect on PCSK9 should be abolished by the

pathway blockers or inhibitors. Our results indicated that our compounds unlikely promoted the proteasomal or lysosomal degradation of PCSK9.

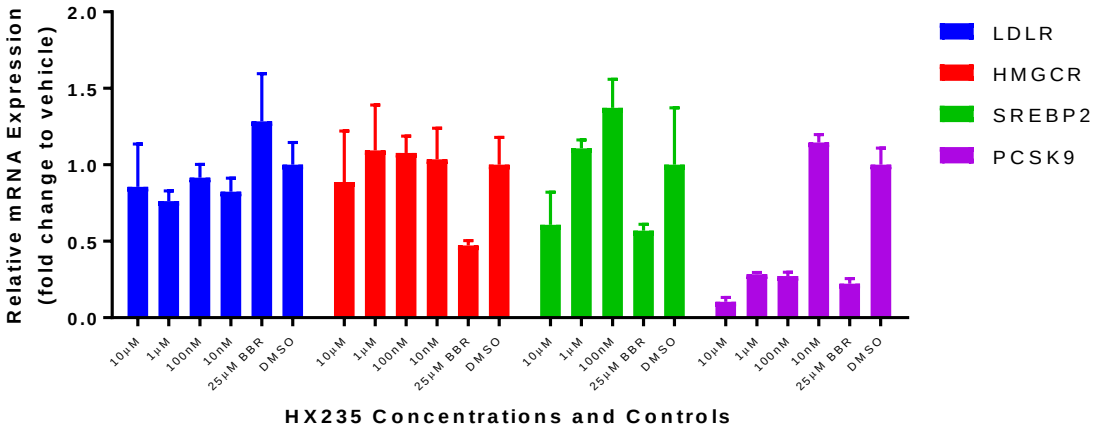

Figure 5.3.3 HX235 affected PCSK9 mRNA level.

We next investigated the possibility of transcriptional regulation. HepG2 cells were treated with HX235, one of the most potent compounds, for 24 h. The total mRNA was extracted and analyzed by reverse transcription quantitative PCR (RT-qPCR, **Figure 5.3.3**). Berberine was reported to suppress the mRNA of both PCSK9 and SREBP-2 while stabilizing LDLR mRNA[206]. Interestingly, PCSK9 mRNA level was decreased by HX235 in a dose-dependent manner. At the meantime, we didn't observe obvious reduction of the mRNA levels for LDLR, HMGCR or SREBP2 in response to the treatment of HX235. SREBP2 was affected only by high concentrations of HX235. This suggested our compounds regulated PCSK9 transcription in a pathway that is distinct from BBR.

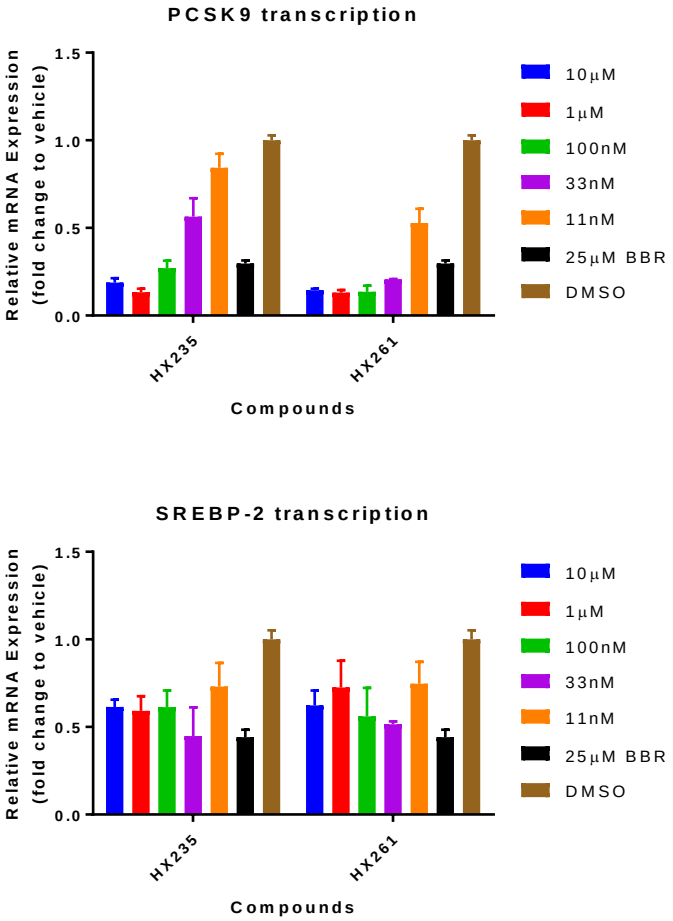

Figure 5.3.4 BIIKs suppress PCSK9 transcription via a novel pathway.

To confirm the effects of our compounds on the transcription of PCSK9, we treated HepG2 cells with HX235 or HX261 at different concentrations (**Figure 5.3.4**). Both compounds reduced the PCSK9 mRNA in response to increased concentrations of compounds. HX261 remarkably suppressed the PCSK9 mRNA level as expected, since it was the most potent compound in previous study. Meanwhile, both compounds had very minimal effects on the

level SREBP2 mRNA. This again confirmed that our compounds acted on a pathway different from BBR.

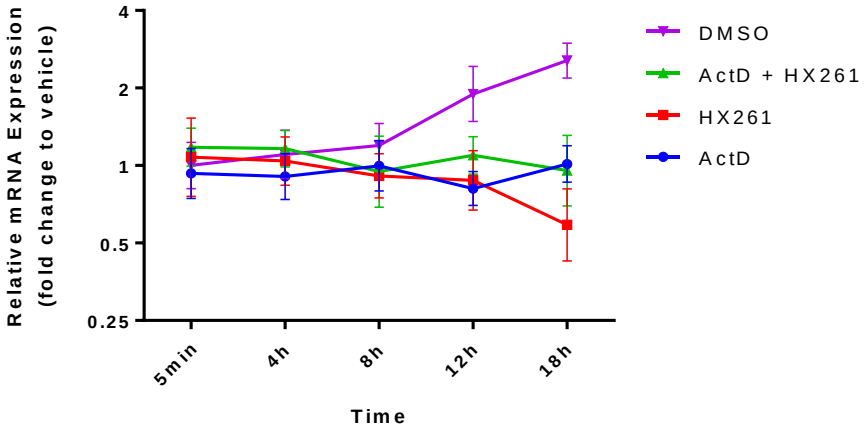

Figure 5.3.5 HX261 targeting transcription rather than mRNA turnover.

We next examined whether our compounds decreased PCSK9 mRNA by suppressing transcription or facilitating mRNA turnover. We used Actinomycin D (ActD)[221] to stall the mRNA synthesis and monitored the PCSK9 mRNA by time (**Figure 5.3.5**). Interestingly, vehicle (DMSO) treated group showed increased mRNA after 12 h, while ActD abolished that increasing as expected. HX261 started decreasing mRNA level after 8 h while the co-treatment with ActD recovered the loss of mRNA. This result suggested that our compound did not promote the degradation of PCSK9 mRNA. Our compounds more likely regulate the transcription of PCSK9 gene.

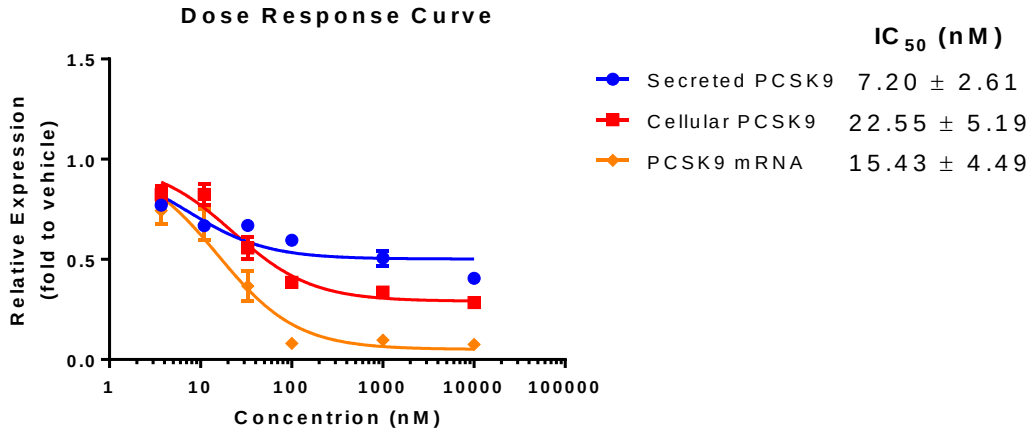

Figure 5.3.6 Dose response curves of HX261 on PCSK9 protein and mRNA change.

To explore the correlation between the changes of protein and mRNA of PCSK9, we performed two parallel experiments by treating HepG2 cells with different concentrations of HX261 (**Figure 5.3.6**). PCSK9 protein (in medium and in cell) and mRNA were extracted for analysis by ELISA or RT-qPCR. The decrease of protein and mRNA was obvious and dose-dependent. The fold change of mRNA was more significant than protein. More significant decrease of cellular protein was observed than that of secreted protein in response to the treatment of compounds, which is consistent with the mechanism of transcriptional downregulation of PCSK9. The calculated IC_{50}s ranged from 7.2 nM to 22.6 nM. Our results suggested HX261 first affected the mRNA of PCSK9, then the cellular PCSK9 protein, and finally secreted PCSK9 protein.

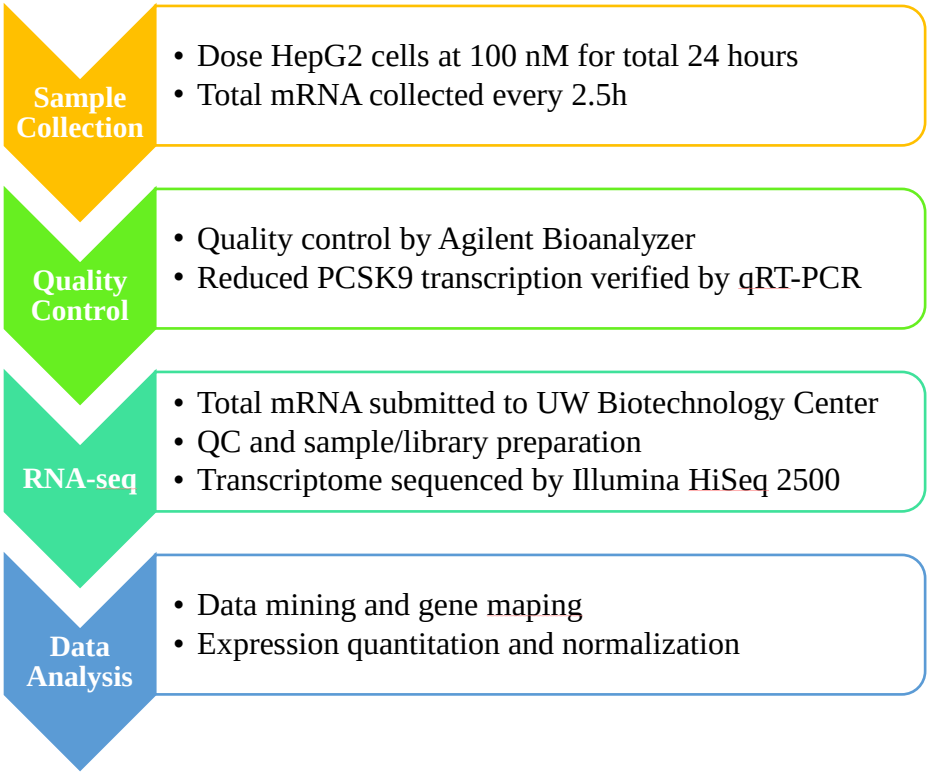

Figure 5.3.7 Workflow of RNA-seq experiment.

Since our compounds act on the transcription of PCSK9, we conducted a RNA-seq experiment to investigate the whole transcriptome after the treatment of our compounds. The workflow was described in **Figure 5.3.7**. In brief, HepG2 cells was treated with 100 nM of HX261 or vehicle for a total of 24 h. Transcriptome was extracted and monitored every 2.5 h. The sequencing was done by UW Biotechnology Center and data analysis was done by Dr. Rhonda Bacher from our collaborator Dr. Christina Kendziorski's lab. We successfully mapped and quantified over 11,000 transcripts. The expression of these transcripts was compared to β-Actin (ACTB), which was the internal reference. Normalization was processed by calculating the expression relative to DMSO-treated groups at the corresponding time points.

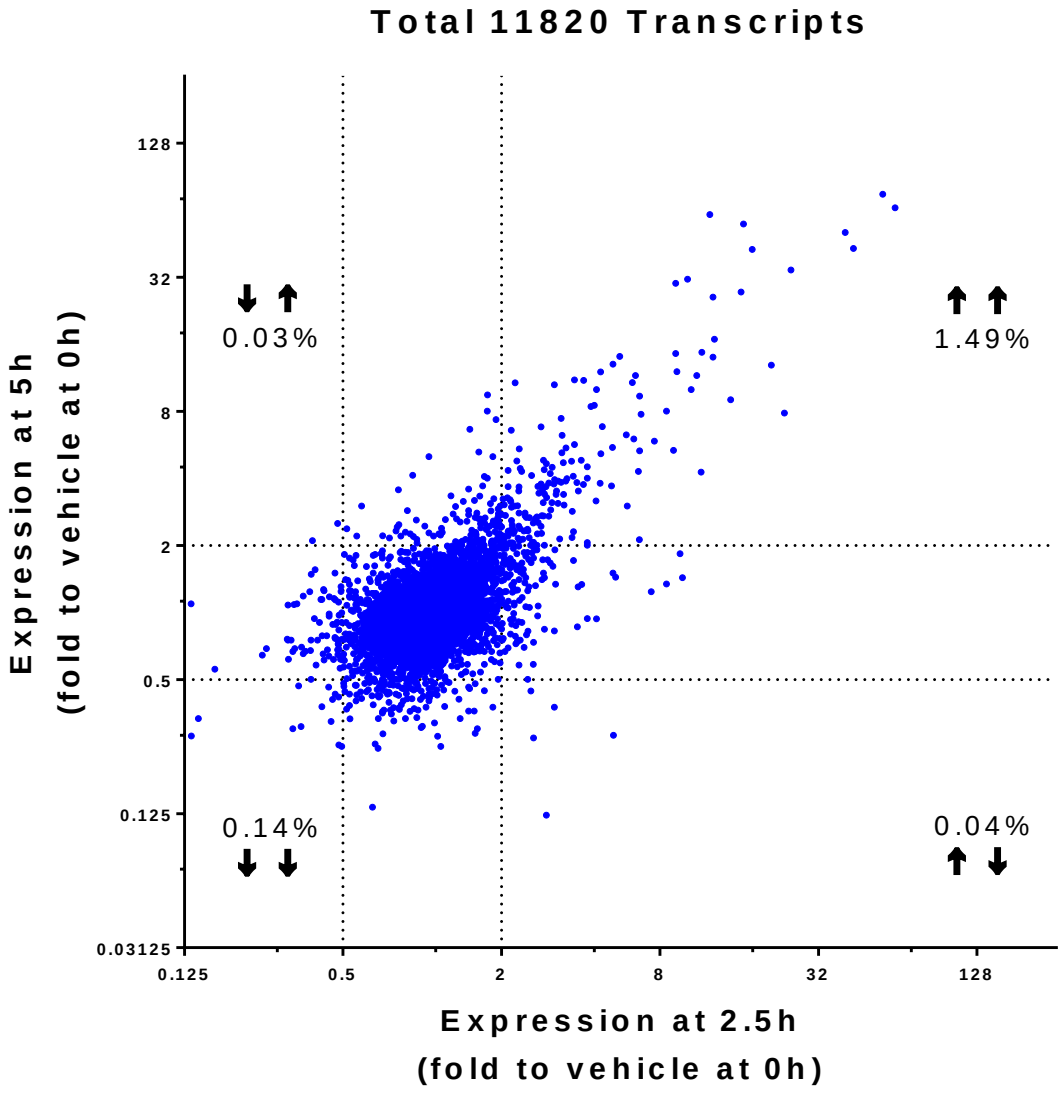

Figure 5.3.8 Whole transcriptome analysis at 2.5 and 5 h treatment points.

Since genes that were affected at the early points were more likely related to the target of our compounds, we plotted the mRNA expression of all transcripts at 2.5 h and 5 h (**Figure 5.3.8**). The upper-right area showed the transcripts with elevated expression. It appeared that a significant number of genes were upregulated. For example, 1.49% of genes had a 2-fold increase at both 2.5 h and 5 h. Among them, we found that CYP1A1 gene was

significantly upregulated. CYP1A1 is one of the targeted genes of aryl hydrocarbon receptor (AhR)[222].

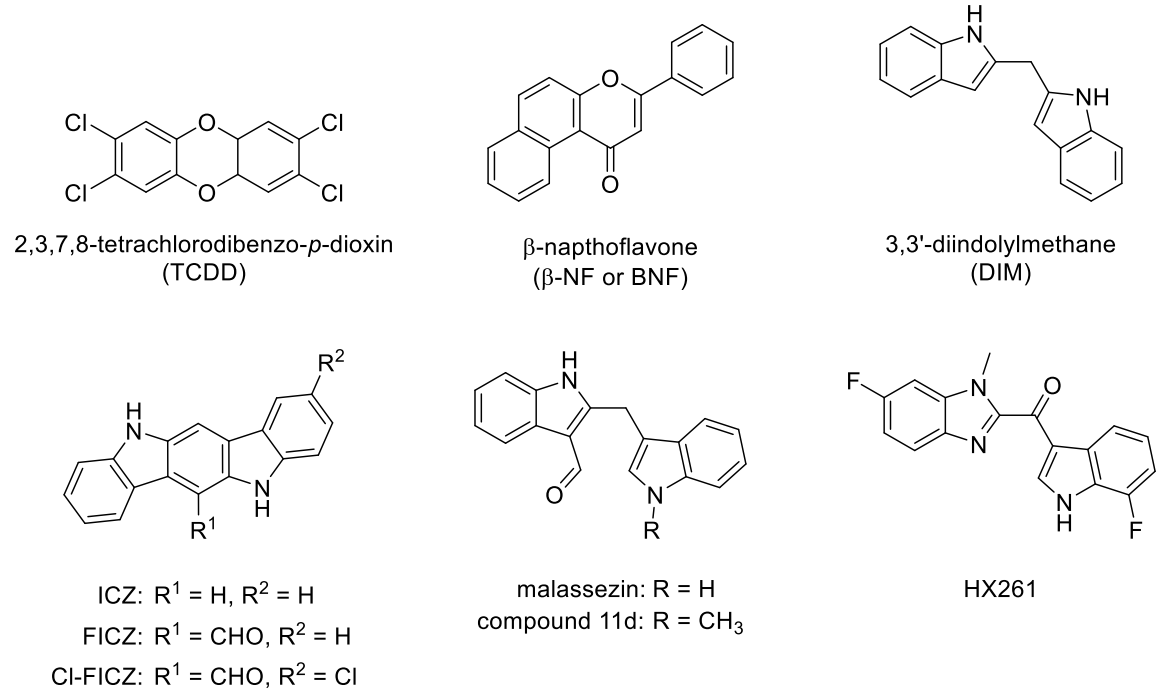

Figure 5.3.9 AhR agonists and HX261.

The activation of genes targeted by AhR is ligand-dependent[223]. AhR ligand or agonist can bind to the PAS domain of AhR and induce conformational change, leading to translocation of AhR to nucleus. AhR will then dimerize with AhR nuclear translocator (ARNT) to recognize xenobiotic-responsive element (XRE) on targeted genes. The known AhR agonist included many flat aromatic heterocycles[213,224–226], such as tetrachlorodibenzo-*p*-dioxin (TCDD), β-napthoflavone (BNF), 3,3'-diindolylmethane (DIM), indolo[3,2-*b*]carbazole (ICZ) and malassezin as illustrated in **Figure 5.3.9**. Our lab has previously prepared chloro-substituted 6-formylindolo[3,2-b]carbazole (Cl-FICZ)[210] and N-

methylated malassezin 11d ("11d" as compound number in original article)[213]. Based on the similarities of some of these structures to **HX261**, it is possible that **HX261** also acted on AhR, though there was no report on the possible connection between AhR and PCSK9 priori to our study.

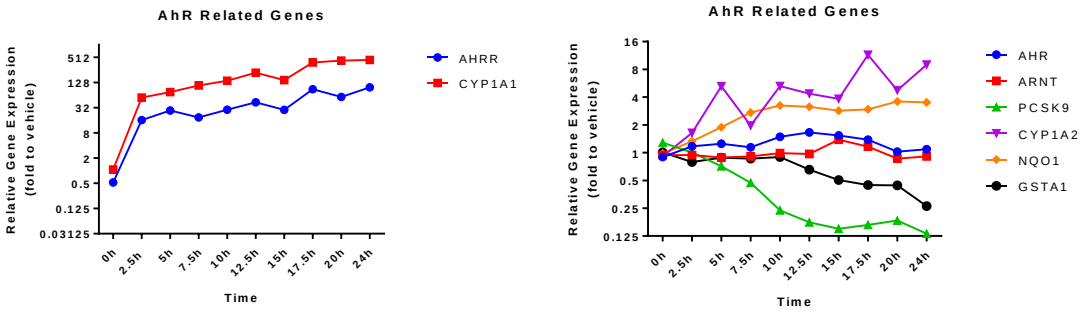

Figure 5.3.10 HX261 affected AhR-related transcripts.

When explored AhR related genes from RNA-seq data, the CYP1A1 mRNA was increased significantly. In addition, we found that AhR repressor (AHRR) was also dramatically increased upon compound treatment (**Figure 5.3.10**). AHRR is a target of AhR and a feedback suppressor[227]. Several other related genes such as NQO1, CYP1A2 and GSTA1 were either up-regulated or down-regulated. After searching the literatures more extensively, we found a 2016 thesis suggesting a possible correlation between AhR and PCSK9[228]. In this thesis, they reported that AhR agonists BNF and TCDD suppressed PCSK9 expression on both mRNA and protein level. They also suggested that AhR may regulate PCSK9 by binding to the one of the XRE elements on the PCSK9 promoter.

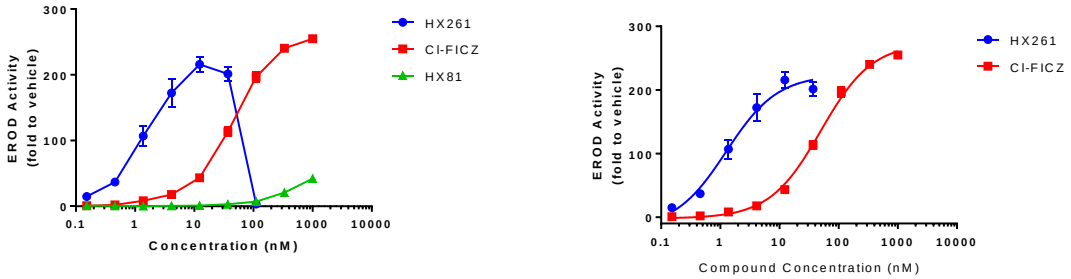

Figure 5.3.11 HX261 and Cl-FICZ induced strong EROD activity.

We next used the 7-ethoxyresorufin-O-deethylase (EROD) assay to examine if our PCKS9 modulators also activate AhR. The EROD assay is based on CYP1A1 enzymatic activity[229]. Activated AhR can translocate from cytoplasm to nuclei and dimerize with ARNT to activate downstream genes, including CYP1A1, which can catalyze the cleavage of the ethyl group in 7-ethoxy-resorufin and convert it to fluorescent resorufin. Three compounds, HX261, HX81 (the precursor of HX261) and Cl-FICZ (a known AhR agonist[210]) were selected to test in the EROD assay using HepG2 cells. After treating cells with these compounds for 24 h, cells were analyzed by the EROD assay. **Figure 2.3.11** showed that both HX261 and Cl-FICZ induced strong fluorescence signal, while HX81 did not. However, the fluorescence signal dropped at high concentration (≥100 nM) of HX261. The calculated EC_{50}s of HX261 and Cl-FICZ were 1.3 nM and 50.1 nM, respectively. This indicated that HX261 could induce the expression of CYP1A1 in HepG2 cells.

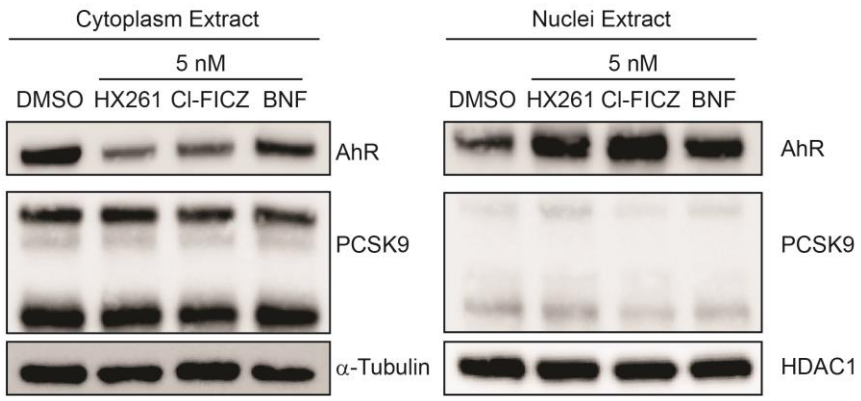

Figure 5.3.12 AhR underwent re-localization upon agonist treatment.

AhR agonists can bind to AhR and activate the translocation of AhR from cytoplasm to nuclei, where AhR triggers the downstream gene expression[230,231]. We next verified the translocation of AhR after the treatment of our compounds. We treated HepG2 cells with 5 nM HX261 and known agonists, Cl-FICZ and BNF, for 1 h. We then harvested the cytoplasmic proteins and nuclei proteins separately according to standard protocols (**Figure 5.3.12**). The expression of selected proteins was examined by western blot. We used α-tubulin and HDAC1 as the loading control for cytoplasmic extract and nuclei extract, respectively. The amount of AhR in cytoplasm was decreased upon treatment of HX261 and Cl-FICZ. BNF induced less reduction of AhR in cytoplasm. At the meantime, AhR was enriched in nuclei in response to all agonists. PCSK9 is a secreted protein and had less expression in nuclei comparing in cytoplasm. The rapid re-localization of ligand-bound AhR confirmed the role of HX261 as a potent agonist.

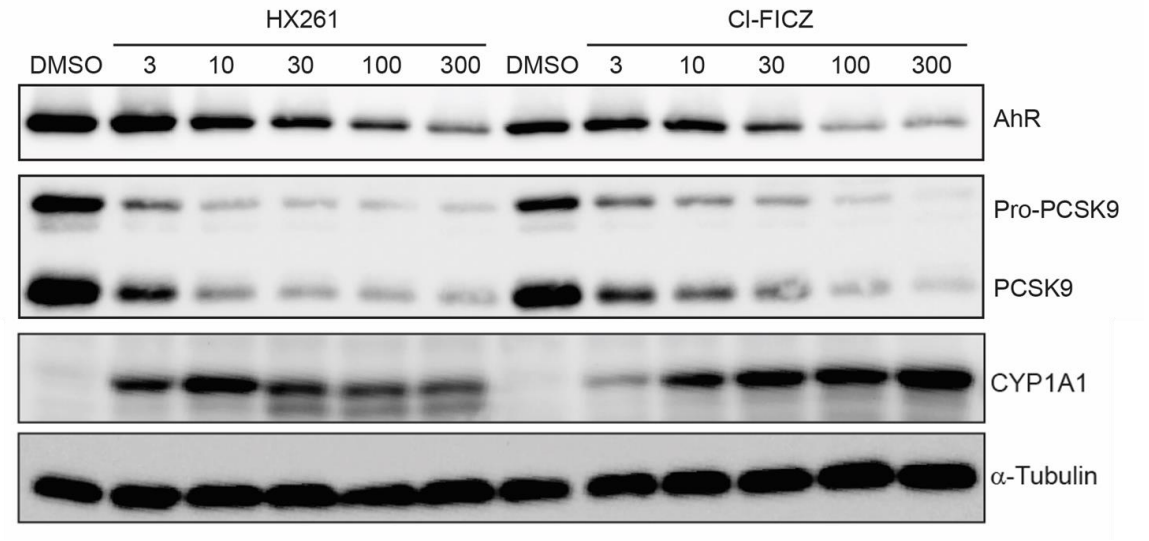

Figure 5.3.13 Dose response study of HX261 and Cl-FICZ.

To probe the effects of AhR agonists, we used western blot to analyze HepG2 cells treated by HX261 and Cl-FICZ at various concentrations for 24 h (**Figure 5.3.13**). Cellular PCSK9 level was significantly suppressed by both compounds at as low as 3 nM. HX261 reached its maximal effects at 10 nM, while the effect of Cl-FICZ was maximized at 100 nM, indicating HX261 was more potent in modulating PCSK9. In addition, we observed that the AhR was decreased at higher concentrations of compounds. It might due to nuclei exportation of AhR followed by proteasome degradation[232]. In comparison with HX261, Cl-FICZ induced more AhR degradation. It suggested that different ligands have different effects on the PCSK9 downregulation and AhR degradation, depending on their structures. Interestingly, HX261 induced significant expression of CYP1A1 at 10 nM, and the effect was decreased with increasing concentrations. In the meantime, Cl-FICZ upregulated CYP1A1 in a dose-dependent manner. This result was consistent with EROD results discussed above. EROD activity should be positively correlated with CYP1A1 expression.

Overdosed HX261 was suspected to undergo unknown inhibition for both CYP1A1 expression and activity. One of the possible reasons is that the AhR agonist may inhibit the enzymatic activity of CYP1A1 as suggested by literature, because most AhR agonists are substrates of CYP1A1 enzumes[229]. The inhibition effect might also trigger unknown negative feedback in the AhR-CYP1A1 regulatory loop.

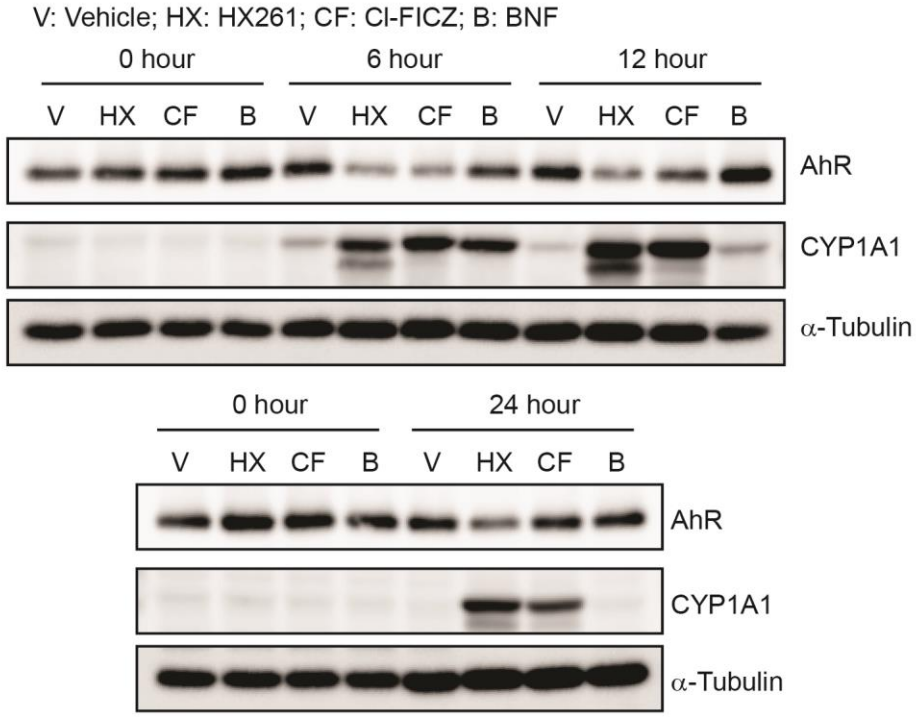

Figure 5.3.14 Time-course study of AhR agonist.

To understand the mechanism of this pathway, we performed a 24 h time-course experiment (**Figure 5.3.14**). HepG2 cells were treated with 30 nM of compounds and were collected at 0 h, 6 h, 12 h and 24 h. We found that the expression of AhR was affected as early as 6 h by HX261 and Cl-FICZ but not BNF. All three compounds induced CYP1A1 expression at 6 h. But only HX261 and Cl-FICZ achieved maximal effects at 12 h and the

effect was decreased slightly afterwards. BNF induced CYP1A1 at 6 h, but not at 12h and 24h. The lower metabolic stability of BNF might be one reason for this observation. A stable compound would sustainably activate AhR and induce the expression of CYP1A1. In the future, comparison of stability of all three compounds will be conducted to confirm this result.

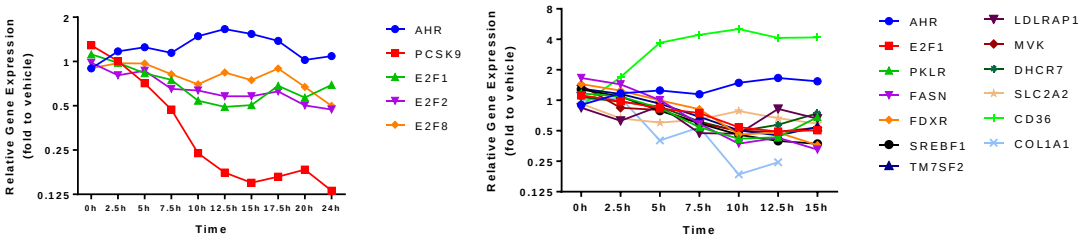

Figure 5.3.15 E2F family and E2F1 related genes affected by HX261 in RNA-seq

The RNA-seq data also indicted that E2F family and E2F1 related genes were affected by HX261 (**Figure 5.3.15**). E2F family were critical transcriptional regulators in multiple pathways[233]. E2F1 can directly interact with AhR and serve as co-factor to regulate transcription of genes such as APAF1, MYCN and PCNA[231,234,235]. E2F1 has also been reported to target PCSK9 promoter and modulate the transcription[236]. E2F1 protein is positively correlated with PCSK9. Knockout of E2F1 decreased the expression of PCSK9 mRNA and protein. Thus, we hypothesized that E2F1 might be the mediator between AhR and PCSK9. For example, activated and translocated AhR might bind to E2F1 and interact with the PCSK9 promoter leading to repressed transcription.

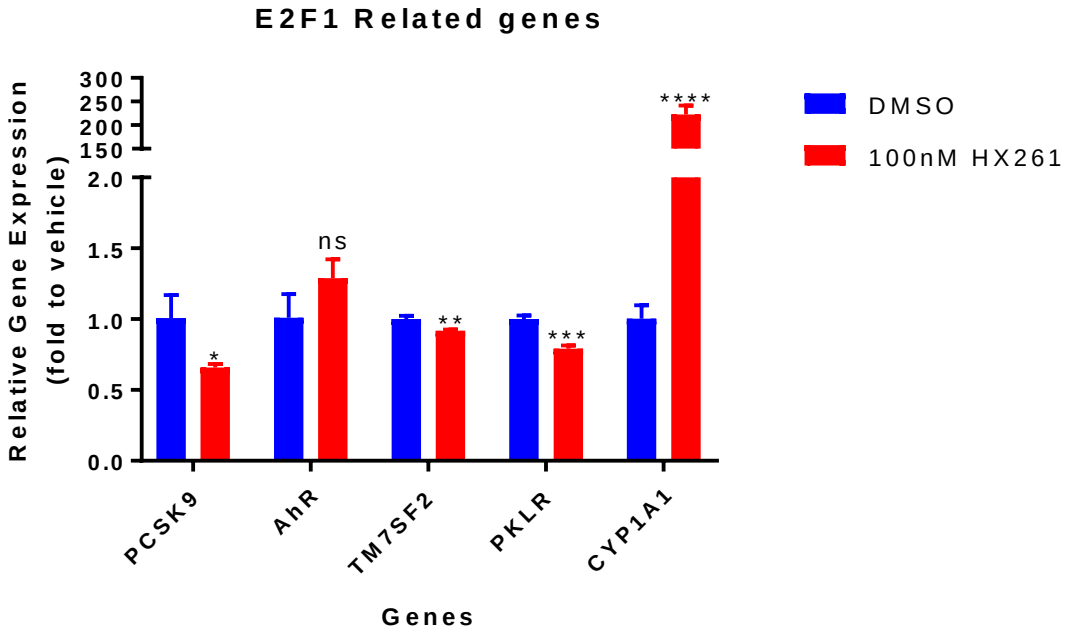

Figure 5.3.16 E2F1 related gene transcription was affected by AhR agonists.

To verify the results from RNA-seq, we investigated the mRNA change of related genes. HepG2 cells were treated with 100 nM HX261 or vehicle for 12 h and examined by qRT-PCR. We observed the reduction of PCSK9 mRNA and the increase of CYP1A1 mRNA, while AhR transcription remained intact. These data verified results from RNA-seq. We also examined genes that were reported to be targeted by E2F1. For example, the DNA of TM7SF2 and PKLR were enriched by E2F1 chromatin immunoprecipitation (ChIP)[236,237]. We only observed 10% (*P = 0.005) and 20% (**P = 0.0005) reduction for TM7SF2 and PKLR gene expression, respectively. Although the fold of change was not dramatic, this result indicated that our compounds affected genes transcriptionally regulated by E2F1. More experiments will be done to confirm this result and our hypothesis that HX261 may affect PCSK9 transcription through AhR-E2F1 pathway.

5.4. Summary and Future Work

To summary, we established a phenotypic screening platform for the development of small-molecule PCSK9 modulators and discovered novel molecule HX261, which could potently suppress PCSK9 expression. Investigation of the mechanism of action of HX261 uncovered a novel regulatory pathway of PCSK9 through AhR. In addition, transcriptional factor E2F1 was hypothesized as mediator in this novel pathway based on our preliminary results and literature.

Future work will focus on validation of this pathway. Orthogonal assays will be developed to confirm the BIIKs as AhR agonist. For example, we will use ITC, SPR or microscale thermophoresis (MST) to verify the binding between AhR and HX261. It has been reported that AhR can be degraded by PROTACs employing apigenin as the ligand of AhR[238,239]. We can develop PROTAC degraders by tethering HX261 with E3 ligase ligand, such as pomalidomide or VHL ligands discussed in **Chapter 2** and **4**. Successful depletion of AhR by this type of PROTACs in cells would support the engagement of AhR in HX261-mediated downregulation of PCSK9. We can also use siRNA/shRNA or CRISPR technology to knockdown or knockout AhR. If PCSK9 was regulated by AhR and its agonist, the absence of AhR would lead to downregulation of PCSK9.

E2F1 was hypothesized to bridge the interaction between AhR and PCSK9 promoter. We can use co-immunoprecipitation (Co-IP) to pull down E2F1 or AhR with interacted proteins from cell lysate. Western blot analysis will confirm the cellular interaction between E2F1 and AhR. Immobilization-free binding assay such as MST can be used to

examine the potential interactions between AhR and E2F1 in the presence or absence of AhR agonists. Since AhR and E2F1 are both transcriptional factors interacting with DNA sequence, we can use ChIP-seq to extract DNA sequence or promoters targeted by them. Alternatively, we can directly analyze ChIP sample to examine whether PCSK9 promoter or DNA sequence is enriched from ChIP or not. If the AhR-E2F1-DNA crosstalk was confirmed, co-crystallization of complex including AhR, E2F1 and targeted DNA fragment can further confirm their interactions .

5.5. Experimental Procedures

Cell line and sample preparation

HepG2, Huh6 and Huh7 cells was cultured in low-glucose DMEM medium supplemented with 10% FBS, 1% Penicillin/Streptomycin, 1% Non-essential amino acid, 1% Sodium pyruvate and 1% L-glutamine. Aml-12 cells was cultured in DMEM/F2 (1:1) medium supplemented with 0.005 mg/ml insulin, 0.005 mg/ml transferrin, 5 ng/ml selenium, and 40 ng/ml dexamethasone, and 10% fetal bovine serum. All cell lines were grown at 37°C in a humidified 5% CO_2 atmosphere.

PCSK9 ELISA assay

When reach 90% confluence, cells were harvested and plated 1 x 10^5 cells per well in 96-well plate. After overnight settle-down, the culture medium was removed. 200 uL of dose medium contain compounds or vehicle in desired compound was added to each well. After 24 hours, each well was refreshed with same medium, followed by another 24-hour

incubation. Finally, 100uL supernatant medium was collected after spin-down at 3000 rpm for 3 mins. Cells was washed twice with cold PBS and lysed with 50 uL RIPA buffer per well after wash with PBS. After 10 mins incubation on ice, the cells were frozen at -20°C overnight. Second day, cells were thawed and span down at 15000 rpm for 15 min. Supernatant was collected. Both medium and/or lysate sample was stored at -20°C if needed.

ELISA assay was processed to measure PCSK9 content in cell culture medium or cell lysate according to manufacture protocol (R&D system, DY3888). 100uL of 2.0 ug/mL PCSK9 capture antibody in PBS was add into high-binding plate (R&D system, DY990). After overnight incubation at room temperature, solution was removed and wash with ~400uL of wash buffer (0.05% Tween-20 in PBS) three times. Then 300 µL of reagent diluent (1% BSA in PBS) was added to each well and incubate for at least 1 hour. The following each step was started with remove of previous solution and wash with wash buffer. Then, 100 µL PCSK9 standard or sample with or without dilution in reagent was added to each well followed with 2-hour incubation. Next, 100 µL of 100 ng/mL PCSK9 detection antibody in reagent was added to each well followed with 2-hour incubation. After detection antibody incubation, 100uL of Streptavidin-HRP was added to each well and incubated for 20 min. Finally, 100uL of TMB solution was added and incubated for 20 mins followed with addition of 50 µL of stop solution (2 N H2SO4). After mixing, determine the optical density of each well immediately, using a microplate reader set to 450 nm and wavelength correction to 570 nm. Subtract readings at 570 nm from the readings at 450 nm.

$$Corrected\ OD = OD_{450}\ of\ Assay\ or\ Standard - OD_{570} of\ Assay\ or\ Standard$$

Corrected ODs of PCSK9 standards were plot and performed linear regression to yield standard curve in GraphPad Prism 7. See example as followed graph.

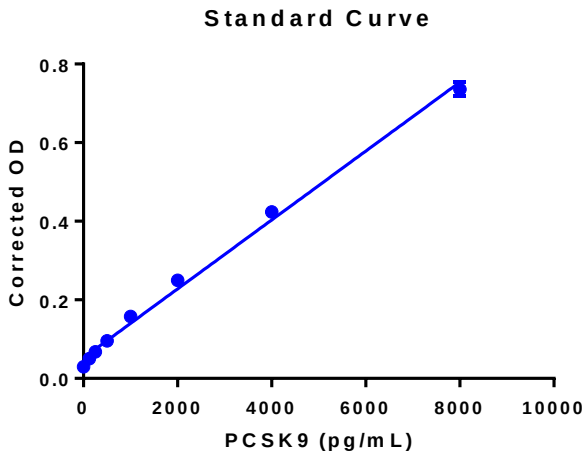

The corrected ODs in assay wells were interpreted to PCSK9 concentrations (PCs) by the standard curve. Normalization was processed by the value of compound-treated groups to vehicle-treated groups give relative PCSK9 expression.

$$Relative\ PCSK9 = \frac{PC\ of\ compound\ treated\ group}{average\ PC\ of\ vehivle\ treated\ groups}$$

Relative PCSK9 was plotted in GraphPad Prism 7. Bar or plot represented the mean of each treatment with ± SD as error. For dose response curve, nonlinear fitting of [Inhibitor] vs. response (three parameters) was generated by GraphPad Prism 7.

Immunoblot

Refer to Chapter 2 section 2.5 for general procedures. Antibodies against PCSK9 (Santa Cruz Biotechnology), LDLR (R&D system), α-Tubulin (R&D system), β-Actin (R&D system) and CYP1A1 (Proteintech) antibodies was purchased. Anti-AhR antibody, anti-mouse- and anti-rabbit HRP-linked antibodies was purchased from Cell Signaling Technology.

Microsomal Stability Assay

Metabolic stability was assessed in the presence of 0.5 mg/mL Human, mouse, and rat liver microsomes (XenoTech). All liquid dispense and transfer steps were performed with the Freedom Evo automated liquid handler (Tecan US). NADPH, a required cofactor for CYP450 metabolism, was provided by the NADPH Regenerating System, Solutions A (BD Biosciences) and B (BD Biosciences). 10 µM compound stock solutions were initially prepared in 100% DMSO and subsequently diluted in acetonitrile for the assay. The pH of the reactions was kept at ~ 7.4 with potassium phosphate buffer (BD Biosciences). The reaction wells were prepared by adding microsomes to a well and allowed to warm to 37 ˚C. Then compound was added to each well. The reactions were started by adding NADPH to the reaction well containing microsomes and compounds. Negative controls received buffer only (instead of NADPH). Immediately after reaction are started, 0 min aliquots were promptly collected and mixed in a separate well with ice cold acetonitrile (spiked with internal standards) to quench the reactions. The remainder of the reaction volume was incubated at 37 °C with shaking. An additional aliquot was collected at 60 min after the start of the reaction and promptly quenched with ice cold acetonitrile (spiked with an internal standard). Samples were vortexed and centrifuged at 3700 rpm for 10 min. The

amount of compound in the supernatant was determined by LC/MS/MS (Thermo Scientific, Endura) and the percent of parent compound remaining after 60 min was calculated by the following formula:

$$\%\ Parent\ Compound\ Remaining = \left[\frac{Concentration\ at\ 60\ min}{Concentration\ at\ 0\ min} \times 100\right]$$

All reactions were run in triplicate, except negative controls (no NADPH) which were performed as single reactions. Results reported are the mean of each reaction triplicate, normalized to the internal standard, and expressed as a percent compound remaining after the incubation time.

RNA extraction and q-PCR assay

When reach 90% confluence, cells were harvested and plated $3X10^5$ cells per well in 24-well plate. Refer to **Chapter 2 Section 2.5** for detail procedures. ACTB or GAPDH was used as internal reference genes. All expression was normalized to vehicle-treated group. The bar graph was generated and by GraphPad Prism. Normalized data was graphed as bar graph representing as mean of relative viability (n = 3) with ± SD as error bar.

Gene-selective primer pairs were generated by Integrated DNA Technologies (IDT). All primer sequences are listed as following table.

Primer Sequence Table

Gene	Forward Primer	Reverse Primer
PCSK9	TGGAACCTGGAGCGGATTA	CTCTGTATGCTGGTGTCTAGGA
PCSK9[a]	GACACCAGCATACAGAGTGACC	GTGCCATGACTGTCACACTTGC
LDLR	CTCCCGCCAAGATCAAGAAA	GTTTGGAGTCAACCCAGTAGAG
SREBP2	GACCTGAAGATCGAGGACTTTAAT	AGAGTCAATGGAGTAGGGAGAG
HMGCR	GAGACAGGGATAAACCGAGAAAG	GGAGGAGTTACCAACCACAAA
ACTB	ATGATGATATCGCCGCGCTC	ATGATGATATCGCCGCGCTC
CYP1A1[a]	GAT TGA GCA CTG TCA GGA GAA GC	ATG AGG CTC CAG GAG ATA GCA G
PKLR[a]	CGG AAG GAC ACG GCA TCA AGA T	GAG CCA GGA AAA CCT TCT CTG C
TM7SF2[a]	GGT CAA TGG CTT CCA GTT GCT C	AAC GCC AGC ATG AAG CCA AAC C
GAPDH[a]	CTCCTCTGACTTCAACAGCGACAC	TGCTGTAGCCAAATTCGTTGTCAT

[a]Primers used for **Figure 5.3.16**

RNA-sequencing experiment

When reach 90% confluence, cells were harvested and plated $1X10^6$ cells per well in 35mm-dish. After overnight settle-down, the cells were treated with dose medium contain either DMSO or 100nM HX261. Cells were harvested and total RNA was isolated follow method above at 0h, 2.5h, 5h, 7.5h, 10h, 12.5h, 15h, 17.5h, 20h and 24h. RNA was then

measured for quality and PCSK9 mRNA level. Purified mRNA was first analyzed for quality control by Agilent 2100 Bioanalyzer. Then mRNA samples were submitted to UW Biotechnology Center for sample QC, library preparation and sequencing. Bioinformatic analysis was done in collaboration with Dr Christina Kendziorski and Dr Rhonda Bacher.

MTT Cell Viability Assay

When reach 90% confluence, cells were harvested and plated $1X10^5$ cells per well in 96-well plate. Refer to **Chapter 2 Section 2.5** for detail procedures.

Pharmacokinetic Study

After mice was IP injected with compound solution, mice blood was collected by retro-orbital method. Crude blood sample was added EDTA and span down. Supernatant plasma was collected and stored at -20 °C. Plasma samples was thawed before use. Compound standard was prepared with pooled plasma sample. 50 µL of plasma samples and standard samples was add into each well of Ostro Sample Preparation Plate for solid-phase extraction. Then 150 µL acetonitrile (1% formic acid) containing internal standard was added and mixed by pipette. Next, clear sample solution was eluted by positive pressure processor under 60 psi for 5 mins. The sample solution can be used directly for LC-MS/MS analysis. In our case, we used QTrap-5500 and Acquity UPLC system to analyze the content of remaining content of compound. While using Waters ACQUITY UPLC BEH C8 column and HX237 as internal standard, 20% to 80% [ACN/water] mobile phase was conducted in 5 mins. MS data was analyzed by Analyst® software and standard curve was processed by four-parameter logistic (4-PL) curve-fit.

EROD assay

HepG2 cells were plated $1X10^5$ cells per well in 96-well plate(s) avoiding side wells by adding 200µL PBS to them. After overnight seeding, cells were treated with compound or vehicle for 24 hours. Then cells were washed cells with 200uL warm PBS twice, followed by addition of 100µl 1uM 7-Ethoxy-Resorufin in PBS. Then the cells were incubated for 2 hours. To prepare Resorufin standard, dilute Resorufin stock in PBS give 2 µM highest standard solution and then make serial 1:2 dilution of 2 µM solution in PBS give 1 µM, 500 nM, 250 nM, 125 nM, 62.5 nM, 31.3 nM and 15.6 nM. After incubation, non-cell wells were added 100µL standard and PBS control to the PBS-filled wells in the plate after remove the original PBS solution. Then read the plate with excitation at 520nm with a 10nm bandwidth and emission at 595nm with a 10nm bandwidth. To calculate the fluorescent intensity (FI), subtract the fluorescent density value of PBS control from standard and assay wells.

$$Corrected\ FI = FI_{595}\ of\ assay\ or\ standard - FI_{595} of\ PBS\ control$$

Corrected FIs of resorufin standards were plot and performed linear regression to yield standard curve in GraphPad Prism 7. See example as followed graph.

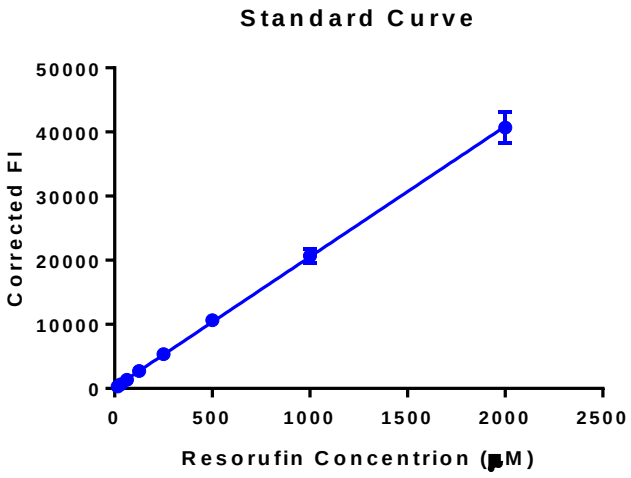

The corrected FIs in assay wells were interpreted to resorufin concentrations (RCs) by the standard curve. Normalization was processed by the value of compound-treated groups to vehicle-treated groups give relative EROD activity.

$$Relative\ EROD\ Activity = \frac{RC\ of\ compound\ treated\ group}{average\ RC\ of\ vehivle\ treated\ groups}$$

Relative EROD activity was plotted in GraphPad Prism 7. Bar or plot represented the mean of each treatment with ± SD as error. For dose response curve, nonlinear fitting of [Inhibitor] vs. response (three parameters) was generated by GraphPad Prism 7.

Statistical Analysis

All statistical analysis was done by GraphPad Prism. Statistical significance was analyzed by performing two-tailed and unpaired t-test of variance. Not significant (ns) $P > 0.05$, $^{*}P \leq 0.05$, $^{**}P \leq 0.01$, $^{****}P \leq 0.001$, $^{****}P \leq 0.0001$.

6. References

(1) Cong, L.; Ran, F. A.; Cox, D.; Lin, S.; Barretto, R.; Habib, N.; Hsu, P. D.; Wu, X.; Jiang, W.; Marraffini, L. A.; Zhang, F. Multiplex Genome Engineering Using CRISPR/Cas Systems. *Science* **2013**, *339* (6121), 819–823.

(2) Bernstein, E.; Caudy, A. A.; Hammond, S. M.; Hannon, G. J. Role for a Bidentate Ribonuclease in the Initiation Step of RNA Interference. *Nature* **2001**, *409* (6818), 363–366.

(3) Bondeson, D. P.; Mares, A.; Smith, I. E. D.; Ko, E.; Campos, S.; Miah, A. H.; Mulholland, K. E.; Routly, N.; Buckley, D. L.; Gustafson, J. L.; Zinn, N.; Grandi, P.; Shimamura, S.; Bergamini, G.; Faelth-Savitski, M.; Bantscheff, M.; Cox, C.; Gordon, D. A.; Willard, R. R.; Flanagan, J. J.; Casillas, L. N.; Votta, B. J.; den Besten, W.; Famm, K.; Kruidenier, L.; Carter, P. S.; Harling, J. D.; Churcher, I.; Crews, C. M. Catalytic in Vivo Protein Knockdown by Small-Molecule PROTACs. *Nat. Chem. Biol.* **2015**, *11* (8), 611–617.

(4) Sun, X.; Wang, J.; Yao, X.; Zheng, W.; Mao, Y.; Lan, T.; Wang, L.; Sun, Y.; Zhang, X.; Zhao, Q.; Zhao, J.; Xiao, R.-P.; Zhang, X.; Ji, G.; Rao, Y. A Chemical Approach for Global Protein Knockdown from Mice to Non-Human Primates. *Cell Discov.* **2019**, *5* (1), 10.

(5) An, Z.; Lv, W.; Su, S.; Wu, W.; Rao, Y. Developing Potent PROTACs Tools for Selective Degradation of HDAC6 Protein. *Protein Cell* **2019**, *10* (8), 606–609.

(6) Tokatlian, T.; Segura, T. SiRNA Applications in Nanomedicine. *Wiley Interdiscip. Rev. Nanomedicine Nanobiotechnology* **2010**, *2* (3), 305–315.

(7) Welchman, R. L.; Gordon, C.; Mayer, R. J. Ubiquitin and Ubiquitin-like Proteins as Multifunctional Signals. *Nat. Rev. Mol. Cell Biol.* **2005**, *6* (8), 599–609.

(8) Lai, A. C.; Crews, C. M. Induced Protein Degradation: An Emerging Drug Discovery Paradigm. *Nat. Rev. Drug Discov.* **2017**, *16* (2), 101–114.

(9) Gadd, M. S.; Testa, A.; Lucas, X.; Chan, K.; Chen, W.; Lamont, D. J.; Zengerle, M.; Ciulli, A. Structural Basis of PROTAC Cooperative Recognition for Selective Protein Degradation. *Nat. Chem. Biol.* **2017**, *13* (5), 514–521.

(10) Ottis, P.; Crews, C. M. Proteolysis-Targeting Chimeras: Induced Protein Degradation as a Therapeutic Strategy. *ACS Chem. Biol.* **2017**, *12* (4), 892–898.

(11) An, S.; Fu, L. Small-Molecule PROTACs: An Emerging and Promising Approach for the Development of Targeted Therapy Drugs. *EBioMedicine* **2018**, *36*, 553–562.

(12) Sakamoto, K. M.; Kim, K. B.; Kumagai, A.; Mercurio, F.; Crews, C. M.; Deshaies, R. J. Protacs: Chimeric Molecules That Target Proteins to the Skp1-Cullin-F Box Complex for Ubiquitination and Degradation. *Proc. Natl. Acad. Sci.* **2001**, *98* (15), 8554–8559.

(13) Yaron, A.; Hatzubai, A.; Davis, M.; Lavon, I.; Amit, S.; Manning, A. M.; Andersen, J. S.; Mann, M.; Mercurio, F.; Ben-Neriah, Y. Identification of the Receptor Component of the IκBα–Ubiquitin Ligase. *Nature* **1998**, *396* (6711), 590–594.

(14) Deshaies, R. J. SCF and Cullin/RING H2-Based Ubiquitin Ligases. *Annu. Rev. Cell Dev. Biol.* **1999**, *15* (1), 435–467.

(15) Griffith, E. C.; Su, Z.; Turk, B. E.; Chen, S.; Chang, Y.-H.; Wu, Z.; Biemann, K.; Liu, J. O. Methionine Aminopeptidase (Type 2) Is the Common Target for Angiogenesis Inhibitors AGM-1470 and Ovalicin. *Chem. Biol.* **1997**, *4* (6), 461–471.

(16) Sakamoto, K. M.; Kim, K. B.; Verma, R.; Ransick, A.; Stein, B.; Crews, C. M.; Deshaies, R. J. Development of Protacs to Target Cancer-Promoting Proteins for Ubiquitination and Degradation. *Mol. Cell. Proteomics* **2003**, *2* (12), 1350–1358.

(17) Schneekloth, J. S.; Fonseca, F. N.; Koldobskiy, M.; Mandal, A.; Deshaies, R.; Sakamoto, K.; Crews, C. M. Chemical Genetic Control of Protein Levels: Selective in Vivo Targeted Degradation. *J. Am. Chem. Soc.* **2004**, *126* (12), 3748–3754.

(18) Hon, W.-C.; Wilson, M. I.; Harlos, K.; Claridge, T. D. W.; Schofield, C. J.; Pugh, C. W.; Maxwell, P. H.; Ratcliffe, P. J.; Stuart, D. I.; Jones, E. Y. Structural Basis for the Recognition of Hydroxyproline in HIF-1α by PVHL. *Nature* **2002**, *417* (6892), 975–978.

(19) Schneekloth, A. R.; Pucheault, M.; Tae, H. S.; Crews, C. M. Targeted Intracellular Protein Degradation Induced by a Small Molecule: En Route to Chemical Proteomics. *Bioorg. Med. Chem. Lett.* **2008**, *18* (22), 5904–5908.

(20) Zhao, Y.; Aguilar, A.; Bernard, D.; Wang, S. Small-Molecule Inhibitors of the MDM2-P53 Protein-Protein Interaction (MDM2 Inhibitors) in Clinical Trials for Cancer Treatment. *J. Med. Chem.* **2015**, *58* (3), 1038–1052.

(21) Hines, J.; Lartigue, S.; Dong, H.; Qian, Y.; Crews, C. M. MDM2-Recruiting PROTAC Offers Superior, Synergistic Antiproliferative Activity via Simultaneous Degradation of BRD4 and Stabilization of P53. *Cancer Res.* **2019**, *79* (1), 251–262.

(22) Clague, M. J.; Heride, C.; Urbé, S. The Demographics of the Ubiquitin System. *Trends Cell Biol.* **2015**, *25* (7), 417–426.

(23) Pettersson, M.; Crews, C. M. PROteolysis TArgeting Chimeras (PROTACs) — Past, Present and Future. *Drug Discov. Today Technol.* **2019**, *31*, 15–27.

(24) Itoh, Y.; Ishikawa, M.; Naito, M.; Hashimoto, Y. Protein Knockdown Using Methyl Bestatin-Ligand Hybrid Molecules: Design and Synthesis of Inducers of Ubiquitination-Mediated Degradation of Cellular Retinoic Acid-Binding Proteins. *J. Am. Chem. Soc.* **2010**, *132* (16), 5820–5826.

(25) Itoh, Y.; Ishikawa, M.; Kitaguchi, R.; Sato, S.; Naito, M.; Hashimoto, Y. Development of Target Protein-Selective Degradation Inducer for Protein Knockdown. *Bioorg. Med. Chem.* **2011**, *19* (10), 3229–3241.

(26) Okuhira, K.; Ohoka, N.; Sai, K.; Nishimaki-Mogami, T.; Itoh, Y.; Ishikawa, M.; Hashimoto, Y.; Naito, M. Specific Degradation of CRABP-II via CIAP1-Mediated Ubiquitylation Induced by Hybrid Molecules That Crosslink CIAP1 and the Target Protein. *FEBS Lett.* **2011**, *585* (8), 1147–1152.

(27) Ohoka, N.; Okuhira, K.; Ito, M.; Nagai, K.; Shibata, N.; Hattori, T.; Ujikawa, O.; Shimokawa, K.; Sano, O.; Koyama, R.; Fujita, H.; Teratani, M.; Matsumoto, H.; Imaeda, Y.; Nara, H.; Cho, N.; Naito, M. In Vivo Knockdown of Pathogenic

Proteins via Specific and Nongenetic Inhibitor of Apoptosis Protein (IAP)-Dependent Protein Erasers (SNIPERs). *J. Biol. Chem.* **2017**, *292* (11), 4556–4570.

(28) Buckley, D. L.; Van Molle, I.; Gareiss, P. C.; Tae, H. S.; Michel, J.; Noblin, D. J.; Jorgensen, W. L.; Ciulli, A.; Crews, C. M. Targeting the von Hippel–Lindau E3 Ubiquitin Ligase Using Small Molecules To Disrupt the VHL/HIF-1α Interaction. *J. Am. Chem. Soc.* **2012**, *134* (10), 4465–4468.

(29) Galdeano, C.; Gadd, M. S.; Soares, P.; Scaffidi, S.; Van Molle, I.; Birced, I.; Hewitt, S.; Dias, D. M.; Ciulli, A. Structure-Guided Design and Optimization of Small Molecules Targeting the Protein–Protein Interaction between the von Hippel–Lindau (VHL) E3 Ubiquitin Ligase and the Hypoxia Inducible Factor (HIF) Alpha Subunit with in Vitro Nanomolar Affinities. *J. Med. Chem.* **2014**, *57* (20), 8657–8663.

(30) Zengerle, M.; Chan, K.-H.; Ciulli, A. Selective Small Molecule Induced Degradation of the BET Bromodomain Protein BRD4. *ACS Chem. Biol.* **2015**, *10* (8), 1770–1777.

(31) Lai, A. C.; Toure, M.; Hellerschmied, D.; Salami, J.; Jaime-Figueroa, S.; Ko, E.; Hines, J.; Crews, C. M. Modular PROTAC Design for the Degradation of Oncogenic BCR-ABL. *Angew. Chemie - Int. Ed.* **2016**, *55* (2), 807–810.

(32) Raina, K.; Lu, J.; Qian, Y.; Altieri, M.; Gordon, D.; Rossi, A. M. K.; Wang, J.; Chen, X.; Dong, H.; Siu, K.; Winkler, J. D.; Crew, A. P.; Crews, C. M.; Coleman, K. G. PROTAC-Induced BET Protein Degradation as a Therapy for Castration-Resistant

Prostate Cancer. *Proc. Natl. Acad. Sci.* **2016**, *113* (26), 7124–7129.

(33) Bondeson, D. P.; Smith, B. E.; Burslem, G. M.; Buhimschi, A. D.; Hines, J.; Jaime-Figueroa, S.; Wang, J.; Hamman, B. D.; Ishchenko, A.; Crews, C. M. Lessons in PROTAC Design from Selective Degradation with a Promiscuous Warhead. *Cell Chem. Biol.* **2018**, *25* (1), 78–87.

(34) Chan, K.-H.; Zengerle, M.; Testa, A.; Ciulli, A. Impact of Target Warhead and Linkage Vector on Inducing Protein Degradation: Comparison of Bromodomain and Extra-Terminal (BET) Degraders Derived from Triazolodiazepine (JQ1) and Tetrahydroquinoline (I-BET726) BET Inhibitor Scaffolds. *J. Med. Chem.* **2017**, *61* (2), 504–513.

(35) Burslem, G. M.; Smith, B. E.; Lai, A. C.; Jaime-Figueroa, S.; McQuaid, D. C.; Bondeson, D. P.; Toure, M.; Dong, H.; Qian, Y.; Wang, J.; Crew, A. P.; Hines, J.; Crews, C. M. The Advantages of Targeted Protein Degradation Over Inhibition: An RTK Case Study. *Cell Chem. Biol.* **2018**, *25* (1), 67–77.

(36) Matyskiela, M. E.; Couto, S.; Zheng, X.; Lu, G.; Hui, J.; Stamp, K.; Drew, C.; Ren, Y.; Wang, M.; Carpenter, A.; Lee, C.-W.; Clayton, T.; Fang, W.; Lu, C.-C.; Riley, M.; Abdubek, P.; Blease, K.; Hartke, J.; Kumar, G.; Vessey, R.; Rolfe, M.; Hamann, L. G.; Chamberlain, P. P. SALL4 Mediates Teratogenicity as a Thalidomide-Dependent Cereblon Substrate. *Nat. Chem. Biol.* **2018**, *14* (10), 981–987.

(37) Quach, H.; Ritchie, D.; Stewart, A. K.; Neeson, P.; Harrison, S.; Smyth, M. J.; Prince, H. M. Mechanism of Action of Immunomodulatory Drugs (IMiDS) in Multiple

Myeloma. *Leukemia* **2010**, *24* (1), 22–32.

(38) Lopez-Girona, A.; Mendy, D.; Ito, T.; Miller, K.; Gandhi, A. K.; Kang, J.; Karasawa, S.; Carmel, G.; Jackson, P.; Abbasian, M.; Mahmoudi, A.; Cathers, B.; Rychak, E.; Gaidarova, S.; Chen, R.; Schafer, P. H.; Handa, H.; Daniel, T. O.; Evans, J. F.; Chopra, R. Cereblon Is a Direct Protein Target for Immunomodulatory and Antiproliferative Activities of Lenalidomide and Pomalidomide. *Leukemia* **2012**, *26* (11), 2326–2335.

(39) Ito, T.; Ando, H.; Suzuki, T.; Ogura, T.; Hotta, K.; Imamura, Y.; Yamaguchi, Y.; Handa, H. Identification of a Primary Target of Thalidomide Teratogenicity. *Science* **2010**, *327* (5971), 1345–1350.

(40) Lu, G.; Middleton, R. E.; Sun, H.; Naniong, M.; Ott, C. J.; Mitsiades, C. S.; Wong, K.-K.; Bradner, J. E.; Kaelin, W. G. The Myeloma Drug Lenalidomide Promotes the Cereblon-Dependent Destruction of Ikaros Proteins. *Science* **2014**, *343* (6168), 305–309.

(41) Winter, G. E.; Buckley, D. L.; Paulk, J.; Roberts, J. M.; Souza, A.; Dhe-Paganon, S.; Bradner, J. E. Phthalimide Conjugation as a Strategy for in Vivo Target Protein Degradation. *Science* **2015**, *348* (6241), 1376–1381.

(42) Lu, J.; Qian, Y.; Altieri, M.; Dong, H.; Wang, J.; Raina, K.; Hines, J.; Winkler, J. D.; Crew, A. P.; Coleman, K.; Crews, C. M. Hijacking the E3 Ubiquitin Ligase Cereblon to Efficiently Target BRD4. *Chem. Biol.* **2015**, *22* (6), 755–763.

(43) Zhou, B.; Hu, J.; Xu, F.; Chen, Z.; Bai, L.; Fernandez-Salas, E.; Lin, M.; Liu, L.;

Yang, C. Y.; Zhao, Y.; McEachern, D.; Przybranowski, S.; Wen, B.; Sun, D.; Wang, S. Discovery of a Small-Molecule Degrader of Bromodomain and Extra-Terminal (BET) Proteins with Picomolar Cellular Potencies and Capable of Achieving Tumor Regression. *J. Med. Chem.* **2018**, *61* (2), 462–481.

(44) Nabet, B.; Roberts, J. M.; Buckley, D. L.; Paulk, J.; Dastjerdi, S.; Yang, A.; Leggett, A. L.; Erb, M. A.; Lawlor, M. A.; Souza, A.; Scott, T. G.; Vittori, S.; Perry, J. A.; Qi, J.; Winter, G. E.; Wong, K.-K.; Gray, N. S.; Bradner, J. E. The DTAG System for Immediate and Target-Specific Protein Degradation. *Nat. Chem. Biol.* **2018**, *14* (5), 431–441.

(45) Schiedel, M.; Herp, D.; Hammelmann, S.; Swyter, S.; Lehotzky, A.; Robaa, D.; Oláh, J.; Ovádi, J.; Sippl, W.; Jung, M. Chemically Induced Degradation of Sirtuin 2 (Sirt2) by a Proteolysis Targeting Chimera (PROTAC) Based on Sirtuin Rearranging Ligands (SirReals). *J. Med. Chem.* **2018**, *61* (2), 482–491.

(46) Matyskiela, M. E.; Lu, G.; Ito, T.; Pagarigan, B.; Lu, C.-C.; Miller, K.; Fang, W.; Wang, N.-Y.; Nguyen, D.; Houston, J.; Carmel, G.; Tran, T.; Riley, M.; Nosaka, L.; Lander, G. C.; Gaidarova, S.; Xu, S.; Ruchelman, A. L.; Handa, H.; Carmichael, J.; Daniel, T. O.; Cathers, B. E.; Lopez-Girona, A.; Chamberlain, P. P. A Novel Cereblon Modulator Recruits GSPT1 to the CRL4CRBN Ubiquitin Ligase. *Nature* **2016**, *535* (7611), 252–257.

(47) Zorba, A.; Nguyen, C.; Xu, Y.; Starr, J.; Borzilleri, K.; Smith, J.; Zhu, H.; Farley, K. A.; Ding, W.; Schiemer, J.; Feng, X.; Chang, J. S.; Uccello, D. P.; Young, J. A.;

Garcia-Irrizary, C. N.; Czabaniuk, L.; Schuff, B.; Oliver, R.; Montgomery, J.; Hayward, M. M.; Coe, J.; Chen, J.; Niosi, M.; Luthra, S.; Shah, J. C.; El-Kattan, A.; Qiu, X.; West, G. M.; Noe, M. C.; Shanmugasundaram, V.; Gilbert, A. M.; Brown, M. F.; Calabrese, M. F. Delineating the Role of Cooperativity in the Design of Potent PROTACs for BTK. *Proc. Natl. Acad. Sci.* **2018**, *115* (31), 7285–7292.

(48) Nowak, R. P.; DeAngelo, S. L.; Buckley, D.; He, Z.; Donovan, K. A.; An, J.; Safaee, N.; Jedrychowski, M. P.; Ponthier, C. M.; Ishoey, M.; Zhang, T.; Mancias, J. D.; Gray, N. S.; Bradner, J. E.; Fischer, E. S. Plasticity in Binding Confers Selectivity in Ligand-Induced Protein Degradation. *Nat. Chem. Biol.* **2018**, *14* (7), 706–714.

(49) Maniaci, C.; Hughes, S. J.; Testa, A.; Chen, W.; Lamont, D. J.; Rocha, S.; Alessi, D. R.; Romeo, R.; Ciulli, A. Homo-PROTACs: Bivalent Small-Molecule Dimerizers of the VHL E3 Ubiquitin Ligase to Induce Self-Degradation. *Nat. Commun.* **2017**, *8* (1), 830.

(50) Steinebach, C.; Lindner, S.; Udeshi, N. D.; Mani, D. C.; Kehm, H.; Köpff, S.; Carr, S. A.; Gütschow, M.; Krönke, J. Homo-PROTACs for the Chemical Knockdown of Cereblon. *ACS Chem. Biol.* **2018**, *13* (9), 2771–2782.

(51) Steinebach, C.; Kehm, H.; Lindner, S.; Vu, L. P.; Köpff, S.; López Mármol, Á.; Weiler, C.; Wagner, K. G.; Reichenzeller, M.; Krönke, J.; Gütschow, M. PROTAC-Mediated Crosstalk between E3 Ligases. *Chem. Commun.* **2019**, *55* (12), 1821–1824.

(52) Girardini, M.; Maniaci, C.; Hughes, S. J.; Testa, A.; Ciulli, A. Cereblon versus VHL: Hijacking E3 Ligases against Each Other Using PROTACs. *Bioorg. Med. Chem.*

2019, *27* (12), 2466–2479.

(53) Bai, Z.; Gust, R. Breast Cancer, Estrogen Receptor and Ligands. *Arch. Pharm. (Weinheim).* **2009**, *342* (3), 133–149.

(54) Hwang, D.-J.; He, Y.; Ponnusamy, S.; Mohler, M. L.; Thiyagarajan, T.; McEwan, I. J.; Narayanan, R.; Miller, D. D. New Generation of Selective Androgen Receptor Degraders: Our Initial Design, Synthesis, and Biological Evaluation of New Compounds with Enzalutamide-Resistant Prostate Cancer Activity. *J. Med. Chem.* **2019**, *62* (2), 491–511.

(55) Tria, G. S.; Abrams, T.; Baird, J.; Burks, H. E.; Firestone, B.; Gaither, L. A.; Hamann, L. G.; He, G.; Kirby, C. A.; Kim, S.; Lombardo, F.; Macchi, K. J.; McDonnell, D. P.; Mishina, Y.; Norris, J. D.; Nunez, J.; Springer, C.; Sun, Y.; Thomsen, N. M.; Wang, C.; Wang, J.; Yu, B.; Tiong-Yip, C.-L.; Peukert, S. Discovery of LSZ102, a Potent, Orally Bioavailable Selective Estrogen Receptor Degrader (SERD) for the Treatment of Estrogen Receptor Positive Breast Cancer. *J. Med. Chem.* **2018**, *61* (7), 2837–2864.

(56) Wang, L.; Guillen, V. S.; Sharma, N.; Flessa, K.; Min, J.; Carlson, K. E.; Toy, W.; Braqi, S.; Katzenellenbogen, B. S.; Katzenellenbogen, J. A.; Chandarlapaty, S.; Sharma, A. New Class of Selective Estrogen Receptor Degraders (SERDs): Expanding the Toolbox of PROTAC Degrons. *ACS Med. Chem. Lett.* **2018**, *9* (8), 803–808.

(57) Neklesa, T. K.; Tae, H. S.; Schneekloth, A. R.; Stulberg, M. J.; Corson, T. W.;

Sundberg, T. B.; Raina, K.; Holley, S. A.; Crews, C. M. Small-Molecule Hydrophobic Tagging–Induced Degradation of HaloTag Fusion Proteins. *Nat. Chem. Biol.* **2011**, *7* (8), 538–543.

(58) Shi, Y.; Long, M. J. C.; Rosenberg, M. M.; Li, S.; Kobjack, A.; Lessans, P.; Coffey, R. T.; Hedstrom, L. Boc 3 Arg-Linked Ligands Induce Degradation by Localizing Target Proteins to the 20S Proteasome. *ACS Chem. Biol.* **2016**, *11* (12), 3328–3337.

(59) Banik, S.; Pedram, K.; Wisnovsky, S.; Riley, N.; Bertozzi, C. Lysosome Targeting Chimeras (LYTACs) for the Degradation of Secreted and Membrane Proteins. *ChemRexiv* **2019**, *(preprint).*

(60) Coutinho, M. F.; Prata, M. J.; Alves, S. A Shortcut to the Lysosome: The Mannose-6-Phosphate-Independent Pathway. *Mol. Genet. Metab.* **2012**, *107* (3), 257–266.

(61) Han, X.; Wang, C.; Qin, C.; Xiang, W.; Fernandez-Salas, E.; Yang, C.-Y.; Wang, M.; Zhao, L.; Xu, T.; Chinnaswamy, K.; Delproposto, J.; Stuckey, J.; Wang, S. Discovery of ARD-69 as a Highly Potent Proteolysis Targeting Chimera (PROTAC) Degrader of Androgen Receptor (AR) for the Treatment of Prostate Cancer. *J. Med. Chem.* **2019**, *62* (2), 941–964.

(62) Li, Y.; Yang, J.; Aguilar, A.; McEachern, D.; Przybranowski, S.; Liu, L.; Yang, C.-Y.; Wang, M.; Han, X.; Wang, S. Discovery of MD-224 as a First-in-Class, Highly Potent, and Efficacious Proteolysis Targeting Chimera Murine Double Minute 2 Degrader Capable of Achieving Complete and Durable Tumor Regression. *J. Med. Chem.* **2019**, *62* (2), 448–466.

(63) Qin, C.; Hu, Y.; Zhou, B.; Fernandez-Salas, E.; Yang, C.-Y.; Liu, L.; McEachern, D.; Przybranowski, S.; Wang, M.; Stuckey, J.; Meagher, J.; Bai, L.; Chen, Z.; Lin, M.; Yang, J.; Ziazadeh, D. N.; Xu, F.; Hu, J.; Xiang, W.; Huang, L.; Li, S.; Wen, B.; Sun, D.; Wang, S. Discovery of QCA570 as an Exceptionally Potent and Efficacious Proteolysis Targeting Chimera (PROTAC) Degrader of the Bromodomain and Extra-Terminal (BET) Proteins Capable of Inducing Complete and Durable Tumor Regression. *J. Med. Chem.* **2018**, *61* (15), 6685–6704.

(64) Bassi, Z. I.; Fillmore, M. C.; Miah, A. H.; Chapman, T. D.; Maller, C.; Roberts, E. J.; Davis, L. C.; Lewis, D. E.; Galwey, N. W.; Waddington, K. E.; Parravicini, V.; Macmillan-Jones, A. L.; Gongora, C.; Humphreys, P. G.; Churcher, I.; Prinjha, R. K.; Tough, D. F. Modulating PCAF/GCN5 Immune Cell Function through a PROTAC Approach. *ACS Chem. Biol.* **2018**, *13* (10), 2862–2867.

(65) Okuhira, K.; Demizu, Y.; Hattori, T.; Ohoka, N.; Shibata, N.; Nishimaki-Mogami, T.; Okuda, H.; Kurihara, M.; Naito, M. Development of Hybrid Small Molecules That Induce Degradation of Estrogen Receptor-Alpha and Necrotic Cell Death in Breast Cancer Cells. *Cancer Sci.* **2013**, *104* (11), 1492–1498.

(66) Buckley, D. L.; Raina, K.; Darricarrere, N.; Hines, J.; Gustafson, J. L.; Smith, I. E.; Miah, A. H.; Harling, J. D.; Crews, C. M. HaloPROTACS: Use of Small Molecule PROTACs to Induce Degradation of HaloTag Fusion Proteins. *ACS Chem. Biol.* **2015**, *10* (8), 1831–1837.

(67) Lebraud, H.; Wright, D. J.; Johnson, C. N.; Heightman, T. D. Protein Degradation

by In-Cell Self-Assembly of Proteolysis Targeting Chimeras. *ACS Cent. Sci.* **2016**, *2* (12), 927–934.

(68) Buhimschi, A. D.; Armstrong, H. A.; Toure, M.; Jaime-Figueroa, S.; Chen, T. L.; Lehman, A. M.; Woyach, J. A.; Johnson, A. J.; Byrd, J. C.; Crews, C. M. Targeting the C481S Ibrutinib-Resistance Mutation in Bruton's Tyrosine Kinase Using PROTAC-Mediated Degradation. *Biochemistry* **2018**, *57* (26), 3564–3575.

(69) Jiang, Y.; Deng, Q.; Zhao, H.; Xie, M.; Chen, L.; Yin, F.; Qin, X.; Zheng, W.; Zhao, Y.; Li, Z. Development of Stabilized Peptide-Based PROTACs against Estrogen Receptor α. *ACS Chem. Biol.* **2018**, *13* (3), 628–635.

(70) Cromm, P. M.; Samarasinghe, K. T. G.; Hines, J.; Crews, C. M. Addressing Kinase-Independent Functions of Fak via PROTAC-Mediated Degradation. *J. Am. Chem. Soc.* **2018**, *140* (49), 17019–17026.

(71) Yang, K.; Song, Y.; Xie, H.; Wu, H.; Wu, Y.-T.; Leisten, E. D.; Tang, W. Development of the First Small Molecule Histone Deacetylase 6 (HDAC6) Degraders. *Bioorg. Med. Chem. Lett.* **2018**, *28* (14), 2493–2497.

(72) Hu, J.; Hu, B.; Wang, M.; Xu, F.; Miao, B.; Yang, C.-Y.; Wang, M.; Liu, Z.; Hayes, D. F.; Chinnaswamy, K.; Delproposto, J.; Stuckey, J.; Wang, S. Discovery of ERD-308 as a Highly Potent Proteolysis Targeting Chimera (PROTAC) Degrader of Estrogen Receptor (ER). *J. Med. Chem.* **2019**, *62* (3), 1420–1442.

(73) Wang, B.; Wu, S.; Liu, J.; Yang, K.; Xie, H.; Tang, W. Development of Selective Small Molecule MDM2 Degraders Based on Nutlin. *Eur. J. Med. Chem.* **2019**, *176*,

476–491.

(74) Wu, H.; Yang, K.; Zhang, Z.; Leisten, E. D.; Li, Z.; Xie, H.; Liu, J.; Smith, K. A.; Novakova, Z.; Barinka, C.; Tang, W. Development of Multifunctional Histone Deacetylase 6 Degraders with Potent Antimyeloma Activity. *J. Med. Chem.* **2019**, *62* (15), 7042–7057.

(75) Hopkins, A. L.; Groom, C. R. The Druggable Genome. *Nat. Rev. Drug Discov.* **2002**, *1* (9), 727–730.

(76) Tinworth, C. P.; Lithgow, H.; Dittus, L.; Bassi, Z. I.; Hughes, S. E.; Muelbaier, M.; Dai, H.; Smith, I. E. D.; Kerr, W. J.; Burley, G. A.; Bantscheff, M.; Harling, J. D. PROTAC-Mediated Degradation of Bruton's Tyrosine Kinase Is Inhibited by Covalent Binding. *ACS Chem. Biol.* **2019**, *14* (3), 342–347.

(77) Saenz, D. T.; Fiskus, W.; Qian, Y.; Manshouri, T.; Rajapakshe, K.; Raina, K.; Coleman, K. G.; Crew, A. P.; Shen, A.; Mill, C. P.; Sun, B.; Qiu, P.; Kadia, T. M.; Pemmaraju, N.; DiNardo, C.; Kim, M.-S.; Nowak, A. J.; Coarfa, C.; Crews, C. M.; Verstovsek, S.; Bhalla, K. N. Novel BET Protein Proteolysis-Targeting Chimera Exerts Superior Lethal Activity than Bromodomain Inhibitor (BETi) against Post-Myeloproliferative Neoplasm Secondary (s) AML Cells. *Leukemia* **2017**, *31* (9), 1951–1961.

(78) Jo, M.; Stolz, D. B.; Esplen, J. E.; Dorko, K.; Michalopoulos, G. K.; Strom, S. C. Cross-Talk between Epidermal Growth Factor Receptor and c-Met Signal Pathways in Transformed Cells. *J. Biol. Chem.* **2000**, *275* (12), 8806–8811.

(79) Holohan, C.; Van Schaeybroeck, S.; Longley, D. B.; Johnston, P. G. Cancer Drug Resistance: An Evolving Paradigm. *Nat. Rev. Cancer* **2013**, *13* (10), 714–726.

(80) Burslem, G. M.; Song, J.; Chen, X.; Hines, J.; Crews, C. M. Enhancing Antiproliferative Activity and Selectivity of a FLT-3 Inhibitor by Proteolysis Targeting Chimera Conversion. *J. Am. Chem. Soc.* **2018**, *140* (48), 16428–16432.

(81) Zhang, X.; Lee, H. C.; Shirazi, F.; Baladandayuthapani, V.; Lin, H.; Kuiatse, I.; Wang, H.; Jones, R. J.; Berkova, Z.; Singh, R. K.; Lu, J.; Qian, Y.; Raina, K.; Coleman, K. G.; Crews, C. M.; Li, B.; Wang, H.; Hailemichael, Y.; Thomas, S. K.; Wang, Z.; Davis, R. E.; Orlowski, R. Z. Protein Targeting Chimeric Molecules Specific for Bromodomain and Extra-Terminal Motif Family Proteins Are Active against Pre-Clinical Models of Multiple Myeloma. *Leukemia* **2018**, *32* (10), 2224–2239.

(82) Tarantelli, C.; Gaudio, E.; Arribas, A. J.; Kwee, I.; Hillmann, P.; Rinaldi, A.; Cascione, L.; Spriano, F.; Bernasconi, E.; Guidetti, F.; Carrassa, L.; Pittau, R. B.; Beaufils, F.; Ritschard, R.; Rageot, D.; Sele, A.; Dossena, B.; Rossi, F. M.; Zucchetto, A.; Taborelli, M.; Gattei, V.; Rossi, D.; Stathis, A.; Stussi, G.; Broggini, M.; Wymann, M. P.; Wicki, A.; Zucca, E.; Cmiljanovic, V.; Fabbro, D.; Bertoni, F. PQR309 Is a Novel Dual PI3K/MTOR Inhibitor with Preclinical Antitumor Activity in Lymphomas as a Single Agent and in Combination Therapy. *Clin. Cancer Res.* **2018**, *24* (1), 120–129.

(83) Lipinski, C. A. Lead- and Drug-like Compounds: The Rule-of-Five Revolution.

Drug Discov. Today Technol. **2004**, *1* (4), 337–341.

(84) Churcher, I. Protac-Induced Protein Degradation in Drug Discovery: Breaking the Rules or Just Making New Ones? *J. Med. Chem.* **2018**, *61* (2), 444–452.

(85) Salami, J.; Alabi, S.; Willard, R. R.; Vitale, N. J.; Wang, J.; Dong, H.; Jin, M.; McDonnell, D. P.; Crew, A. P.; Neklesa, T. K.; Crews, C. M. Androgen Receptor Degradation by the Proteolysis-Targeting Chimera ARCC-4 Outperforms Enzalutamide in Cellular Models of Prostate Cancer Drug Resistance. *Commun. Biol.* **2018**, *1* (1), 100.

(86) Shibata, N.; Nagai, K.; Morita, Y.; Ujikawa, O.; Ohoka, N.; Hattori, T.; Koyama, R.; Sano, O.; Imaeda, Y.; Nara, H.; Cho, N.; Naito, M. Development of Protein Degradation Inducers of Androgen Receptor by Conjugation of Androgen Receptor Ligands and Inhibitor of Apoptosis Protein Ligands. *J. Med. Chem.* **2018**, *61* (2), 543–575.

(87) Zhang, Y.; Loh, C.; Chen, J.; Mainolfi, N. Targeted Protein Degradation Mechanisms. *Drug Discov. Today Technol.* **2019**, *31*, 53–60.

(88) Lu, M.; Liu, T.; Jiao, Q.; Ji, J.; Tao, M.; Liu, Y.; You, Q.; Jiang, Z. Discovery of a Keap1-Dependent Peptide PROTAC to Knockdown Tau by Ubiquitination-Proteasome Degradation Pathway. *Eur. J. Med. Chem.* **2018**, *146*, 251–259.

(89) Rodbard, D.; Feldman, Y.; Jaffe, M. L.; Miles, L. E. M. Kinetics of Two-Site Immunoradiometric (‘Sandwich’) Assays—II. *Immunochemistry* **1978**, *15* (2), 77–82.

(90) Douglass, E. F.; Miller, C. J.; Sparer, G.; Shapiro, H.; Spiegel, D. A. A Comprehensive Mathematical Model for Three-Body Binding Equilibria. *J. Am. Chem. Soc.* **2013**, *135* (16), 6092–6099.

(91) Roy, M. J.; Winkler, S.; Hughes, S. J.; Whitworth, C.; Galant, M.; Farnaby, W.; Rumpel, K.; Ciulli, A. SPR-Measured Dissociation Kinetics of PROTAC Ternary Complexes Influence Target Degradation Rate. *ACS Chem. Biol.* **2019**, *14* (3), 361–368.

(92) Shi, Y. A Glimpse of Structural Biology through X-Ray Crystallography. *Cell* **2014**, *159* (5), 995–1014.

(93) Drummond, M. L.; Williams, C. I. In Silico Modeling of PROTAC-Mediated Ternary Complexes: Validation and Application. *J. Chem. Inf. Model.* **2019**, *59* (4), 1634–1644.

(94) Riching, K. M.; Mahan, S.; Corona, C. R.; McDougall, M.; Vasta, J. D.; Robers, M. B.; Urh, M.; Daniels, D. L. Quantitative Live-Cell Kinetic Degradation and Mechanistic Profiling of PROTAC Mode of Action. *ACS Chem. Biol.* **2018**, *13* (9), 2758–2770.

(95) Brand, M.; Jiang, B.; Bauer, S.; Donovan, K. A.; Liang, Y.; Wang, E. S.; Nowak, R. P.; Yuan, J. C.; Zhang, T.; Kwiatkowski, N.; Müller, A. C.; Fischer, E. S.; Gray, N. S.; Winter, G. E. Homolog-Selective Degradation as a Strategy to Probe the Function of CDK6 in AML. *Cell Chem. Biol.* **2019**, *26* (2), 300–306.

(96) Savitski, M. M.; Zinn, N.; Faelth-Savitski, M.; Poeckel, D.; Gade, S.; Becher, I.;

Muelbaier, M.; Wagner, A. J.; Strohmer, K.; Werner, T.; Melchert, S.; Petretich, M.; Rutkowska, A.; Vappiani, J.; Franken, H.; Steidel, M.; Sweetman, G. M.; Gilan, O.; Lam, E. Y. N.; Dawson, M. A.; Prinjha, R. K.; Grandi, P.; Bergamini, G.; Bantscheff, M. Multiplexed Proteome Dynamics Profiling Reveals Mechanisms Controlling Protein Homeostasis. *Cell* **2018**, *173* (1), 260–274.

(97) van Kasteren, S. I.; Kramer, H. B.; Jensen, H. H.; Campbell, S. J.; Kirkpatrick, J.; Oldham, N. J.; Anthony, D. C.; Davis, B. G. Expanding the Diversity of Chemical Protein Modification Allows Post-Translational Mimicry. *Nature* **2007**, *446* (7139), 1105–1109.

(98) Falkenberg, K. J.; Johnstone, R. W. Histone Deacetylases and Their Inhibitors in Cancer, Neurological Diseases and Immune Disorders. *Nat. Rev. Drug Discov.* **2014**, *13* (9), 673–691.

(99) Johnstone, R. W. Histone-Deacetylase Inhibitors: Novel Drugs for the Treatment of Cancer. *Nat. Rev. Drug Discov.* **2002**, *1* (4), 287–299.

(100) Xu, W. S.; Parmigiani, R. B.; Marks, P. Histone Deacetylase Inhibitors: Molecular Mechanisms of Action. *Oncogene* **2007**, *26*, 5541–5552.

(101) Losson, H.; Schnekenburger, M.; Dicato, M.; Diederich, M. Natural Compound Histone Deacetylase Inhibitors (HDACi): Synergy with Inflammatory Signaling Pathway Modulators and Clinical Applications in Cancer. *Molecules* **2016**, *21* (11), 1608.

(102) Bradner, J. E.; West, N.; Grachan, M. L.; Greenberg, E. F.; Haggarty, S. J.; Warnow,

T.; Mazitschek, R. Chemical Phylogenetics of Histone Deacetylases. *Nat. Chem. Biol.* **2010**, *6* (3), 238–243.

(103) Grant, S.; Easley, C.; Kirkpatrick, P. Vorinostat. *Nat. Rev. Drug Discov.* **2007**, *6* (1), 21–22.

(104) Miller, T. A.; Witter, D. J.; Belvedere, S. Histone Deacetylase Inhibitors. *J. Med. Chem.* **2003**, *46* (24), 5097–5116.

(105) Finnin, M. S.; Donigian, J. R.; Cohen, A.; Richon, V. M.; Rifkind, R. A.; Marks, P. A.; Breslow, R.; Pavletich, N. P. Structures of a Histone Deacetylase Homologue Bound to the TSA and SAHA Inhibitors. *Nature* **1999**, *401* (6749), 188–193.

(106) Dokmanovic, M.; Clarke, C.; Marks, P. A. Histone Deacetylase Inhibitors: Overview and Perspectives. *Mol. Cancer Res.* **2007**, *5* (10), 981–989.

(107) Guha, M. Erratum: HDAC Inhibitors Still Need a Home Run, despite Recent Approval. *Nat. Rev. Drug Discov.* **2015**, *14* (5), 225–226.

(108) Gryder, B. E.; Rood, M. K.; Johnson, K. A.; Patil, V.; Raftery, E. D.; Yao, L. P. D.; Rice, M.; Azizi, B.; Doyle, D. F.; Oyelere, A. K. Histone Deacetylase Inhibitors Equipped with Estrogen Receptor Modulation Activity. *J. Med. Chem.* **2013**, *56* (14), 5782–5796.

(109) Gryder, B. E.; Akbashev, M. J.; Rood, M. K.; Raftery, E. D.; Meyers, W. M.; Dillard, P.; Khan, S.; Oyelere, A. K. Selectively Targeting Prostate Cancer with Antiandrogen Equipped Histone Deacetylase Inhibitors. *ACS Chem. Biol.* **2013**, *8*

(11), 2550–2560.

(110) Guerrant, W.; Patil, V.; Canzoneri, J. C.; Yao, L. P.; Hood, R.; Oyelere, A. K. Dual-Acting Histone Deacetylase-Topoisomerase i Inhibitors. *Bioorg. Med. Chem. Lett.* **2013**, *23* (11), 3283–3287.

(111) Sodji, Q. H.; Kornacki, J. R.; Mcdonald, J. F.; Mrksich, M.; Oyelere, A. K. Design and Structure Activity Relationship of Tumor-Homing Histone Deacetylase Inhibitors Conjugated to Folic and Pteroic Acids. *Eur. J. Med. Chem.* **2015**, *96*, 340–359.

(112) Ojha, R.; Huang, H. L.; HuangFu, W. C.; Wu, Y. W.; Nepali, K.; Lai, M. J.; Su, C. J.; Sung, T. Y.; Chen, Y. L.; Pan, S. L.; Liou, J. P. 1-Aroylindoline-Hydroxamic Acids as Anticancer Agents, Inhibitors of HSP90 and HDAC. *Eur. J. Med. Chem.* **2018**, *150*, 667–677.

(113) Dong, G.; Chen, W.; Wang, X.; Yang, X.; Xu, T.; Wang, P.; Zhang, W.; Rao, Y.; Miao, C.; Sheng, C. Small Molecule Inhibitors Simultaneously Targeting Cancer Metabolism and Epigenetics: Discovery of Novel Nicotinamide Phosphoribosyltransferase (NAMPT) and Histone Deacetylase (HDAC) Dual Inhibitors. *J. Med. Chem.* **2017**, *60* (19), 7965–7983.

(114) Lu, D.; Yan, J.; Wang, L.; Liu, H.; Zeng, L.; Zhang, M.; Duan, W.; Ji, Y.; Cao, J.; Geng, M.; Shen, A.; Hu, Y. Design, Synthesis, and Biological Evaluation of the First c-Met/HDAC Inhibitors Based on Pyridazinone Derivatives. *ACS Med. Chem. Lett.* **2017**, *8* (8), 830–834.

(115) Qian, C.; Lai, C.-J.; Bao, R.; Wang, D.-G.; Wang, J.; Xu, G.-X.; Atoyan, R.; Qu, H.; Yin, L.; Samson, M.; Zifcak, B.; Ma, A. W. S.; DellaRocca, S.; Borek, M.; Zhai, H.-X.; Cai, X.; Voi, M. Cancer Network Disruption by a Single Molecule Inhibitor Targeting Both Histone Deacetylase Activity and Phosphatidylinositol 3-Kinase Signaling. *Clin. Cancer Res.* **2012**, *18* (15), 4104–4113.

(116) Kalin, J. H.; Wu, M.; Gomez, A. V.; Song, Y.; Das, J.; Hayward, D.; Adejola, N.; Wu, M.; Panova, I.; Chung, H. J.; Kim, E.; Roberts, H. J.; Roberts, J. M.; Prusevich, P.; Jeliazkov, J. R.; Roy Burman, S. S.; Fairall, L.; Milano, C.; Eroglu, A.; Proby, C. M.; Dinkova-Kostova, A. T.; Hancock, W. W.; Gray, J. J.; Bradner, J. E.; Valente, S.; Mai, A.; Anders, N. M.; Rudek, M. A.; Hu, Y.; Ryu, B.; Schwabe, J. W. R.; Mattevi, A.; Alani, R. M.; Cole, P. A. Targeting the CoREST Complex with Dual Histone Deacetylase and Demethylase Inhibitors. *Nat. Commun.* **2018**, *9* (1), 53.

(117) Griffith, D.; Morgan, M. P.; Marmion, C. J. A Novel Anti-Cancer Bifunctional Platinum Drug Candidate with Dual DNA Binding and Histone Deacetylase Inhibitory Activity. *Chem. Commun.* **2009**, *0* (44), 6735–6737.

(118) Grozinger, C. M.; Hassig, C. a; Schreiber, S. L. Three Proteins Define a Class of Human Histone Deacetylases Related to Yeast Hda1p. *Proc. Natl. Acad. Sci. U. S. A.* **1999**, *96* (9), 4868–4873.

(119) Boyault, C.; Sadoul, K.; Pabion, M.; Khochbin, S. HDAC6, at the Crossroads between Cytoskeleton and Cell Signaling by Acetylation and Ubiquitination. *Oncogene* **2007**, *26* (37), 5468–5476.

(120) Hubbert, C.; Guardiola, A.; Shao, R.; Kawaguchi, Y.; Ito, A.; Nixon, A.; Yoshida, M.; Wang, X.-F.; Yao, T.-P. HDAC6 Is a Microtubule-Associated Deacetylase. *Nature* **2002**, *417* (6887), 455–458.

(121) Zhang, X.; Yuan, Z.; Zhang, Y.; Yong, S.; Salas-Burgos, A.; Koomen, J.; Olashaw, N.; Parsons, J. T.; Yang, X. J.; Dent, S. R.; Yao, T. P.; Lane, W. S.; Seto, E. HDAC6 Modulates Cell Motility by Altering the Acetylation Level of Cortactin SI. *Mol. Cell* **2007**, *27* (2), 197–213.

(122) Wu, Y.; Song, S. W.; Sun, J.; Bruner, J. M.; Fuller, G. N.; Zhang, W. IIp45 Inhibits Cell Migration through Inhibition of HDAC6. *J. Biol. Chem.* **2010**, *285* (6), 3554–3560.

(123) Keremu, A.; Aimaiti, A.; Liang, Z.; Zou, X. Role of the HDAC6/STAT3 Pathway in Regulating PD-L1 Expression in Osteosarcoma Cell Lines. *Cancer Chemother. Pharmacol.* **2019**, *83* (2), 255–264.

(124) Lienlaf, M.; Perez-Villarroel, P.; Knox, T.; Pabon, M.; Sahakian, E.; Powers, J.; Woan, K. V.; Lee, C.; Cheng, F.; Deng, S.; Smalley, K. S. M.; Montecino, M.; Kozikowski, A.; Pinilla-Ibarz, J.; Sarnaik, A.; Seto, E.; Weber, J.; Sotomayor, E. M.; Villagra, A. Essential Role of HDAC6 in the Regulation of PD-L1 in Melanoma. *Mol. Oncol.* **2016**, *10* (5), 735–750.

(125) Hideshima, T.; Bradner, J. E.; Wong, J.; Chauhan, D.; Richardson, P.; Schreiber, S. L.; Anderson, K. C. Small-Molecule Inhibition of Proteasome and Aggresome Function Induces Synergistic Antitumor Activity in Multiple Myeloma. *Proc. Natl.*

Acad. Sci. U. S. A. **2005**, *102* (24), 8567–8572.

(126) Kawaguchi, Y.; Kovacs, J. J.; McLaurin, A.; Vance, J. M.; Ito, A.; Yao, T.-P. The Deacetylase HDAC6 Regulates Aggresome Formation and Cell Viability in Response to Misfolded Protein Stress. *Cell* **2003**, *115* (6), 727–738.

(127) Kalin, J. H.; Bergman, J. A. Development and Therapeutic Implications of Selective Histone Deacetylase 6 Inhibitors. *J. Med. Chem.* **2013**, *56* (16), 6297–6313.

(128) Kanno, K.; Kanno, S.; Nitta, H.; Uesugi, N.; Sugai, T.; Masuda, T.; Wakabayashi, G.; Maesawa, C. Overexpression of Histone Deacetylase 6 Contributes to Accelerated Migration and Invasion Activity of Hepatocellular Carcinoma Cells. *Oncol. Rep.* **2012**, *28* (3), 867–873.

(129) Bradbury, C. A.; Khanim, F. L.; Hayden, R.; Bunce, C. M.; White, D. A.; Drayson, M. T.; Craddock, C.; Turner, B. M. Histone Deacetylases in Acute Myeloid Leukaemia Show a Distinctive Pattern of Expression That Changes Selectively in Response to Deacetylase Inhibitors. *Leukemia* **2005**, *19* (10), 1751–1759.

(130) Bazzaro, M.; Lin, Z.; Santillan, A.; Lee, M. K.; Wang, M. C.; Chan, K. C.; Bristow, R. E.; Mazitschek, R.; Bradner, J.; Roden, R. B. S. Ubiquitin Proteasome System Stress Underlies Synergistic Killing of Ovarian Cancer Cells by Bortezomib and a Novel HDAC6 Inhibitor. *Clin. Cancer Res.* **2008**, *14* (22), 7340–7347.

(131) Wang, X.-X.; Wan, R.-Z.; Liu, Z.-P. Recent Advances in the Discovery of Potent and Selective HDAC6 Inhibitors. *Eur. J. Med. Chem.* **2018**, *143*, 1406–1418.

(132) Tang, W.; Luo, T.; Greenberg, E. F.; Bradner, J. E.; Schreiber, S. L. Discovery of Histone Deacetylase 8 Selective Inhibitors. *Bioorg. Med. Chem. Lett.* **2011**, *21* (9), 2601–2605.

(133) Hideshima, T.; Qi, J.; Paranal, R. M.; Tang, W.; Greenberg, E.; West, N.; Colling, M. E.; Estiu, G.; Mazitschek, R.; Perry, J. A.; Ohguchi, H.; Cottini, F.; Mimura, N.; Görgün, G.; Tai, Y.-T.; Richardson, P. G.; Carrasco, R. D.; Wiest, O.; Schreiber, S. L.; Anderson, K. C.; Bradner, J. E. Discovery of Selective Small-Molecule HDAC6 Inhibitor for Overcoming Proteasome Inhibitor Resistance in Multiple Myeloma. *Proc. Natl. Acad. Sci.* **2016**, *113* (46), 13162–13167.

(134) Santo, L.; Hideshima, T.; Kung, A. L.; Tseng, J.-C.; Tamang, D.; Yang, M.; Jarpe, M.; van Duzer, J. H.; Mazitschek, R.; Ogier, W. C.; Cirstea, D.; Rodig, S.; Eda, H.; Scullen, T.; Canavese, M.; Bradner, J.; Anderson, K. C.; Jones, S. S.; Raje, N. Preclinical Activity, Pharmacodynamic, and Pharmacokinetic Properties of a Selective HDAC6 Inhibitor, ACY-1215, in Combination with Bortezomib in Multiple Myeloma. *Blood* **2012**, *119* (11), 2579–2589.

(135) Vogl, D. T.; Raje, N. S.; Jagannath, S.; Richardson, P. G.; Hari, P.; Orlowski, R. Z.; Supko, J.; Tamang, D.; Jones, S. S.; Wheeler, C.; Markelewicz, R. J.; Lonial, S. Ricolinostat (ACY-1215), the First Selective HDAC6 Inhibitor, in Combination with Bortezomib and Dexamethasone in Patients with Relapsed or Relapsed-and-Refractory Multiple Myeloma: Phase 1b Results (ACY-100 Study). *Blood* **2015**, *126* (23), 1827.

(136) Yee, A. J.; Bensinger, W. I.; Supko, J. G.; Voorhees, P. M.; Berdeja, J. G.; Richardson, P. G.; Libby, E. N.; Wallace, E. E.; Birrer, N. E.; Burke, J. N.; Tamang, D. L.; Yang, M.; Jones, S. S.; Wheeler, C. A.; Markelewicz, R. J.; Raje, N. S. Ricolinostat plus Lenalidomide, and Dexamethasone in Relapsed or Refractory Multiple Myeloma: A Multicentre Phase 1b Trial. *Lancet Oncol.* **2016**, *17* (11), 1569–1578.

(137) Kronke, J.; Udeshi, N. D.; Narla, A.; Grauman, P.; Hurst, S. N.; McConkey, M.; Svinkina, T.; Heckl, D.; Comer, E.; Li, X.; Ciarlo, C.; Hartman, E.; Munshi, N.; Schenone, M.; Schreiber, S. L.; Carr, S. A.; Ebert, B. L. Lenalidomide Causes Selective Degradation of IKZF1 and IKZF3 in Multiple Myeloma Cells. *Science* **2014**, *343* (6168), 301–305.

(138) Fass, D. M.; Reis, S. A.; Ghosh, B.; Hennig, K. M.; Joseph, N. F.; Zhao, W. N.; Nieland, T. J. F.; Guan, J. S.; Groves Kuhnle, C. E.; Tang, W.; Barker, D. D.; Mazitschek, R.; Schreiber, S. L.; Tsai, L. H.; Haggarty, S. J. Crebinostat: A Novel Cognitive Enhancer That Inhibits Histone Deacetylase Activity and Modulates Chromatin-Mediated Neuroplasticity. *Neuropharmacology* **2013**, *64*, 81–96.

(139) Jaskula-Sztul, R.; Eide, J.; Tesfazghi, S.; Dammalapati, A.; Harrison, A. D.; Yu, X.-M.; Scheinebeck, C.; Winston-McPherson, G.; Kupcho, K. R.; Robers, M. B.; Hundal, A. K.; Tang, W.; Chen, H. Tumor-Suppressor Role of Notch3 in Medullary Thyroid Carcinoma Revealed by Genetic and Pharmacological Induction. *Mol. Cancer Ther.* **2015**, *14* (2), 499–512.

(140) Jang, S.; Yu, X. M.; Odorico, S.; Clark, M.; Jaskula-Sztul, R.; Schienebeck, C. M.; Kupcho, K. R.; Harrison, A. D.; Winston-Mcpherson, G. N.; Tang, W.; Chen, H. Novel Analogs Targeting Histone Deacetylase Suppress Aggressive Thyroid Cancer Cell Growth and Induce Re-Differentiation. *Cancer Gene Ther.* **2015**, *22* (8), 410–416.

(141) Ortmeyer, C. P.; Haufe, G.; Schwegmann, K.; Hermann, S.; Schäfers, M.; Börgel, F.; Wünsch, B.; Wagner, S.; Hugenberg, V. Synthesis and Evaluation of a [18F]BODIPY-Labeled Caspase-Inhibitor. *Bioorg. Med. Chem.* **2017**, *25* (7), 2167–2176.

(142) Poolman, J. M.; Maity, C.; Boekhoven, J.; van der Mee, L.; le Sage, V. A. A.; Groenewold, G. J. M.; van Kasteren, S. I.; Versluis, F.; van Esch, J. H.; Eelkema, R. A Toolbox for Controlling the Properties and Functionalisation of Hydrazone-Based Supramolecular Hydrogels. *J. Mater. Chem. B* **2016**, *4* (5), 852–858.

(143) Hideshima, T.; Cottini, F.; Ohguchi, H.; Jakubikova, J.; Gorgun, G.; Mimura, N.; Tai, Y.-T.; Munshi, N. C.; Richardson, P. G.; Anderson, K. C. Rational Combination Treatment with Histone Deacetylase Inhibitors and Immunomodulatory Drugs in Multiple Myeloma. *Blood Cancer J.* **2015**, *5* (5), 312.

(144) Bergman, J. A.; Woan, K.; Perez-Villarroel, P.; Villagra, A.; Sotomayor, E. M.; Kozikowski, A. P. Selective Histone Deacetylase 6 Inhibitors Bearing Substituted Urea Linkers Inhibit Melanoma Cell Growth. *J. Med. Chem.* **2012**, *55* (22), 9891–9899.

(145) Papadas, A.; Asimakopoulos, F. Mechanisms of Resistance in Multiple Myeloma. In *M. Mandala, E. Romano (eds.), Mechanisms of Drug Resistance in Cancer Therapy*, *Handbook of Experimental Pharmacology*; Springer, 2017; Vol. 249, pp. 251–288.

(146) Niesvizky, R.; Richardson, P. G.; Yee, A. J.; Nooka, A. K.; Raab, M. S.; Shain, K. H.; Gabrail, N. Y.; Matous, J.; Agarwal, A. B.; Hoffman, J.; Madan, S.; Pagel, J. M.; San Miguel, J.; Moreau, P.; Mateos, M.-V.; Facon, T.; Tamang, D.; Jones, S. S.; Markelewicz, R. J.; Wheeler, C.; Trede, N. S.; Raje, N.; Terpos, E.; Bensinger, W. I. Selective HDAC6 Inhibitor ACY-241, an Oral Tablet, Combined with Pomalidomide and Dexamethasone: Safety and Efficacy of Escalation and Expansion Cohorts in Patients with Relapsed or Relapsed-and-Refractory Multiple Myeloma (ACE-MM-200 Study). *Blood* **2016**, *128* (22), 3307.

(147) Ray, A.; Das, D. S.; Song, Y.; Hideshima, T.; Tai, Y.; Chauhan, D.; Anderson, K. C. Combination of a Novel HDAC6 Inhibitor ACY-241 and Anti-PD-L1 Antibody Enhances Anti-Tumor Immunity and Cytotoxicity in Multiple Myeloma. *Leukemia* **2018**, *32* (3), 843–846.

(148) Fischer, E. S.; Böhm, K.; Lydeard, J. R.; Yang, H.; Stadler, M. B.; Cavadini, S.; Nagel, J.; Serluca, F.; Acker, V.; Lingaraju, G. M.; Tichkule, R. B.; Schebesta, M.; Forrester, W. C.; Schirle, M.; Hassiepen, U.; Ottl, J.; Hild, M.; Beckwith, R. E. J.; Harper, J. W.; Jenkins, J. L.; Thomä, N. H. Structure of the DDB1–CRBN E3 Ubiquitin Ligase in Complex with Thalidomide. *Nature* **2014**, *512* (7512), 49–53.

(149) Chamberlain, P. P.; Lopez-Girona, A.; Miller, K.; Carmel, G.; Pagarigan, B.; Chie-Leon, B.; Rychak, E.; Corral, L. G.; Ren, Y. J.; Wang, M.; Riley, M.; Delker, S. L.; Ito, T.; Ando, H.; Mori, T.; Hirano, Y.; Handa, H.; Hakoshima, T.; Daniel, T. O.; Cathers, B. E. Structure of the Human Cereblon-DDB1-Lenalidomide Complex Reveals Basis for Responsiveness to Thalidomide Analogs. *Nat. Struct. Mol. Biol.* **2014**, *21* (9), 803–809.

(150) Miyake, Y.; Keusch, J. J.; Wang, L.; Saito, M.; Hess, D.; Wang, X.; Melancon, B. J.; Helquist, P.; Gut, H.; Matthias, P. Structural Insights into HDAC6 Tubulin Deacetylation and Its Selective Inhibition. *Nat. Chem. Biol.* **2016**, *12* (9), 748–754.

(151) Soucy, T. A.; Smith, P. G.; Milhollen, M. A.; Berger, A. J.; Gavin, J. M.; Adhikari, S.; Brownell, J. E.; Burke, K. E.; Cardin, D. P.; Critchley, S.; Cullis, C. A.; Doucette, A.; Garnsey, J. J.; Gaulin, J. L.; Gershman, R. E.; Lublinsky, A. R.; McDonald, A.; Mizutani, H.; Narayanan, U.; Olhava, E. J.; Peluso, S.; Rezaei, M.; Sintchak, M. D.; Talreja, T.; Thomas, M. P.; Traore, T.; Vyskocil, S.; Weatherhead, G. S.; Yu, J.; Zhang, J.; Dick, L. R.; Claiborne, C. F.; Rolfe, M.; Bolen, J. B.; Langston, S. P. An Inhibitor of NEDD8-Activating Enzyme as a New Approach to Treat Cancer. *Nature* **2009**, *458* (7239), 732–736.

(152) Agnarelli, A.; Chevassut, T.; Mancini, E. J. IRF4 in Multiple Myeloma—Biology, Disease and Therapeutic Target. *Leuk. Res.* **2018**, *72*, 52–58.

(153) Bjorklund, C. C.; Lu, L.; Kang, J.; Hagner, P. R.; Havens, C. G.; Amatangelo, M.; Wang, M.; Ren, Y.; Couto, S.; Breider, M.; Ning, Y.; Gandhi, A. K.; Daniel, T. O.;

Chopra, R.; Klippel, A.; Thakurta, A. G. Rate of CRL4CRBN Substrate Ikaros and Aiolos Degradation Underlies Differential Activity of Lenalidomide and Pomalidomide in Multiple Myeloma Cells by Regulation of C-Myc and IRF4. *Blood Cancer J.* **2015**, *5* (10), 354.

(154) Harada, T.; Hideshima, T.; Anderson, K. C. Histone Deacetylase Inhibitors in Multiple Myeloma: From Bench to Bedside. *Int. J. Hematol.* **2016**, *104* (3), 300–309.

(155) Rosenblatt, J.; Avigan, D. Targeting the PD-1/PD-L1 Axis in Multiple Myeloma: A Dream or a Reality? *Blood* **2017**, *129* (3), 275–279.

(156) Keir, M. E.; Liang, S. C.; Guleria, I.; Latchman, Y. E.; Qipo, A.; Albacker, L. A.; Koulmanda, M.; Freeman, G. J.; Sayegh, M. H.; Sharpe, A. H. Tissue Expression of PD-L1 Mediates Peripheral T Cell Tolerance. *J. Exp. Med.* **2006**, *203* (4), 883–895.

(157) Liu, J.-R.; Yu, C.-W.; Hung, P.-Y.; Hsin, L.-W.; Chern, J.-W. High-Selective HDAC6 Inhibitor Promotes HDAC6 Degradation Following Autophagy Modulation and Enhanced Antitumor Immunity in Glioblastoma. *Biochem. Pharmacol.* **2019**, *163*, 458–471.

(158) Carew, J. S.; Espitia, C. M.; Zhao, W.; Visconte, V.; Anwer, F.; Kelly, K. R.; Nawrocki, S. T. Rational Cotargeting of HDAC6 and BET Proteins Yields Synergistic Antimyeloma Activity. *Blood Adv.* **2019**, *3* (8), 1318–1329.

(159) Li, Y.; Shin, D.; Kwon, S. H. Histone Deacetylase 6 Plays a Role as a Distinct Regulator of Diverse Cellular Processes. *FEBS J.* **2013**, *280* (3), 775–793.

(160) Zhang, L.; Liu, S.; Liu, N.; Zhang, Y.; Liu, M.; Li, D.; Seto, E.; Yao, T. P.; Shui, W.; Zhou, J. Proteomic Identification and Functional Characterization of MYH9, Hsc70, and DNAJA1 as Novel Substrates of HDAC6 Deacetylase Activity. *Protein Cell* **2014**, *6* (1), 42–54.

(161) Livak, K. J.; Schmittgen, T. D. Analysis of Relative Gene Expression Data Using Real-Time Quantitative PCR and the 2−ΔΔCT Method. *Methods* **2001**, *25* (4), 402–408.

(162) Lequin, R. M. Enzyme Immunoassay (EIA)/Enzyme-Linked Immunosorbent Assay (ELISA). *Clin. Chem.* **2005**, *51* (12), 2415–2418.

(163) Andersen, P. L.; Vermette, P. Intracellular Insulin Quantification by Cell-ELISA. *Exp. Cell Res.* **2016**, *347* (1), 14–23.

(164) Falahat, R.; Wiranowska, M.; Gallant, N. D.; Toomey, R.; Hill, R.; Alcantar, N. A Cell ELISA for the Quantification of MUC1 Mucin (CD227) Expressed by Cancer Cells of Epithelial and Neuroectodermal Origin. *Cell. Immunol.* **2015**, *298* (1–2), 96–103.

(165) Zhang, J.-H. A Simple Statistical Parameter for Use in Evaluation and Validation of High Throughput Screening Assays. *J. Biomol. Screen.* **1999**, *4* (2), 67–73.

(166) Simon, G. M.; Niphakis, M. J.; Cravatt, B. F. Determining Target Engagement in Living Systems. *Nat. Chem. Biol.* **2013**, *9* (4), 200–205.

(167) Schürmann, M.; Janning, P.; Ziegler, S.; Waldmann, H. Small-Molecule Target

Engagement in Cells. *Cell Chem. Biol.* **2016**, *23* (4), 435–441.

(168) Chessum, N. E. A. A.; Sharp, S. Y.; Caldwell, J. J.; Pasqua, A. E.; Wilding, B.; Colombano, G.; Collins, I.; Ozer, B.; Richards, M.; Rowlands, M.; Stubbs, M.; Burke, R.; McAndrew, P. C.; Clarke, P. A.; Workman, P.; Cheeseman, M. D.; Jones, K. Demonstrating In-Cell Target Engagement Using a Pirin Protein Degradation Probe (CCT367766). *J. Med. Chem.* **2018**, *61* (3), 918–933.

(169) Sievers, Q. L.; Petzold, G.; Bunker, R. D.; Renneville, A.; Słabicki, M.; Liddicoat, B. J.; Abdulrahman, W.; Mikkelsen, T.; Ebert, B. L.; Thomä, N. H. Defining the Human C2H2 Zinc Finger Degrome Targeted by Thalidomide Analogs through CRBN. *Science* **2018**, *362* (6414), eaat0572.

(170) Hagner, P. R.; Man, H.-W.; Fontanillo, C.; Wang, M.; Couto, S.; Breider, M.; Bjorklund, C.; Havens, C. G.; Lu, G.; Rychak, E.; Raymon, H.; Narla, R. K.; Barnes, L.; Khambatta, G.; Chiu, H.; Kosek, J.; Kang, J.; Amantangelo, M. D.; Waldman, M.; Lopez-Girona, A.; Cai, T.; Pourdehnad, M.; Trotter, M.; Daniel, T. O.; Schafer, P. H.; Klippel, A.; Thakurta, A.; Chopra, R.; Gandhi, A. K. CC-122, a Pleiotropic Pathway Modifier, Mimics an Interferon Response and Has Antitumor Activity in DLBCL. *Blood* **2015**, *126* (6), 779–789.

(171) Matyskiela, M. E.; Zhang, W.; Man, H.-W.; Muller, G.; Khambatta, G.; Baculi, F.; Hickman, M.; LeBrun, L.; Pagarigan, B.; Carmel, G.; Lu, C.-C.; Lu, G.; Riley, M.; Satoh, Y.; Schafer, P.; Daniel, T. O.; Carmichael, J.; Cathers, B. E.; Chamberlain, P. P. A Cereblon Modulator (CC-220) with Improved Degradation of Ikaros and

Aiolos. *J. Med. Chem.* **2018**, *61* (2), 535–542.

(172) Ishoey, M.; Chorn, S.; Singh, N.; Jaeger, M. G.; Brand, M.; Paulk, J.; Bauer, S.; Erb, M. A.; Parapatics, K.; Müller, A. C.; Bennett, K. L.; Ecker, G. F.; Bradner, J. E.; Winter, G. E. Translation Termination Factor GSPT1 Is a Phenotypically Relevant Off-Target of Heterobifunctional Phthalimide Degraders. *ACS Chem. Biol.* **2018**, *13* (3), 553–560.

(173) Epstein, A. C. R.; Gleadle, J. M.; McNeill, L. A.; Hewitson, K. S.; O'Rourke, J.; Mole, D. R.; Mukherji, M.; Metzen, E.; Wilson, M. I.; Dhanda, A.; Tian, Y.-M.; Masson, N.; Hamilton, D. L.; Jaakkola, P.; Barstead, R.; Hodgkin, J.; Maxwell, P. H.; Pugh, C. W.; Schofield, C. J.; Ratcliffe, P. J. C. Elegans EGL-9 and Mammalian Homologs Define a Family of Dioxygenases That Regulate HIF by Prolyl Hydroxylation. *Cell* **2001**, *107* (1), 43–54.

(174) Maxwell, P. H.; Wiesener, M. S.; Chang, G.-W.; Clifford, S. C.; Vaux, E. C.; Cockman, M. E.; Wykoff, C. C.; Pugh, C. W.; Maher, E. R.; Ratcliffe, P. J. The Tumour Suppressor Protein VHL Targets Hypoxia-Inducible Factors for Oxygen-Dependent Proteolysis. *Nature* **1999**, *399* (6733), 271–275.

(175) Min, J.-H. Structure of an HIF-1alpha -PVHL Complex: Hydroxyproline Recognition in Signaling. *Science* **2002**, *296* (5574), 1886–1889.

(176) Soares, P.; Gadd, M. S.; Frost, J.; Galdeano, C.; Ellis, L.; Epemolu, O.; Rocha, S.; Read, K. D.; Ciulli, A. Group-Based Optimization of Potent and Cell-Active Inhibitors of the von Hippel–Lindau (VHL) E3 Ubiquitin Ligase: Structure–Activity

Relationships Leading to the Chemical Probe (2S ,4R)-1-((S)-2-(1-Cyanocyclopropanecarboxamido)-3,3-Dimethylbutanoyl)-4-Hy. *J. Med. Chem.* **2018**, *61* (2), 599–618.

(177) Pagidipati, N. J.; Gaziano, T. A. Estimating Deaths from Cardiovascular Disease: A Review of Global Methodologies of Mortality Measurement. *Circulation* **2013**, *127* (6), 749–756.

(178) Hajhosseiny, R.; Sabir, I.; Khavandi, K.; Wierzbicki, a S. The Ebbs and Flows in the Development of Cholesterol-Lowering Drugs: Prospects for the Future. *Clin. Pharmacol. Ther.* **2014**, *96* (1), 64–73.

(179) Daniels, T. F.; Killinger, K. M.; Michal, J. J.; Wright Jr., R. W.; Jiang, Z. Lipoproteins, Cholesterol Homeostasis and Cardiac Health. *Int. J. Biol. Sci.* **2009**, *5* (5), 474–488.

(180) Wasan, K. M.; Brocks, D. R.; Lee, S. D.; Sachs-Barrable, K.; Thornton, S. J. Impact of Lipoproteins on the Biological Activity and Disposition of Hydrophobic Drugs: Implications for Drug Discovery. *Nat. Rev. Drug Discov.* **2008**, *7* (1), 84–99.

(181) Stone, N. J.; Robinson, J. G.; Lichtenstein, A. H.; Bairey Merz, C. N.; Blum, C. B.; Eckel, R. H.; Goldberg, A. C.; Gordon, D.; Levy, D.; Lloyd-Jones, D. M.; McBride, P.; Schwartz, J. S.; Shero, S. T.; Smith, S. C.; Watson, K.; Wilson, P. W. F. 2013 ACC/AHA Guideline on the Treatment of Blood Cholesterol to Reduce Atherosclerotic Cardiovascular Risk in Adults. *Circulation* **2014**, *129*, 1–45.

(182) Choudhury, R. P.; Fuster, V.; Fayad, Z. a. Molecular, Cellular and Functional

Imaging of Atherothrombosis. *Nat. Rev. Drug Discov.* **2004**, *3* (11), 913–925.

(183) Goldstein, J. L.; Brown, M. S. The LDL Receptor. *Arterioscler. Thromb. Vasc. Biol.* **2009**, *29* (4), 431–438.

(184) Toth, P. P.; Patti, A. M.; Giglio, R. V.; Nikolic, D.; Castellino, G.; Rizzo, M.; Banach, M. Management of Statin Intolerance in 2018: Still More Questions Than Answers. *Am. J. Cardiovasc. Drugs* **2018**, *18* (3), 157–173.

(185) Seidah, N. G. Proprotein Convertase Subtilisin Kexin 9 (PCSK9) Inhibitors in the Treatment of Hypercholesterolemia and Other Pathologies. *Curr. Pharm. Des.* **2013**, *19* (17), 3161–3172.

(186) Weinreich, M.; Frishman, W. H. Antihyperlipidemic Therapies Targeting PCSK9. *Cardiol. Rev.* **2014**, *22* (3), 140–146.

(187) Reiner, Z. Resistance and Intolerance to Statins. *Nutr. Metab. Cardiovasc. Dis.* **2014**, *24* (10), 1057–1066.

(188) Seidah, N. G.; Benjannet, S.; Wickham, L.; Marcinkiewicz, J.; Jasmin, S. B.; Stifani, S.; Basak, A.; Prat, A.; Chretien, M. The Secretory Proprotein Convertase Neural Apoptosis-Regulated Convertase 1 (NARC-1): Liver Regeneration and Neuronal Differentiation. *Proc. Natl. Acad. Sci. U. S. A.* **2003**, *100* (3), 928–933.

(189) Poirier, S.; Mayer, G.; Benjannet, S.; Bergeron, E.; Marcinkiewicz, J.; Nassoury, N.; Mayer, H.; Nimpf, J.; Prat, A.; Seidah, N. G. The Proprotein Convertase PCSK9 Induces the Degradation of Low Density Lipoprotein Receptor (LDLR) and Its

Closest Family Members VLDLR and ApoER2. *J. Biol. Chem.* **2008**, *283* (4), 2363–2372.

(190) Seidah, N. G.; Awan, Z.; Chrétien, M.; Mbikay, M. PCSK9: A Key Modulator of Cardiovascular Health Nabil. *Circ. Res.* **2014**, *114* (6), 1022–1036.

(191) Cohen, J. C.; Boerwinkle, E.; Mosley, T. H.; Hobbs, H. H. Sequence Variations in PCSK9, Low LDL, and Protection against Coronary Heart Disease. *Hear. Dis.* **2006**, *354* (12), 1264–1272.

(192) Hampton, E. N.; Knuth, M. W.; Li, J.; Harris, J. L.; Lesley, S. a; Spraggon, G. The Self-Inhibited Structure of Full-Length PCSK9 at 1.9 A Reveals Structural Homology with Resistin within the C-Terminal Domain. *Proc. Natl. Acad. Sci. U. S. A.* **2007**, *104* (37), 14604–14609.

(193) Timms, K. M.; Wagner, S.; Samuels, M. E.; Forbey, K.; Goldfine, H.; Jammulapati, S.; Skolnick, M. H.; Hopkins, P. N.; Hunt, S. C.; Shattuck, D. M. A Mutation in PCSK9 Causing Autosomal-Dominant Hypercholesterolemia in a Utah Pedigree. *Hum. Genet.* **2004**, *114* (4), 349–353.

(194) Cunningham, D.; Danley, D. E.; Geoghegan, K. F.; Griffor, M. C.; Hawkins, J. L.; Subashi, T. a; Varghese, A. H.; Ammirati, M. J.; Culp, J. S.; Hoth, L. R.; Mansour, M. N.; McGrath, K. M.; Seddon, A. P.; Shenolikar, S.; Stutzman-Engwall, K. J.; Warren, L. C.; Xia, D.; Qiu, X. Structural and Biophysical Studies of PCSK9 and Its Mutants Linked to Familial Hypercholesterolemia. *Nat. Struct. Mol. Biol.* **2007**, *14* (5), 413–419.

(195) Allard, D.; Amsellem, S.; Abifadel, M.; Trillard, M.; Devillers, M.; Luc, G.; Krempf, M.; Reznik, Y.; Girardet, J.-P.; Fredenrich, A.; Junien, C.; Varret, M.; Boileau, C.; Benlian, P.; Rabès, J.-P. Novel Mutations of ThePCSK9 Gene Cause Variable Phenotype of Autosomal Dominant Hypercholesterolemia. *Hum. Mutat.* **2005**, *26* (5), 497–497.

(196) Zaid, A.; Roubtsova, A.; Essalmani, R.; Marcinkiewicz, J.; Chamberland, A.; Hamelin, J.; Tremblay, M.; Jacques, H.; Jin, W.; Davignon, J.; Seidah, N. G.; Prat, A. Proprotein Convertase Subtilisin/Kexin Type 9 (PCSK9): Hepatocyte-Specific Low-Density Lipoprotein Receptor Degradation and Critical Role in Mouse Liver Regeneration. *Hepatology* **2008**, *48* (2), 646–654.

(197) Rashid, S.; Curtis, D. E.; Garuti, R.; Anderson, N. N.; Bashmakov, Y.; Ho, Y. K.; Hammer, R. E.; Moon, Y.-A.; Horton, J. D. Decreased Plasma Cholesterol and Hypersensitivity to Statins in Mice Lacking Pcsk9. *Proc. Natl. Acad. Sci. U. S. A.* **2005**, *102* (15), 5374–5379.

(198) Dubuc, G.; Chamberland, A.; Wassef, H.; Davignon, J.; Seidah, N. G.; Bernier, L.; Prat, A. Statins Upregulate PCSK9, the Gene Encoding the Proprotein Convertase Neural Apoptosis-Regulated Convertase-1 Implicated in Familial Hypercholesterolemia. *Arterioscler. Thromb. Vasc. Biol.* **2004**, *24* (8), 1454–1459.

(199) Dong, B.; Wu, M.; Li, H.; Kraemer, F. B.; Adeli, K.; Seidah, N. G.; Park, S. W.; Liu, J. Strong Induction of PCSK9 Gene Expression through HNF1alpha and SREBP2: Mechanism for the Resistance to LDL-Cholesterol Lowering Effect of Statins in

Dyslipidemic Hamsters. *J. Lipid Res.* **2010**, *51*, 1486–1495.

(200) Sabatine, M. S.; Giugliano, R. P.; Keech, A. C.; Honarpour, N.; Wiviott, S. D.; Murphy, S. A.; Kuder, J. F.; Wang, H.; Liu, T.; Wasserman, S. M.; Sever, P. S.; Pedersen, T. R. Evolocumab and Clinical Outcomes in Patients with Cardiovascular Disease. *N. Engl. J. Med.* **2017**, *376* (18), 1713–1722.

(201) Robinson, J. G.; Farnier, M.; Krempf, M.; Bergeron, J.; Luc, G.; Averna, M.; Stroes, E. S.; Langslet, G.; Raal, F. J.; El Shahawy, M.; Koren, M. J.; Lepor, N. E.; Lorenzato, C.; Pordy, R.; Chaudhari, U.; Kastelein, J. J. P.; ODYSSEY LONG TERM Investigators. Efficacy and Safety of Alirocumab in Reducing Lipids and Cardiovascular Events. *N. Engl. J. Med.* **2015**, *372* (16), 1489–1499.

(202) Frank-Kamenetsky, M.; Grefhorst, A.; Anderson, N. N.; Racie, T. S.; Bramlage, B.; Akinc, A.; Butler, D.; Charisse, K.; Dorkin, R.; Fan, Y.; Gamba-Vitalo, C.; Hadwiger, P.; Jayaraman, M.; John, M.; Jayaprakash, K. N.; Maier, M.; Nechev, L.; Rajeev, K. G.; Read, T.; Rohl, I.; Soutschek, J.; Tan, P.; Wong, J.; Wang, G.; Zimmermann, T.; de Fougerolles, A.; Vornlocher, H.-P.; Langer, R.; Anderson, D. G.; Manoharan, M.; Koteliansky, V.; Horton, J. D.; Fitzgerald, K. Therapeutic RNAi Targeting PCSK9 Acutely Lowers Plasma Cholesterol in Rodents and LDL Cholesterol in Nonhuman Primates. *Proc. Natl. Acad. Sci.* **2008**, *105* (33), 11915–11920.

(203) Zhang, Y.; Eigenbrot, C.; Zhou, L.; Shia, S.; Li, W.; Quan, C.; Tom, J.; Moran, P.; Lello, P. Di; Skelton, N. J.; Kong-Beltran, M.; Peterson, A.; Kirchhofer, D.

Identification of a Small Peptide That Inhibits PCSK9 Protein Binding to the Low Density Lipoprotein Receptor. *J. Biol. Chem.* **2014**, *289* (2), 942–955.

(204) Landlinger, C.; Pouwer, M. G.; Juno, C.; van der Hoorn, J. W. A.; Pieterman, E. J.; Jukema, J. W.; Staffler, G.; Princen, H. M. G.; Galabova, G. The AT04A Vaccine against Proprotein Convertase Subtilisin/Kexin Type 9 Reduces Total Cholesterol, Vascular Inflammation, and Atherosclerosis in APOE*3Leiden.CETP Mice. *Eur. Heart J.* **2017**, *38* (32), 2499–2507.

(205) Ding, Q.; Strong, A.; Patel, K. M.; Ng, S. L.; Gosis, B. S.; Regan, S. N.; Cowan, C. A.; Rader, D. J.; Musunuru, K. Permanent Alteration of PCSK9 with in Vivo CRISPR-Cas9 Genome Editing. *Circ. Res.* **2014**, *115* (5), 488–492.

(206) Dong, B.; Li, H.; Singh, A. B.; Cao, A.; Liu, J. Inhibition of PCSK9 Transcription by Berberine Involves Down-Regulation of Hepatic HNF1α Protein Expression through the Ubiquitin-Proteasome Degradation Pathway. *J. Biol. Chem.* **2015**, *290* (7), 4047–4058.

(207) Taechalertpaisarn, J.; Zhao, B.; Liang, X.; Burgess, K. Small Molecule Inhibitors of the PCSK9·LDLR Interaction. *J. Am. Chem. Soc.* **2018**, *140* (9), 3242–3249.

(208) Londregan, A. T.; Wei, L.; Xiao, J.; Lintner, N. G.; Petersen, D.; Dullea, R. G.; McClure, K. F.; Bolt, M. W.; Warmus, J. S.; Coffey, S. B.; Limberakis, C.; Genovino, J.; Thuma, B. A.; Hesp, K. D.; Aspnes, G. E.; Reidich, B.; Salatto, C. T.; Chabot, J. R.; Cate, J. H. D.; Liras, S.; Piotrowski, D. W. Small Molecule Proprotein Convertase Subtilisin/Kexin Type 9 (PCSK9) Inhibitors: Hit to Lead Optimization

of Systemic Agents. *J. Med. Chem.* **2018**, *61* (13), 5704–5718.

(209) Gustafsen, C.; Olsen, D.; Vilstrup, J.; Lund, S.; Reinhardt, A.; Wellner, N.; Larsen, T.; Andersen, C. B. F.; Weyer, K.; Li, J.; Seeberger, P. H.; Thirup, S.; Madsen, P.; Glerup, S. Heparan Sulfate Proteoglycans Present PCSK9 to the LDL Receptor. *Nat. Commun.* **2017**, *8* (1), 503.

(210) Gabrielle Noel Winston-McPherson. Chemical Synthesis and Biological Evaluation of Novel Indole-Containing Heterocycles, University of Wisconsin-Madison, 2016.

(211) Winston-McPherson, G. N.; Xie, H.; Yang, K.; Li, X.; Shu, D.; Tang, W. Discovery of 2,3′-Diindolylmethanes as a Novel Class of PCSK9 Modulators. *Bioorg. Med. Chem. Lett.* **2019**, *29* (16), 2345–2348.

(212) Shu, D.; Winston-Mcpherson, G. N.; Song, W.; Tang, W. Platinum-Catalyzed Tandem Indole Annulation/Arylation for the Synthesis of Diindolylmethanes and Indolo[3,2-b]Carbazoles. *Org. Lett.* **2013**, *15* (16), 4162–4165.

(213) Winston-McPherson, G. N.; Shu, D.; Tang, W. Synthesis and Biological Evaluation of 2,3′-Diindolylmethanes as Agonists of Aryl Hydrocarbon Receptor. *Bioorg. Med. Chem. Lett.* **2014**, *24* (16), 4023–4025.

(214) Kuhnz, W.; Gieschen, H. Predicting the Oral Bioavailability of 19-Nortestosterone Progestins In Vivo from Their Metabolic Stability in Human Liver Microsomal Preparations In Vitro. *Drug Metab. Dispos.* **1998**, *26* (11), 1120–1127.

(215) Guengerich, F. P. Cytochrome P450 Enzymes in the Generation of Commercial

Products. *Nat. Rev. Drug Discov.* **2002**, *1* (5), 359–366.

(216) Pirali, T.; Serafini, M.; Cargnin, S.; Genazzani, A. A. Applications of Deuterium in Medicinal Chemistry. *J. Med. Chem.* **2019**, *62* (11), 5276–5297.

(217) Giles, P. M.; Andrews, B. J.; Cheshire, J.; Noble, N.; Muller, D. P. R.; Slack, J.; Wolff, O. H. Effects of Delipidated Serum and Lipoprotein-Deficient Serum on Sterol Biosynthesis and Efflux in Cultured Skin Fibroblasts—a Comparison of the Behaviour of Cells from a Control with Those from a Heterozygote and Homozygote for Familial Hypercholesterolae. *Clin. Chim. Acta* **1981**, *113* (2), 183–191.

(218) Scotti, E.; Hong, C.; Yoshinaga, Y.; Tu, Y.; Hu, Y.; Zelcer, N.; Boyadjian, R.; de Jong, P. J.; Young, S. G.; Fong, L. G.; Tontonoz, P. Targeted Disruption of the Idol Gene Alters Cellular Regulation of the Low-Density Lipoprotein Receptor by Sterols and Liver X Receptor Agonists. *Mol. Cell. Biol.* **2011**, *31* (9), 1885–1893.

(219) Yan, H.; Ma, Y.; Gui, Y.; Wang, S.; Wang, X.; Gao, F.; Wang, Y. MG132, a Proteasome Inhibitor, Enhances LDL Uptake in HepG2 Cells in Vitro by Regulating LDLR and PCSK9 Expression. *Acta Pharmacol. Sin.* **2014**, *35* (8), 994–1004.

(220) Nassoury, N.; Blasiole, D. A.; Tebon Oler, A.; Benjannet, S.; Hamelin, J.; Poupon, V.; McPherson, P. S.; Attie, A. D.; Prat, A.; Seidah, N. G. The Cellular Trafficking of the Secretory Proprotein Convertase PCSK9 and Its Dependence on the LDLR. *Traffic* **2007**, *8* (6), 718–732.

(221) Miyosawa, K.; Watanabe, Y.; Murakami, K.; Murakami, T.; Shibata, H.; Iwashita,

M.; Yamazaki, H.; Yamazaki, K.; Ohgiya, T.; Shibuya, K.; Mizuno, K.; Tanabe, S.; Singh, S. A.; Aikawa, M. New CETP Inhibitor K-312 Reduces PCSK9 Expression: A Potential Effect on LDL Cholesterol Metabolism. *Am. J. Physiol. Metab.* **2015**, *309* (2), 177–190.

(222) Schmidt, J. V.; Bradfield, C. A. AH RECEPTOR SIGNALING PATHWAYS. *Annu. Rev. Cell Dev. Biol.* **1996**, *12* (1), 55–89.

(223) Ohtake, F.; Fujii-Kuriyama, Y.; Kato, S. AhR Acts as an E3 Ubiquitin Ligase to Modulate Steroid Receptor Functions. *Biochem. Pharmacol.* **2009**, *77* (4), 474–484.

(224) Larigot, L.; Juricek, L.; Dairou, J.; Coumoul, X. AhR Signaling Pathways and Regulatory Functions. *Biochim. Open* **2018**, *7*, 1–9.

(225) Hooper, L. V. You AhR What You Eat: Linking Diet and Immunity. *Cell* **2011**, *147* (3), 489–491.

(226) Rothhammer, V.; Quintana, F. J. The Aryl Hydrocarbon Receptor: An Environmental Sensor Integrating Immune Responses in Health and Disease. *Nat. Rev. Immunol.* **2019**, *19* (3), 184–197.

(227) Mimura, J.; Ema, M.; Sogawa, K.; Fujii-Kuriyama, Y. Identification of a Novel Mechanism of Regulation of Ah (Dioxin) Receptor Function. *Genes Dev.* **1999**, *13* (1), 20–25.

(228) Yang, G. E. The Role of AHR in the Regulation of PCSK9 Expression and Elucidation of Its Mechanism, Yonsei University, 2016.

(229) Ortiz-Delgado, J. B.; Behrens, A.; Segner, H.; Sarasquete, C. Tissue-Specific Induction of EROD Activity and CYP1A Protein in Sparus Aurata Exposed to B(a)P and TCDD. *Ecotoxicol. Environ. Saf.* **2008**, *69* (1), 80–88.

(230) Bisson, W. H.; Koch, D. C.; O'Donnell, E. F.; Khalil, S. M.; Kerkvliet, N. I.; Tanguay, R. L.; Abagyan, R.; Kolluri, S. K. Modeling of the Aryl Hydrocarbon Receptor (AhR) Ligand Binding Domain and Its Utility in Virtual Ligand Screening to Predict New AhR Ligands. *J. Med. Chem.* **2009**, *52* (18), 5635–5641.

(231) Marlowe, J. L.; Fan, Y.; Chang, X.; Peng, L.; Knudsen, E. S.; Xia, Y.; Puga, A. The Aryl Hydrocarbon Receptor Binds to E2F1 and Inhibits E2F1-Induced Apoptosis. *Mol. Biol. Cell* **2008**, *19*, 3263–3271.

(232) Davarinos, N. A.; Pollenz, R. S. Aryl Hydrocarbon Receptor Imported into the Nucleus Following Ligand Binding Is Rapidly Degraded via the Cytosplasmic Proteasome Following Nuclear Export. *J. Biol. Chem.* **1999**, *274* (40), 28708–28715.

(233) Poppy Roworth, A.; Ghari, F.; La Thangue, N. B. To Live or Let Die – Complexity within the E2F1 Pathway. *Mol. Cell. Oncol.* **2015**, *2* (1), e970480.

(234) Wu, P.-Y.; Liao, Y.-F.; Juan, H.-F.; Huang, H.-C.; Wang, B.-J.; Lu, Y.-L.; Yu, I.-S.; Shih, Y.-Y.; Jeng, Y.-M.; Hsu, W.-M.; Lee, H. Aryl Hydrocarbon Receptor Downregulates MYCN Expression and Promotes Cell Differentiation of Neuroblastoma. *PLoS One* **2014**, *9* (2), 88795.

(235) Watabe, Y.; Nazuka, N.; Tezuka, M.; Shimba, S. Aryl Hydrocarbon Receptor Functions as a Potent Coactivator of E2F1-Dependent Trascription Activity. *Biol.*

Pharm. Bull **2010**, *33* (3), 389–397.

(236) Lai, Q.; Giralt, A.; Le May, C.; Zhang, L.; Cariou, B.; Denechaud, P.-D.; Fajas, L. E2F1 Inhibits Circulating Cholesterol Clearance by Regulating Pcsk9 Expression in the Liver. *JCI Insight* **2017**, *2* (10), e89729.

(237) Denechaud, P.-D.; Annicotte, J.-S.; Fajas, L. E2F1 Mediates Sustained Lipogenesis and Contributes to Hepatic Steatosis. *J Clin Invest* **2016**, *126* (1).

(238) Lee, H.; Puppala, D.; Choi, E.-Y.; Swanson, H.; Kim, K.-B. Targeted Degradation of the Aryl Hydrocarbon Receptor by the PROTAC Approach: A Useful Chemical Genetic Tool. *ChemBioChem* **2007**, *8* (17), 2058–2062.

(239) Puppala, D.; Lee, H.; Kim, K. B.; Swanson, H. I. Development of an Aryl Hydrocarbon Receptor Antagonist Using the Proteolysis-Targeting Chimeric Molecules Approach: A Potential Tool for Chemoprevention. *Mol. Pharmacol.* **2008**, *73* (4), 1064–1071.

Appendices

Abbreviations and Acronyms

ActD	actinomycin D
AhR	aryl hydrocarbon receptor
AhRR	AhR repressor
AML	acute myeloid leukemia
AR	androgen receptor
ARNT	AhR nuclear translocator
ATRA	all-trans retinoic acid
BBR	berberine
BET	bromodomain and extra terminal domain
BET/Brd	bromodomain and extra-terminal motif proteins
BIIK	benzimidazole indolyl ketone
BIIM	benzimidazole-indolyl methane
BNF	β-napthoflavone
BRET	bioluminescence resonance energy transfer
BTK	Bruton's tyrosine kinase
CD1/2	catalytic domain 1 or 2
$CDCl_3$	chloroform-d
CDK	cyclin-dependent kinases
ChIP	chromatin immunoprecipitation
cIAP1	cellular inhibitor of apoptosis protein 1
CI-M6PR	cation-independent mannose-6-phosphate receptor
Cl-FICZ	chloro-substituted 6-formylindolo[3,2-b]carbazole
CLIPTAC	click-formed proteolysis targeting chimera
CLL	chronic lymphocytic leukemia
Co-IP	co-immunoprecipitation
Cpd	compound

CRBN	cereblon
CRISPR	clustered regularly interspaced short palindromic repeats
CRL	cullin–RING (really interesting new gene) E3 ubiquitin ligase
CST	cell Signaling Technology
CVD	cardiovascular diseases
CYP	cytochrome P450
CYP1A1	cytochrome P450 family 1 subfamily A member 1
DC_{50}	concentration where half of maximal degradation is achieved
DHT	dihydrotestosterone
DIIK	diindolyl ketone
DIIM	diindolyl methane
DIM	3,3’-diindolylmethane
D_{max}	maximal degradation
E2F1	E2F transcription factor 1
EC_{50}	concentration of compound that gives half-maximal response
EGFR	epidermal growth factor receptor
ELISA	enzyme-linked immunosorbent assay
ER	estrogen receptor
ERK1/2	extracellular signal-regulated protein kinases 1 and 2
ERRα	estrogen-related receptor alpha
FBS	fetal bovine serum
FICZ	6-formylindolo[3,2-b]carbazole
FKBP12	FK506 binding protein 12
FLT-3	fms related tyrosine kinase 3
FRET	fluorescence resonance energy transfer
FYTTD1	forty-two-three domain containing 1
GFP	green fluorescent protein
GOF	gain-of-function
H3	histone 3
HAT	histone acetyltransferase

HDAC	histone deacetylase
HDACi	HDAC inhibitors
HDL	high density lipoprotein
HMG-CoA	3-hydroxy-3- methylglutaryl coenzyme A
HRMS	high resolution mass spectra
HRP	horseradish peroxidase
HSP90	Heat shock protein 90
HSPG	heparan sulfate proteoglycans
Hyp	hydroxyproline
IAP	inhibitor of apoptosis protein
ICZ	indolo[3,2-*b*]carbazole
IKZF1/3	Ikaros family zinc finger proteins 1/3
IMiDs	immunomodulatory drugs
IPP	IκBα phosphopeptide
IRF4	interferon regulatory factor 4
ITC	isothermal titration calorimetry
Lac	lactacystin
LDL	low density lipoprotein
LDLR	low density lipoprotein receptor
LDPS	lipoprotein-deficient fetal bovine serum
LHR	left heterocycle ring
LHS	left hand side
LOF	loss-of-function
LTR	lysosomal targeting receptor
LYTAC	lysosome targeting chimeras
M6Pn	mannose-6-phosphonate
mAb	monoclonal antibodies
MDM2	mouse double minute 2 homolog
MDR1	multidrug resistance protein 1
MeBS	methyl Bestatin

MM	multiple myeloma
MoA	mode of action
mPDP	multiplexed proteome dynamic profiling
MST	microscale thermophoresis
MTD	maximal tolerated dose
MTT	3-(4,5-dimethylthiazol-2-yl)-2,5-diphenyltetrazolium bromide
NAD^+	nicotinamide adenine dinucleotide
NES	nuclear export signal
Next-A	nexturastat a
NH_4Cl	ammonium chloride
NMR	nuclear magnetic resonance
NTD	N-terminal domain
OIDD	open innovation drug discovery
OVA	ovalicin
PARP	poly ADP ribose polymerase
PC	proprotein convertases
PCSK9	proprotein convertase subtilisin/kexin type 9
PD	pharmacodynamic
PD-1	programmed cell death protein 1
PD-L1	programmed cell death ligand 1
PDP	pirin degradation probe
PK	pharmacokinetic
POI	protein of interest
Poma	pomalidomide
PPI	protein-protein interaction
PROTAC	proteolysis targeting chimera
PTM	post-translational modification
RHR	right heterocycle ring
RHS	right hand side
RIPK2	receptor-interacting serine/threonine-protein kinase 2

RMSD	root-mean-square deviation
RTK	receptor tyrosine kinases
RT-qPCR	real-time quantitative reverse transcription PCR
S/N	signal-to-noise ratio
SAR	structure-activity-relationship
SARM	selective androgen receptor modulator
SCBT	Santa Cruz Biotechnology
SDS-PAGE	sodium dodecyl sulfate polyacrylamide gel electrophoresis
SERD/SARD	selective estrogen/androgen receptor degrader
shRNA	small hairpin RNA
siRNA	small interfering RNA
SIRT	sirtuin
SNIPER	specific and nongenetic IAP-dependent protein erasers
SPR	surface plasmon resonance
STAT3	signal transducer and activator of transcription 3
$T_{1/2}$	half-life
TCDD	tetrachlorodibenzo-*p*-dioxin
TF_{50}	ternary formation 50%
TI_{50}	ternary inhibition 50%
TLC	thin layer chromatography
TPD	targeted protein degradation
UPS	ubiquitination-proteasome system
VCB	VHL, EloinginC and ElonginB
VHL	von Hippel-Lindau tumor suppressor protein
XIAP	X-linked IAP
XRE	xenobiotic-responsive element
ZnF-UBP	zinc-finger ubiquitin binding domain

LC-MS Analysis

9a: retention time, 1.207 min; MS $(M+H)^+$ found 688.3

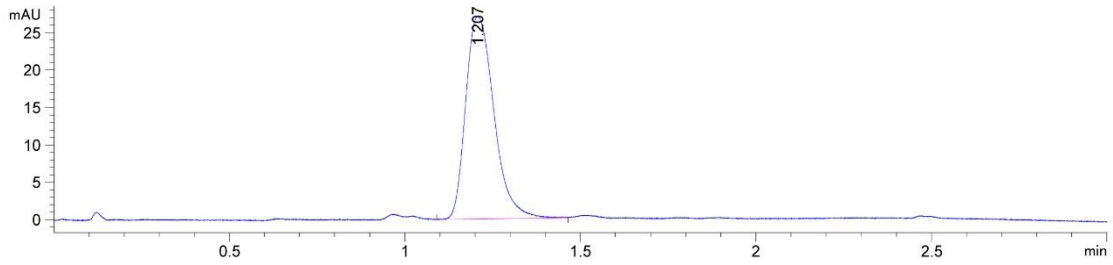

9b: retention time, 1.237 min; MS $(M+H)^+$ found 732.3

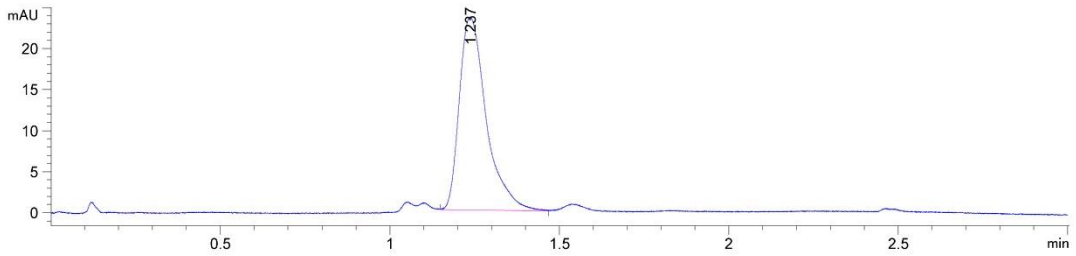

9c: retention time, 1.571 min; MS $(M+H)^+$ found 776.3

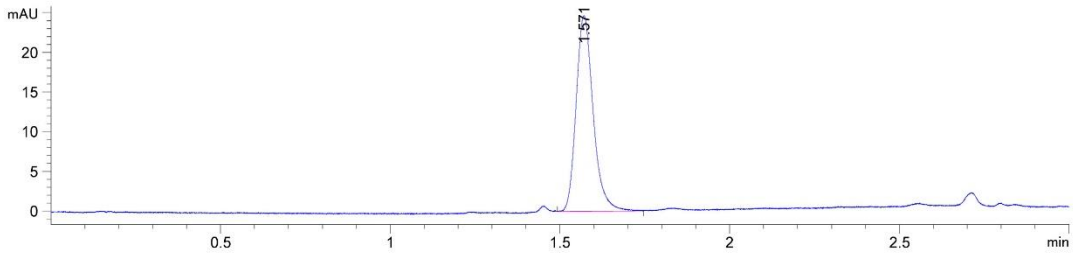

9d: retention time, 1.634 min; MS $(M+H)^+$ found 820.3

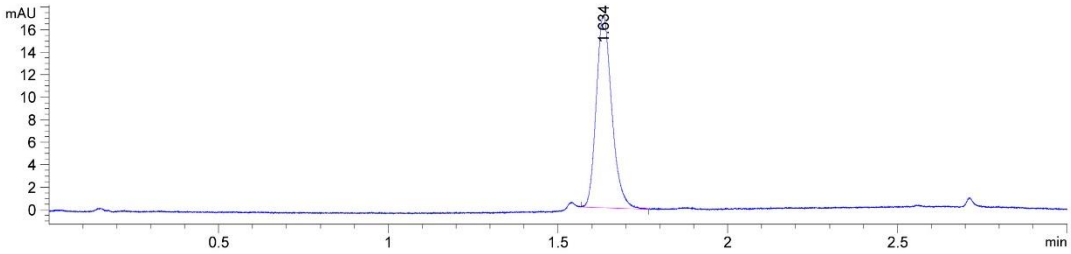
mAU
16
14
12
10
8
6
4
2
0
1.634
0.5
1
1.5
2
2.5
min

NMR Spectrums

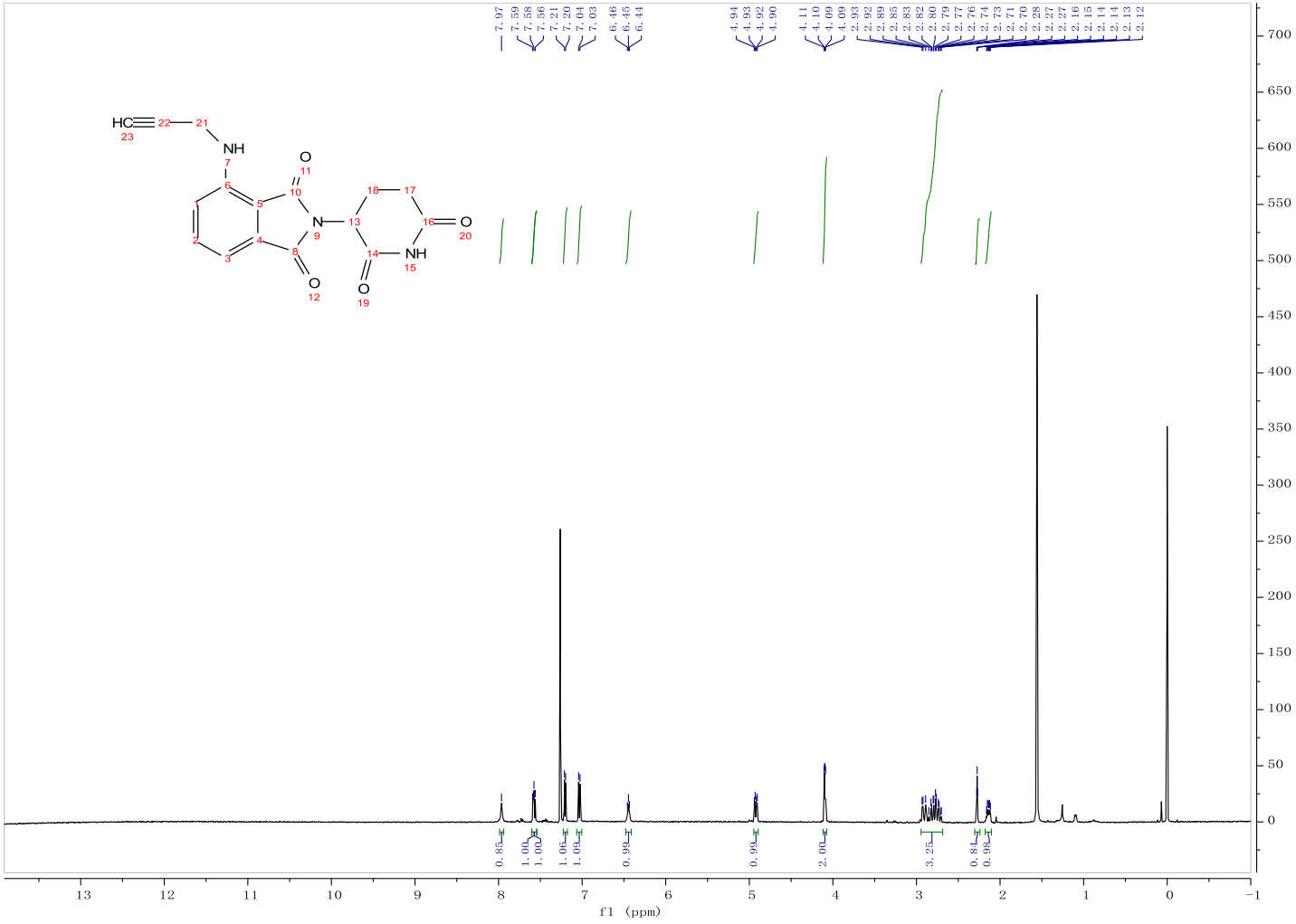

6: ^{1}H

6: ^{13}C

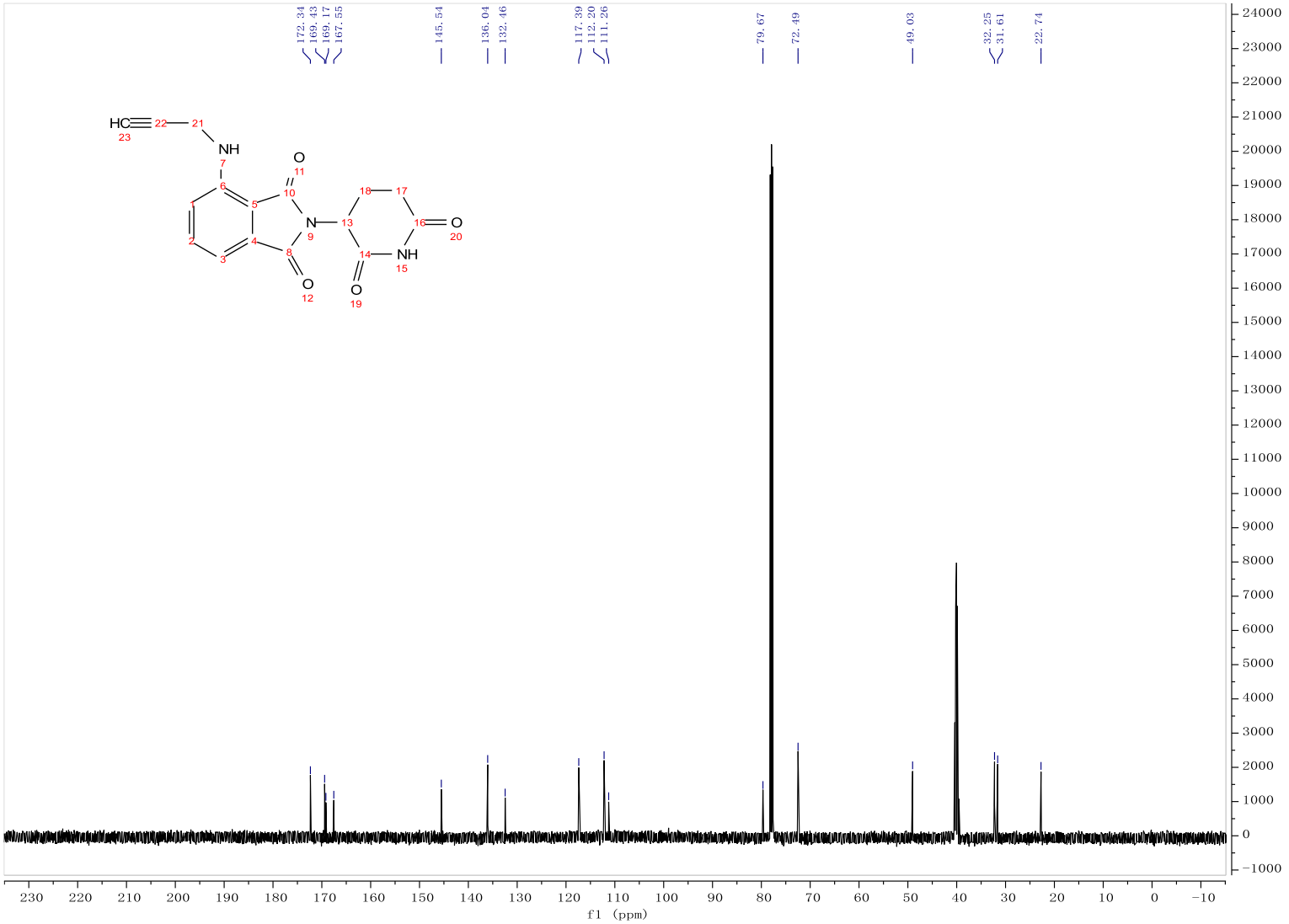
172.34
169.43
169.17
167.55
145.54
136.04
132.46
117.39
112.20
111.26
79.67
72.49
49.03
32.25
31.61
22.74
HC
22
21
23
NH
7
6
5
1
2
3
4
8
O
12
O
11
10
N
9
13
18
17
16
O
20
14
NH
15
O
19
f1 (ppm)

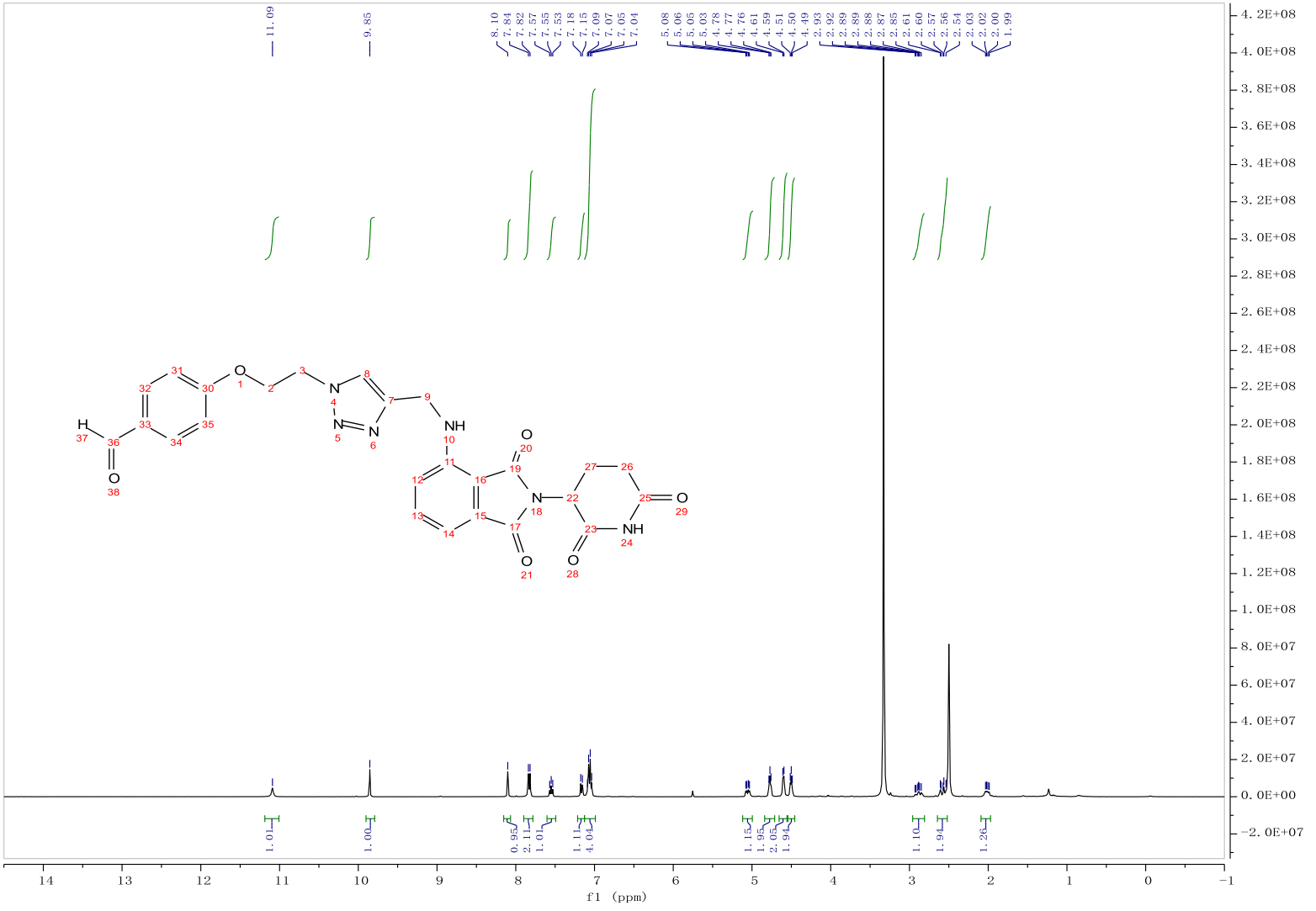
11.09
9.85
8.10
7.84
7.82
7.57
7.55
7.53
7.18
7.15
7.09
7.07
7.05
7.04
5.08
5.06
5.05
5.03
4.78
4.77
4.76
4.61
4.59
4.51
4.50
4.49
2.93
2.92
2.89
2.89
2.88
2.87
2.85
2.61
2.60
2.57
2.56
2.54
2.03
2.02
2.00
1.99
f1 (ppm)

8a: ^{1}H

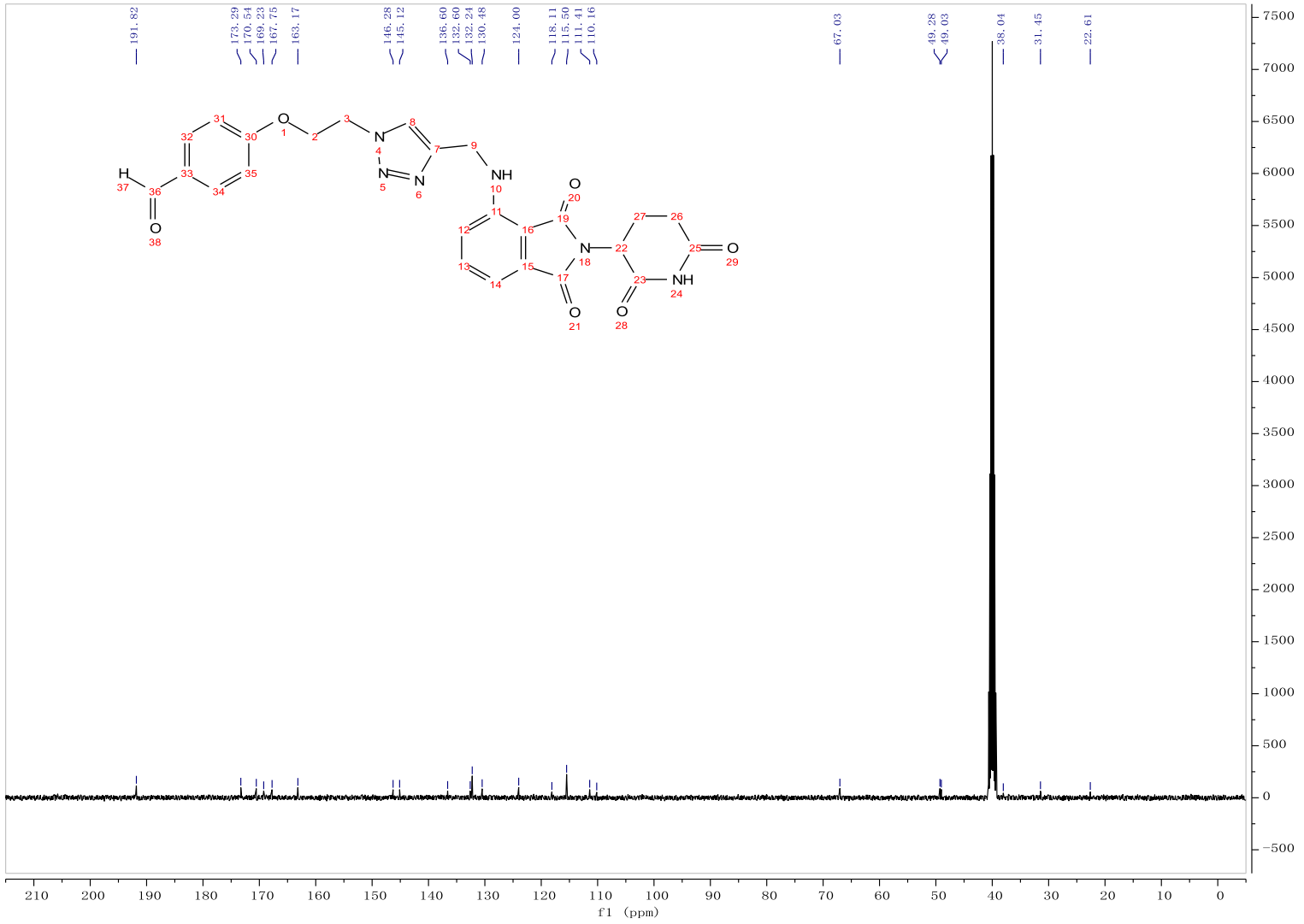
191.82
173.29
170.54
169.23
167.75
163.17
146.28
145.12
136.60
132.60
132.24
130.48
124.00
118.11
115.50
111.41
110.16
67.03
49.28
49.03
38.04
31.45
22.61
f1 (ppm)

8a: ^{13}C

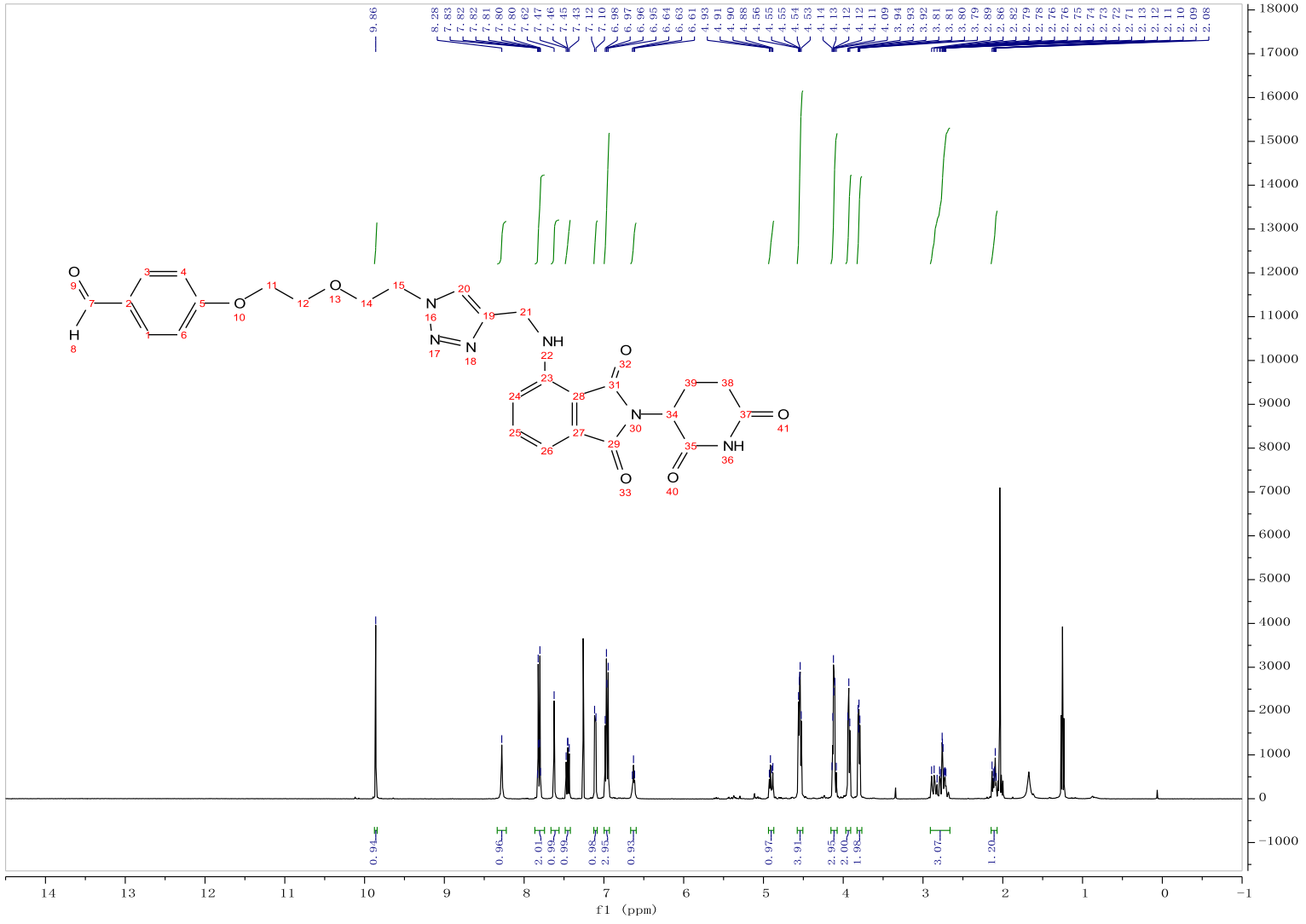
9.86
8.28
7.83
7.82
7.82
7.81
7.80
7.80
7.62
7.47
7.46
7.45
7.43
7.12
7.10
6.98
6.97
6.96
6.95
6.64
6.63
6.61
4.93
4.91
4.90
4.88
4.56
4.55
4.55
4.54
4.53
4.14
4.13
4.12
4.12
4.11
4.09
3.94
3.93
3.92
3.81
3.81
3.80
3.79
2.89
2.86
2.82
2.79
2.78
2.76
2.76
2.75
2.74
2.73
2.72
2.71
2.13
2.12
2.11
2.10
2.09
2.08
0.94
0.96
2.01
0.99
0.99
0.98
2.95
0.93
0.97
3.91
2.95
2.00
1.98
3.07
1.20
f1 (ppm)

8b: ^{1}H

8b: ^{13}C

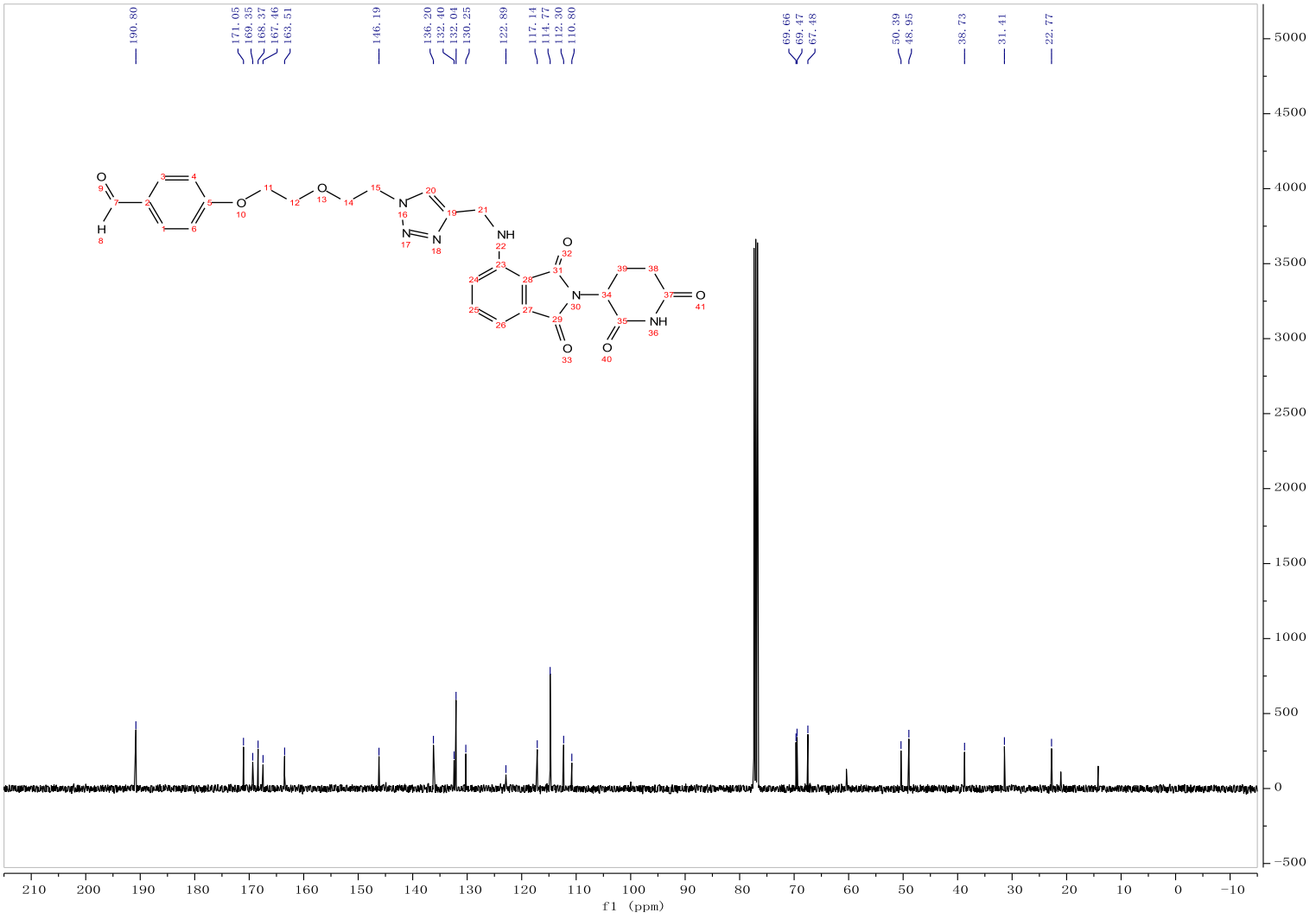
190.80
171.05
169.35
168.37
167.46
163.51
146.19
136.20
132.40
132.04
130.25
122.89
117.14
114.77
112.30
110.80
69.66
69.47
67.48
50.39
48.95
38.73
31.41
22.77
5000
4500
4000
3500
3000
2500
2000
1500
1000
500
0
−500
210
200
190
180
170
160
150
140
130
120
110
100
90
80
70
60
50
40
30
20
10
0
−10
f1 (ppm)

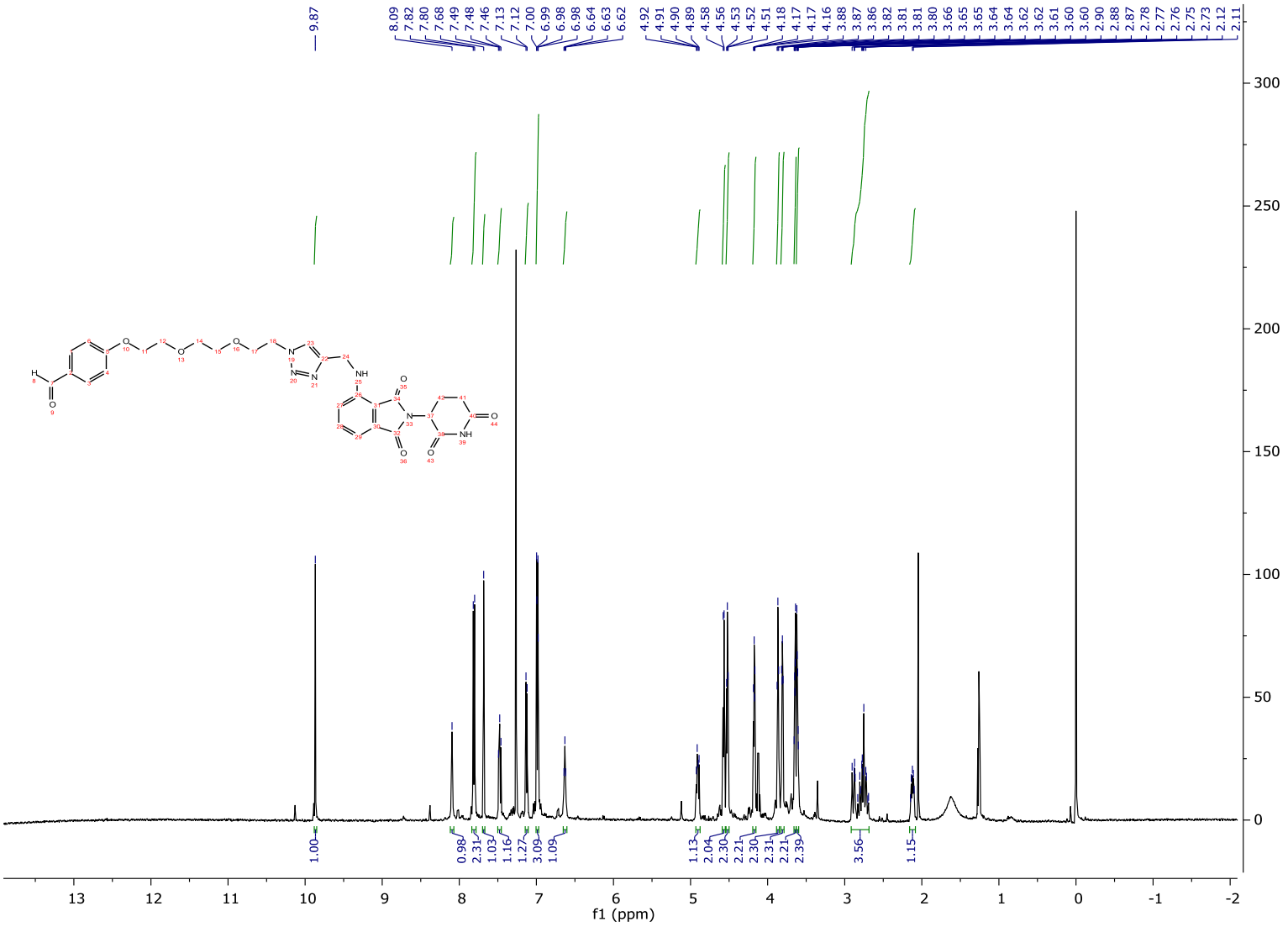
9.87
8.09
7.82
7.80
7.68
7.49
7.48
7.46
7.13
7.12
7.00
6.99
6.98
6.98
6.64
6.63
6.62
4.92
4.91
4.90
4.89
4.58
4.56
4.53
4.52
4.51
4.18
4.17
4.17
4.16
3.88
3.87
3.86
3.82
3.81
3.81
3.80
3.66
3.65
3.65
3.64
3.62
3.62
3.61
3.60
3.60
2.90
2.88
2.87
2.78
2.77
2.76
2.75
2.73
2.12
2.11
1.00
0.98
2.31
1.03
1.16
1.27
3.09
1.09
1.13
2.04
2.30
2.21
2.30
2.31
2.21
2.39
3.56
1.15
f1 (ppm)

8c: ^{1}H

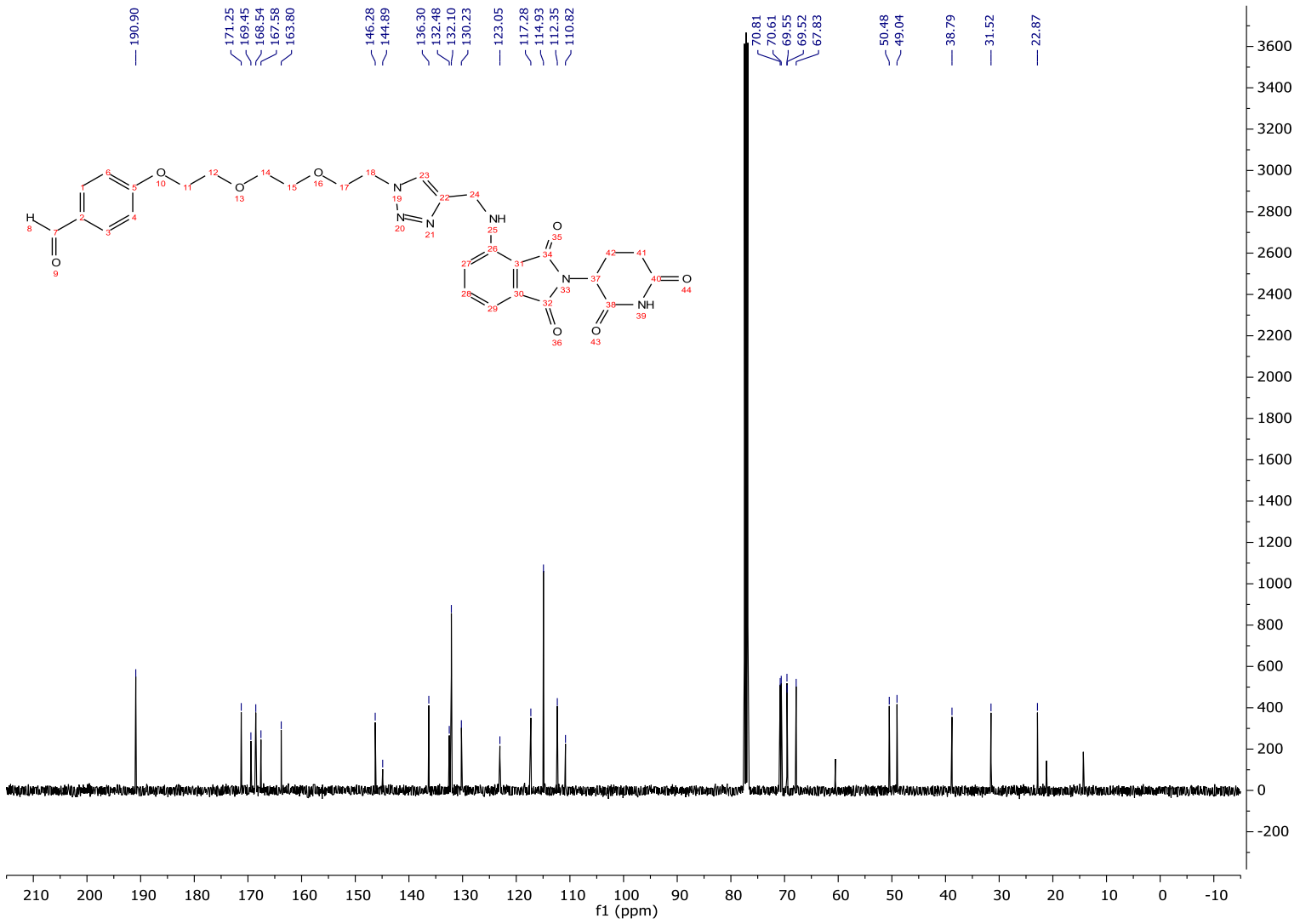
190.90
171.25
169.45
168.54
167.58
163.80
146.28
144.89
136.30
132.48
132.10
130.23
123.05
117.28
114.93
112.35
110.82
70.81
70.61
69.55
69.52
67.83
50.48
49.04
38.79
31.52
22.87
f1 (ppm)

8c: ^{13}C

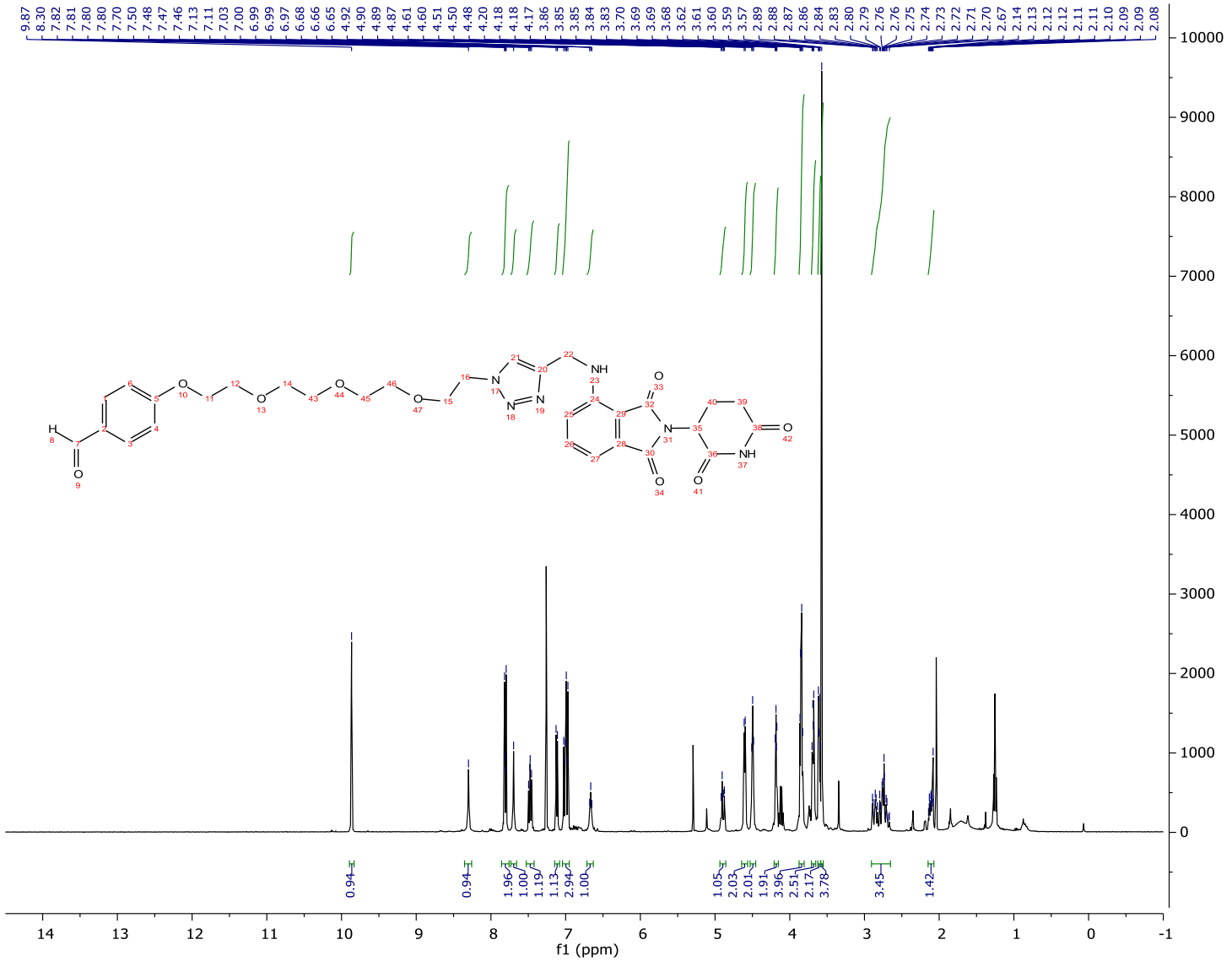
9.87 8.30 7.82 7.81 7.80 7.80 7.70 7.50 7.48 7.47 7.46 7.13 7.11 7.03 7.00 6.99 6.99 6.97 6.68 6.66 6.65 4.92 4.90 4.89 4.87 4.61 4.60 4.51 4.50 4.48 4.20 4.18 4.18 4.17 3.86 3.85 3.85 3.84 3.83 3.70 3.69 3.69 3.68 3.62 3.61 3.60 3.59 3.57 2.89 2.88 2.87 2.86 2.84 2.83 2.80 2.79 2.76 2.76 2.75 2.74 2.73 2.72 2.71 2.70 2.67 2.14 2.13 2.12 2.12 2.11 2.11 2.10 2.09 2.09 2.08
10000
9000
8000
7000
6000
5000
4000
3000
2000
1000
0
0.94 0.94 1.96 1.00 1.19 1.13 2.94 1.00 1.05 2.03 2.01 1.91 3.96 2.51 2.17 3.78 3.45 1.42
14 13 12 11 10 9 8 7 6 5 4 3 2 1 0 -1
f1 (ppm)

8d: ^{1}H

8d: ^{13}C

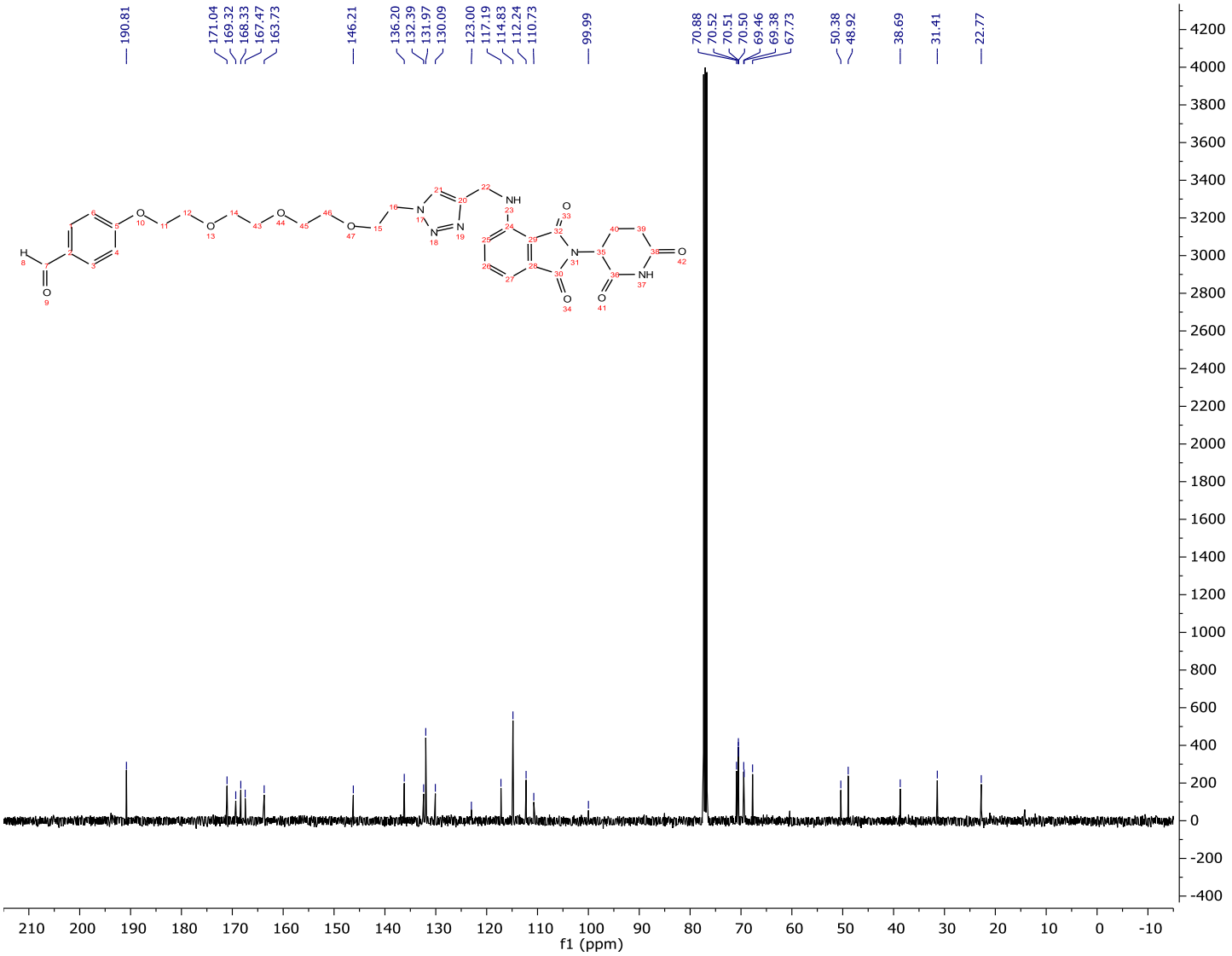
190.81
171.04
169.32
168.33
167.47
163.73
146.21
136.20
132.39
131.97
130.09
123.00
117.19
114.83
112.24
110.73
99.99
70.88
70.52
70.51
70.50
69.46
69.38
67.73
50.38
48.92
38.69
31.41
22.77
f1 (ppm)

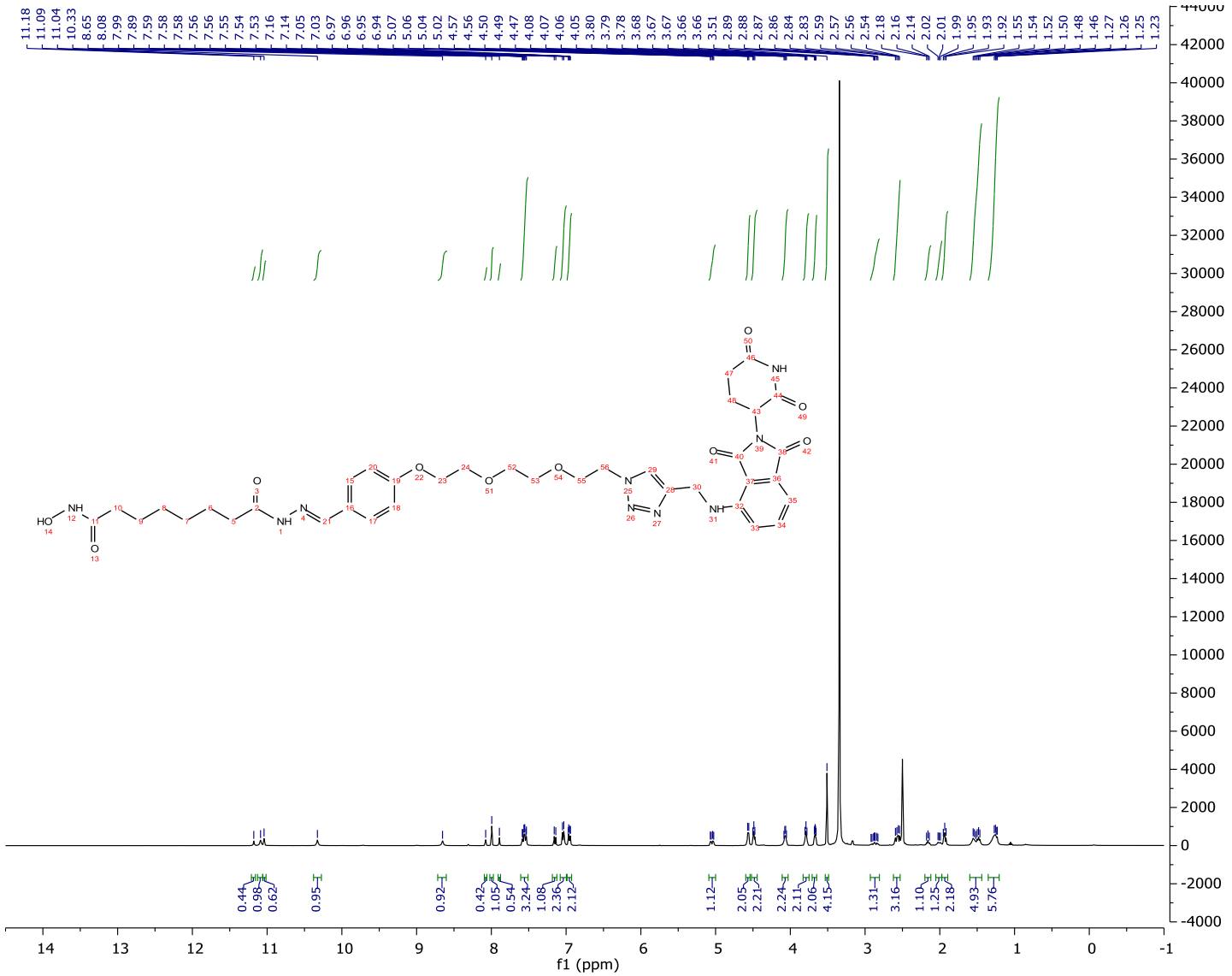
11.18
11.09
11.04
10.33
8.65
8.08
7.99
7.89
7.59
7.58
7.58
7.56
7.56
7.55
7.54
7.53
7.16
7.14
7.05
7.03
6.97
6.96
6.95
6.94
5.07
5.06
5.04
5.02
4.57
4.56
4.50
4.49
4.47
4.08
4.07
4.06
4.05
3.80
3.79
3.78
3.68
3.67
3.67
3.66
3.66
3.51
2.89
2.88
2.87
2.86
2.84
2.83
2.59
2.57
2.56
2.54
2.18
2.16
2.14
2.02
2.01
1.99
1.95
1.93
1.92
1.55
1.54
1.52
1.50
1.48
1.46
1.27
1.26
1.25
1.23
0.44
0.98
0.62
0.95
0.92
0.42
1.05
0.54
3.24
1.08
2.36
2.12
1.12
2.05
2.21
2.24
2.11
2.06
4.15
1.31
3.16
1.10
1.25
2.18
4.93
5.76
f1 (ppm)

9c: ^{1}H

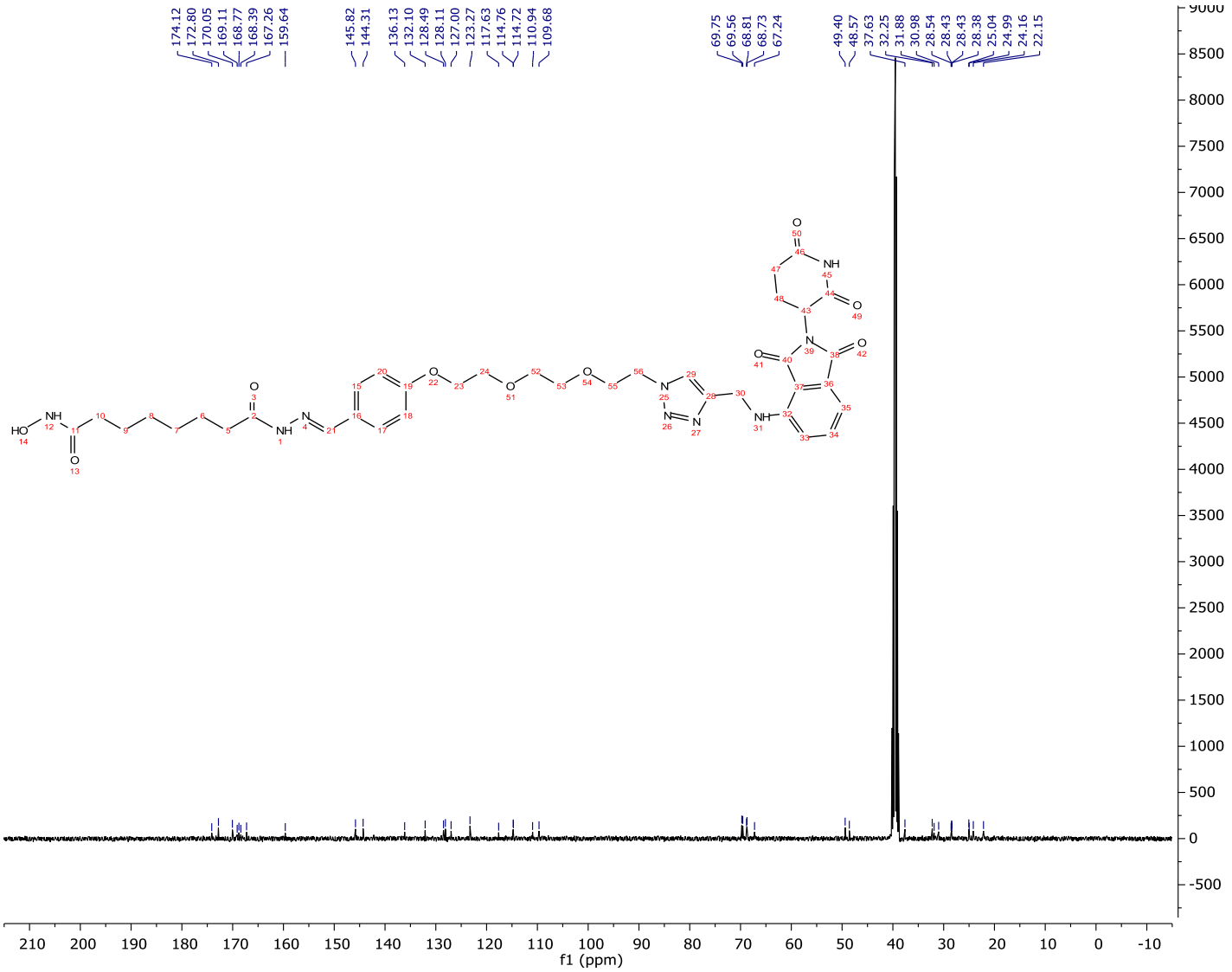
174.12
172.80
170.05
169.11
168.77
168.39
167.26
159.64
145.82
144.31
136.13
132.10
128.49
128.11
127.00
123.27
117.63
114.76
114.72
110.94
109.68
69.75
69.56
68.81
68.73
67.24
49.40
48.57
37.63
32.25
31.88
30.98
28.54
28.43
28.43
28.38
25.04
24.99
24.16
22.15
f1 (ppm)

9c: ^{13}C